DNA-surfactant complexes:

preparation, self-assembly properties and applications in synthesis and bioelectronics

Kai Liu

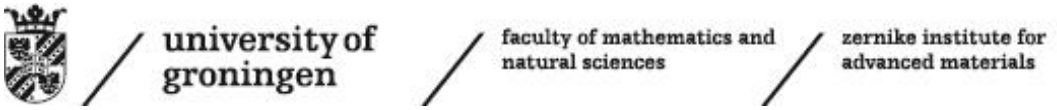

The work described in this thesis was carried out at the Zernike Institute for Advanced Materials, University of Groningen, The Netherlands.

This work was supported financially by the European Research Council (ERC).

Printed by: University Services Department, Blauwborgje 8, 9747 AC Groningen

Cover design by: Alessio Marcozzi and Kai Liu

Zernike Institute PhD thesis series 2015-25

ISSN: 1570-1530

ISBN: 978-90-367-8443-6 (printed version)

ISBN: 978-90-367-8444-3 (electronic version)

university of groningen

DNA-surfactant complexes: preparation, self-assembly properties and applications in synthesis and bioelectronics

PhD thesis

to obtain the degree of PhD at the
University of Groningen
on the authority of the
Rector Magnificus Prof. E. Sterken
and in accordance with
the decision by the College of Deans.

This thesis will be defended in public on

Monday 7 December 2015 at 09.00 hours

by

Kai Liu

born on 10 December 1983
in Shandong, China

Supervisor

Prof. A. Herrmann

Assessment committee

Prof. T. Weil

Prof. S. Lecommandoux

Prof. G. Roelfes

Dedicated to my beloved family

Contents

Chapter 1

DNA-surfactant complexes: an overview

Abstract

The powerful ionic self-assembly behavior of DNA-surfactant complexes, driven by electrostatic interaction, make it a unique material for various applications from optoelectronics to biomedicine. Different packing modes, including ordered lamellar, hexagonal, cubic structures, and disordered isotropic phases have been developed and are summarized herein. The reported DNA-surfactant complexes were organized in the form of bulk films, lyotropic liquid crystals, and hydrogles. The complexes are soluble in organic solvents allowing facile processing, and thus bulk thin films were produced, which lead to nuclease resistance and the ability to long-term storage. These films tend to form well-ordered supramolecular assemblies, resulting in extraordinary electron conductive properties along DNA. The DNA-surfactant complex is a very promising host material for dye dispersion to minimize fluorescence quenching. Different optical applications in lasing and nonlinear optics have been investigated and discussed. Due to their high dielectric properties, DNA-surfactant films are good candidates as electron blocking layers and hole transport materials for optoelectronic devices (light-emitting diodes and solar cells) with enhanced performance. Furthermore, biomedical applications based on DNA-surfactant bulk films and soft DNA-surfactant lyotropic liquid crystals and hydrogels have been reviewed. Gene delivery and drug release are the major application fields for these materials, which have made significant steps forward in the last decades. Delivery efficiencies and internalization mechanisms into cells have been investigated extensively by many research groups. In a series of comprehensive studies, delivery efficiencies were indeed found to be structure-dependent. The advantages and drawbacks of each material in these applications have been evaluated. We end with some prospects for the future development and applications of DNA-surfactant complexes.

1. Introduction of DNA-surfactant complexes

1.1 DNA overview

Deoxyribonucleic acid (DNA), carrying the hereditary information of all living cells, was found by Miescher in 1869[1]. Later, Watson & Crick succeeded in elucidating the double-stranded helix structure of DNA in 1953[2]. DNA is a stable polymeric biomacromolecule, consisting of 2'-deoxyribose, a phosphate group and nitrogenous heterocyclic nucleobases, which are linked together in a linear fashion. In nature, four nucleotide bases exist; adenine (A) and guanine (G) are pyrimidines while thymine (T) and cytosine (C) represent purines. Each polynucleotide is hence characterized by a specific nucleobase sequence, conventionally written in the direction from the 5'-end to the 3'-end of the sugar phosphate backbone. In the double-stranded state, they pair in two by the natural Watson Crick pairing G:C and A:T (Figure 1a), and form the hydrophobic center of the helix. DNA exhibits a highly hydrophilic surface due to the negatively charged phosphate groups, which are responsible for the solubility of DNA in water and buffered aqueous solutions. In the most common structure of DNA, the B-form[3], the bases side on average perpendicular to the molecule axis. Helix periodicity is ~10 base pairs, equivalent to ~3.4 nm, while the diameter of the bare DNA is ~2 nm. Double-stranded DNA is characterized by a distinct melting point at which one double-strand separates into two single strands, a phenomenon that is highly dependent on the GC content[4], the number of base pairs and therefore, on the length of the DNA strands and the surrounding buffer and salt concentrations. Therefore, DNA strands have extraordinary specificity, as they can recognize and bind to complementary partner strands in very dilute solutions. This specific binding of DNA is due to a combination of diverse forces such as electrostatic repulsion of the charged hydrophilic phosphate backbone, a combination of van der Waals forces and base stacking or π–π interactions in the hydrophobic core, and hydrogen bonding between nucleobases.

Nowadays, oligonucleotides (short DNA strands) are routinely fabricated by employing automated synthesizers using phosphoramidite building blocks[5] with lengths larger than 100 nucleotides (100mers) of defined nucleotide sequence. The solid phase synthesis technology is suited to incorporate unnatural monomers as well. Thus, the development of DNA synthesis and modifications[6] has dramatically extended the knowledge about DNA in a broad sense. Synthetic DNA has not only played an important role in the investigation of nucleic acids in the field of biology, but also in the area of nanotechnology. The concept of folding DNA strands into well-defined structures of higher hierarchy was pioneered by Seeman[7]. In an early study, branched DNA molecules were employed to form specific motifs (small building units with specific sticky ends) that could further self-assemble into 3D structures (Figure 1b). These properties of DNA make it a very appealing material for use in various fields[8-10], including drug and gene delivery, molecular computing, biosensors, and even photoelectric and micro-electronic devices.

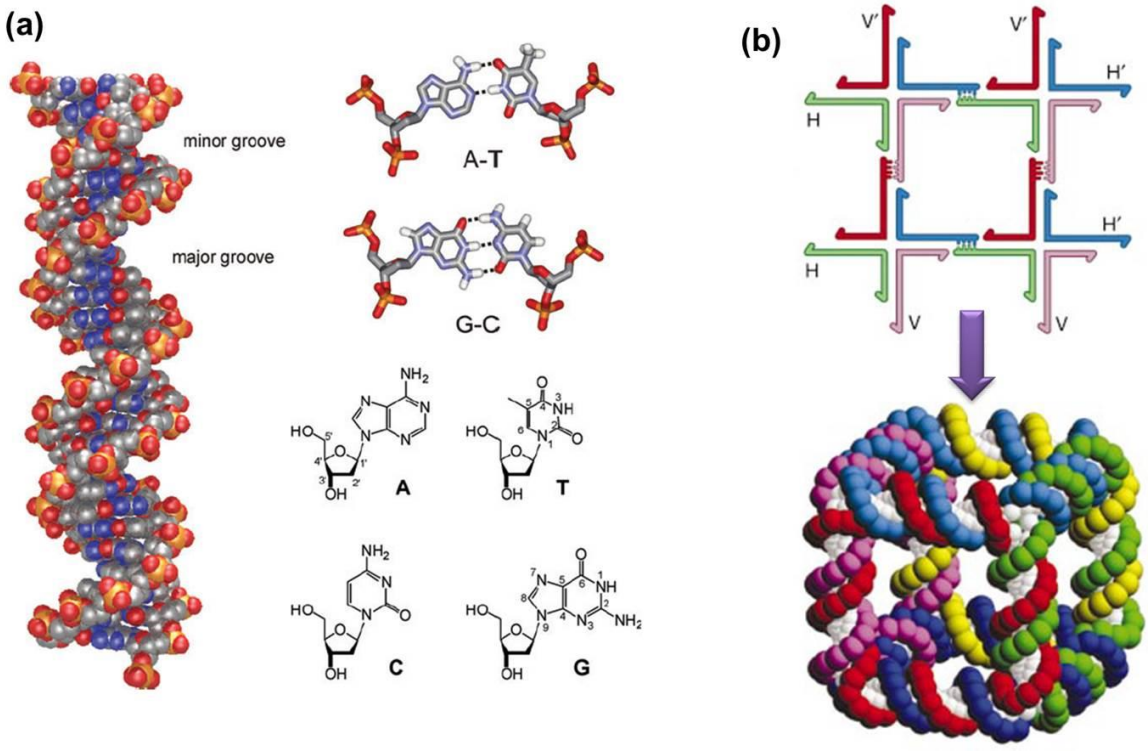

Figure 1. Representation of common structures of DNA. (a) Structure of B-type DNA duplex[6], A–T and G–C base-pairs and numbered structures of the four nucleosides, deoxyadenosine, thymidine, deoxycytidine and deoxyguanosine. (b) DNA oligonucleotides with programmed sequences self-assemble into 3D wireframe structures like a cube[7].

1.2 Ionic Self-assembly of DNA-surfactant complexes

Self-assembling hierarchical and supramolecular materials have attracted considerable interest among materials scientists who are interested in obtaining new properties and functions[11,12]. Researchers can control intermolecular forces for non-covalent tethering by manipulating π-π interactions, van der Waals forces, ionic forces, and hydrogen bonding, and thereby control the functional and structural properties of the self-assembled materials in the bulk. In this vein, the ionic self-assembly strategy, driven by Coulomb forces, was recently introduced for the production of supramolecular materials[13]. Specifically, the addition of charged surfactants to oppositely charged poly- and oligoelectrolytic species yielded nanostructured bulk materials in a cooperative process. The modular assembly strategy allows to include organic and inorganic electrolytes of varying size, charge, molecular weight, and functionality into hybrid materials[14].

As for any charged surfactant-polyelectrolyte pair[15], the complexation of cationic surfactants and DNA occurs at a very low concentration (the critical aggregation concentration), which is usually a few orders of magnitude lower than the critical micelle concentration of the surfactant. This is attributed primarily to the strong electrostatic interaction between surfactant and the phosphate groups of DNA[15,16]. As shown in Figure 2a, the binding between surfactant and DNA follows a two-step process:

first, binding of a surfactant molecule to an isolated phosphate site on the DNA strand; second, a highly cooperative binding event which is due to the hydrophobic interactions between the alkyl chains of surfactant[17]. The phase diagrams of DNA-cationic surfactant systems show a strongly associative behavior[18]. The phase separation starts at very low concentration of DNA or surfactant and is enhanced as the alkyl chain length of the surfactant increases. As a consequence, different kinds of soft matter aggregates[19], like viscous liquids, gels, liquid crystalline phases in solution, and precipitates may form at the critical aggregation concentration or higher, depending on the DNA concentration and other properties of the system (salinity, hydrophobicity and backbone rigidity of DNA, tail length and head-group structure of the surfactant)[20].

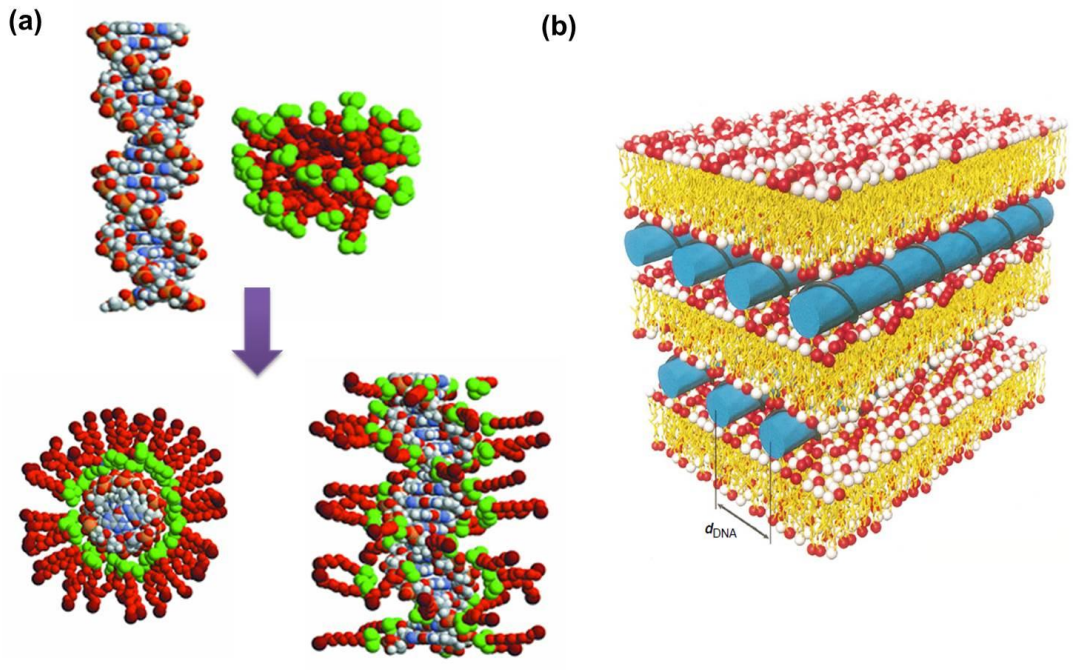

Figure 2. (a) The cooperative binding of DNA and surfactants by electrostatic interaction[20]. The interactions of surfactants (depicted as micelle) and the helical DNA, results in rod-like (right), or spherical structure (left). (b) Multilamellar structure of DNA-lipid complex in aqueous environment[30], where DNA is sandwiched between cationic lipid bilayers.

The interactions of cationic surfactants with DNA have been studied extensively. Changes in the hydrophobic moiety of the surfactants affect their complexation with DNA. The surfactant, cetyltrimethylammonium bromide (C16, CTAB) binds more readily to DNA than dodecyltrimethylammonium bromide (C12, DTAB)[18], leading to formation of a precipitate a lower concentrations for CTAB than for DTAB. The interactions of surfactants with DNA can also be tuned efficiently by controlling the head-group structure. The chemical structure of the head group markedly influences the interaction: for instance, negatively charged and non-ionic surfactants will not associate directly with DNA. It has also been observed that when structural modifications at the head group increase the hydrophobicity of the surfactant[21], such as the addition of an aromatic ring between the head group and the tail, the effect is

similar to that of an increase in the surfactant chain length. Modifications of the head group, like the introduction of a hydroxyl substituent, can lead to other more subtle changes in the interactions between DNA and a surfactant[22]. In addition, the effect of salt (counterions) on the phase behavior is complex, since the phase separation can be either stronger or weaker depending on experimental conditions. In general, oppositely charged macro-ions in solution attract each other, tending to form a bound complex. When separated, each macro-ion is surrounded by a diffuse layer of spatially confined counterions. Upon approach, the fixed macro-ion charges partially, and sometimes fully neutralize each other, releasing mobile counterions into the bulk solution, thereby increasing their translational entropy. This scenario suggests that macro-ion association in solution is, to a large extent, an entropically driven process[23]. Therefore, the actual contribution of the counterion entropy to the free energy of association depends on the detailed geometries and charge distributions of the separated and bound macro-ions[23-25].

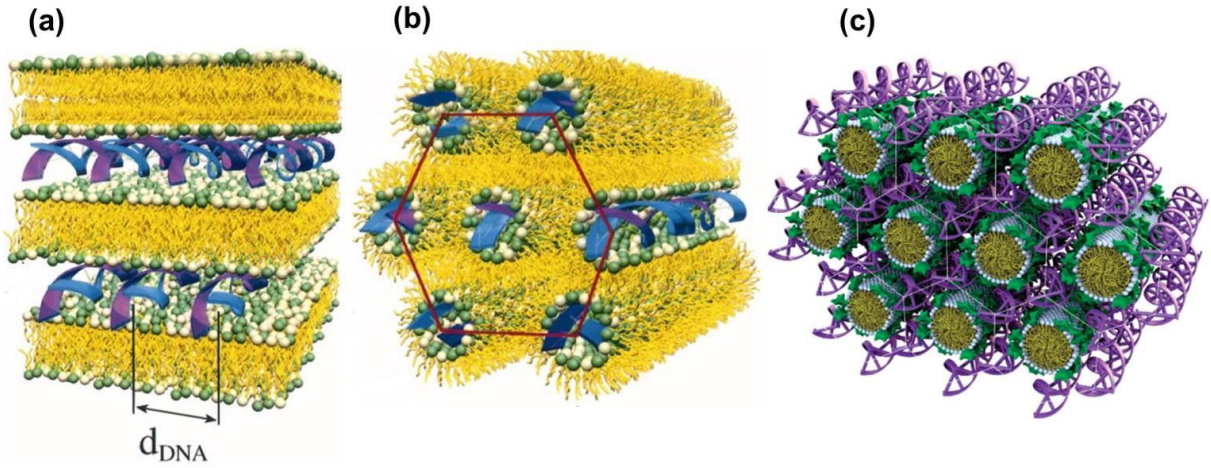

Figure 3. Schematic representation of the three representative structures of DNA-lipid complexes. (a) Structure of the lamellar phase (Lα) with alternating lipid bilayers and DNA monolayers[35]. (b) Structure of the inverted hexagonal phase (HII), comprised of DNA inserted within inverse lipid tubules, which are arranged on a hexagonal lattice[35]. (c) Structure of the hexagonal phase (HI), where the large dendritic cationic lipid headgroup leads to the formation of rod-like lipid micelles arranged on a hexagonal lattice with DNA inserted within the interstices with honeycomb symmetry[37].

The self-assembled structures of DNA-surfactant (lipid) complexes have been investigated very broadly. The earliest structure presented, known as the bead-on-string structure, consists of liposomes attached to the DNA strands[26,27]. Electron microscopy studies revealed a variety of structures including oligo lamellar structures[28] and tube-like structures, indicating lipid bilayer-covered DNA[29]. Detailed X-ray diffraction studies have been carried out on complexes of DNA and mixtures of cationic lipids[30-32] like DOTAP (dioleoyltrimethylammonium propane) or DMTAP (dimyristoyltrimethylammonium propane) and neutral lipids like DOPC (dioleoyl-phosphatidylcholine) or DOPE (dioleoyl-phosphatidylethanolamine). In

aqueous solution, the complexes exhibit optically birefringent liquid-crystalline phases originating from a multi-lamellar structure with alternating lipid bilayer and DNA monolayers (Figure 2b). There are no trans-bilayer positional correlations of the DNA strands when the bilayers are in the L_α fluid phase. The DNA chains confined between the bilayers form a 2D smectic phase[33]. At low temperatures, when the bilayers are in the L_β phase and hence more rigid[34], positional correlations develop across the bilayers, and a 2D rectangular lattice of DNA emerges. When the neutral lipids DOPC are replaced by the cosurfactant DOPE in the complex[35], the mesophase changes from a multi-lamellar structure (L_α) (Figure 3a) into an inverted hexagonal (H_{II}) (Figure 3b) liquid-crystalline phase, which is induced by DOPE negative curvature. In addition, a similar structural transition to the hexagonal (H_{II}) phase was achieved as a function of increasing ratio of hexanol (a membrane-soluble cosurfactant) to DOPC, which reduces the membrane bending rigidity. Recently, very short DNA with non-paring overhanging end groups were complexed with DOTAP and DOPC[36]. Nematic ordering arising from the interplay between shape anisotropy and DNA end-to-end interactions for short DNA with single-stranded oligo-thymine (T) overhangs were studied. The 11 base pair (bp) DNA rods with 5- and 10-T overhangs remain in anisotropic phase. When the overhangs are decreased to 2-T, a 2D columnar nematic phase with finite-length columns forms. These results offer new possibilities for the design of LC stacking of anisotropic rods in lipid-based complexes. In the Safinya group, a new type of highly charged (16+) multivalent cationic lipid with a dendritic headgroup (MVLBG2) was synthesized[37] for the study of DNA-lipid self-assembly. Complexes of DNA with mixtures of MVLBG2 and DOPC exhibit novel dual lattice structures. In the H_I phase, hexagonally arranged tubular lipid micelles are surrounded by DNA rods, forming a three-dimensional continuous substructure with honeycomb symmetry (Figure 3c). Furthermore, a series of multivalent lipids with dendritic headgroups from MVLG2 (4+), MVLG33 (8+), MVLBisG1 (8+), to MVLBisG2 (16+) were used to investigate the influence of the headgroup charge on the DNA-lipid structures[38]. It was found that lamellar phase, hexagonal phase (H_I), disordered hexagonal phase of DNA-lipid complexes coexisted with hexagonally ordered DNA bundles at different molar ratios of dendritic lipids and DOPC.

Apart from those complexes, there have been many structural studies involving nucleic acids combined with other alkylmethylammonium bromides, including dodecyltrimethylammonium bromide (DTAB), cetyltrimethylammonium bromide (CTAB), didodecyldimethylammonium bromide (DDAB), dioctadecyldimethylammonium bromide (DIAB), decyltrimethylammonium bromide (ETAB), and tetradecyltrimethylammonium bromide (TTAB). In 1992, Minsky and coworkers systematically investigated DNA packing within DNA-surfactant complexes by X-ray scattering[39]. A normal 2D hexagonal packing (H_I) of DNA-TTAB and DNA-CTAB was proposed, where DNA is interspersed between surfactant aggregates. Mel'nikov et al. confirmed the 2D hexagonal structure for DNA-CTAB complexes[40]

based on the first two diffraction peaks, which have a spacing ratio of $1/3^{1/2}$. A multi-lamellar structure was also determined by small-angle X-ray scattering (SAXS) in DNA-DIAB complexes[32,40]. On the basis of these experimentally observed structures, a number of theoretical calculations has been carried out to explain the interactions and structures in the DNA-surfactant complexes[41-45]. Furthermore, the addition of a co-surfactant, such as hexanol, to a CTAB solution is known to decrease the spontaneous curvature of the surfactant aggregates, transforming them from cylinders to bilayers[46]. Short-chain alcohols also substantially lower the bending rigidity of bilayers[47], indicating that co-surfactants can significantly influence the structure of these complexes. Reentrant phase transitions and the formation of two hexagonal structures H_I and H_{II}, driven by variations in the DNA and hexanol concentrations in CTAB-DNA-hexanol complexes were observed[48,49]. When mixing sodium 3-hydroxy-2-naphthoate (SHN) in the DNA-CTAB system, the DNA-CTAB-SHN complexes exhibit a hexagonal phase at low SHN concentration. However, at high SHN concentration, the complex transitions into a lamellar structure with intercalated DNA sublayers[50]. The Chu group used different cationic surfactants (CTAB or DDAB) and the zwitterionic lipid 1-palmitoyl-2-hydroxy-sn-glycero-3-phosphocholine (PHGPC) with double-stranded or single-stranded DNA to study the self-assembly properties[51]. The complexes of dsDNA and double-tail DDAB formed a bilayered lamellar structure, whereas the complexes between dsDNA and single-tail CTAB preferred a structure of 2D hexagonal closed-packed cylinders. The ssDNA-CTAB complex forms a cubic structure due to the different stiffness of dsDNA and ssDNA. The addition of PHGPC to the dsDNA-CTAB induced a structural transition from a 2D hexagonal to a multi-bilayered lamellar structure. In the DNA sublayers, the DNA-DNA spacing depends on the ratios of CTAB to PHGPC and CTAB to DNA, respectively. Recently, Lindman et al. investigated the self-assembly behavior of a ternary system, which included DNA-DTAB, water, and nonionic surfactant (dodecyl tetraethylene glycol, $C_{12}EO_4$; or dodecyl octaethylene glycol, $C_{12}EO_8$)[52]. The supramolecular assemblies evolve from a 2D hexagonal structure to a lamellar phase as one increases the concentration of nonionic surfactant. In the lamellar phases, short $C_{12}EO_4$ separates in the DTAB layer. Thereby, the DTAB headgroup interacts with the DNA while the $C_{12}EO_4$ headgroup protrudes into the aqueous reservoirs (Figure 4a). However, when $C_{12}EO_8$ with a longer non-ionic headgroup is incorporated into the ternary system, a fully swollen mesophase of $C_{12}EO_8$ alone coexists, wherein the ethyleneoxide moieties are present within the DNA-DTAB layers (Figure 4b). In addition to the development of the lamellar and hexagonal phases of DNA-surfactant complexes, cubic phases were also realized by combining short DNA and cationic surfactant with short alkyl tails, like ETAB[53] or DTAB[54]. Gemini surfactants such as bis(quaternary ammonium) surfactants have also been extensively studied in the context of DNA-surfactant superstructures[55-58]. Balgavý et al. found that multi-lamellar vesicles of dilauroylphosphatidylcholine (DLPC) with DNA in the presence of butane-1,4-diyl-bis(dodecyldimethylammonium bromide) ($C_{12}GS$) form a

condensed lamellar phase with ordered DNA monolayers intercalated between lipid bilayers[55]. Recently, Amenitsch et al. observed trans-bilayer correlation in the DNA ordering in lamellar structures by combining the cationic gemini surfactant and a neutral lipid[58]. A simple rectangular DNA packing and a centered rectangular columnar phase were obtained by controlling memory rigidity.

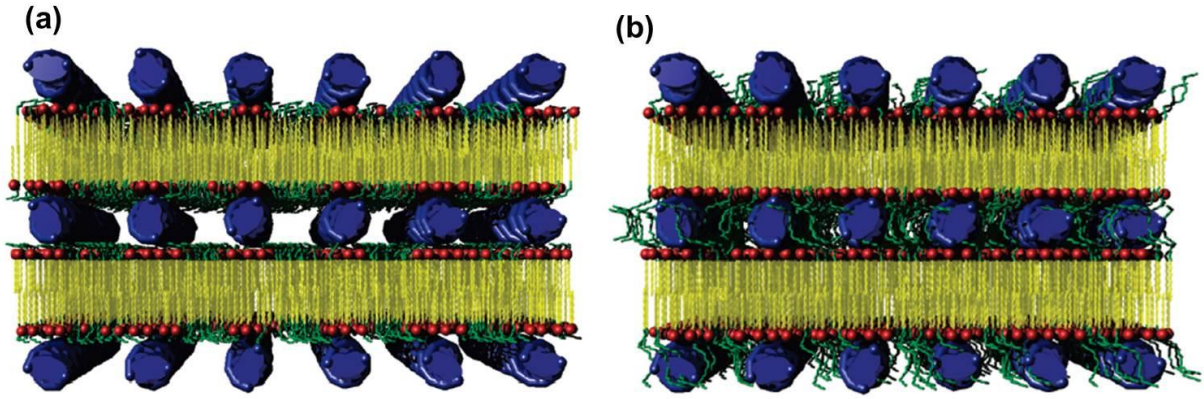

Figure 4. Schematic depictions of the intercalated lamellar structures of DNA-DTAB-$C_{12}EO_4$ complex (a) and DNA-DTAB-$C_{12}EO_8$ complex (b) in aqueous solution[52]. In a, $C_{12}EO_4$ units (green) are penetrated in the DNA sublayer. In b, all $C_{12}EO_8$ units are incorporated in the DNA-DTAB lamellar layers.

In addition to the study of self-assembly of DNA-surfactant complexes in solutions, their structures were investigated in aligned bulk films that were fabricated by casting the materials from organic solvents. Okahata and coworkers directed a great deal of effort toward developing an oriented DNA-surfactant film. The cationic surfactant N,N,N-trimethyl-N-(3,6,9,12-tetraoxadocosyl)ammonium bromide was mixed with DNA[59]. Poly-ion complex precipitates were gathered by centrifugation and freeze-dried. The DNA-surfactant complex obtained in this way was soluble only in organic solvents such as chloroform, benzene, and ethanol, but not in aqueous buffer solution. A free standing water-insoluble DNA film was prepared by drop-casting and was stretched to produce oriented DNA strands with their axes aligned along the stretching direction (Figure 5a). The as-cast film gave a circular reflection with 41 Å which corresponds to the diameter of a DNA-lipid complex. Once the film was stretched in the wet state, diffraction on the equator of 41 Å and on the meridian of 3.4 Å were observed. These findings clearly show that the DNA strands aligned parallel to the stretching direction of the film and that base pairs stacked perpendicular to the direction of DNA strands. When the stretched film was dried, only the diffraction peaks on the equator at 41 Å were observed, but no diffraction on the meridian for the base pairs. This suggests that the orientation of base pairs is not perpendicular to the stretching direction, although DNA strands are aligned in this direction. A similar procedure was later reported for aligned RNA-surfactant films[60]. In the same group, the Langmuir-Blodgett (LB) method was introduced to align a dye-intercalated DNA-surfactant complex[61,62]. DNA strands were uniformly oriented by the vertical dipping

method. However, when the DNA-surfactant monolayers were deposited by a horizontal lifting method, DNA strands were randomly oriented in the film. Recently, Wu and coworkers reported the self-organization of DNA into honeycomb structures on solid substrates by a simple solution casting of DNA-ditetradecyldimethylammonium (DTDA) complex at high relative humidity (Figure 5b)[63]. The structure results from self-assembly of the complex due to condensation of water droplets in a particular pattern at the interface of the film and surrounding air. The morphology of the microporous structures can be adjusted by slightly changing the concentration of the complex solution. The choice of solvent for film casting has a significant effect on the regularity of the honeycomb structure due to differences in evaporation rates. These self-organizing honeycomb structures might be a promising feature for applications in biosensors, optical, and optoelectronic devices[63-66].

Besides investigating pristine films composed of DNA-surfactant complexes, their response to humidity was studied. The Tirrell group found that a film composed of DNA and the cationic surfactant dimethyldidodecylammonium bromide (DDAB) exhibits structural switching between double-stranded DNA-DDAB in a solvated state and single-stranded DNA-DDAB in a dry state (Figure 5c)[67]. It is known that the double-stranded structure of DNA is stabilized in aqueous media primarily by a hydrophobic core consisting of π-stacked bases stabilized by hydrogen bonds and repulsion of the charged phosphate groups in the DNA backbone[68]. However, when the aqueous media is exchanged for a less polar solvent such as isopropanol, the base interactions weaken, leading to a less stable double helix. A similar process is responsible for the separation of the double-stranded DNA into two single strands in the presence of DDAB in the dry film, as discussed above. The cationic surfactant DDAB is bound to the DNA through electrostatic interactions and is thus forced to undergo a structural transition such that the tails of the surfactant interact with the exposed hydrophobic bases of the DNA. This means that the surfactant bilayer with interdigitated alkyl chains is disrupted, and a monolayer of surfactant is formed (Figure 5c). The hydrophilic head group of the surfactant monolayer interacts with the phosphate backbone of the DNA while the surfactant alkyl chains interact with the bases of the single stranded DNA. Once the DNA-DDAB film is hydrated, the two complementary DNA strands hybridize quickly and structure reorganization is observed. The threshold relative humidity level to induce structural switching of the film is around 60%[69]. Furthermore, temperature has an effect on the structure of DNA within the wet film. The measured melting temperature of DNA complexed in the film is slightly lower and spans a wider temperature range than that of pristine DNA insolution, presumably due to the presence of DDAB. Therefore, the self-assembled structure of DNA-DDAB is responsive to various environmental conditions like heat and humidity.

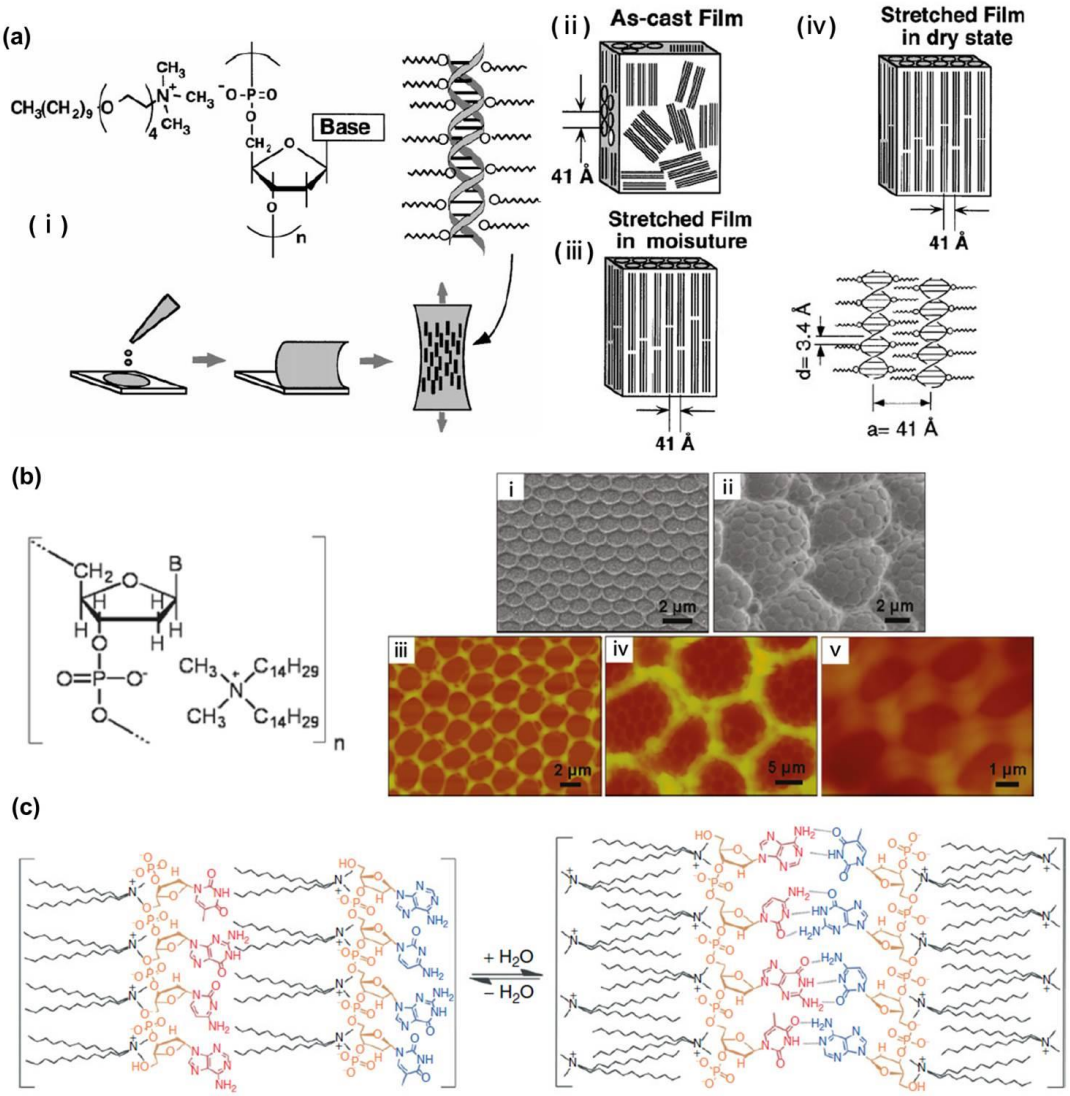

Figure 5. Self-assembly of DNA-surfactant complexes in bulk films. (a) Schematic diagram of stretchable DNA-surfactant film with aligned DNA helices[59,60]. The film was cast on a Teflon plate, and the solvent was evaporated slowly under saturated vapor at room temperature (i). The as-cast film (ii), the stretched film of the DNA-lipid complex in water moisture and its DNA packing (iii), and the stretched DNA-lipid film in dry state (iv) are shown. The DNA strands in as-cast films were found to align with respect to each other in both wet and dry states as the film was stretched. (b) Honeycomb-patterned DNA-surfactant films cast on a glass substrate under a moist airflow[63]. Characterization of the microstructure via SEM (i,ii) and AFM (iii-v). (c) Schematic structure of DNA-DDAB film indicating the structural change that takes place upon wetting and drying the film[67].

2. Applications of DNA-surfactant complexes

At present, self-assembled DNA-surfactant (lipid) complexes are mainly being investigated in two forms: the solvent-free phase (bulk film materials) and the solution phase (lyotropic liquid crystals). Both are good examples of materials with well-defined structures, high structural stability, and easy processability. Therefore, diverse potential applications ranging from optoelectronics to biomedicine and therapeutics have been investigated.

2.1 Bulk materials and applications based on DNA-surfactant complexes

2.2.1 Electrical conductivity of bulk DNA-surfactant complex films

There is considerable interest in using DNA as a building block for molecular electronics and computation[70]. However, the debate over whether DNA behaves primarily as a conductor, semiconductor, or insulator is still open to debate today[71-73]. DNA is also widely recognized as a good model material to study charge transport mechanisms in 1D polymers, particularly because of its complementary strand recognition and self-assembly properties[74]. Okahata et al. have investigated the anisotropic conductivity of DNA-surfactant films that were mechanically stretched to align the DNA strands[59-62]. When a 2000bp DNA film was put on the comb-shaped electrode with the DNA helices aligned perpendicular to the Au electrodes, a large ohmic current was observed with a conductivity of 5.6×10^{-5} S cm^{-1} (Figure 6a)[75,76]. On the contrary, when the film was placed with DNA strands aligned parallel to the two electrodes, electric conductivity was only 10^{-9} S cm^{-1}. Unstretched DNA films (dsDNA strands orient randomly in the film plane) exhibited a conductivity of 10^{-7}-10^{-8} S cm^{-1}. From these measurements it was concluded that DNA films conduct current more efficiently along the DNA axis than in a perpendicular orientation.

When longer DNA (30,000bp, ca. 10 mm length) was used, the stretched DNA film on the comb-type electrodes with the DNA helix axis aligned perpendicularly to the electrodes gave large ohmic currents (0–0.7 mA) that increased linearly with an increase of the applied voltage in the range of ± 0.5 V. The conductivity was calculated to be 5×10^{-3} S cm^{-1} (Figure 6b)[77]. When the aligned DNA film prepared from short DNA molecules (500bp, ca. 0.2 mm length) was put perpendicularly to the electrodes, very small conductivities (10^{-6} S cm^{-1}) were measured. Additionally, temperature-dependent conductance experiments of the DNA-surfactant films were performed. When the film was heated above 60 °C, the conductivity decreased drastically to 10^{-6} S cm^{-1}. This temperature-dependent behavior was found to be reversible. The thermal conductivity characteristics can be explained by reversible changes in the intramolecular stacking of nucleobases within the double stranded DNA of the aligned films. Similar anisotropic conductivity was observed for DNA films prepared by the LB method, in which 200 DNA-surfactant monolayers were deposited on the same comb-shaped electrode by vertical dipping[78]. The electric current along the DNA strands was ca. 300 times larger than that in the cast-stretched film. A possible reason is an improved contact between electrodes and films. DNA strands were directly deposited on Au electrodes when using the LB method, while the DNA-surfactant cast film was mechanically pressed on the surface of electrodes.

Furthermore, photo-induced electron transfer mediated by intercalated dye molecules within the double helix of aligned DNA films was investigated[75,79]. Acridine orange was intercalated between base-pairs and aligned perpendicularly to DNA strands in the

film. As shown in Figure 6c, a large ohmic photocurrent was observed when DNA strands were aligned perpendicular to the two electrodes. Photocurrents increased linearly with increasing voltage, indicating that photoelectrons pass through stacked base-pairs of the aligned DNA strands in the film.

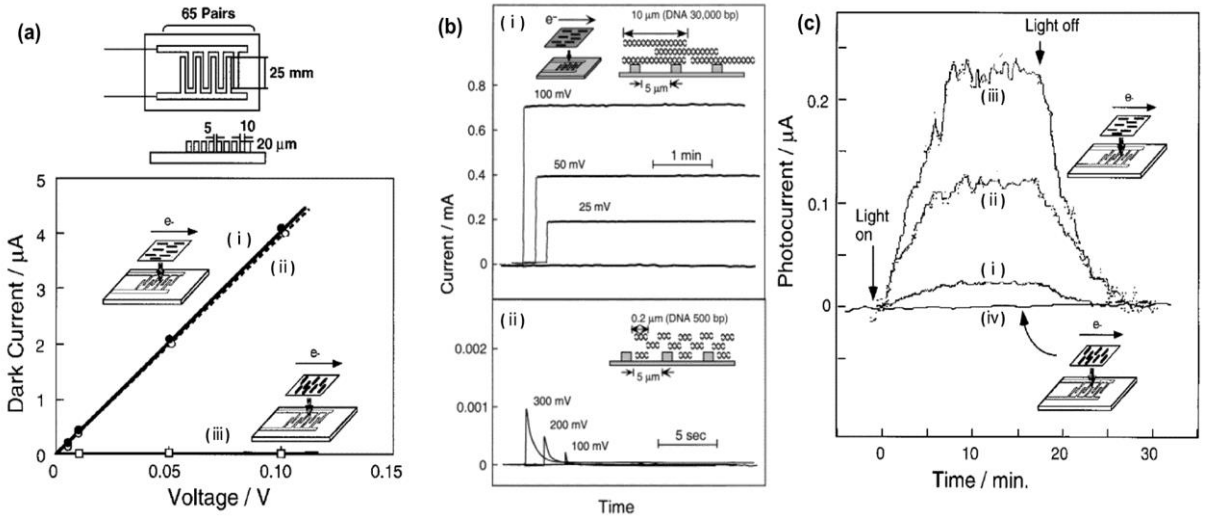

Figure 6. Anisotropic conductivities of oriented DNA-surfactant films. (a) Dark currents for aligned 2000bp DNA-surfactant films on comb-type electrodes at 25 °C[75]. DNA double helices in the film were orientated perpendicular to the two electrodes and were measured in ambient conditions (i), the same film measured in vacuum (ii), and DNA strands in the film were placed parallel to the electrodes both in a vacuum and in ambient conditions (iii). (b) Direct currents of aligned DNA films on a comb-type electrode at 25 °C in a dry box[77]. (i) The film prepared from long DNA (10 mm, 30,000bp) and (ii) from short DNA (0.2 mm, 500bp). In both films the DNA was aligned perpendicularly to the two electrodes. (c) Photoinduced currents for aligned DNA films in which acridine orange intercalates between base-pairs[75]. (i) At 0.01 V, (ii) 0.05 V, and (iii) 0.1 V applied voltage on comb electrodes with DNA strands aligned perpendicular to the two electrodes. (iv) DNA strands in the film oriented parallel to the two electrodes at 0.1 V. Pulsed light above 380 nm was irradiated from a 150 W xenon lamp at 25 °C.

2.1.2 Optical properties of bulk DNA-surfactant complex films

Besides characterizing the electrical properties of DNA-surfactant films, their optical and optoelectronic properties were investigated. The optical properties of DNA-surfactant films are mainly dependent on parameters like the type of surfactant, the length of the DNA, and the amount of doped dyes. DNA films generated from quaternary ammonium-based surfactants, particularly cetyltrimethyl ammonium chloride (CTMA), have been investigated extensively due to their high transmission from the near infrared to the visible region[80,81]. The refractive index of these thin films vary broadly with wavelength but remain constant in the range of 1000–1250 nm (slightly >1.526), which means that they can be considered a low-loss optical material[82]. The films are thermostable up to temperatures of 200 °C while retaining electrical resistance of 10-105 GΩ. These results suggest that DNA-CTMA is a potential candidate in optical waveguides and for optical cladding in nonlinear electro-optic modulators. Furthermore, Ogata and coworkers prepared a series of dye doped DNA-

surfactant films (Figure 7a)[83], which were thermo-extensive over a temperature range of 100 to 148 °C. These films exhibit a high transparency from 300 to about 1000 nm, with good processability for multilayer integration into large-area optoelectronic devices.

It is known that the fluorescence efficiency (or quantum yield) diminishes when one increases the concentration of dyes in solution. This effect is called concentration quenching. Preventing the formation of dye aggregates is one of the most important factors for minimizing the concentration quenching effect. DNA-surfactant complexes have been utilized as a matrix to separate the dye molecules for fluorescence enhancement[81,84,85]. The fluorescent dye 4-[4-(dimethylamino)styryl]-1-dodecyl pyridinium bromide (DMASDPB) was doped into the DNA-CTMA complex[81]. The film containing the lowest concentration of dye exhibited the greatest fluorescence intensity. Efficient compartmentalization of the dye with negligible electronic interactions between them in the DNA-CTMA matrix is a likely reason for this observation. Furthermore, europium (Eu) complexes were blended into the DNA-CTMA. The films exhibited strong amplification of fluorescence at 614 nm when irradiated with UV light. The Eu fluorescence amplification in DNA-CTMA film was 100 times higher than in poly(methyl methacrylate) (PMMA) films. In addition, relaxation times in DNA-CTMA film were twice as long as those for Eu in PMMA films. Choi and coworkers investigated the absorption and photoluminescence (PL) behaviors of DNA-CTMA and PMMA thin films doped with (E)-2-(2-(4-(diethylamino)styryl)-4Hpyran-4-ylidene)malononitrile (DCM) [84]. It was found that the PL intensity of the DCM-doped DNA increases up to a dopant concentration of 10 wt%, whereas in PMMA, the PL intensity starts to diminish at only 3 wt% of the dopant. These results indicated that DNA accommodates and separates the DCM molecules more efficiently than PMMA. Moreover, the conjugated polymer poly(fluorenevinylene) containng alkyl chains with terminal quaternary ammonium groups (Q) was complexed with DNA in order to prevent aggregation of the π-conjugated system[85]. As a consequence, the fluorescence life-time of Q was greatly increased from picoseconds to nanoseconds, indicating that the desired task was achieved successfully. DNA-surfactant complexes can also be used as an effective scaffold for fluorescence resonance energy transfer (FRET)[86,87]. Choi et al. prepared a DNA complex bearing two different fluorophores (carbazole (Cz) and pyrenylvinylenephenylene (PVP)) in the surfactant side chains. It was found that an inclusion of only 2.2 wt% of PVP in the ternary complex completely quenched the PL emissions of the Cz and that only emission of PVP was observed[87]. This result indicates efficient energy transfer from the Cz unit (donor) to PVP (acceptor) via FRET. More interestingly, when 2-{2-[2-(4-diethylamino-phenyl)-vinyl]-6-methyl-pyran-4-ylidene}-malononitrile (DCM) was doped into the Cz-DNA-PVP complexes, tunable colors from blue, to orange, to red can be realized due to cascade energy transfer from the Cz moieties to the DCM molecules through the PVP as transmitter unit (Figure 7b).

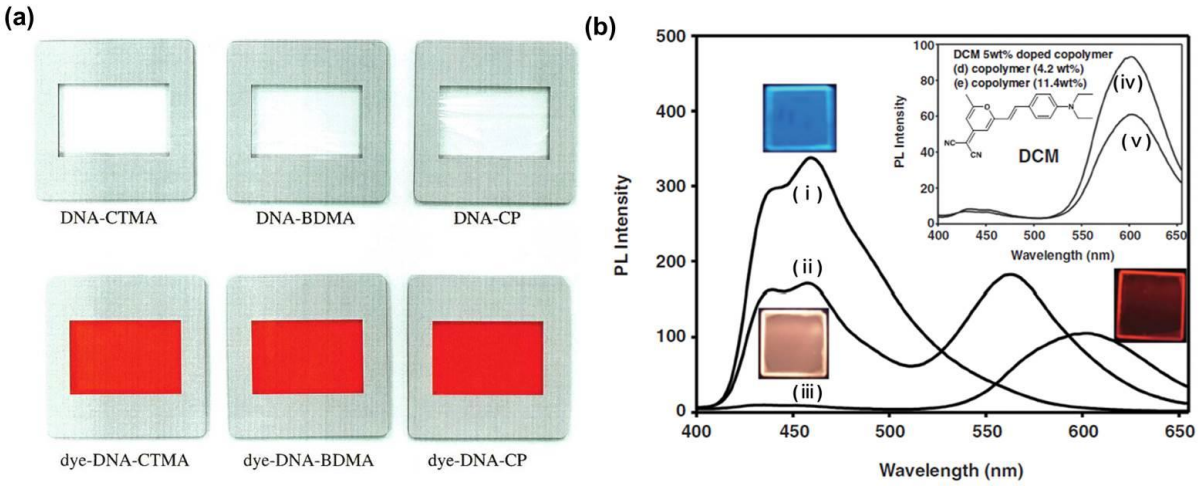

Figure 7. Optical properties of DNA-surfactant bulk films. (a) Photographs of a series of DNA-surfactant complex films and functional-dye-doped DNA-surfactant complex films[83]. (b) Photoluminescence spectra of the ternary Cz-DNA-PVP complex film bearing 11.4 wt % PVP and its mixtures with DCM dye[87]. (i) Cz-DNA-PVP (PVP, 11.4 wt %), (ii) Cz-DNA-PVP (PVP, 11.4 wt %) doped with 0.3 wt % DCM, (iii) Cz-DNA-PVP (PVP, 11.4 wt %) doped with 5.0 wt % DCM, (iv) Cz-DNA-PVP (PVP, 4.2 wt %) doped with 5.0 wt % DCM, and (v) Cz-DNA-PVP (PVP , 11.4 wt %) doped with 5.0 wt % DCM. Tunable colors from blue, orange to red were achieved, indicating the cascade energy transfer from the Cz moieties to the DCM molecules through the PVP units. CTMA: Cetyltrimethylammonium, CP: cetylpyridinium, BDMA: benzyldimethylcetylammonium, DMASDPB: 4-[4-(dimethylamino)styryl]-1-dodecyl pyridinium bromide, Cz: carbazole, PVP: pyrenylvinylenephenylene, DCM: 2-{2-[2-(4-diethylamino-phenyl)-vinyl]-6-methyl-pyran-4-ylidene}-malononitrile.

In addition, the lasing capacities of dye-doped DNA-surfactant complexes have been studied. Ogata et al. presented an investigation in which the DNA-CTMA/Rhodamine 6G film was pumped by a nanosecond 532 nm laser beam[88]. In the experiments, one-photon excited amplified spontaneous emission (ASE) was observed for the first time. The Grote group created distributed feedback (DFB) lasing structures that consist of a grating etched into an SiO2-Si wafer substrate with a DNA-CTMA/sulforhodamine 640 (SRh) dye layer[89]. They found that both the output energy and the line-width of the emission peaks of the DFB structure are considerably more responsive to changes in the pumping energy than the planar structure. Furthermore, DNA-CTMA-based devices exhibited considerably better lasing characteristics than PMMA-based ones. Lopez and coworkers studied the optical gains of lasing in DNA-CTMA/DCM composites[90]. The optimal amplification density was observed at ~2.5 wt% of DCM. Quenching occurred at higher concentrations. ASE and lasing in a two layer system composed of a DNA-CTMA/Rhodamine 6G layer superimposed on a periodic SRG (surface relief grating) structure were investigated and compared[91]. The signal intensity of the emitted light increased considerably faster than the ASE. These studies indicate that DNA intercalation and minor groove binding of fluorescent dyes appear to be very efficient supramolecular structures for lasing.

Due to the versatility and easy processability of DNA-surfactant complexes, their nonlinear optical properties have been investigated for use in optical communication systems. Grote et al. succeeded in preparing a DNA-CTMA thin film containing DR1 chromophore on an indium tin oxide-coated glass. An electro-optic coefficient of 2.13 pm V^{-1} at λ = 633 nm, which is comparable to the value for a PMMA film with the same concentration of DR1, was achieved[81]. In nonlinear optics, second- and third-harmonics were generated in ternary DNA-surfactant complexes[92]. It was found that the second-harmonic generation signals were very weak, due to the absence of any orientation of the dye molecules due to DNA double-helical structure. The third-order nonlinear susceptibility values are greater than in a cured epoxy resin matrix, which can be attributed to the better dispersion of the dye molecules in the DNA-surfactant matrices[93]. Therefore, the intercalation of dye molecules into DNA-surfactant must promote charge migration and nonlinear optical activities. On the other hand, nonlinear optics can be utilized to study the electronic, vibrational, electrostatic, and chiral characteristics of DNA at its surfaces, interfaces, and in its native state[94]. An understanding of these properties is crucial for tracking DNA recognition events in real time and for learning about the specific molecular kinetics.

2.1.3 Optoelectronics with bulk DNA-surfactant complex films

Organic light-emitting diodes (OLEDs) containing DNA-surfactant complexes have been fabricated, and led to significant enhancement of luminance and device efficiency over conventional device structures[95-97]. DNA-CTMA complex shows a large band gap (4.7 eV) and a high dielectric constant, which may function as an electron blocking layer (EBL) in OLEDs[98]. The purpose of blocking electron flow is to enhance the probability of radiative electron-hole recombination in the emitting layer of the device and to reduce the leakage of electrons to the anode region. This can lead to increased device luminous efficiency and luminance. Significantly enhanced electroluminescence (EL) is obtained by fabricating green- (Alq_3, tris-8-hydroxyquinoline aluminum) and blue-emitting (NPD,N,N-bisnaphthalene-1-yl)-N,N-bisphenylbenzidine) OLEDs with a DNA-CTMA complex such as EBL (Figure 8a). The luminous performances of the blue and green OLEDs with and without the DNA-CTMA electron-blocking layer are compared in Figure 8b. The energy level diagram in Figure 8b intuitively confirms that DNA-CTMA acts as an EBL in the device. Maximum luminous efficiencies for the green and blue OLEDs are 8.2 and 0.8 cd A^{-1}, respectively. The OLED containing DNA-CTMA has higher device efficiency and luminance compared to traditional OLEDs lacking the DNA-surfactant layer: it is as much as 10 times more efficient and 30 times brighter. Similarly impressive results have been reported in quantum dot-LEDs (QD-LEDs)[99], where the DNA-CTMA complex acts as a combined hole transporting and electron-blocking layer (HTL/EBL). A high external quantum efficiency (~ 4%), high brightness (~ 6580 cd/m^2), low turn-on voltage (~ 2.6 V), and significantly improved color purity were achieved for QD-LEDs. The material combination of DNA with Cz modified

CTMA was utilized as a host for phosphorescent material ($Ir(Cz\text{-}ppy)_3$) in OLEDs[100]. Efficient energy transfer from the DNA-Cz host to the metal-to-ligand charge transfer (MLCT) band of $Ir(Cz\text{-}ppy)_3$ was found. When the electron transport compound PBD (5,4-tert-butylphenyl-1,3,4-oxadiazole) was co-doped into the phosphorescent light-emitting layer, the OLED performance was significantly improved. The maximum luminance was raised from 244 cd m^{-2} to 1135 cd m^{-2}, and the maximum luminous efficiencies were up to 3.41 cd A^{-1}.

Even a more sophisticated OLED device containing DNA was produced. This color-tunable OLED composed of a DNA/polyaniline/$Ru(bpy)_3^{2+}$ complex was reported by Kobayashi and coworkers[101]. In the device, red-emitting DNA/polyaniline/$Ru(bpy)_3^{2+}$ was the hole transport layer, and green-emitting Alq_3 was chosen as the electron transport layer (for structure of the device see insert in Figure 8c). As the electric field is increased, the colors of the light emitted by the OLED device changed from green (5 V) to yellow (14 V), orange (16 V), and red (18 V) (Figure 8c). The corresponding EL spectra and the International Commission on Illumination emission coordinates at various voltages are shown in Figure 8d. In depth experiments indicated that the shift in the carrier recombination region increases with the applied voltage and is responsible for the color tuning. At low voltage, the hole mobility of the DNA/polyaniline/$Ru(bpy)_3^{2+}$ complex layer was superior to the electron mobility of the Alq_3 layer. Thus, recombination occurred mainly in the Alq_3 layer. As the voltage was increased, the electron mobility of the Alq_3 layer increased rapidly with the electric field, and the electrons could move through the interface and recombine with the holes in the DNA complex layer. This resulted in a continuous shift in the recombination region from the Alq_3 layer to the DNA/polyaniline/$Ru(bpy)_3^{2+}$ complex layer. Therefore, multicolor emission could be realized in this OLED structure. Furthermore, Sotzing et al. reported the electrospun DNA-CTMA nanofiber doped with the dye coumarin 102 (donor) and 4-(4-dimethylaminostyryl)-1-dodecylpyridinium bromide (acceptor)[102]. Efficient energy transfer between both componets was observed, even at low acceptor-loading levels. The emission wavelength was controlled by varying the donor-to-acceptor ratio, which shifts the fluorescence from blue to orange through pure white. Moreover, solid-state LEDs were coated with white-light-emitting DNA-CTMA-based nanofibers. By changing the total dye loading from 1.33 to 10% in the DNA-CTMA matrix, the LED color temperature was tuned from cool white to warm white.

In a very simple view, the photovoltaic process can be regarded as the reverse scenario of that in an OLED, which was discussed above. Therefore, it is expected that DNA-surfactant complex-containing photovoltaic devices might have favorable properties. It has been reported that double-stranded calf-thymus DNA and the nucleobase adenine were employed as hole transporting materials in a dye sensitized nanocrystalline titanium dioxide solar cell[103]. The short circuit currents were found to be two and four times larger for calf-thymus DNA and adenine cells, respectively, compared to the non-

DNA containing counterparts. The stability of adenine-based devices was found to be higher than those made of calf-thymus DNA because double strands might break under the prolonged exposure of light. Jin and coworkers reported a solar cell in which DNA-CTMA complex was employed as a hole injection layer to replace the commonly used PEDOT:PSS[104]. The solar cells exhibited rectifying behavior in the dark and solar energy conversion occurred under illumination by a 300-W projector lamp. However, further characterization of such devices is necessary to confirm the utility of DNA-CTMA as the hole injection layer in organic solar cells.

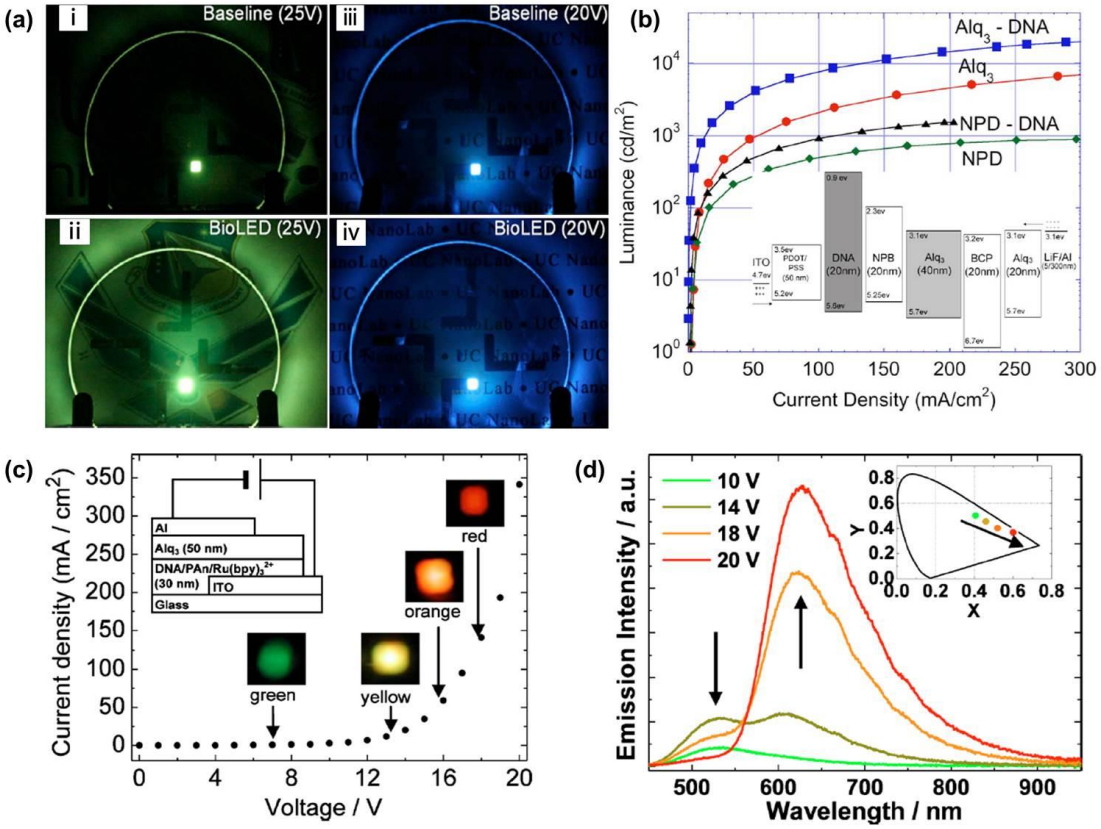

Figure 8. OLED studies involving DNA-surfactant complexes. (a) DNA-CTMA complex working as electron blocking layer (EBL) in OLEDs increases device luminous efficiency and luminance as evidenced by photographs of EL emission[98]. (i)Green Alq3 baseline OLED at 25V (707 mA cm^{-2}) - 590 cd m^{-2}, 0.35 cd A^{-1}. (ii)Green Alq_3 OLED with DNA-CTMA EBL at 25 V (308 mA cm^{-2}) - 21, 100 cd m^{-2}, 6.56 cd A^{-1}. (iii)Blue NPD baseline OLED at 20 V (460 mA cm^{-2}) - 700 cd m^{-2}, 0.14 cd A^{-1}. (iv) Blue NPB OLED with DNA-CTMA EBL at 20 V (200 mA cm^{-2}) - 1500 cd m^{-2}, 0.76 cd A^{-1}. (b) Luminance vs current density plot in green Alq_3 and blue NPD EL devices with and without DNA-CTMA EBL. The inset shows an energy level diagram in a green-emitting OLED structure with DNA-CTMA EBL. (c) Current density vs voltage relationship and photographs of an OLED prepared from DNA/polyaniline/$Ru(bpy)_3^{2+}$ complex as the hole transport layer and Alq_3 as the electron transport layer, with inset showing the OLED structure[101]. The luminescence color changed dramatically with increasing voltage above the bias voltage of 5 V. (d) The corresponding EL spectra and the International Commission on Illumination emission coordinates at various voltages.

DNA-surfactant complexes are attractive for incorporation into optoelectronic devices including OLEDs and solar cells due to the material properties of the

complexes[95,96,105], such as good temperature stability, a wide HOMO/LUMO band-gap, low optical absorption, low optical scattering losses, and mechanical robustness. However, DNA-surfactant complexes are polyelectrolytes, which respond to external electric fields. The DNA chains are likely to undergo conformational change and the DNA helical structures might be destroyed. These processes may even lead to their migration in the devices. Diverse problems associated with the long-term stability of the devices still need to be resolved. Therefore, research efforts should be directed to evaluate and understand material properties of various DNA-surfactant complexes in devices, which might ultimately lead to improved performance.

2.1.4 Drug and gene delivery with bulk DNA-surfactant complex films

Besides for bioelectronic applications, DNA-surfactant complexes were employed in the fields of drug and gene delivery. Bulk DNA-surfactant complexes may be fabricated for achieving long term in vivo stability of the DNA component and subsequently may recover biological activity once wetted. These materials contain a high local concentration of the therapeutic nucleic acid agent. For these reasons, the study of bulk DNA-surfactant materials has become a new and exciting field for drug and gene delivery. Tirrell and coworkers have recently simulated a drug release system by employing an ethidium bromide-labeled DNA-DDAB film[69]. The film disassembled in a layer-by-layer fashion and the release of ethidium bromide occurred when exposed to a buffer solution (such as PBS) due to electrostatic screening of the charges by salts. Thus, it is reasonable to expect that the film will disassemble easily in vivo and may act as a drug delivery vehicle or DNA depot. Similar to ethidium bromide, anticancer drug molecules like daunorubicin and doxorubicin also intercalate into DNA and thus inhibit the enzyme topoisomerase II, which prevents the DNA from duplication in fast-replicating cells[106]. These drugs are potentially useful in DNA-surfactant films as they could be incorporated into the complex and then locally elute after implantation as the film degrades either through nuclease action or ion replacement. Such drug delivery system was developed in which the DNA-surfactant complex was blended with poly(lactide-co-glycolide) and the drug daunorubicin[107]. The complex was obtained by casting a film from DMSO/$CHCl_3$ solution, which was later incubated in an aqueous solution of daunorubicin. The drug loading was controlled by the immersion time. The pharmaceutically active payload was released from the films after immersion in PBS solution and the release rate was dependent on the chemical structure of the surfactants. These results clearly indicated that a film of the three components DNA, surfactant, and PLGA is a promising scaffold for anticancer drug delivery. In addition, cationic polymers have been used to complex DNA for drug and gene delivery applications, including local gene delivery to cells and vascular delivery from stent coatings[108-110]. Venkatraman et al. reported the release and transfection efficiencies of plasmid DNA-lipofectamine complex films[111a]. The release was slow, but could be accelerated using additives. The results also demonstrated that bioactivity of the

released plasmid DNA was higher than naked DNA. The layer-by-layer (LBL) deposition of polyelectrolytes is a convenient and well-established method for the incorporation of natural and synthetic polyelectrolytes into thin nanostructured assemblies[111b]. This technique can also be used for the generation of thin DNA-polymer films[112]. Multilayered polyelectrolyte films fabricated from plasmid DNA and a polycation were utilized to achieve localized transfection of cells without the aid of a secondary transfection agent[108]. A mechanism for the immobilization of DNA at the cell/surface interface was proposed. The cationic polymer in these materials plays an important role for the internalization and expression of the plasmid. Such materials represent an attractive framework for the local or non-invasive delivery of DNA from the surfaces of implants or biomedical devices. Other cationic polymers such as poly(lysine), poly(histidine), polyethyleneimine, polylysine, and poly(amidoamine) have been employed to complex with DNA for gene delivery applications[113-115]. Among them, improved transfection efficiency and sustained delivery have been realized[116-119]. However, the major barriers for cell transfection including endosomal escape and penetration into the nucleus still need to be overcome by developing new materials.

2.2 Soft materials and applications based on DNA-surfactant (lipid) complexes

2.2.1 Lyotropic liquid crystals and gene therapy based on DNA-surfactant complexes

As discussed in **1.2**, DNA-surfactant complexes spontaneously assemble into distinct lyotropic liquid crystalline phases in a hydrated environment. Several nanoscale structures of DNA-surfactant complexes probed with synchrotron X-ray diffraction have been discovered by Safinya and coworkers. As shown in Figure 3, the prevalent lamellar phases are given by DNA sandwiched between cationic membranes (L_α), the inverted hexagonal phase with DNA encapsulated within inverse lipid tubes (H_{II}), and the more recently discovered H_I phase with hexagonally arranged rod-like micelles surrounded by DNA chains, which form a continuous substructure with honeycomb symmetry. These lyotropic liquid crystals are being studied primarily because of their applications in gene delivery and gene silencing, and their implications for ongoing clinical gene therapy efforts worldwide. As synthetic non-viral delivery systems, DNA-surfactant complexes were first investigated for gene transfection by Felgner et al[27]. It was found that transfection efficiencies (TEs) are significantly higher than for other chemical delivery systems (e.g. anionic liposomes with encapsulated DNA, calcium phosphate precipitation, and polycationic reagents such as DEAE-dextran or polylysine). In the last twenty years, Safinya et al. have directed a great deal of effort toward developing new DNA-surfactant complexes for gene therapy studies, in particular to understand the correlation between transfection mechanism and internal DNA-surfactant structural characteristics for improving the TE[120-123]. In a series of comprehensive studies, the TE was indeed found to be structure dependent. In particular, it was found that for

lamellar DNA-surfactant complexes, the membrane charge density (σ_M) is a universal parameter which is predictive of the TE[124,125]. For this study, a series of multivalent surfactants (MVLs) were synthesized, which allowed for systematic variation of the charge (between 2+ and 5+ electron charge). The complexation between DNA, cationic MVLs, and neutral DOPC led to the formation of lamellar structures (L_α). In the mesophases, the membrane charge density was varied by changing the amount of neutral DOPC while keeping the amount of DNA and cationic MVLs per sample constant.

As shown in Figure 9a, the universal TE curve of lamellar complexes exhibits three well-defined regimes. Regime I (dark gray), corresponding to low σ_M, features an exponential increase in efficiency over three orders of magnitude. Regime III (light gray), corresponding to high σ_M, is characterized by a decrease in efficiency with increasing σ_M, suggesting that there is an obstacle of electrostatic nature to successful DNA delivery by lamellar DNA-surfactant complexes. The competition of the two effects that give rise to regimes I and III leads to the existence of the intermediate regime II (white) as the region of optimal charge density, corresponding to the highest TE. Therefore, this identifies σ_M as a universal parameter for transfection by lamellar DNA-surfactant complexes (i.e. a predictor of TE)[124].

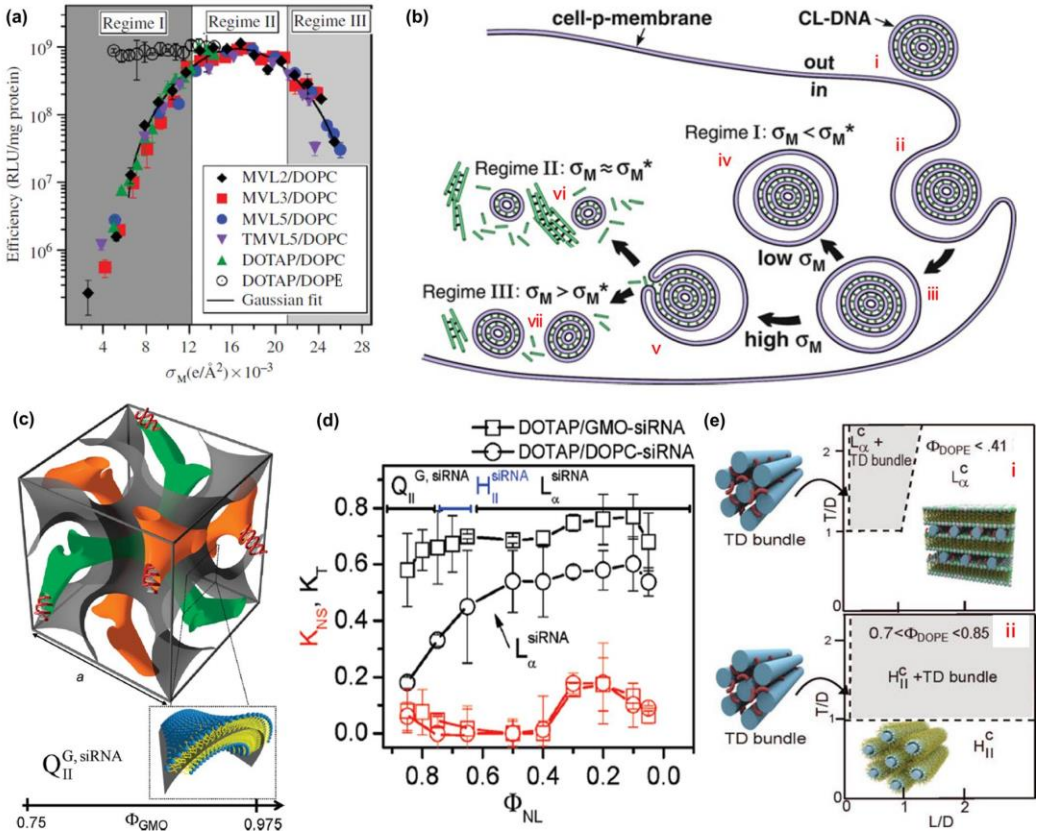

Figure 9. Gene therapy applications based on lyotropic liquid crystals of DNA-surfactant complexes. (a) Transfection efficiency (TE) as a function of the membrane charge density σ_M for lamellar DNA-surfactant complexes prepared with MVL2, MVL3, MVL5, TMVL5, DOTAP, and neutral DOPC[124]. The TE of the lamellar complexes may be described by a universal, bell-shaped curve as a function of σ_M. TE data for hexagonal DNA-DOTAP-DOPE complex (open circles) deviate from the universal curve, indicative of a distinctly different transfection mechanism for the inverted hexagonal mesophase. (b) Model of cellular uptake of the lamellar DNA-surfactant liquid crystals[124]. Complexes adhere to cells due to electrostatics (i) and enter through endocytosis (ii, iii). Low σ_M complexes remain trapped in the endosome (iv). High σ_M complexes escape the endosome (v) where released DNA may form aggregates with cationic biomolecules (vi) or the complexes are less able to dissociate and less DNA is available (vii). (c) Double gyroid lipid cubic phase of siRNA-DOTAP-GMO complex containing two (green and orange) water channels[133]. A lipid bilayer surface separates the two intertwined but independent water channels. For clarity, the bilayer is represented by a surface (grey) corresponding to a thin layer in the center of the membrane as indicated in the enlarged inset. (d) Total specific gene knockdown (KT, black lines and symbols) and nonspecific gene knockdown (KNS, red lines and symbols) for siRNA-DOTAP-GMO complexes (squares) and siRNA-DOTAP-DOPC complexes (circles) as a function of mole fraction of neutral surfactants (Φ_{NL})[133]. Optimal silencing corresponds to KT approaching 1 and KNS approaching 0. siRNA-DOTAP-GMO complexes in the gyroid cubic phase at low cationic DOTAP content show remarkably improved sequence-specific gene silencing over complexes in the lamellar phase. (e) Schematic phase diagrams showing different self-assembled DNA-tobramycin-surfactant liquid crystalline structures observed as a function of tobramycin-to-DNA charge ratio (T/D) and lipid-to-DNA charge ratio (L/D) for the hexagonal DNA-tobramycin bundles, lamellar DNA-DOTAP-DOPE-tobramycin (i) and inverse hexagonal phase DNA-DOTAP-DOPE with free tobramycin (ii), assuming a fixed DNA concentration[135]. Dashed lines show approximate boundaries between single phase regions and the shaded coexistence region where both tobramycin-DNA close-packed bundles (DNA-tobramycin bundle) and the DNA-DOTAP-DOPE complexes are observed. Tobramycin is represented as a red 'C' shape in the models.

The TE data, combined with confocal microscopy data for low and high TE complexes interacting with cells[125], suggested a model of cellular uptake of lamellar complexes depicted schematically in Figure 9b. An increase in σ_M (regime I) enhances fusion between the cationic membranes of lamellar complexes (trapped in endosomes) and anionic endosomal membranes facilitating the release of complexes to the cell cytoplasm. However, a very large σ_M (regime III) inhibits cationic membranes from efficiently releasing anionic DNA upon cell entry after endosomal escape. This then gives rise to the optimal σ_M (regime II) observed in experiments (i.e. σ_M just large enough to fuse with and escape the endosome but not too large to prevent complex dissociation upon cell entry)[124]. In contrast, the inverted hexagonal phase of DNA-DOTAP-DOPE complex[35] exhibits high TE even at low σ_M (independent of σ_M), due to their distinct mechanism of cellular entry, which relies on the fusogenic properties of DOPE[125,126]. This has made DOPE a popular choice as a co-surfactant for DNA complexes. In addition, other hexagonal mesophases (H_I and disordered H_I) of DNA-MVLBG2-DOPC complexes showed enhanced transfection efficiency, which deviates from the universal bell curve observed for lamellar complexes (Figure 9a)[37,38]. This suggests a distinctly new mechanism of action for these dendritic DNA-surfactant complexes, which still remains to be understood. In order to stabilize DNA-DOTAP-DOPC complexes sterically for in vivo gene therapy, PEG2000-lipids were introduced[127]. However, gene delivery efficiency was strongly reduced, likely due to the weakened electrostatic binding of DNA-DOTAP-DOPC-PEG2000 complexes to cells (leading to reduced uptake). In this system, RGD-peptide-grafted PEG2000-lipids were also used for cell attachment and uptake investigations. The RGD-tagged DNA complexes exhibited strongly increased cellular attachment as well as a uptake independent of σ_M. The TE of RGD-tagged DNA-DOTAP-DOPC-PEG2000 increased by about an order of magnitude between the complexes with low and high membrane charge density, which confirmed that the TE of RGD-tagged DNA-surfactant complexes is improved by high σ_M.

Recently, the discovery that cytoplasmic delivery of exogenous small interfering RNA (siRNA) induces gene silencing[128,129] (as part of the RNA interference pathway) has motivated major research efforts towards developing siRNA-surfactant complexes as efficient gene silencing vectors[130-132]. However, the current limiting step in realizing the full potential of siRNA gene silencing technology is the development of efficient chemical carriers for siRNA. A series of siRNA-surfactant complexes (siRNA-DOTAP/DOPE, siRNA-DOTAP/DOPC, siRNA-MVL5/DOPC) were fabricated, which exhibited lamellar and inverted hexagonal mesophases[132]. It was found that inverted hexagonal siRNA-DOTAP/DOPE had high toxicity and much lower target-specific gene silencing than lamellar siRNA complexes. This may result from an excessive fusion of DOPE containing complexes with the cell membrane, possibly creating pores and leading to membrane instability. The siRNA complex combined with pentavalent surfactant MVL5 exhibited lower toxicity and superior silencing efficiency when

compared to monovalent DOTAP. More recently, a new double-gyroid cubic mesophase was developed[133], in which cationic DOTAP and nonionic glycerol monooleate (GMO, 1-monooleoyl-glycerol) were combined with siRNA. Figure 9c shows a schematic representation of the unit cell of an inverse bicontinuous cubic phase (Q_{II}^{G}) containing siRNA. This phase is comprised of a bilayer surface that divides two intertwined but independent water channels (hosting the siRNA molecules). As anticipated, these complexes allowed for high levels of sequence-specific gene knockdown in the regime of low charge density where lamellar complexes are considerably less efficient. This mesophase was found to be highly efficient in cytoplasmic delivery of siRNA-surfactant complexes, leading to sequence-specific gene silencing and low cell toxicity (Figure 9d). The high degree of silencing was achieved with virtually no negative implications for cell viability and plasma membrane integrity, which was attributed to the low charge density of the cubic phase membranes. This significant discovery is consistent with the aforementioned hypothesis[134] that the tendency of cubic phase forming lipids for pore formation leads to fusion of the membranes of the gyroid siRNA-surfactant complex and endosomal membranes upon endocytosis. Pores, in turn, allow for efficient cytoplasmic siRNA delivery, leading to gene silencing. Aside from the applications in gene delivery and gene silencing with DNA-surfactant and siRNA-surfactant complexes, enhanced antimicrobial function for cystic fibrosis (CF) was observed for DNA-surfactant lyotropic liquid crystals[135]. Tobramycin, which is an aminoglycoside antibiotic commonly administered to CF patients via inhalation, can induce DNA to pack into hexagonal aggregates. Therefore, it would be unavailable for interaction with bacteria in the DNA-containing CF airway surface liquid. Wong and coworkers found that interactions between DNA and tobramycin can be significantly modified by the presence of mixtures of surfactants (DOTAP+DOPE). Different phase transitions, from hexagonal packed DNA-tobramycin, lamellar structured DNA-DOTAP-DOPE-tobramycin, and inverse hexagonal DNA-DOTAP-DOPE with free tobramycin were detected (Figure 9e). As a consequence, recovery of tobramycin's antimicrobial activity was realized. These results suggest that optimized cationic amphiphile surfactant solutions have the potential to enhance antimicrobial function in highly infected environments that contain increased concentrations of anionic inflammatory polymers (like DNA bundles) [135].

Based on the above discussions, lyotropic liquid crystals of DNA-surfactant complexes for therapeutics exhibit several outstanding features. They are relatively safe for use in human because no viral genes are present to cause disease. Furthermore, the lack of proteins makes the synthetic vector relatively non-immunogenic. These DNA-surfactant mesophases used for gene delivery are found to be significantly less toxic to cells than other DNA complexes combined with quaternary ammonium surfactants. Another exciting advantage of these synthetic vectors, as compared to engineered viral vectors for gene delivery, is the potential of transferring and expressing large pieces of DNA (one million base pairs) into cells[136,137]. However, delivery efficiencies of these liquid

crystalline complexes remain low compared to those of engineered viral vectors. Therefore, it is necessary to further develop a comprehensive understanding of the interactions of optimal DNA-surfactant complexes with cell membranes and other components such as the cytoskeleton network, which lead to cytosol delivery of complexes followed by DNA release and gene expression.

2.2.2 Hydrogels and release based on DNA-surfactant complexes

A general understanding of the interactions between DNA and oppositely-charged surfactants, and in particular the phase behavior, has given a basis for developing novel DNA-based materials, including the above-mentioned bulk DNA-surfactant films and soft-matter lyotropic liquid crystals. In addition, another type of soft DNA-surfactant material, i.e. DNA-surfactant hydrogel, has been developed based on associative phase separation and interfacial diffusion[138]. For the preparation of this type of structures, DNA solutions were added dropwise via a needle to gently agitated surfactant solutions. Under optimal conditions, droplets from DNA solutions instantaneously gelled into discrete particles upon contact with the surfactant solution. Hydrogel particles of DNA-surfactant complexes can be fabricated very easily and efficiently without adding any kind of cross-linker or organic solvent. Thus, the procedure is significantly different from that used to fabricate traditional DNA hydrogels[139]. The driving force for this strong association is the electrostatic interaction between the two components, as induced by the entropic increase due to the release of the respective counter-ions[140]. The association strength, which is tuned by varying the chemical structure of the cationic surfactant, allows control over the spatial homogeneity of the gelation process, producing either a homogeneous DNA matrix or different DNA reservoir devices. This gives rise to various applications for the controlled encapsulation and release of ssDNA and dsDNA. Lindman et al. reported the formation of DNA hydrogel particles by mixing solutions of DNA (either ssDNA or dsDNA) with solutions of cationic surfactant CTAB[141]. The size of the resulting DNA-CTAB gel particles varied between 1 and 2 mm. DNA entrapment in the gels has been determined, and the obtained loading efficiencies in dsDNA-CTAB and ssDNA-CTAB were higher than 99%. Further studies explored the effect of ionic strength on the release of DNA from the gel particles. Total release of DNA was obtained when dsDNA-CTAB hydrogels were placed in aqueous solutions containing high salt concentrations. A lower percentage of DNA release in ssDNA-CTAB gels was observed. This striking release difference suggests that the interaction of surfactant with DNA is much stronger in the case of ssDNA than dsDNA. Scanning electron microscopy images indicated that dsDNA-CTAB hydrogels are more porous, which is consistent with the higher degree of swelling compared to hydrogels containing ssDNA-CTAB. In order to investigate the influence of the surfactant structure on hydrogel particle formation and their release properties, double chain surfactant DDAB was combined with DNA and compared with single chain surfactant DTAB[142]. DNA-DTAB gel particles exhibited a rapid DNA release by a dissolution

mechanism. The corresponding half-life for dsDNA-DTAB and ssDNA-DTAB are 4 and 8 hours (h), respectively. However, in the case of DNA-DDAB hydrogels, an initial burst release (24 h) is observed which is independent of the secondary structure of the nucleic acid used. After that, a linear cumulative release was observed until the end of the experiment (1500 h). The amount of DNA released from dsDNA-DDAB and ssDNA-DDAB was 63 and 34%, respectively. Furthermore, the effect of different counter-ions on the formation of the DNA-surfactant hydrogel particles was examined[143]. In particular, single chain surfactant dodecyltrimethylammonium with different counter-ions (HSO_4^-, $CF_3SO_3^-$, Cl^-, and Br^-) was complexed with DNA. The degree of counter-ion dissociation from the surfactant micelles and the polar/hydrophobic character of the counter-ion are important for controlling DNA entrapment, swelling/shrinking behavior, and DNA release kinetics of the DNA hydrogels. Regarding biological evaluation these gel particles were assessed for haemolysis. It was found that the stronger the DNA-surfactant interaction, the lower haemolysis and the slower the DNA release kinetics. Therefore, these DNA-surfactant hydrogels represent a conceptually new design of nonviral vectors for the delivery of therapeutic DNA. The colloidal carrier protects nucleic acid molecules from deleterious degradation and may provide sustained release of payload in a therapeutically advantageous fashion. Although these carriers may offer various advantages over conventional gene-delivery systems, their safety must still be investigated. The toxicity of these materials may be significant due to the presence of cationic surfactants. A continuous effort focused on improving safety, feasibility, and efficacy of colloidal carriers is a challenging future goal.

3. Summary and Outlook

The ionic self-assembly of DNA-surfactant complexes is an exciting area of nucleic acid research and has received increasing attention in recent years. The driving force for this 'bottom-up' self-assembly process is the electrostatic interaction between anionic DNA and cationic surfactants. As summarized in Figure 10, the organization DNA-surfactant complexes into bulk films, lyotropic liquid crystals, and hydrogels was resulted in striking applications ranging from electronics, optics, and optoelectronics to biomedicine (gene therapy and drug delivery). Ordered films of aligned DNA have been fabricated by complexation with surfactant and exhibit high electronic conductivity. Enhanced fluorescence efficiency could be realized via DNA-surfactant complex as a matrix for the efficient dispersion of fluorescent dyes. Biological OLEDs and solar cells based on bulk DNA-surfactant films have been developed with improved device performance. However, the sensitivity of the DNA-surfactant complex to light and electric fields should be considered, because it may impair with long-term device stability. Under ambient conditions, water molecules may diffuse into ionic DNA-surfactant materials and might negatively influence device performance. Therefore, controlling the amount of water molecules attached to the DNA chains appears to be a critical factor for obtaining stable devices. Biological activity of DNA-surfactant bulk

films can be recovered once wetted. Thus, they may be suitable for gene therapy and drug release by direct implantation in vivo in combination with controlled delivery and dosage adjustment.

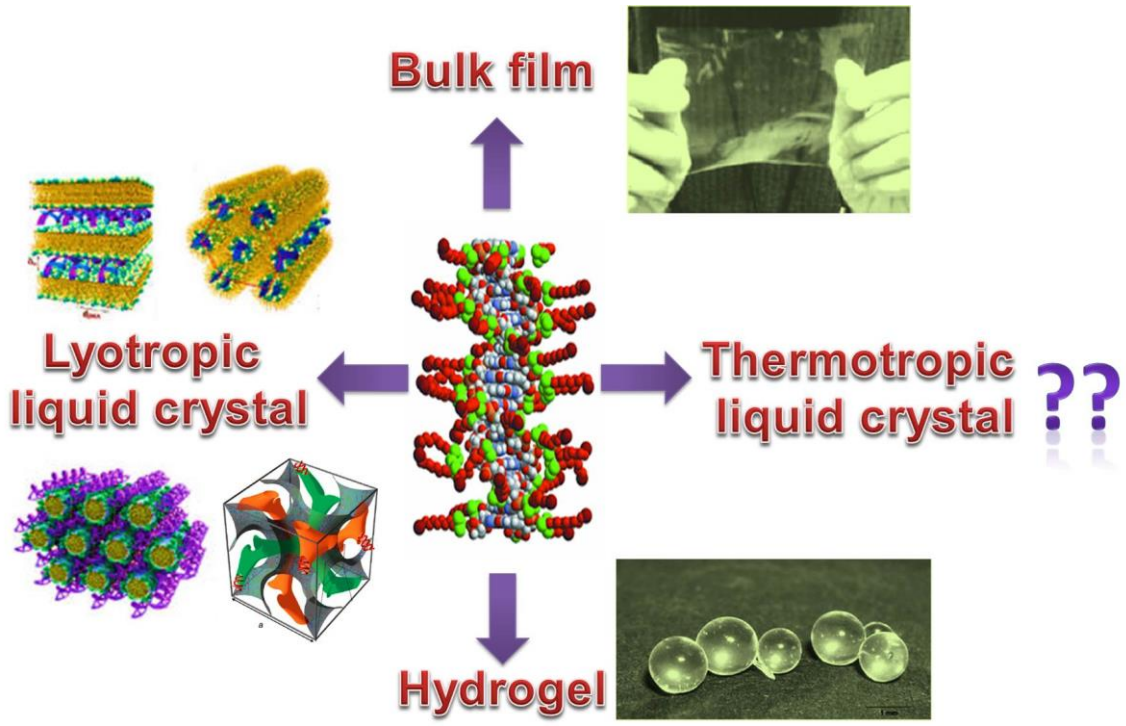

Figure 10. Summary of DNA-surfactant complexes forming different types of materials. Bulk films could be fabricated conveniently by casting the complexes from organic medium[79]. Packing mode of lyotropic liquid crystalline mesophases are strongly dependent on the DNA chains, headgroup charge and chain length of chosen surfactants, counterions, and other polyelectrolytes in solutions[123]. DNA-surfactant hydrogel particles are fabricated very easily and efficiently without adding any kind of cross-linker or organic solvent[140]. Up to now, solvent-free thermotropic liquid crystals based on DNA-surfactant complex have not been reported so far.

Furthermore, soft materials of DNA-surfactant complexes including lyotropic liquid crystals and hydrogels have been developed, especially for gene therapeutics. They are relatively safe for gene transfection and gene silencing when compared to viral vectors. A preliminary understanding of delivery mechanism at the individual complex level has been achieved by a combination of structural analysis and fluorescence microscopy. However, a comprehensive understanding of the nature of the interactions of DNA-surfactant complexes with cell membranes, and events leading to release of active nucleic acids within the cell cytoplasm is urgently needed for successful medical applications. Moreover, a continuous search to understand the role of amphiphilic surfactants, salts, and other polyelectrolytes in DNA-surfactant assembly behavior is imperative to enhance delivery efficiencies within current gene therapy trials and other drug delivery systems.

While studying DNA-surfactant complexes in bulk films, lyotropic liquid crystals, and hydrogels, up to now thermotropic liquic crystals have not been pursued (Figure 10). Since this class of DNA-surfactant materials would be solvent-free ordered fluids, new ensemble properties significantly different from bulk films and solvent-supported lyotropic liquid crystals are expected.

4. Motivation and thesis outline

Liquid crystals (LCs) are a state of matter with fluidic properties as found in liquids and molecular ordering like that found in crystals. In nature, LCs play an important role because the combination of order and mobility is a basic requirement for self-organization and structure formation in living systems. LCs observed in biology are usually dispersed in a solvent, typically water, and are therefore classified as lyotropic. As discussed above (**chapter 1**), lyotropic liquid crystals of DNA-surfactant complexes have been developed. Their mesophase behaviors are strongly dependent on DNA chains, headgroup charge, and the chain length of the chosen surfactants, counterions, and other polyelectrolytes in solutions. However, the principal thrust and achievement of LCs has been in the science and application of solvent-free thermotropic materials, structures, and phases, leading to various liquid crystal display technologies. The importance and technological success of thermotropic LCs based on organic molecules suggests the development of solvent-free DNA-LC systems in which the nucleic acid macromolecules and their assemblies can be investigated in the thermotropic regime. This characteristic likely enables DNA thermotropic LCs to adopt a wide variety of phases and to exhibit responses to external stimuli like electric fields.

In this thesis, we have successfully realized lamellar-structured thermotropic LCs from DNA and RNA (**chapter 2**). A general, simple, and effective strategy was developed whereby negatively charged DNA and RNA act as rigid parts, and cationic surfactants comprise flexible units to contain the typical structural features of a mesogen. Due to electrostatic interactions, stable thermotropic LC structures were realized where the components self-assemble into a multilayer architecture. Both this and the remarkably low LC-isotropic transition temperatures, enable the study and application of thermotropic LC phase behavior without thermal degradation of the DNA components.

In **chapter 3**, solvent-free DNA fluids (liquid crystals and liquids) have been developed by combining DNA with suitable cationic surfactants. The lengths of the DNA and surfactant are found to be extremely important in tuning the physical properties of the fluids, including the thermal and mechanical behaviors. Fluid DNA has been achieved at temperatures as low as -20°C and the transition from the crystal to the liquid crystal state can be adjusted up to 65°C. The liquid crystal to isotropic liquid-transition can be tuned between 41°C and 130°C. In the liquid crystals, in addition to the normal smectic mesophase, a two-dimensional modulated smectic structure of DNA-surfactant liquid crystal is observed when employing surfactants with long aliphatic chains.

Opto-electric effects of solvent-free DNA-surfactant liquid crystals have been investigated in **chapter 4**. We successfully fabricated a novel electrochromic device with extraordinary properties. Switching between coloration (magenta) and bleaching (colorless) is realized in the isotropic liquid phase. It is found that switch time of these materials is correlated with the length of the chosen DNA segments. Thus, the response time between coloration and bleaching could be controlled from a few seconds to several minutes. Remarkably enough, the red-color impression for many hours can be preserved in the smectic mesophase without color decay or application of a voltage. Additionally, the crystalline phase can further increase the durability of the stored optical information. Therefore, the volatility of optoelectronic information can be controlled simply by changing the phase of DNA-surfactant complex. This novel mode of device operation is especially appealing with respect to smart tags with incorporated clock and ceiling temperature functionalities.

Electrostatic complexes between DNA and surfactants are not only important for the formation of bulk LC phases but also for chemical functionalization in organic solvents. Functional DNA is a key material, which is required for many technologies, including molecular diagnostics, DNA sequencing, and gene therapy. In many cases, the functional moiety is hydrophobic, which renders the coupling to hydrophilic DNA very difficult. One can couple hydrophobic molecules in the form of phosphoramidites on the solid phase. However, this unit must then be compatible with harsh reaction conditions. Alternatively, hydrophobic structures can be coupled to oligonucleotides in solution, but typically with low yields due to solvent incompatibility between the hydrophilic DNA and the hydrophobic entity.

To overcome these limitations, we report a general organic-phase coupling strategy for nucleic acid functionalization by introducing a hydrophobic DNA-surfactant complex as a general reactive scaffold (**chapter 5**). Large hydrophobic π-systems, long hydrocarbon chains, and even hydrophobic polymers like poly(propylene oxide), polystyrene, and polyisoprene can be covalently linked to DNA efficiently by amine acylation. High yields for amphiphilic DNA conjugates are achieved, relative to existing methods. The reactions are simple, easily controllable, and applicable to a variety of hydrophobic moieties. More importantly, this approach avoids the large instrumental investment of acquiring an automated DNA synthesizer in the laboratory, thus expanding the accessibility of custom-synthesized amphiphilic DNA conjugates to many more research groups.

References

1. R. Dahm, Developmental Biology 2005, 278, 274.
2. J. D. Watson, F. H. C. Crick, Nature 1953, 171, 737.
3. X. J. Lu, W. K. Olson, Nucleic Acids Res 2003, 31, 5108.
4. E. Yeramian, Gene 2000, 255, 139.
5. S. L. Beaucage, M. H. Caruthers, Tetrahedron Lett. 1981, 22, 1859.
6. T. J. Bandy, A. Brewer, J. R. Burns, G. Marth, T. Nguyen, E. Stulz, Chem. Soc. Rev. 2011, 40, 138.
7. J. Chen, N. C. Seeman, Nature 1991, 350, 631.
8. D. Yang, M. J. Campolongo, T. N. Nhi Tran, R. C. H. Ruiz, J. S. Kahn, Luo D. WIREs NanomedNanobiotechnol 2010, 2, 648.
9. A. V. Pinheiro, D. Han, W. M. Shih, H. Yan, Nature Nanotech. 2011, 6, 763.
10. M. Kwak, A. Herrmann, Chem. Soc. Rev. 2011, 40, 5745.
11. T. Kato, N. Mizoshita, K. Kishimoto, Angew. Chem., Int. Ed. 2006, 45, 38.
12. O. Ikkala, G. ten Brinke, Science 2002, 295, 2407.
13. C. F. J. Faul, M. Antonietti, Adv. Mater. 2003, 15, 673.
14. C. F. J. Faul, Mol. Cryst. Liq. Cryst. 2006, 450, 255.
15. K. Hayakawa, J. P. Santerre, J. C. T. Kwak, Biophys. Chem. 1983, 17, 175.
16. V. A. Izumrudov, M. V. Zhiryakova, A. A. Goulko, Langmuir 2002, 18, 10348.
17. C. H. Spink, J. B. Chaires, J. Am. Chem. Soc. 1997, 119, 10920.
18. R. Dias, S. Mel'nikov, B. Lindman, M. G. Miguel, Langmuir 2000, 16, 9577.
19. L. Piculell, B. Lindman, Adv. Colloid Interface Sci. 1992, 41, 149.
20. P. Smith, R. M. Lynden-Bell, W. Smith. Phys. Chem. Chem. Phys. 2000, 2, 1305.
21. L. Goracci, R. Germani, G. Savelli, D. M. Bassani, ChemBioChem 2005, 6, 197.
22. A. Dasgupta, P. K. Das, R. S. Dias, M. G. Miguel, B. Lindman, V. M. Jadhav, M. Gnanamani, S. Maiti, J. Phys. Chem. B 2007, 111, 8502.
23. M. T. Record, Jr, C. F. Anderson, T. M. Lohman, Q. Rev. Biophys. 1978, 2, 103.
24. K. A. Sharp, R. A. Friedman, V. Misra, J. Hecht, B. Honig, Biopolymers 1995, 36, 245.
25. S. A. Palkar, A. M. Lenhoff, J. Colloid Interface Sci. 1994, 165, 177.
26. P. L. Felgner, G. Rhodes, Nature 1991, 349, 351.
27. P. L. Felgner, T. R. Gadek, M. Holm, R. Roman, H. W. Chan, M. Wenz, J. P. Northrop, G. M. Ringold, M. Danielsen, Proc. Natl. Acad. Sci. U.S.A. 1987, 84, 7413.
28. J. Gustafsson, G. Arvidson, G. Karlsson, M. Almgren, Biochim. Biophys. Acta 1995, 1235, 305.
29. F. L. Sorgi, L. Huang, FEBS Lett. 1994, 356, 361.
30. J. O. Rädler, I. Koltover, T. Salditt, C. R. Safinya, Science 1997, 275, 810.
31. T. Salditt, I. Koltover, J. O. Rädler, C. R. Safinya, Phys. Rev. Lett. 1997, 79, 2582.
32. D. D. Lasic, H. Strey, M. C. A. Stuart, R. Podgornik, P. M. Frederik, 1997, 119, 832.
33. T. Salditt, I. Koltover, J. O. Rädler, C. R. Safinya, Phys. Rev. E 1998, 58, 889.
34. F. Artzner, R. Zantl, G. Rapp, J. O. Rädler, Phys. Rev. Lett. 1998, 81, 5015.
35. I. Koltover, T. Salditt, J. O. Rädler, C. R. Safinya, Science 1998, 281, 78.
36. N. F. Bouxsein, C. Leal, C. S. Mcallister, K. K. Ewert, Y. Li, C. E. Samuel, C. R. Safinya, J. Am. Chem. Soc. 2011, 133, 7585.

37. K. K. Ewert, H. M. Evans, A. Zidovska, N. F. Bouxsein, A. Ahmad, C. R. Safinya, J. Am. Chem. Soc. 2006, 128, 3998.
38. A. Zidovska, H. M. Evans, K. K. Ewert, J. Quispe, B. Carragher, C. S. Potter, C. R. Safinya, J. Phys. Chem. B 2009, 113, 3694.
39. R. Ghirlando, E. J. Wachtel, T. Arad, A. Minsky, Biochemistry 1992, 31, 7110.
40. S. M. Mel'nikov, V. G. Sergeyev, K. Yoshikawa, H. Takahashi, I. Hatta, J. Chem. Phys. 1997, 107, 6917.
41. D. Harries, S. May, W. M. Gelbart, A. Ben-Shaul, Biophys. J. 1998, 75, 159.
42. L. Goluboric, M. Gloubovic, Phys. Rev. Lett. 1998, 80, 4341.
43. C. S. O'Hern, T. C. Lubensky, Phys. Rev. Lett. 1998, 80, 4345; 1999, 83, 2745.
44. N. Dan, Biophys. Biochim. Acta 1998, 1369, 34.
45. S. May, D. Harries, A. Ben-Shaul, Biophys. J. 2000, 78, 1681.
46. P. Ekwall, L. Mandell, K. Fontell, J. Colloid Interface Sci. 1969, 29, 639.
47. C. R. Safinya, E. B. Sirota, D. Roux, and G. S. Smith, Phys. Rev. Lett. 1989, 62, 1134.
48. R. Krishnaswamy, V. A. Raghunathan, A. K. Sood, Phys. Rev. E 2004, 69, 031905.
49. R. Krishnaswamy, G. Pabst, M. Rappolt, V. A. Raghunathan, A. K. Sood, Phys. Rev. E 2006, 73, 031904.
50. R. Krishnaswamy, P. Mitra, V. A. Raghunathan, A. K. Sood, Europhys. Lett. 2003, 62, 357.
51. S. Zhou, D. Liang, C. Burger, F. Yeh, B. Chu, Biomacromolecules 2004, 5, 1256.
52. C. Leal , A. Bilalov, B. Lindman, J. Phys. Chem. B 2009, 113, 9909.
53. D. McLoughlin, M. Impéror-Clerc, D. Langevin, ChemPhysChem 2004, 5, 1619.
54. A. Bilalov, U. Olsson, B. Lindman, Soft Matter 2009, 5, 3827; 2011, 7, 730.
55. D. Uhríková, G. Rapp, P. Balgavý, Bioelectrochemistry 2002, 58, 87.
56. X. Zhao, Y. Shang, J. Hu, H. Liu, Y. Hu, Biophys. Chem. 2008, 138, 144.
57. Q. Chen, X. Kang, R. Li, X. Du , Y. Shang, H. Liu , Y. Hu, Langmuir 2012, 28, 3429.
58. G. Caracciolo, D. Pozzi, R. Caminiti, G. Mancini, P. Luciani, H. Amenitsch, J. Am. Chem. Soc. 2007, 129, 10092.
59. K. Tanaka, Y. Okahata, J. Am. Chem. Soc. 1996, 118, 10679.
60. Y. Hoshino, S. Tajima, H. Nakayama, Y. Okahata, Macromol. Rapid Commun. 2002, 23, 253.
61. Y. Okahata, T. Kobayashi, K. Tanaka, Langmuir 1996, 12, 1326.
62. Y. Okahata , K. Tanaka, Thin Solid Films 1996, 284-285, 6.
63. H. Sun, W. Li, L. Wu, Langmuir 2009, 25, 10466.
64. S. May, A. Ben-Shaul, Biophys. J. 1997, 73, 2427.
65. M. H. Stenzel Austral. J. Chem. 2002, 55, 239.
66. B. Martin, M. Sainlos, A. Aissaoui, N. Oudrhiri, M. Hauchecorne, J. P. Vigneron, J. M. Lehn, P. Lehn, Curr. Pharma. Des. 2005, 11, 375.
67. T. Neumann, S. Gajria, M. Tirrell, L. Jaeger, J. Am. Chem. Soc. 2009, 131, 3440.
68. O. Sinanoglu, S. Abdulnur, Photochem. Photobiol. 1964, 3, 333.
69. T. Neumann, S. Gajria, N. F. Bouxsein, L. Jaeger, M. Tirrell, J. Am. Chem. Soc. 2010, 132, 7025.
70. T. Omabegho, R. Sha, N. C. Seeman, Science 2009, 324, 67.
71. C. J. Murphy, M. R. Arkin, Y. Jenkins, N. D. Ghatlia, S. H. Bossmann, N. J. Turro, J. K. Barton, Science 1993, 262, 1025.
72. E. Braun, Y. Eichen, U. Sivan, G. Ben-Yoseph, Nature 1998, 391, 775.
73. D. Porath, A. Bezryadin, S. de Vries, C. Dekker, Nature 2000, 403, 635.

74. D. Porath, G. Cuniberti, R. Di Felice, Top. Curr. Chem. 2004, 237, 183.
75. Y. Okahata, T. Kobayashi, K. Tanaka, M. Shimomura, J. Am. Chem. Soc. 1998, 120, 6165.
76. Y. Okahata, T. Kobayashi, H. Nakayama, K. Tanakat, Supramol. Sci. 1998, 5, 317.
77. H. Nakayama, H. Ohnob, Y. Okahataa, Chem. Commun. 2001, 2300.
78. Y. Okahata, H. Nakayama, Proc. Japan Acad. 2000, 76, 145.
79. Y. Okahata, T. Kawasaki, Top. Curr. Chem. 2005, 260, 57.
80. J. Mysliwiec, A. Kochalska, A. Miniewicz, Appl. Opt. 2008, 47, 1902.
81. J. G. Grote, J. A. Hagen, J. S. Zetts, R. L. Nelson, D. E. Diggs, M. O. Stone, P. P. Yaney, E. Heckman, C. Zhang, W. H. Steier, A. K. Y. Jen, L. R. Dalton, N. Ogata, M. J. Curley, S. J. Clarson, F. K. Hopkins, J. Phys. Chem. B 2004, 108, 8584.
82. J. G. Grote, D. E. Diggs, R. L. Nelson, J. S. Zetts, F. K. Hopkins, N. Ogata, J. A. Hagen, E. Heckman, P. P. Yaney, M. O. Stone, L. R. Dalton, Mol. Cryst. Liq. Cryst. 2005, 426, 3.
83. L. Wang, J. Yoshida, N. Ogata, S. Sasaki, T. Kajiyama, Chem. Mater. 2001, 13, 1273.
84. J. E. Lee, E. D. Do, U. R. Lee, M. J. Cho, K. H. Kim, J. -I. Jin, D. H. Shin, S. H. Choi, D. H. Choi, Polymer 2008, 49, 5417.
85. Y. J. Yu, Y. -W. Kwon, K. N. Kim, E. D. Do, D. H. Choi, J. -I. Jin, H. W. Shin, Y. R. Kim, I. J. Kang, J. A. Mikroyannidis, Macromol. Res. 2009, 17, 245.
86. B. Liu, B. S. Gaylord, S. Wang, G. C. Bazan, J. Am. Chem. Soc. 2003, 125, 6705.
87. U. R. Lee, J. E. Lee, M. J. Cho, K. H. Kim, Y. -W. Kwon, J. -I. Jin, D. H. Choi, J. Polym. Sci. Part A: Polym. Chem. 2009, 47, 5416.
88. Y. Kawabe, L. Wang, S. Horinouchi, N. Ogata, Adv. Mater. 2000, 12, 1281.
89. Z. Yu, W. Li, J. A. Hagen, Y. Zhou, D. Klotzkin, J. G. Grote, A. J. Steckl, Appl. Opt. 2007, 46, 1507.
90. M. Leonetti, R. Sapienza, M. Ibisate, C. Conti, C. Lopez, Opt. Lett. 2009, 34, 3764.
91. J. Mysliwiec, L. Sznitko, A. Sobolewska, S. Bartkiewicz, A. Miniewicz, Appl. Phys. Lett. 2010, 96, 141106.
92. B. Sahraoui, M. Pranaitis, D. Gindre, J. Niziol, V. Kazukauskas, J. Appl. Phys. 2011, 110, 083117.
93. B. Derkowska, O. Krupka, V. Smokal, B. Sahraoui, Opt. Mater. 2011, 33, 1429.
94. S. R. Walter, F. M. Geiger, J. Phys. Chem. Lett. 2010, 1, 9.
95. T. Singh, N. Sariciftci, J. Grote, Adv. Poly. Sci. 2010, 223, 189.
96. Y-W. Kwon, D. H. Choi, J-I. Jin, Polymer Journal 2012, 44, 1191.
97. A. J. Steckl, H. Spaeth, H. You, E. Gomez, J. Grote, Opt. Photonics News 2011, 22, 34.
98. J. A. Hagen, W. Li, J. Steckl, J. Grote, Appl. Phys. Lett. 2006, 88, 171109.
99. Q. Sun, G. Subramanyam, L. Dai, M. Check, A. Campbell, R. Naik, J. Grote, Y. Wang, ACS Nano 2009, 3, 737.
100. M. J. Cho, U. R. Lee, Y. S. Kim, J. Shin, Y. M. Kim, Y. W. Park, B. K. Ju, J. I. Jin, D. H. Choi, J. Polym. Sci. Part A: Polym. Chem. 2010, 48, 1913.
101. K. Nakamura, T. Ishikawa, D. Nishioka, T. Ushikubo, N. Kobayashi, Appl. Phys. Lett. 2010, 97, 193301.
102. Y. Ner, J. G. Grote, J. A. Stuart, G. A. Sotzing, Angew. Chem. Int. Ed. 2009, 48, 5134.
103. A. Bandyopadhyay, A. K. Ray, A. K. Sharma, J. Appl. Phys. 2007,102, 064508.
104. V. Kolachure, & M. H. -C. Jin, 33rd IEEE Photovoltaic Specialists Conference, 2008, (IEEE, San Diego, CA, USA).
105. S. Gajria, T. Neumann, M. Tirrell, Wires Nanomed. Nanobio. 2011, 3, 479.

106. A. Bodley, L. F. Liu, M. Israel, R. Seshadri, Y. Koseki, F. C. Giuliani, S. Kirschenbaum, R. Silber, M. Potmesil, Cancer Res. 1989, 49, 5969.
107. T. Fukushima, M. Kawaguchi T., Hayakawa, S. Takeda, Y. Inoue J. Ohno, K. Taniguchi, Dental. Mater. J. 2007, 26, 854.
108. C. M. Jewell, J. Zhang, N. J. Fredin, D. M. Lynn, J. Control. Rel. 2005, 106, 214.
109. J. Zhang, D. M. Lynn, Adv. Mater. 2007, 19, 4218.
110. J. Blacklock, Y. Z. You, Q. H. Zhou, G. Mao, D. Oupick, Biomaterials 2009, 30, 939.
111. (a) Y. Ramgopal, D. Mondal, S. S. Venkatraman, W. T. Godbey, J. Biomed. Mater. Res. Part B: Appl. Biomater. 2008, 85, 496. (b) A. Kolbe , L. L. del Mercato , A. Z. Abbasi , P. Rivera Gil , S. J. Gorzini , W. H. C. Huibers , A. Poolman , W. J. Parak , A. Herrmann , Macromol. Rapid Commun. 2011 , 32 , 186 .
112. Y. Lvov, G. Decher, G. Sukhorukov, Macromolecules 1993, 26, 5396.
113. T. Segura, L. D. Shea, Bioconj. Chem. 2002, 13, 621.
114. T. Segura, M. J. Volk, L. D. Shea, J. Control. Rel. 2003, 93, 69.
115. P. Midoux, C. Pichon, J. J. Yaouanc, P. A. Jaffès, Brit. J. Pharmacol. 2009, 157, 166.
116. G. Iacomino, G. Picariello, F. Sbrana, A. Di Luccia, R. Raiteri, L. D'Agostino, Biomacromolecules 2011, 12, 1178.
117. E. V. B. van Gaal, R. S. Oosting, W. E. Hennink, D. J. A. Crommelin, E. Mastrobattista Int. J. Pharm. 2010, 390, 76.
118. J. C. Rea, R. F. Gibly, A. E. Barron, L. D. Shea, Acta. Biomater. 2009, 5, 903.
119. J. C Rea., A. E. Barron, L. D. Shea, J. Pharma. Sci. 2008, 97, 4794.
120. K. K. Ewert, A. Ahmad, H. M. Evans, C. R. Safinya, Expert Opin. Biol. Ther. 2005, 5, 33.
121. S. Chesnoy, L. Huang, Annu. Rev. Biophys. Biomol. Struct. 2000, 29, 27.
122. K. K. Ewert, A. Zidovska, A. Ahmad, N. F. Bouxsein, H. M. Evans, C. S. McAllister, C. E. Samuel, C. R. Safinya, Topics Curr. Chem. 2010, 296, 191.
123. C. R. Safinya, K. K. Ewert, C. Leal, Liq. Cryst. 2011, 38, 1715.
124. A. Ahmad, H. M. Evans, K. Ewert, C. X. George, C. E. Samuel, C. R. Safinya, J. Gene Med. 2005, 7, 739.
125. A. J. Lin, N. L. Slack, A. Ahmad, C. X. George, C. E. Samuel, C. R. Safinya, Biophys. J. 2003, 84, 3307.
126. R. I. Mahato, S. W. Kim (editors). Pharmaceutical Perspectives of Nucleic Acid Based Therapeutics, Taylor and Francis: London, 2002.
127. R. N. Majzoub, C.-L. Chan, B. F. B. Silva, K. K. Ewert, K. S. Liang, E. L. Jacovetty, B. Carragher, C. S. Potter, C. R. Safinya Biomaterials 2014, 35, 4996.
128. S. M. Elbashir, J. Harborth, W. Lendeckel, A. Yalcin, K. Weber, T. Tuschl, Nature 2001, 411, 494.
129. N. J. Caplen, S. Parrish, F. Imani, A. Fire, R. A. Morgan, Proc. Natl. Acad. Sci. U.S.A. 2001, 98, 9742.
130. T. C. Karagiannis, A. El-Osta, Cancer Gene Ther. 2005, 12, 787.
131. M. Sioud, Trends Pharm. Sci. 2004, 25, 22.
132. N. F. Bouxsein, C. S. McAllister, K. K. Ewert, C. E. Samuel, C. R. Safinya, Biochemistry 2007, 46, 4785.
133. C. Leal, N. F. Bouxsein, K. K. Ewert, C. R. Safinya, J. Am. Chem. Soc. 2010, 132, 16841.
134. D.P. Siegel, Biophys. J. 1999, 76, 291.
135. K. R. Purdy Drew, L. K. Sanders, Z. W. Culumber, O. Zribi, G. C. Wong, J. Am. Chem. Soc. 2008, 132, 16841.
136. J. J. Harrington, G. Van Bokkelen, R. W. Mays, K. Gustashaw, H. F. Williard, Nat. Gen. 1997, 15, 345.
137. W. Roush, Science 1997, 276, 38.

138. R. S. Dias and B. Lindman (editors). Cross-Linked DNA Gels and Gels Particles, Wiley Interscience, New York, 2008.
139. D. Costa, A. J. Valente, M. G. Miguel, J. Queiroz, Adv Colloid Interface Sci. 2014, 205, 257.
140. M. C. Morán, M. P. Vinardell, M. R. Infante, M. G. Miguel, B. Lindman, Adv Colloid Interface Sci. 2014, 205, 240.
141. M. C. Morán, M. G. Miguel, B. Lindman, Biomacromolecules 2007, 8, 3886.
142. M. C. Morán, M. G. Miguel, B. Lindman, Soft Matter 2011, 7, 2001.
143. M. C. Morán, T. Alonso, F. S. Lima, M. P. Vinardell, M. G. Miguelc, B. Lindman, Soft Matter 2012, 8, 3200.

Chapter 2

Thermotropic liquid crystals from nucleic acids

Abstract

Complexation of nucleic acids (DNA and RNA) with surfactants containing flexible alkyl tails, followed by dehydration, is shown to be a simple generic method for the production of thermotropic liquid crystals. The anhydrous smectic phases that result exhibit nucleic acid sublayers intercalated between aliphatic hydrocarbon sublayers at or near room temperature. Both this and low transition temperatures to other phases enable the study and application of thermotropic LC phase behavior without thermal degradation of the nucleic acid components.

Introduction

Liquid crystals (LCs) play an important role in biology because their essential characteristic, the combination of order and mobility, is a basic requirement for self-organization and structure formation in living systems[1-3]. Thus, it is not surprising that the study of liquid crystals emerged as a scientific discipline in part from biology in the study of myelin figures, lipids, and cell membranes[4]. These and the LC phases formed from many other biomolecules, including nucleic acids[5,6], proteins[7,8], and viruses[9,10], are classified as lyotropic, the general term applied to LC structures formed in water and stabilized by the distinctly biological theme of amphiphilic partitioning of hydrophilic and hydrophobic molecular components into separate domains. However, the principal thrust and achievement of the study of LCs has been in the science and application of thermotropic materials, structures and phases in which molecules that are only weakly amphiphilic exhibit LC ordering by virtue of their steric molecular shape, flexibility, and/or weak intermolecular interactions (e.g., van der Waals and dipolar forces[11]). These characteristics enable thermotropic LCs (TLCs) to adopt a wide variety of exotic phases and to exhibit dramatic and useful responses to external forces, including, for example, the electro-optic effects that have led to LC displays and the portable computing revolution. This general distinction between lyotropic and thermotropic LCs suggests that there may be interesting possibilities in the development of biomolecular or bio-inspired LC systems in which the importance of amphiphilicity is reduced and the LC phases obtained are more thermotropic in nature. Such biological TLC materials are very appealing for several reasons. Most biomacromolecules were extensively characterized in aqueous environments but in TLC phases their solvent-free properties and functions could be investigated in a state where no or only traces of water are present. Water exhibits a high dielectric constant and has the ability to form hydrogen bonds greatly influencing the structure and functions of biomacromolecules or compromising electronic properties like charge transport[12-15]. Indeed, anhydrous TLC systems containing glycolipids[16-19], ferritin[20], and polylysine have been reported[21-23]. However, a general approach to fabricate TLCs based on nucleic acids remains elusive.

Here we propose that the combination of nucleic acids with suitably chosen surfactants followed by dehydration, can be effectively applied as a simple generic scheme for producing nucleic acids-based TLCs. We demonstrate TLCs made from single stranded DNA and RNA. TLC materials typically combine rigid or semi-rigid anisometric units, which introduce orientational anisotropy, with flexible alkyl chains, which suppress crystallization[24]. In the present experiments negatively charged nucleic acids act as rigid part, and cationic surfactants comprise the flexible units to produce TLC phases with remarkably low LC-isotropic clearing temperatures, which is another TLC signature. Electrostatic interactions couple these rigid and flexible components into hybrid assemblies which then order into lamellar phases of alternating rigid and flexible

layers (Figure 1a), stabilized by the tendency in TLCs for rigid and flexible to spatially segregate[25].

Results and discussions

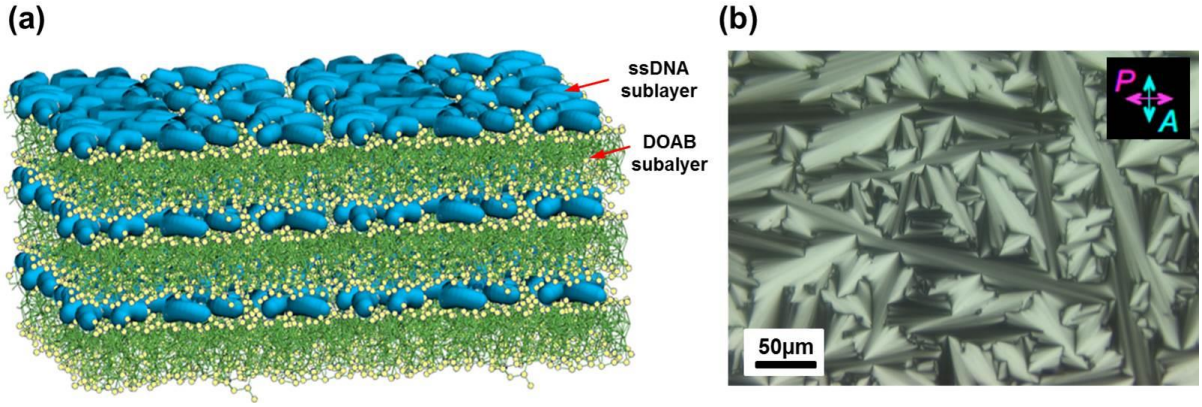

Figure 1. Lamellar structured thermotropic liquid crystal (TLC) formation from DNA-surfactant complex. (a) Proposed mesophase structure of DNA-DOAB complex (DOAB: dimethyldioctylammonium bromide). The lamellar bilayer structure is made of alternately one sublayer of the single-stranded (ss) 22mer DNA and one interdigitated sublayer of the surfactant, where the negatively charged phosphate groups of ssDNA electrostatically interact with the cationic head groups of DOAB. For the ssDNA-DOAB smectic TLC, the oligonucleotides are randomly orientated in the DNA sublayers. (b) Polarized optical microscopy (POM) image of the mesophase cooled from isotropic of DNA-DOAB complex, showing well-defined focal-conic textures of smectic layers at 25 °C.

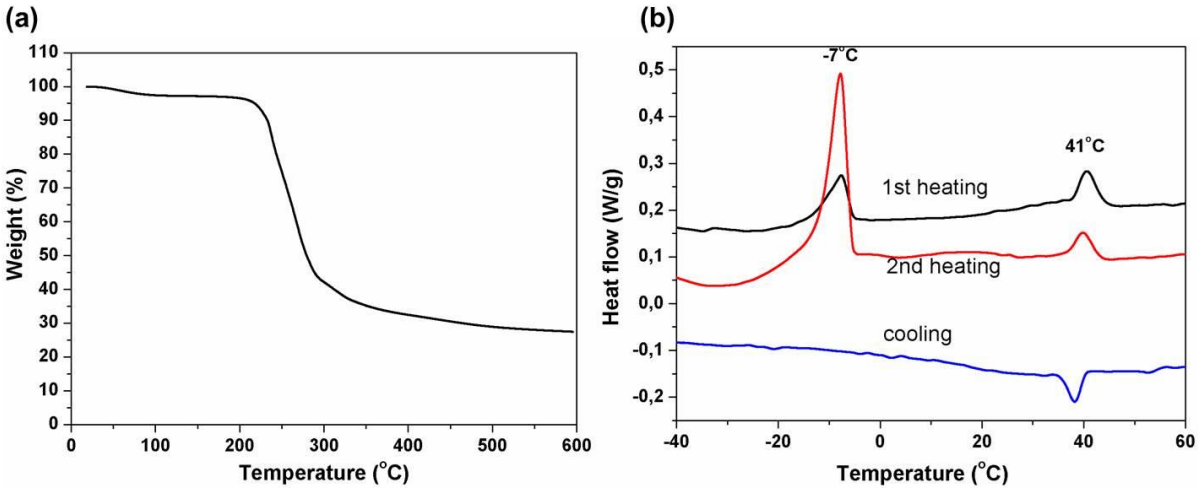

Figure 2. Thermal behaviors of DNA-DOAB complex. (a) Thermogravimetric analysis (TGA) of DNA-surfactant complex (DNA-DOAB). It gave a water content of less than 3%, confirming only traces of water present in the bulk material and the thermal degradation starts from around 200 °C. (b) Differential scanning calorimetry (DSC) traces (at a heating/cooling rate of 5 °C/min) with phase transition temperatures of the DNA-DOAB complex. DSC revealed two discrete endothermic peaks upon 1st heating at -7 and 41 °C, corresponding to crystalline–smectic and smectic–isotropic transitions, respectively. Upon cooling, the exothermic transition from isotropic liquid to smectic phase was evident at around 40 °C, but the recrystallization phase transition at low temperature was not observed anymore, possibly due to a slow crystallization process. The DSC curve of the 2nd heating was identical to the 1st one, indicating reversibility of the thermal cycles.

Inspired by previous work dealing with polyelectrolyte-lipid complexes[2,26-31], for the preparation of nucleic acid TLCs an oligonucleotide (22mer single-stranded (ss) DNA) and the cationic surfactant dimethyldioctylammonium bromide (DOAB) were complexed in a simple procedure including a final lyophylization step (**Experimental Section**). The solvent-free DNA-DOAB complex was birefringent (supplementary Figure S2), viscous and did not solidify at room temperature. Thermogravimetric analysis (TGA) of the DNA-surfactant melts revealed a water content of less than 3% (wt), confirming that only traces of water are present in the bulk material and that they are thermally stable up to 200 °C (Figure 2a). The phase sequence was then investigated by polarized optical microscopy (POM). The typical focal-conic textures characteristic for smectic order[32] were observed upon cooling from isotropic to the mesophase (Figure 1b). Differential scanning calorimetry (DSC) revealed two discrete endothermic peaks at -7 and 41 °C, corresponding to crystalline–LC and LC–isotropic transitions, respectively (Figure 2b). This finding suggests the formation of a TLC due to electrostatic complexation between the phosphate backbone of the oligonucleotide and the cationic head groups of DOAB because pristine DOAB is isotropic at the same temperature range.

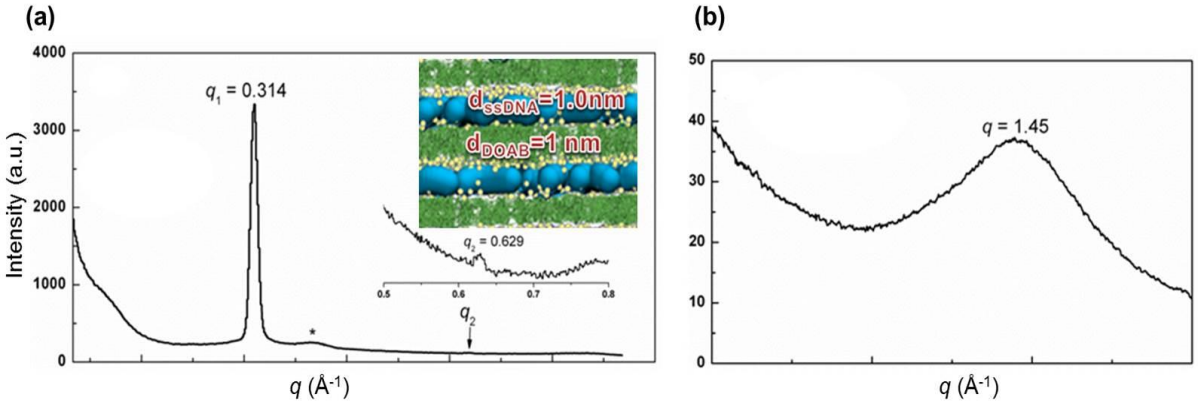

Figure 3. Small-angle X-ray scattering (SAXS, a) and wide-angle X-ray scattering (WAXS, b) profiles of the 22mer single-stranded DNA-DOAB complex cooled from isotropic to the smectic mesophase (25 °C). The corresponding molecular organization of the smectic structures (side view) is given in the inset. The peak at q_2 is also magnified in the inset. The diffraction peak at q~0.4 Å^{-1} (labeled with * in a) is due to the kapton, which is used for sample loading and sealing.

The sharp reflection peak q_1 = 0.314 Å^{-1} and its harmonics q_2 = 0.629 Å^{-1} at small-angle X-ray scattering (SAXS) (Figure 3a) indicate long-range ordered smectic layers of the DNA-DOAB complexes with a periodicity of 20.0 Å (d = $2\pi/q_1$). Considering the dimensions of the ssDNA and the DOAB, the layer spacing of 20.0 Å suggests that the lamellar structure is composed of a ssDNA sublayer of ~10 Å thickness[33] that electrostatically interacts with a interdigitaed DOAB sublayer of ~10 Å, as modeled in Figure 1a and shown in the inset of Figure 3a. In the wide-angle X-ray scattering (WAXS) experiment (Figure 3b), the broad peak at q = 1.45 Å^{-1} corresponds to repeat distance of 4.3 Å, which is attributed to the intralayer packing of the alkyl chains of the

surfactant[20]. Regarding the X-ray results, no peak from the DNA intralayer packing was observed, which suggests that the oligonucleotide chains of ssDNA are randomly packed within the sublayer without any positional or orientational order[34]. The lamellar structure of the DNA-DOAB complex was directly visualized by freeze-fracture transmission electron microscopy (FF-TEM). As shown in Figure 4a, stacks of flat and smooth layers with occasional distinct layer steps (red arrows) indicate a long-range order of the DNA-DOAB smectic mesophase. No specific or identifiable features were observed at the fracturing surface even at high magnification (Figure 4b), indicating that DNA molecules are randomly, homogeneously orientated, and uncorrelated within the sublayer, consistent with the X-ray analysis.

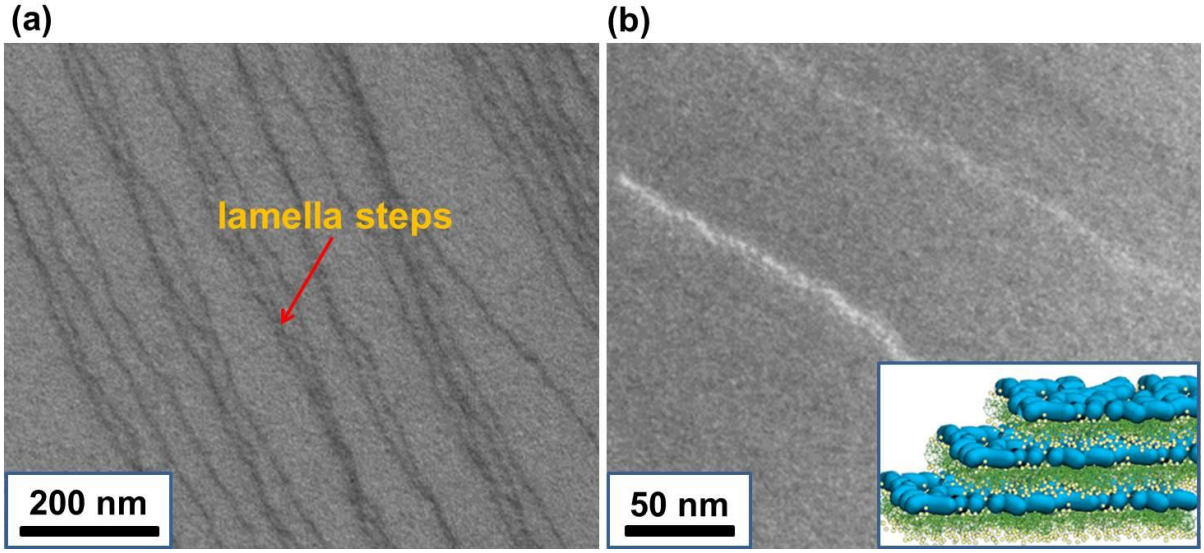

Figure 4. Freeze-fracture transmission electron microscopy (FF-TEM) images of the 22mer single-stranded DNA-DOAB mesophase. The sample was quenched after cooling from isotropic (45 °C) to the desired temperature in the mesophase (25 °C), and then fractured in the bulk. The model is sketched in the inset. (a) Lamellar structure of the DNA-DOAB with fractured distinct layer steps, and magnified in (b), homogeneous layer surfaces where ssDNA molecules randomly oriented within the sublayer.

To show the generality of our approach in regard to other nucleic acids, TLCs from RNA were fabricated following the same complexation procedure (**Experimental Section**). The resulting TLC phase ranged from -7 to 42 °C (supplementary Figure S3). POM of the RNA-DOAB complex displayed a typical focal-conic texture (supplementary Figure S4), and the analysis of SAXS and WAXS data indicated a smectic mesophase with a layer spacing of 20.3 Å (supplementary Figure S5). The periodic lamellar structures are also directly confirmed by FF-TEM (supplementary Figure S6).

Conclusions

We report here a generic molecular architecture and preparative scenario whereby thermotropic liquid crystals can be fabricated from nucleic acids. DNA and RNA that

exhibit negative charges were complexed with cationic surfactants by a simple fabrication procedure. The biological materials represent a new class of thermotropic liquid crystals, which form mesophases that are stabilized by electrostatic interactions. It is important to note that single-stranded short DNA and RNA assemble into periodic lamellar structures in spite of the fact that these molecules lack sufficient rigidity. In the future we will study the properties of the biological components within this novel class of TLCs providing a hydrophobic environment and lacking high dielectric water content. The flexibility of incorporating various different biological building blocks in nucleic acids will enable many technological applications including biosensing, biocatalysis and bioelectronic devices.

Experimental Section

Materials

Surfactant of dioctyldimethylammonium bromide (DOAB) used for the electrostatic complex formation was purchased from ABCR (Germany). 22mer single-stranded DNA (sequence: 5'-CCTCGCTCTGCTAATCCTGTTA-3', Mw = 6612 g/mol) was synthesized employing conventional solid-phase synthesis method. 22mer single-stranded RNA (sequence: 5'-CCUCGCUCUGCUAAUCCUGUUA-3', Mw = 6853 g/mol) was purchased from biomers (Germany). Other solvents and reagents for DNA synthesis were purchased from Novabiochem (Merck, UK), GE Healthcare, Sigma-Aldrich, Entelechon (Regensburg, Germany), and LaserBio (Sophia-Antipolis, France) and were used without further purification. During all experiments, ultrapure water (18.2 MΩ) purified by a MilliQ-Millipore system (Millipore, Germany) was used.

Characterization

UV absorption of DNA and RNA were recorded on a fluorimeter (SpectraMax M2, Molecular Devices, Sunnyvale, CA). DNA purity was determined by denaturing polyacrylamide gel electrophoresis (PAGE) with subsequent SYBR Gold staining. Photographs of the gel was taken with a LAS-3000 Image Reader (Fuji Photo Film (Europe) GmbH, Dusseldorf, Germany). Mass spectrometry of DNA was performed using a 4800 MALDI-TOF/TOF Analyzer (Applied Biosystems, Foster City, CA, USA). Differential scanning calorimetry (DSC) was carried out using a TA Instruments Q1000 system in a nitrogen atmosphere and with a heating/cooling rate of 5 °C/min. Polarized optical microscopy (POM) was conducted on a Zeiss Axiophot using the same temperature program as employed for the DSC experiments. Small-angle and wide-angle X-ray scattering (SAXS and WAXS) with heating and cooling systems were performed by employing a conventional X-ray source. For SAXS, a Bruker Nano/microstar instrument with radiation wavelength of λ = 1.54 Å was used to obtain small angle scattering profiles, where the sample-to-detector distance was 240 cm for DNA and RNA samples. The scattering vector q is defined as $q = 4\pi \cdot \sin\theta/\lambda$ with 2θ being the scattering angle. WAXS was carried out by a home-made, rotating-anode–based

setup. The goal of the WAXS experiments was to probe the halo diffusion of the alkyl chains of the surfactants. The sample-to-detector distance was 13 cm with X-ray wavelength of 1.54 Å. SAXS and WAXS profiles were obtained by cooling the samples (5 °C/min) from the isotropic phase to a selected temperature of the mesophase. Freeze-fractured transmission electron microscopy (FF-TEM) was carried out according to standard protocols[35]. FF-TEM was performed by sandwiching the samples between 2 mm by 3 mm glass planchettes and cooling from the isotropic melt to a selected temperature in the LC range. The samples were then rapidly quenched to T < -180 °C by immersion in liquid propane, fractured in vacuum at -140 °C, and then coated with 2 nm of platinum deposited at 45° and then with 25 nm of carbon deposited at 90°. After dissolving the liquid crystal, the Pt–C replicas were placed in the TEM, where the topographic structure of the fracture plane was observed. Smectic layer surfaces are generally smooth but have occasional layer steps that are distinct and can be identified unambiguously.

Synthesis of DNA

DNA with the sequence 5'-CCTCGCTCTGCTAATCCTGTTA-3' was synthesized through conventional solid-phase synthesis method as reported before[36]. For purification, anionic exchange (AIEX) chromatography was performed using a HiTrap Q HP 1 mL column (GE Healthcare) through linear gradient using buffer A (25 mM Tris-HCl, pH 8.0) and buffer B (25 mM Tris-HCl and 1.0 M NaCl, pH 8.0). For recording the MALDI-TOF mass spectra of the different DNA sequences the following matrix was employed: 20 mg 3-hydroxypicolinic acid, 2 mg picolinic acid, 3 mg ammonium citrate, 0,5 mL of a mixture of ultrapure water/acetonitrile (7:3); ratio sample/matrix = 1:2 (v/v). The concentration of the DNA solution was 100 µM. Gel electrophoresis (PAGE) and MALDI-TOF mass spectrometry (supplementary Figure S1) clearly indicate the identity and purity of 22mer ssDNA.

Preparation of DNA-DOAB complex

The DNA was pretreated by precipitating a 250 µM DNA solution containing 5 M NaCl with cold ethanol. Subsequently, a 250 µM aqueous solution of DNA was prepared by dissolving the single-stranded 22mer DNA in ultrapure water. In a second solution made from ultrapure water the concentration of cationic surfactant DOAB was adjusted to 60 mM at room temperature. Both the DNA and DOAB solutions (~5 mol equivalents of surfactant relative to nucleotides of the DNA) were mixed together and as a result the insoluble complex precipitated from the aqueous phase. After centrifugation the water and unreacted DOAB were removed and the complex was lyophilized before further characterization.

Preparation and characterization of RNA-DOAB complex

The RNA was pretreated by precipitating a 250 μM RNA solution containing 5 M NaCl with cold ethanol. Subsequently, a 250 μM aqueous solution of RNA was prepared by dissolving the single-stranded 22mer RNA in ultrapure water. In a second solution made from ultrapure water the concentration of cationic surfactant DOAB was adjusted to 60 mM at room temperature. Both the RNA and DOAB solutions (~5 mol equivalents of surfactant relative to nucleotides of the RNA) were mixed together and as a result the insoluble complex precipitated from the aqueous phase. After centrifugation the water and unreacted DOAB were removed and the complex was lyophilized before further characterization.

Supplementary Figures

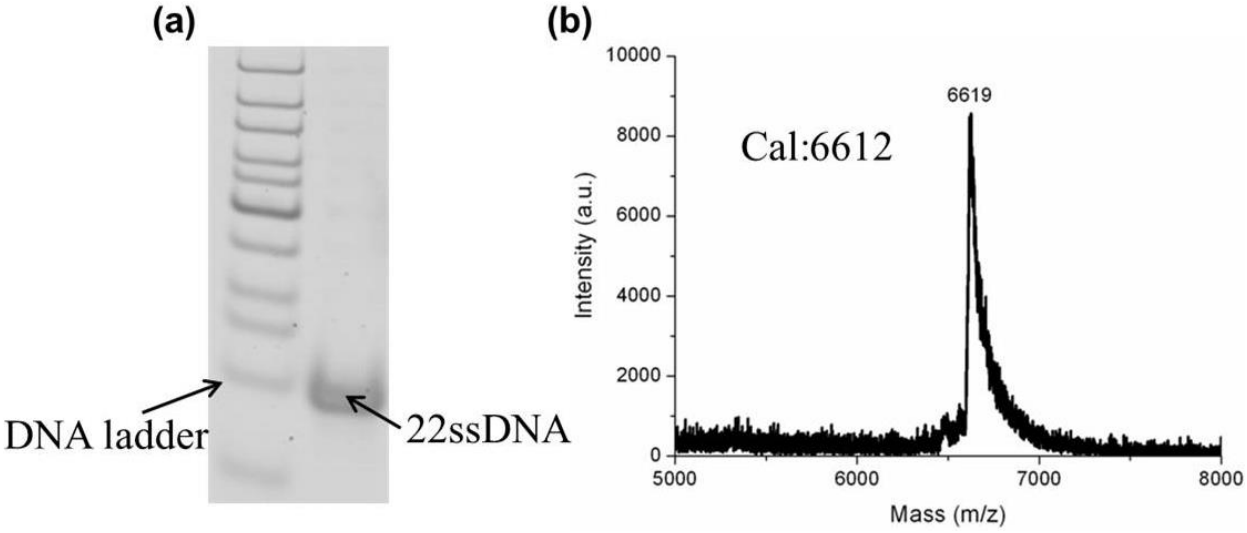

Figure S1. Denatured PAGE (a) and MALDI-TOF mass spectrum (b) of 22mer ssDNA. Both of them clearly indicate the identity and purity of 22mer ssDNA.

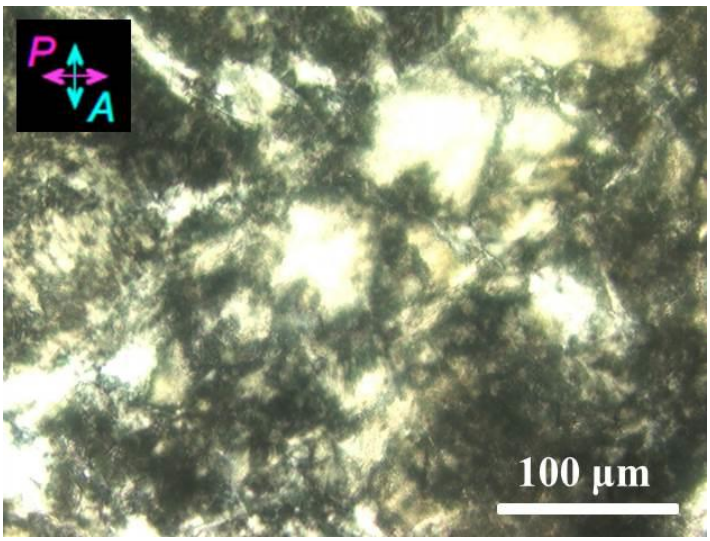

Figure S2. Polarized optical microscopy image showing the strong birefringence of viscous DNA-DOAB complex at room temperature, suggesting the presence of a non-crystalline soft anisotropic phase at room temperature that remained viscous until clearing into an isotropic liquid at 42 °C.

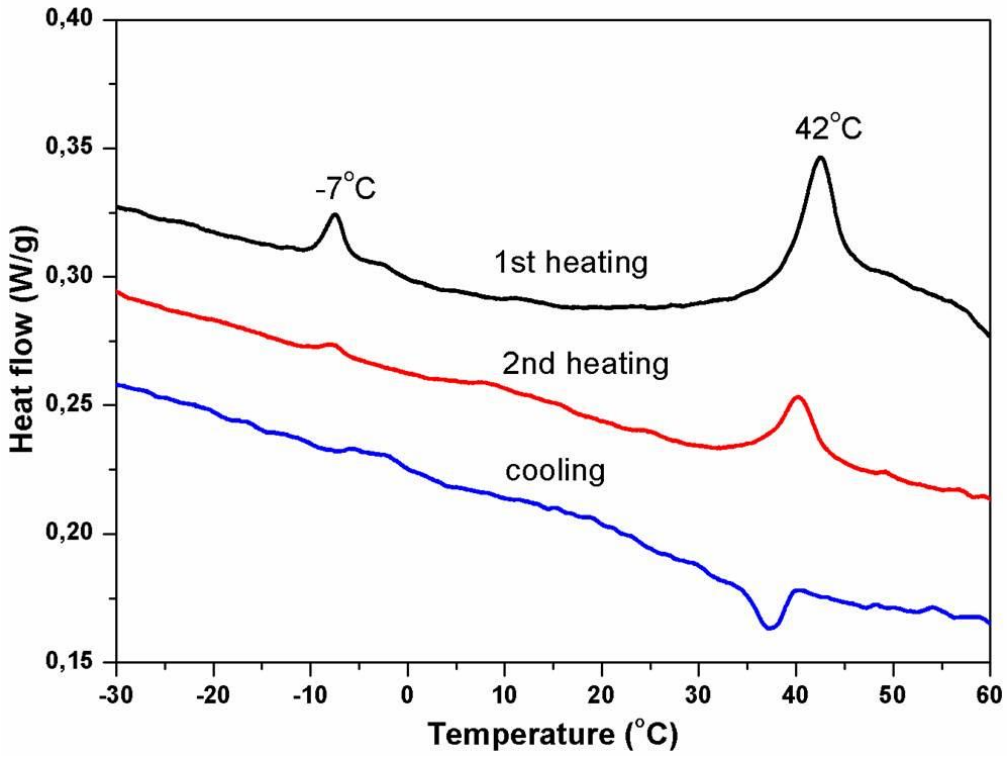

Fig. S3. DSC traces (at a heating/cooling rate of 5 °C/min) with phase transition temperatures of RNA-DOAB complex, showing two transitions at -7 and 42 °C, corresponding to crystalline–smectic and smectic–isotropic transitions, respectively, showing complete reversibility of thermal cycles.

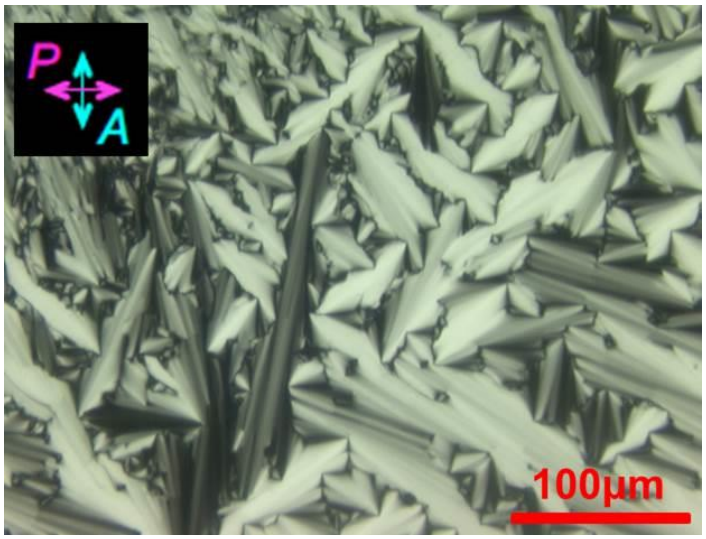

Fig. S4. POM image of the mesophase cooled from isotropic of RNA-DOAB complexes, showing well-defined focal-conic textures of smectic layers.

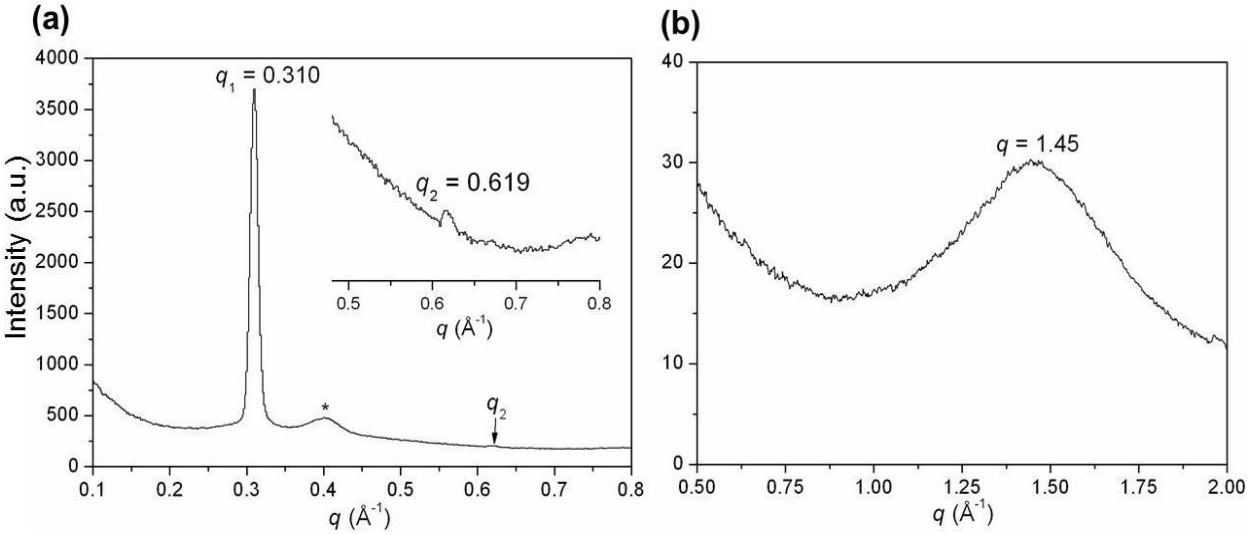

Figure S5. SAXS (a) and WAXS (b) profiles of unoriented RNA-DOAB sample at 25 °C upon cooling from the isotropic liquid to the smectic phase. The diffraction peaks at q_1 and q_2 are the first and second orders of the 20.3 Å layer spacing, whereas the broad peak (0.4 Å^{-1}) is due to the kapton diffraction, which is used for sample loading and sealing. The broad peak at 1.45 Å^{-1} confirms the amorphous halo of the disordered alkyl chains of DOAB.

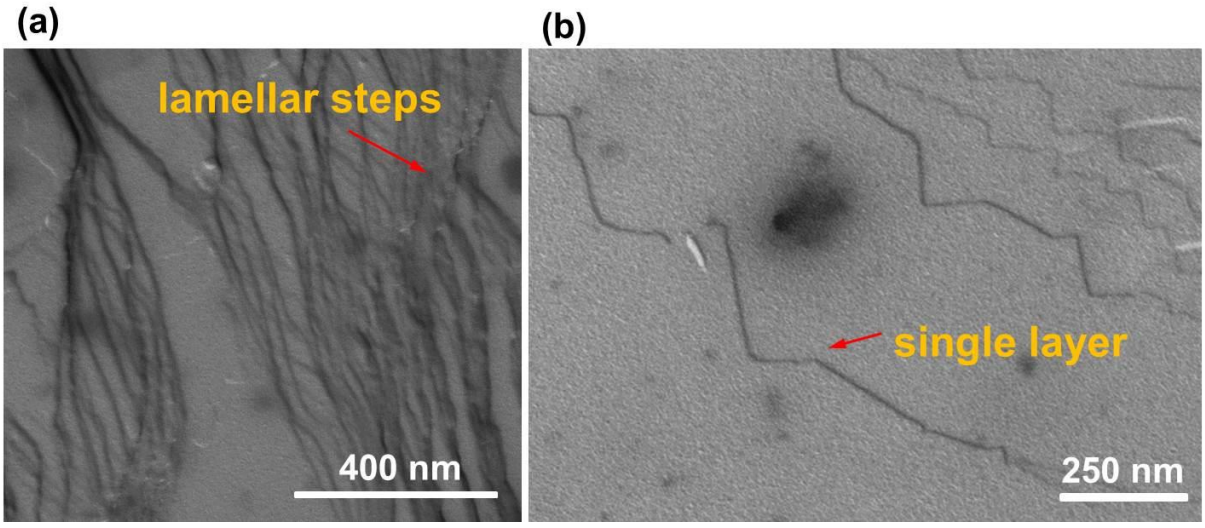

Figure S6. FF-TEM images of the 22mer single-stranded RNA-DOAB mesophase. The sample was quenched after cooling from isotropic (45 °C) to the desired temperature in the mesophase (25 °C), and then fractured in the bulk. (a) Lamellar structure of the RNA-DOAB with fractured distinct layer steps, and magnified in (b), homogeneous layer surfaces where ssRNA molecules randomly oriented within the sublayer.

References

1. M. Nakata, G. Zanchetta, B. D. Chapman, C. D. Jones, J. O. Cross, R. Pindak, T. Bellini, N. A. Clark, 2007, Science 318, 1276.
2. I. Koltover, T. Salditt, J. O. Rädler, C. R. Safinya, Science 1998, 281, 78.
3. I. W. Hamley, Soft Matter 2010,6, 1863.
4. A. D. Bangham, Liposome letters 1983 (Academic Press, New York).
5. T. E. Strzelecka, M. W. Davidson, R. L. Rill, Nature 1988, 331, 457.
6. F. Livolant, Physica A 1991, 176, 117.
7. F. Livolant, Y. Bouligand, J. Physique 1986, 47, 1813.
8. S. M. Yu, V. P. Conticello, G. Zhang, C. Kayser, M. J. Fournier, T. L. Mason, D. A. Tirrell, Nature 1997, 389, 167.
9. Z. Dogic, S. Fraden, Curr. Opinion in Coll. & Inter. Sci. 2006, 11, 47.
10. W. J. Chung, J. W. Oh, K. Kwak, B. Y. Lee, J. Meyer, E. Wang, A. Hexemer, S. W. Lee, Nature 2011, 478, 364.
11. A. Ramamoorthy, Thermotropic liquid crystals 2007 (Springer).
12. M. Briman , N. P. Armitage, E. Helgren, G. Grüner, Nano Lett. 2004, 4, 733.
13. C. Yamahata, D. Collard, T. Takekawa, M. Kumemura, G. Hashiguchi, H. Fujita, Biophys. J. 2008, 94, 63.
14. F. D. Lewis, T. Wu, Y. Zhang, R. L. Letsinger, S. R. Greenfield, M. R. Wasielewski, Science 1997, 277, 673.
15. K. Hamad-Schifferli, J. J. Schwartz, A. T. Santos, S. Zhang, J. M. Jacobson, Nature 2002, 415, 152.
16. G. A. Jeffrey, Acc. Chem. Res. 1986, 19, 168.
17. P. Sakya, J. M. Seddon, Liq. Cryst. 1997, 23, 409.
18. G. Milkereit, V. Vill, J Carbohyd. Chem. 2006,25, 615.
19. J. W. Goodby, V. Görtz, S. J. Cowling, G. Mackenzie, P. Martin, D. Plusquellec, T. Benvegnu, P. Boullanger, D. Lafont, Y. Queneau, S. Chambert, J. Fitremann, Chem. Soc. Rev. 2007, 36, 1971.
20. A. W. Perriman, H. Cölfen, R. W. Hughes, C. L. Barrie, S. Mann, Angew. Chem. Int. Ed. 2009, 48, 6242.
21. A. Wenzel, M. Antonietti, Adv. Mater. 1997, 9, 487.
22. S. Hanski , S. Junnila , L. Almásy , J. Ruokolainen , O. Ikkala, Macromolecules 2008, 41, 866.
23. S. Hanski, S. Junnila, A. J. Soininen, J. Ruokolainen, O. Ikkala, Biomacromolecules 2010, 11, 3440.
24. Tschierske C, Chem. Soc. Rev. 2007, 36, 1930.
25. C. McBride, C. Vega, J. Chem. Phys. 2002, 117, 10370.
26. C. F. J. Faul, M. Antonietti, Adv. Mater. 2003, 15, 673.
27. K. Tanaka, Y. Okahata, J. Am. Chem. Soc. 1996, 118, 10679.
28. Y. Okahata, T. Kobayashi, K. Tanaka, M. Shimomura, J. Am. Chem. Soc. 1998, 120, 6165.
29. T. Neumann, S. Gajria, N. F. Bouxsein, L. Jaeger, M. Tirrell, J. Am. Chem. Soc. 2010, 132, 7025.
30. S. Gajria, T. Neumann, M. Tirrell, Wiley Interdiscip. Rev. Nanomed. Nanobiotechnol. 2011, 3, 479.
31. S. Zhou, D. Liang, C. Burger, F. Yeh, B. Chu, Biomacromolecules 2004, 5, 1256.
32. G. W. Gray, J. W. G. Goodby, Smectic liquid crystals 1984 (Leonard Hill, Glasgow).
33. J. Zhou, S. K. Gregurick, S. Krueger, F. P. Schwarz, Biophys. J. 2006, 90, 544.
34. N. F. Bouxsein, C. Leal, C. S. McAllister, K. K. Ewert, Y. Li, C. E. Samuel, C. R. Safinya, J. Am. Chem. Soc. 2011, 133, 7585.
35. N. J. Servers, Nat. Protoc. 2007, 2, 547.
36. F. E. Alemdaroglu, K. Ding, R. Berger, A. Herrmann, Angew. Chem. Int. Ed. 2006, 45, 4206.

Chapter 3

Solvent-free DNA fluids

Abstract

Since DNA exhibits persistent structures with dimensions that exceed the range of their intermolecular forces, solid-state DNA undergoes thermal degradation at elevated temperatures. Therefore, the realization of solvent-free DNA fluids, including liquid crystals and liquids, still remains a significant challenge. To address this intriguing issue, we demonstrate that combining DNA with suitable cationic surfactants, followed by dehydration, can be a simple generic scheme for producing these solvent-free DNA fluid systems. In the anhydrous smectic liquid crystalline phase, DNA sublayers are intercalated between aliphatic hydrocarbon sublayers. The lengths of the DNA and surfactant are found to be extremely important in tuning the physical properties of the fluids. Stable liquid crystalline and liquid phases are obtained in the -20°C to 200°C temperature range without thermal degradation of the DNA. Thus, a new type of DNA-based soft biomaterial has been achieved which will promote the study and application of DNA in a much broader context.

Introduction

The potential for designing intrinsically addressable and stimuli-responsive functionalities marks DNA as a unique information-encoding biopolymer compatible with technologies that bridge materials and life sciences[1-6]. Although most investigations of DNA-based functional materials are currently limited to aqueous solutions and hydrogels[1-14], research examining the solvent-free and solid-state properties of DNA is gaining momentum, due to its relevance to biomaterials-inspired drug and gene delivery as well as optoelectronic applications[15-18]. Additionally, softening solid-state DNA to realize its fluidity and ordering (in liquids and liquid crystals) in the absence of any solvent would be of much benefit to a variety of scientific and technological pursuits. For instance, DNA melts might replace acrylate based polymeric ionic liquids as dispersion medium for organic and inorganic moieties if biodegradability is desired[19]. As chemically modified oligonucleotides, they might act as reactive inks to functionalize biochips[20]. Moreover, such materials can be processed easily under solvent-free conditions, which offers opportunities for the development of flexible and printable DNA electronic components, where water is detrimental for device performance. From a fundamental perspective, solvent-free DNA liquid crystals allows for the manipulation of ordering and fluidity; these systems may exhibit novel ensemble properties, e.g. regarding their mechanical (viscoelastic) behavior, which are significantly distinct from typical dissolved DNA systems or traditional organic liquid crystals. However, in the absence of any solvent, pristine DNA cannot undergo a heat-induced transition to the liquid-crystalline, or liquid phases because its dimensions exceed the interaction range of the intermolecular forces of its constituent parts[21]. As a consequence, solid-state DNA only undergoes thermal degradation at elevated temperatures in ambient conditions[22]. Thus, we explore several approaches to fabricating solvent-free DNA fluids.

In recent years, the study of supramolecular chemistry has improved our understanding of non-covalent interactions (e.g., hydrogen bonding, electrostatic forces, van der Waals and dipolar forces) between DNA building blocks and synthetic organic and inorganic molecules[23-26]. This approach expands DNA assembly beyond the boundaries of Watson–Crick base pairing into remarkably diverse architectures and sophisticated functionalities. Inspired by some work pertaining to supramolecular ionic assembly[11-19,26-30], herein we report the fabrication of a series of novel solvent-free DNA fluids which exhibit ordered liquid crystalline and isotropic liquid phases (Figure 1). In the present experiments, electrostatic interactions couple these DNA and surfactants into hybrid assemblies, in which the flexible alkyl chains of the surfactants suppress crystallization. A series of solvent-free DNA melts (smectic ordered mesophases and isotropic liquids) has been achieved with controllable phase transition temperatures ranging from -20 °C to 130 °C. These materials are stable up to 200 °C and exhibit low viscosities. This study paves the way to accessing the properties of DNA liquids and

liquid crystals in the absence of any solvent, without thermal degradation of the DNA components.

Results and discussions

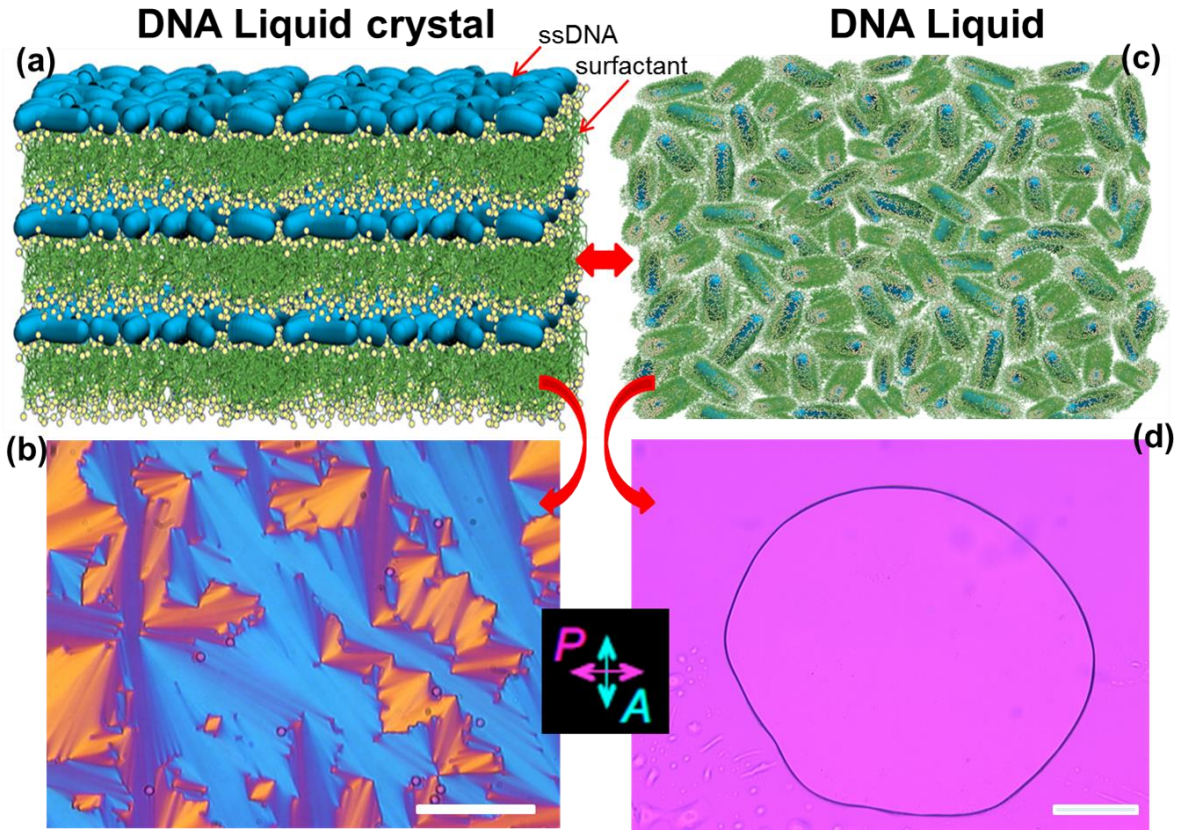

Figure 1. Solvent-free DNA-surfactant melts with phase transitions between liquid crystal and isotropic liquid. (a) Proposed lamellar bilayer structure in the liquid crystalline phase. The bilayer structure is made of one sublayer of single stranded DNA and one sublayer of interdigitated surfactants, where the phosphate groups in the DNA electrostatically interact with the cationic head groups of the surfactants. (b) Typical polarized optical microscopy (POM) image of the DNA-surfactant mesophases (here taking a 14mer DNA-DEAB as an example, 70 °C, DEAB: didecyldimethylammonium bromide), showing well-defined focal-conic textures of smectic layers. (c) Schematic of disordered DNA-surfactant complex in the isotropic liquid phase and (d) corresponding POM image of the isotropic liquid (14mer DNA-DEAB, 125 °C) not showing any birefringent textures. Both POM images were acquired with an inserted one quarter wave plate. The scale bar is 100 μm.

Solvent-free DNA-surfactant melts were prepared by electrostatic complexation of a single-stranded oligonucleotide (6mer, 14mer, 22mer, 50mer and 110mer) with a cationic lipid containing linear, flexible alkyl tails. Three surfactants with two aliphatic chains of variable lengths, i.e. dioctyldimethylammonium bromide (DOAB), didecyldimethylammonium bromide (DEAB), and didodecyldimethylammonium bromide (DDAB), were used to prepare the stable DNA-surfactant mesophases and liquid phases. Polarized optical microscopy (POM) images showed that the DNA liquid crystals which are formed from the melted polycrystalline phases (supplementary Figure S1), exhibit typical focal-conic textures characteristic of smectic lamellar

structures[31,32] (Figure 1b and supplementary S2). After heating above the clearing temperatures, the DNA-surfactant complexes transition into the disordered liquid state (Figure 1c), wherein the oligonucleotide-surfactant chains are randomly disordered. The birefringent focal-conic textures melt away completely (Figure 1d), leaving only the transparent isotropic fluid (supplementary Figure S3).

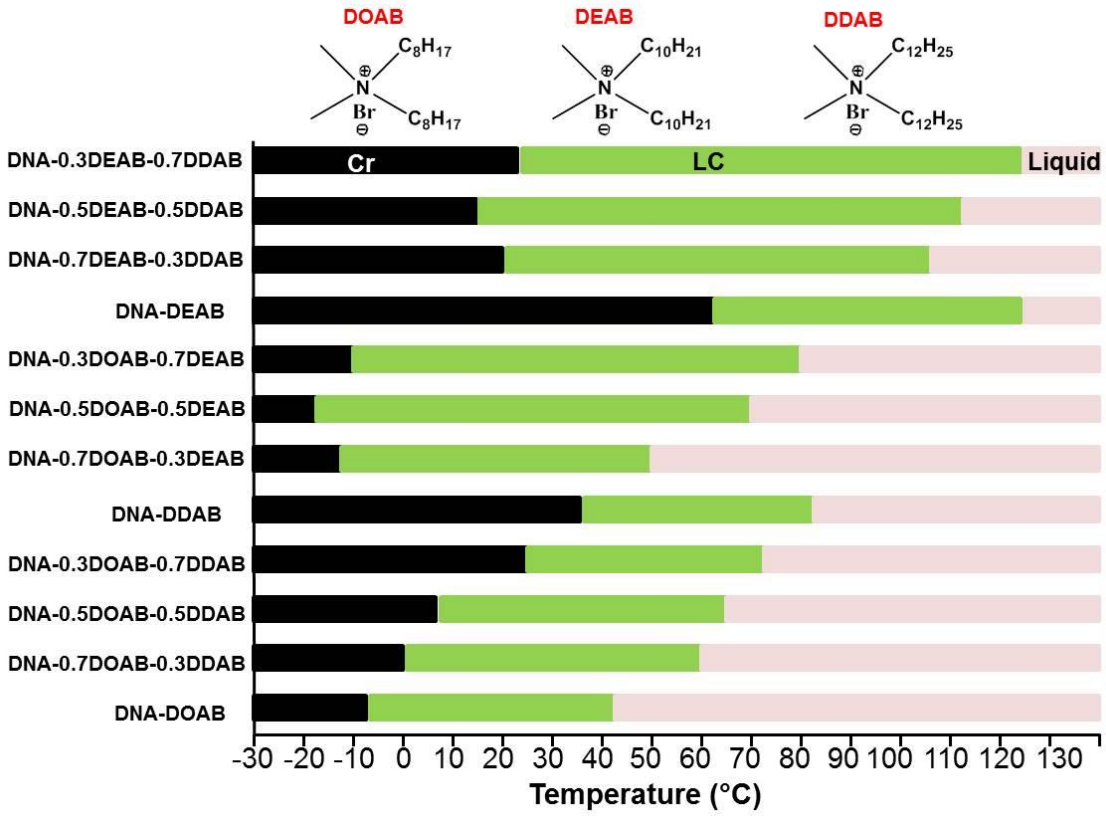

Figure 2. Overview of phase transition temperatures (melting/clearing points) of binary and ternary DNA-surfactant complexes from crystalline (Cr) to liquid crystalline (LC) and then to isotropic liquid, which depend strongly on the specific length of the aliphatic chains of the surfactants. (DOAB: dioctyldimethylammonium bromide, DEAB: didecyldimethylammonium bromide, and DDAB: didodecyldimethylammonium bromide). The data were obtained from the second heating cycle of DSC measurements. Heating/cooling rate was 5 °C/min.

Subsequently, the thermal properties of binary complexes (DNA-DOAB, DNA-DEAB, and DNA-DDAB) and ternary complexes (DNA-xDOAB-yDEAB, DNA-xDOAB-yDDAB, and DNA-xDEAB-yDDAB, x+y=1) were investigated. x and y denote the fraction of the respective surfactant complexed to DNA assuming a ratio of surfactant to nucleotide of 1:1. Thermogravimetric analysis (TGA) showed that the DNA-surfactant melts have a water content of less than 3% (wt) and that they are thermally stable over a wide range of temperatures until decomposition at approximately 200 °C occurs (supplementary Figure S4). Differential scanning calorimetry (DSC) results indicated that all the complexes have two endothermic peaks, corresponding to the crystal-liquid crystal and liquid crystal-isotropic phase transitions, respectively (supplementary Figure S5). As summarized in Figure 2, the phase transition temperatures of DNA-surfactant

complexes can be controlled over a wide temperature range. Melting temperatures are tunable from around -20 °C to 65 °C, and clearing temperatures are broadly dispersed between 41 °C and ~130 °C, indicating that the cooperative interactions between the DNA and the surfactants are very important for preventing DNA aggregation and stabilizing the various phases. Interestingly, we found a correlation between the phase transition temperatures and the length of the surfactant alkyl chains. When the aliphatic chain length of the surfactant is increased in the binary (or ternary) complexes, the melting and clearing points are generally increased. This confirms that the van der Waals interactions between the adjacent alkyl chains of the surfactants[33,34] primarily determine the melting and clearing points in the DNA-surfactant complexes. Longer aliphatic chains of surfactants result in an increase in the melting and clearing temperatures. This behavior is marginally influenced by varying the DNA length from 6 to 110 nucleotides. Thus, the chemical nature of the surfactant dominates the phase transition behavior of the DNA-surfactant melts.

Next, the ordered structural features of DNA-surfactant fluids were analyzed by small-angle X-ray scattering (SAXS). In their mesophases, the sharp first order reflection peaks and the following harmonics are characteristic of long-range ordered lamellar structures (Figure 3a). Elongation of the surfactant alkyl chain length leads to a clear shift in the first-order reflections (from 0.294 to 0.238 $Å^{-1}$), corresponding to an increase in the layer spacing from 21.4 Å to 26.4 Å for different ternary complexes. When DNA of different lengths (6mer, 14mer, 22mer, 50mer, 110mer) are complexed with a given surfactant, lamellar distances are retained (supplementary Figure S6). This indicates that the lamellar spacing of the mesophase DNA-surfactant assemblies can be controlled by choosing surfactants with desired alky chains. Considering the dimensions of the single-stranded DNA and the surfactants, the smectic lamellar structures must be made of alternating DNA sublayers of ~10 Å thickness[35] and interdigitated surfactant bilayers of ~11.4–16.4 Å thickness (Figure 1a). Each repeating layer consists of tail-to-tail interacting cationic surfactants that electrostatically interact with the anionic DNA segments. Short range alignment of the DNA-surfactant liquid crystals was investigated by wide-angle X-ray scattering (WAXS) (supplementary Figure S7). When the alkyl chain length of a surfactant is short, only one broad peak at around 1.41 $Å^{-1}$ is observed, corresponding to the typical distance of ~4.5Å between neighboring alkyl chains[36,37]. As the length of the aliphatic chains was increased, the WAXS profiles exhibit one or two reflections between 1.38-1.52 $Å^{-1}$, indicating ordered intralayer packing of the molten alky chains. We observed no reflection peak from the DNA intralayer packing, which suggests that the oligonucleotide chains are randomly packed within the sublayer without any preferential orientation. The topography of the lamellar structure was visualized directly by freeze-fracture transmission electron microscopy (FF-TEM) (Figure 3b). The flat and smooth layer surfaces of the DNA-surfactant liquid crystal exhibit long-range ordering, and are separated by distinct and continuous steps. This confirms liquid crystalline smectic layer ordering.

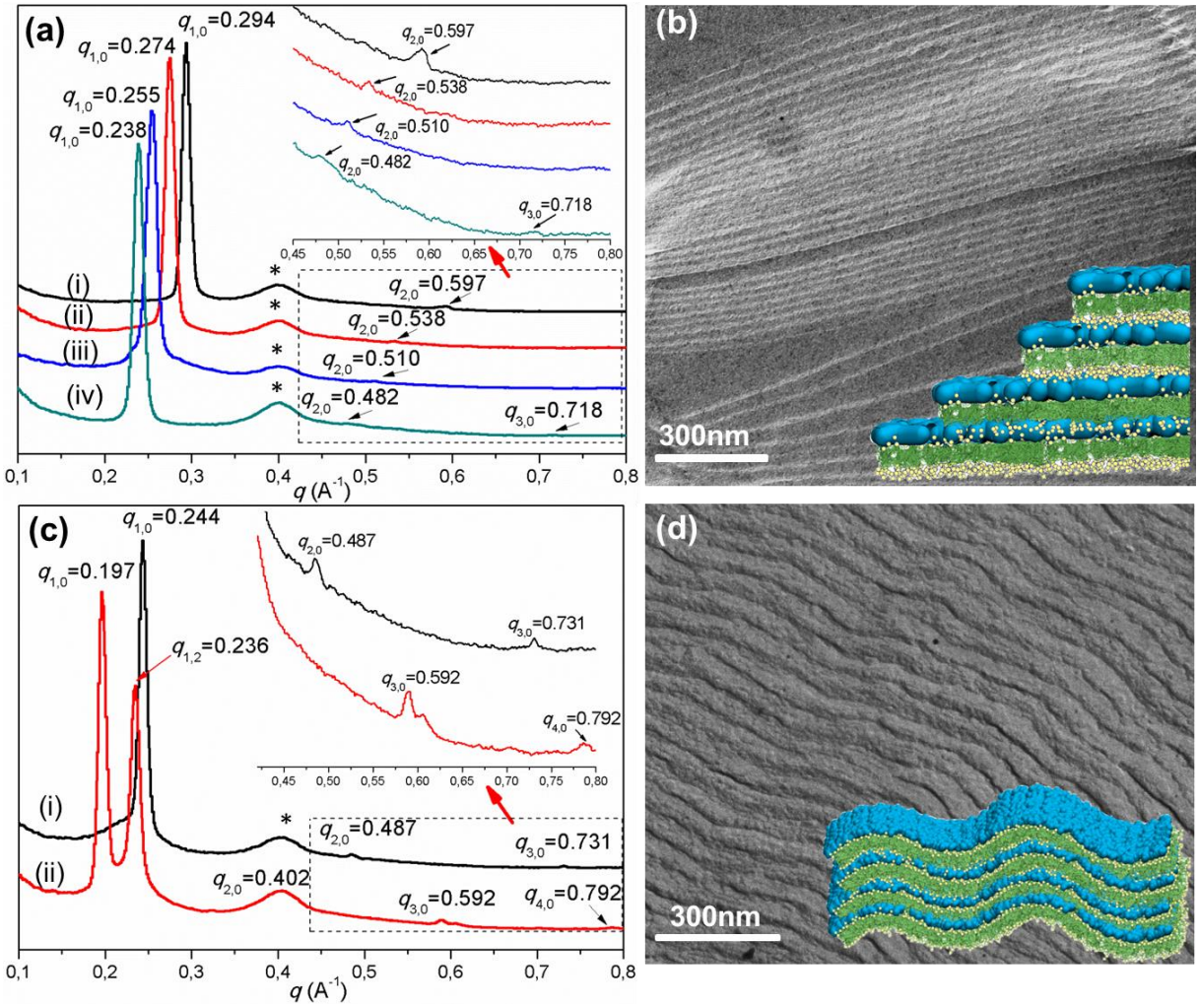

Figure 3. Structure analysis of DNA-surfactant complex mesophases. (a) Representative SAXS profiles of the first order reflections and their harmonics (25 °C, black curve, 14mer DNA-0.7DOAB-0.3DEAB; red curve, 14mer DNA-0.3DOAB-0.7DEAB; blue curve, 14mer DNA-0.5DOAB-0.5DDAB; green curve, 14mer DNA-0.5DEAB-0.5DDAB), indicating long-range ordered smectic liquid crystal phases. The lamellar layer spacing depends on the length of the aliphatic chains on the surfactants. The broad diffraction peak at q=0.4 Å^{-1} (labeled with *) is due to the kapton, which is used for sample loading and sealing. (b) Corresponding freeze-fracture transmission electron microscopy (FF-TEM) image (here taking 14mer DNA-0.5DOAB-0.5DEAB as the example), showing distinct layer steps, with the molecular model of the fracture topography sketched in the inset. (c) SAXS profiles of 14mer DNA-DDAB complex with the typical smectic (black cruve, 75 °C) and modulated smectic (red curve, 50 °C) mesophases. In (a) and (c), q vector is indexed as (*s, m*), where s is along the layer normal and m is in the layer plane. The multiple peaks ($q_{1,0}$ = 0.197, $q_{1,2}$ = 0.236) in (c, red curve), indicate an modulated smectic structure of two-dimensional ordering. (d) Corresponding FF-TEM image of undulation stripes, and a corresponding model of the modulation in the inset, showing the two-dimensional periodic structure.

During the X-ray analysis of DNA-DDAB complex an isotropic-smectic-modulated smectic phase (Sm_{mod}) sequence was found. As expected for a typical smectic phase, at 70 °C the SAXS spectrum of DNA-DDAB revealed a well-defined lamellar diffraction peak at q = 0.244 Å^{-1} and its harmonics (q = 0.487, 0.731 Å^{-1}), indicating a layer spacing of 25.7 Å (Figure 3c). However, when cooled to 50 °C, the layer spacing increased from d

= 25.7 Å to d = 31.8 Å (Figure 3c, q = 0.197 $Å^{-1}$). Moreover, a subsidiary satellite peak at 0.236 $Å^{-1}$ close to the smectic layer reflection peak was detected. It is indexed as (*s, m*) = (*1, 2*), where s indicates the direction along the layer normal and m represents the orientation in the layer plane, expressing an additional periodicity perpendicular to the layer normal, i.e. an in-plane layer undulation[38,39]. The periodic pattern of layer undulations was clearly observed by FF-TEM (Figure 3d). Modulated crests and troughs are aligned alternatively on the fractured surfaces and propagate along different layers without disruption of the smectic lamellar structure.

Furthermore, SAXS analysis of the DNA-surfactant melts in the isotropic liquid states showed no clear diffraction, with only one very broad halo at 0.29 $Å^{-1}$ associated with disordered DNA-surfactant scattering (21.7 Å) (supplementary Figure S8). WAXS gave another broad halo at ~1.40 $Å^{-1}$ that corresponds to the average distance (4.5 Å) between the liquid-like aliphatic chains (supplementary Figure S9).

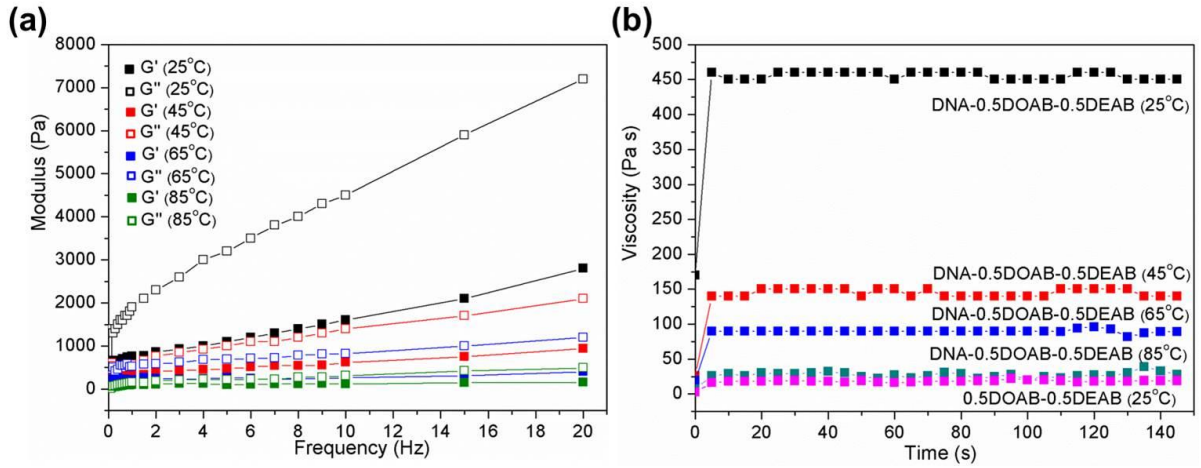

Figure 4. Rheological behavior of solvent-free DNA-surfactant fluids. (a) Temperature-dependent storage (*G′*) and loss (*G″*) moduli curves as a function of frequency with the strain amplitude (γ = 10%) and (b) viscosity (*f* = 1 Hz, γ = 10%) (here 14mer DNA-0.5DOAB-0.5DEAB as an example).

To study the viscoelastic properties of solvent-free DNA-surfactant fluids, shear rheometry was applied. Storage modulus (*G′*) representing the elastic portion and loss modulus (*G″*) representing the viscous portion were measured at an applied strain amplitude (γ) of 10%. We observed liquid-like behaviors in both liquid crystalline and isotropic liquid phases, as evidenced by the larger loss modulus (*G″*) compared to the storage modulus (*G′*) over the measured frequency range (Figure 4a). Notably, the values of the loss and storage moduli become much smaller with heating from the liquid crystalline to isotropic liquid phases. It is also noteworthy that when the shear strain amplitude increased in the mesophase, the frequency-dependent *G″* and *G′* moduli values decreased (supplementary Figure S10a), implying that the existing lamellar structure was disrupted over the course of the experiment. In contrast, the isotropic liquids did not show such a strong dependence on the shear strain (supplementary Figure S10b). In addition, it was found that viscosity decreased significantly upon

transition from the liquid crystal to the isotropic liquid (Figure 4b). This might be due to the absence of inter-layer friction of DNA-surfactant complex layers and the increased molecular mobility at higher temperatures in the melt. The viscosity of the 14mer DNA-surfactant fluid in the isotropic liquid phase equals to approximately 24 Pa•s, which is indicative of a Newtonian liquid. It should be added that there is a clear correlation between the viscosity of the soft DNA-surfactant biomaterials and the alkyl chain lengths of the surfactants. The magnitude of the viscosity increases with longer alkyl chain length (supplementary Figure S11a). We presume that the friction is partly due to the strong alkyl chain tail-tail interactions of the elongated surfactants. Furthermore, rheological investigations of the 6mer, 22mer, 50mer and 110mer DNA melts clearly indicate that the viscosity increases with DNA length (supplementary Figure S11b).

The above POM, TGA, DSC, SAXS, WAXS, FF-TEM, and rheology results indicate that fluidity and ordering are inherent characteristics of the DNA-surfactant complex in the absence of solvents. Electrostatic complexation between the DNA and surfactant increases the range of the intermolecular force field to a length scale that is commensurate with the size of the DNA molecules, and simultaneously coordinates them into hybrid assemblies which order into lamellar structures of alternating DNA and surfactant layers, thereby enabling thermally induced liquid crystal and isotropic liquid formation. This new class of DNA fluids is a bulk material, which differs significantly from other reported electrostatic complexes of DNA. With its characteristics of being solvent free and at the same time mosophase forming it does not compare to simple DNA liquids containing electrostatically bound poly(ethylene glycol) units[27,28], neither to DNA lipid complexes that require a solvent to adopt mesophases[11-14] nor to DNA-surfactant complex solids missing a liquid crystalline phase[15-18]. Furthermore, the DNA molecules can be liberated from the dehydrated fluidic phases by exposure to saturated NaCl solution allowing dissolution in aqueous phase.

Conclusions

A series of solvent-free DNA fluids exhibiting both liquid crystal ordering and melting into isotropic liquids have been generated by electrostatic complexation of DNA with surfactants containing two flexible alkyl chains. Equipping the nucleic acid backbone with surfactants allows disrupting of attractive intermolecular DNA interactions (π-π and hydrogen bonds) and at the same time introduces van der Waals forces enabling fluid and ordering behavior. Well-defined lamellar superstructures of planar and undulated DNA sublayers separated by surfactant bilayers have been realized. Phase transitions in these materials can be controlled over an extremely broad temperature range. Fluid DNA was already achieved at temperatures as low as -20 °C and the transition from the crystal to the liquid crystal can be adjusted up to 65 °C. The liquid crystal to isotropic liquid-transition can be tuned between 41 °C and 130 °C by selection

of the appropriate surfactants. Our solvent-free DNA fluids have negligible volatility, exhibit high DNA content and low viscosity that depends on the surfactant alkyl chain length and molecular weight of the DNA, which might be suitable for use as injectable biomaterials. Finally, the high thermal stability up to 200 °C might make this class of soft condensed DNA material amenable to a broad range of new investigations differing a lot from current applications of DNA pursued in an aqueous environment.

Experimental Section

Materials

The surfactants used for the DNA complex formation, including dioctyldimethylammonium bromide (DOAB) and didodecyldimethylammonium bromide (DDAB) were purchased from ABCR (Germany), and didecyldimethylammonium bromide (DEAB) was aquired from Sigma–Aldrich. Single-stranded DNA, including 6mer (5'-CCT CGC-3', Mw=1728 g/mol), 14mer (5'-CCT CGC TCT GCT AA-3', Mw=4175 g/mol) and 22mer (5'-CCT CGC TCT GCT AAT CCT GTT A-3', Mw=6612 g/mol) were synthesized by conventional solid-phase synthesis method.[10] Longer DNA strands, including the 50mer (5'-CCT CGC TCT GCT AAT CCT GTT ACC TCG CTC TGC TAA TCC TGT TAC CTC GC-3', Mw=15077 g/mol) and 110mer (5'-CCT CGC TCT GCT AAT CCT GTT ACC TCG CTC TGC TAA TCC TGT TAC CTC GCT CTG CTA ATC CTG TTA CCT CGC TCT GCT AAT CCT GTT ACC TCG CTC TGC TAA TCC TGT TA-3', Mw=33309 g/mol) were purchased from BIOMERS (Germany).

DNA-surfactant complex preparation

The single-stranded DNA (6mer, 14mer, 22mer, 50mer and 110mer) was pretreated by precipitating a ~300 μM DNA solution containing 5 M NaCl with cold ethanol (-20 °C). From this precipitate an aqueous DNA solution (~300 μM) was prepared employing ultrapure water. In a second solution made from ultrapure water, the concentration of single surfactant (DOAB, DEAB and DDAB) or two surfactant mixtures (DOAB:DEAB, DOAB:DDAB and DEAB:DDAB, molar ratios 7:3, 5:5 and 3:7) were adjusted to 5-10 mM at room temperature. Both the DNA and surfactant solutions (~5 mol equivalents of surfactant relative to nucleotides of the DNA) were mixed together and as a result the insoluble complexes precipitated from the aqueous phase. After centrifugation, the water and unreacted surfactants were removed, and finally the complexes were lyophilized overnight before further characterization.

Characterization of DNA-surfactant complexes

Thermogravimetric analysis (TGA) and differential scanning calorimetry (DSC) were carried out using a TA Instruments Q1000 system in a nitrogen atmosphere and with a heating/cooling rate of 5 °C/min. Polarized optical microscopy (POM) was conducted on a Zeiss Axiophot using the same temperature program as employed for the DSC

experiments. Small-angle and wide-angle X-ray scattering (SAXS and WAXS) with heating and cooling systems were performed by employing a conventional X-ray source with radiation wavelength of λ = 1.54 Å. For SAXS, a Bruker Nano/microstar instrument was used to obtain small angle scattering profiles, where the sample-to-detector distance was 24 cm. WAXS was carried out with a home-made, rotating-anode-based setup[40], where the sample-to-detector distance was 13 cm. Freeze-fractured transmission electron microscopy (FF-TEM) was carried out according to standard protocols[41]. A shear strain controlled Bohlin VOR rheometer (Bohlin Reologi AB) with two stainless steel fixtures[42] was used to study the viscoelastic properties.

Supplementary Figures

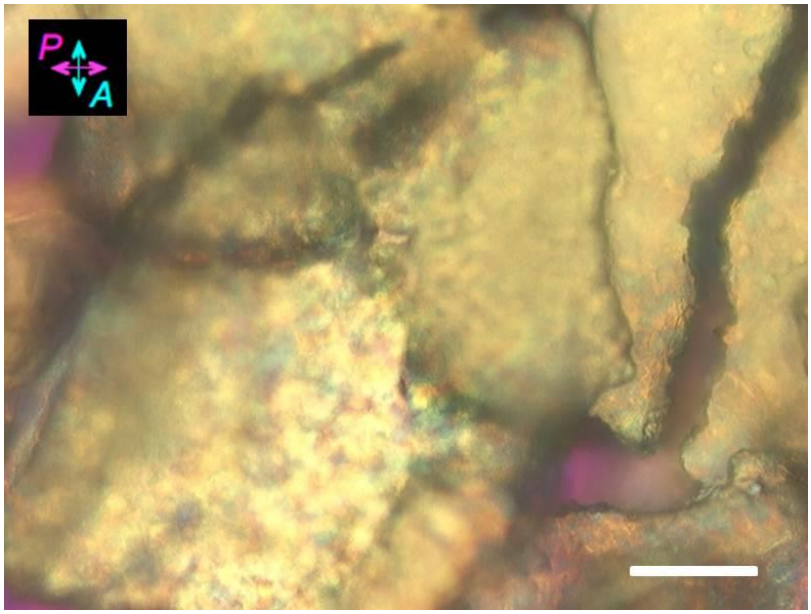

Figure S1. Typical polarized optical microscopy (POM) image of the DNA-surfactant complex in the polycrystalline phase (example is 14mer DNA-DEAB below 65 °C, DEAB: didecyldimethylammonium bromide). Scale bar is 100 μm. POM image was acquired with an inserted one quarter wave plate.

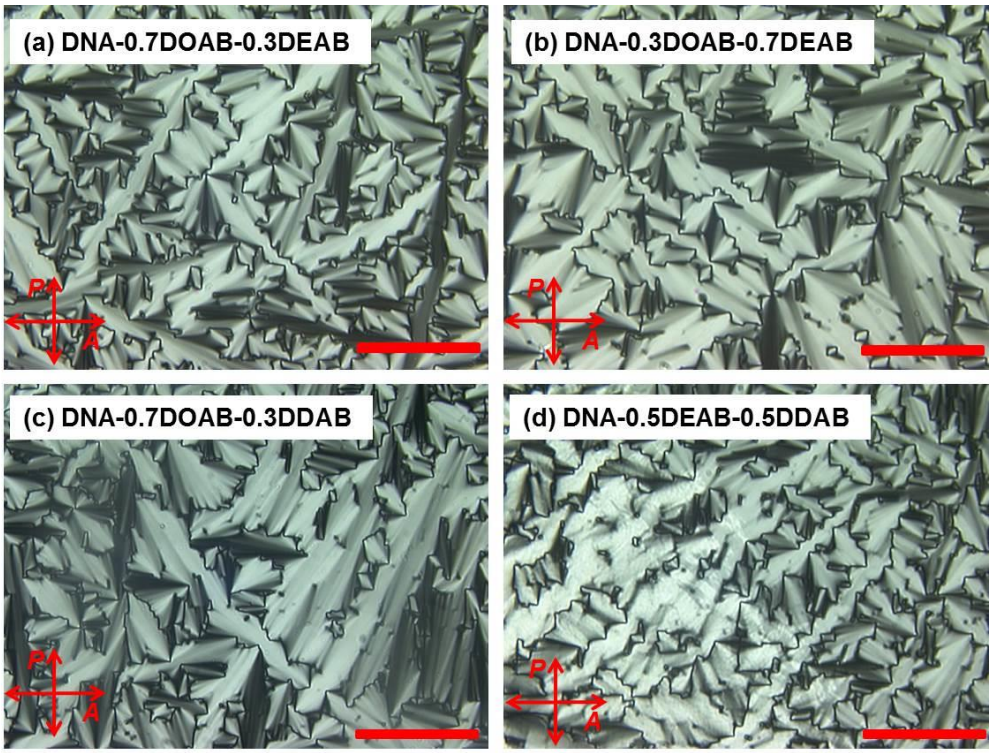

Figure S2. Representative POM images of solvent-free 14mer DNA-surfactant liquid crystals at 25 °C. Typical focal-conic textures characteristic of smectic lamellar structures were observed (scale bar is 100 μm).

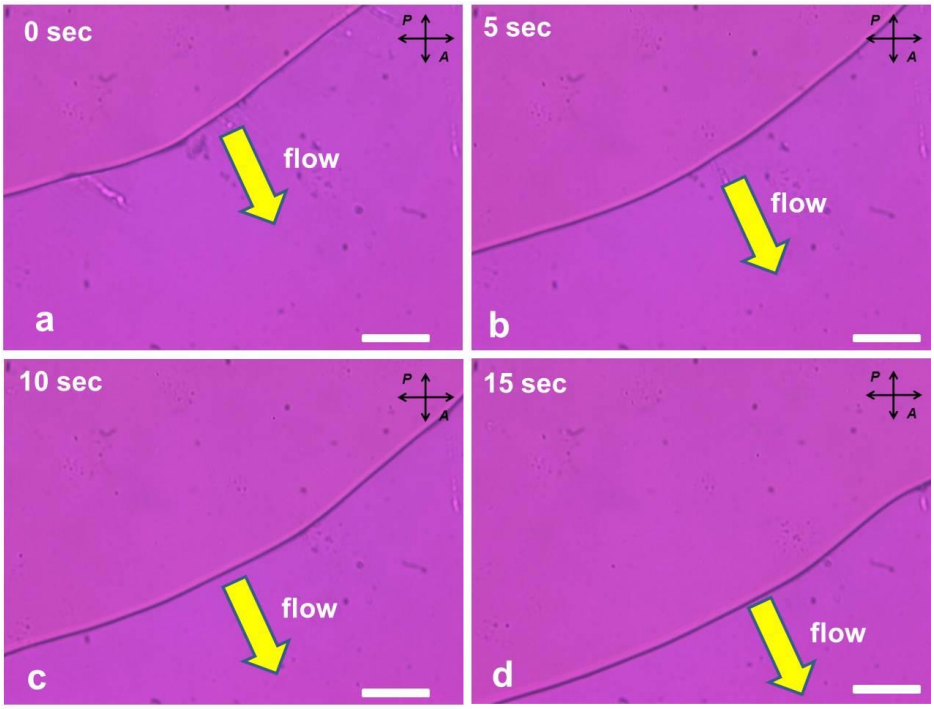

Figure S3. A series of POM images (insertion of a quarter wave plate) of molten DNA-surfactant complex (here taking 14mer DNA-DEAB as an example) in the liquid phase at 130 °C. The images confirm the fluidity of the DNA-surfactant melts. The scale bar is 100 μm.

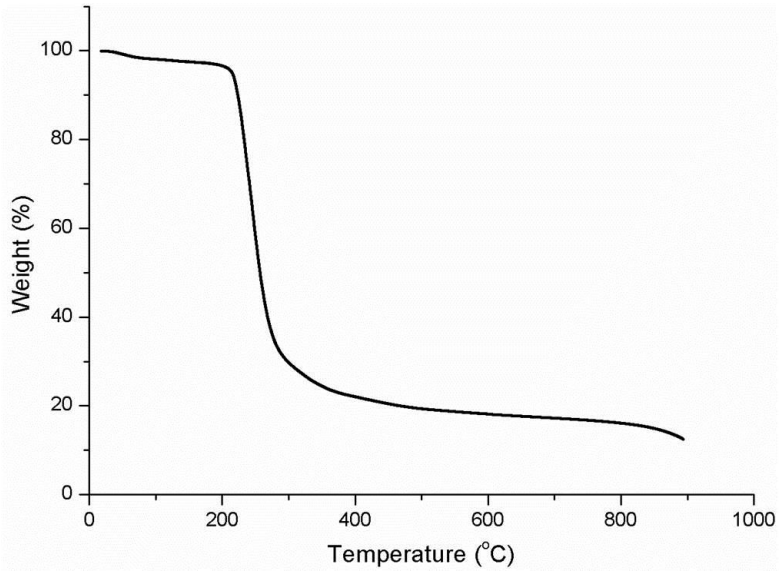

Figure S4. TGA analysis of a solvent-free DNA-surfactant complex (here taking 14mer DNA-DDAB as an example). It indicates that the complex had a water content of less than 3% and thermal degradation started at around 200 °C.

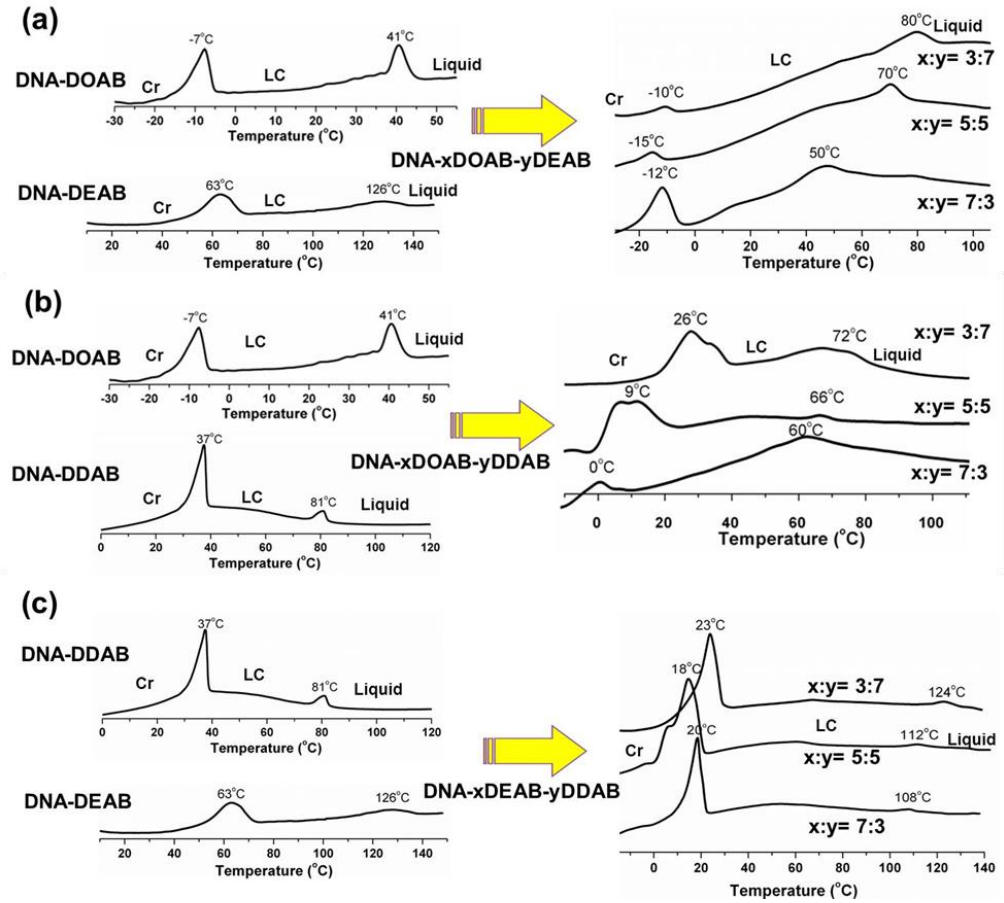

Figure S5. DSC analysis of binary and ternary 14mer DNA-surfactant complexes. The traces represent the second heating cycle. Heating rate was 5 °C/min. (a) DNA-DOAB-DEAB system. (b) DNA-DOAB-DDAB system. (c) DNA-DEAB-DDAB system. The DSC results demonstrate that the phase transition temperatures of the DNA-surfactant complexes can be controlled over a wide temperature range.

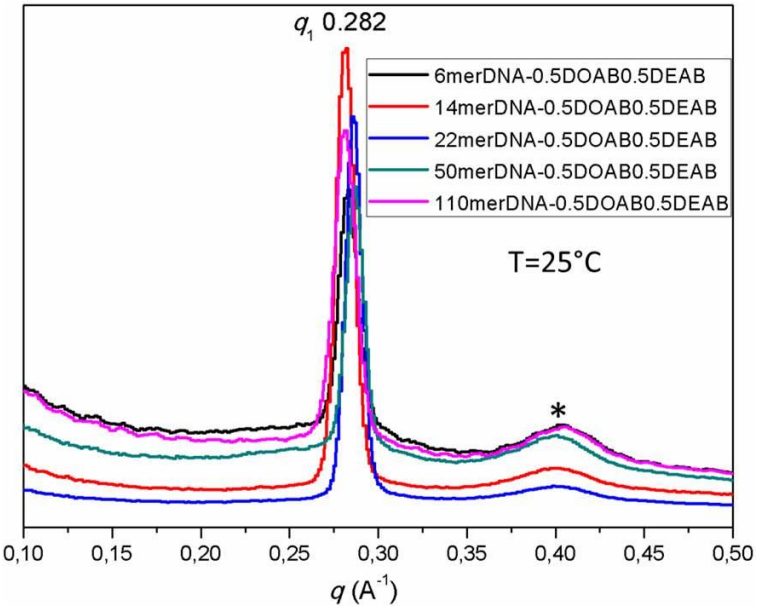

Figure S6. SAXS profiles of a series of DNA-surfactant melts (6mer DNA, 14mer DNA, 22mer DNA, 50mer DNA, 110mer DNA) complexed with the same mixed surfactants (here taking 0.5DOAB-0.5DEAB as the surfactant mixture). All the sharp first order reflection peaks at 0.282 Å^{-1}, correspond to a layer spacing of about 22.3 Å, which consists of alternating DNA sublayers of ~10 Å thickness and interdigitated surfactant bilayers of ~12.3 Å thickness. The broad diffraction peak at q~0.4 Å^{-1} (labeled with *) is due to the kapton, which is used for sample loading and sealing.

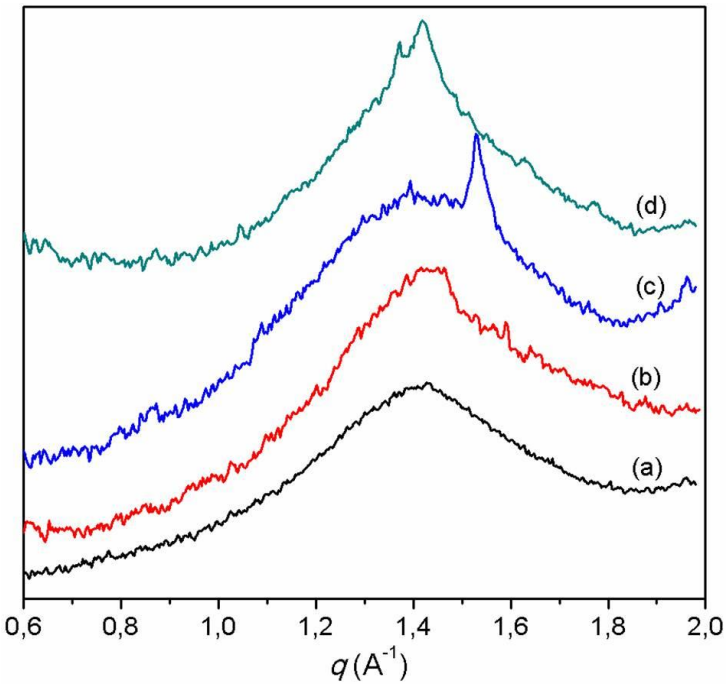

Figure S7. WAXS profiles of solvent-free 14mer DNA-surfactant complexes in their liquid crystal phases (25 °C, a, DNA-0.7DOAB-0.3DEAB; b, DNA-0.3DOAB-0.7DEAB; c, DNA-0.5DOAB-0.5DDAB; d, DNA-0.5DEAB-0.5DDAB). As we increase the lengths of aliphatic hydrocarbon tails, one or two reflections at 1.38-1.52 Å^{-1} become more and more prominent, indicating that the intralayer packing of the molten alky chains becomes more ordered.

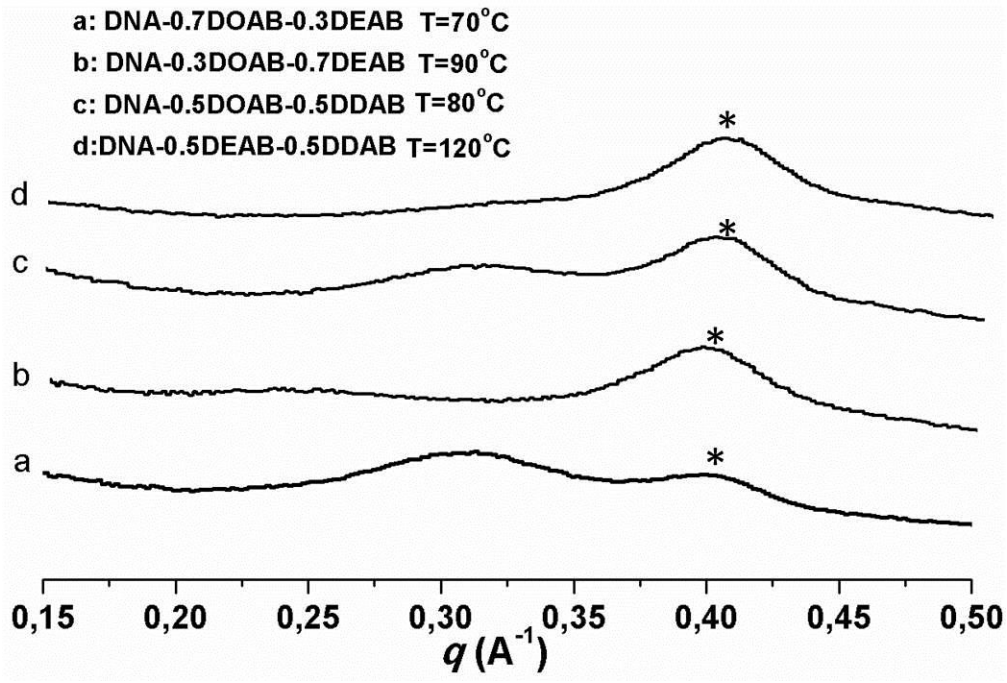

Figure S8. SAXS profiles of solvent-free 14mer DNA-surfactant complexes in the isotropic liquid phases. We observe no diffraction peaks associated with discrete layers, and only a very broad and weak halo at 0.29 Å-1 associated with disordered DNA-surfactant scattering (21.7 Å). The broad diffraction peak at q~0.4 $Å^{-1}$ (labeled with *) is due to the kapton, which is used for sample loading and sealing.

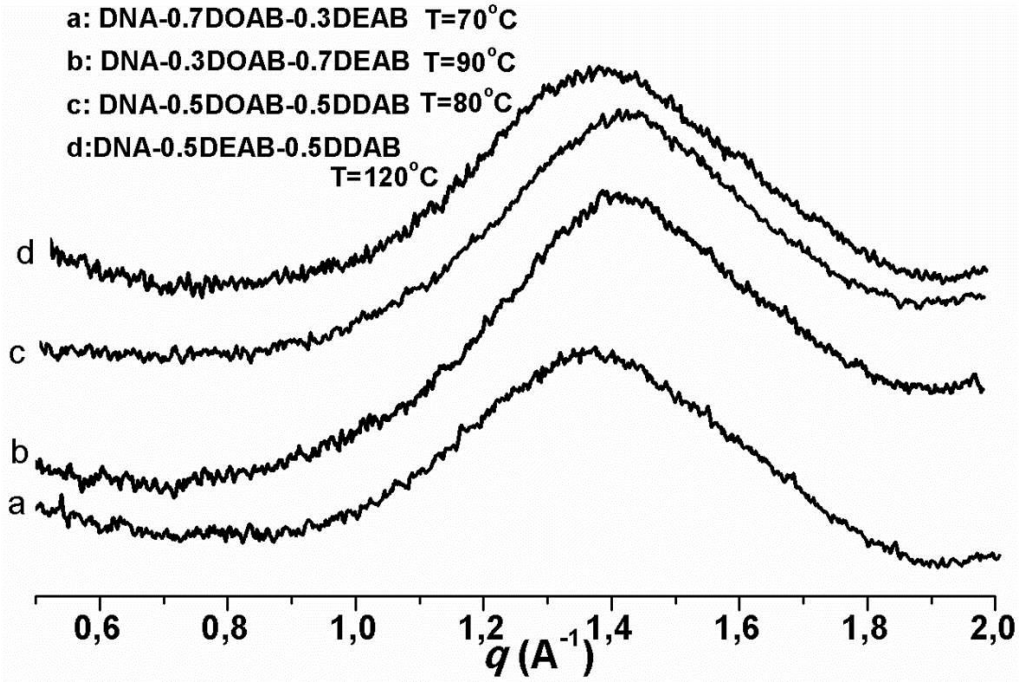

Figure S9. WAXS profiles of solvent-free 14mer DNA-surfactant complexes in the isotropic liquid phases. Only one broad halo appears at 1.40-1.45 $Å^{-1}$ in the samples, corresponding to the scattering of the liquid-like aliphatic chains.

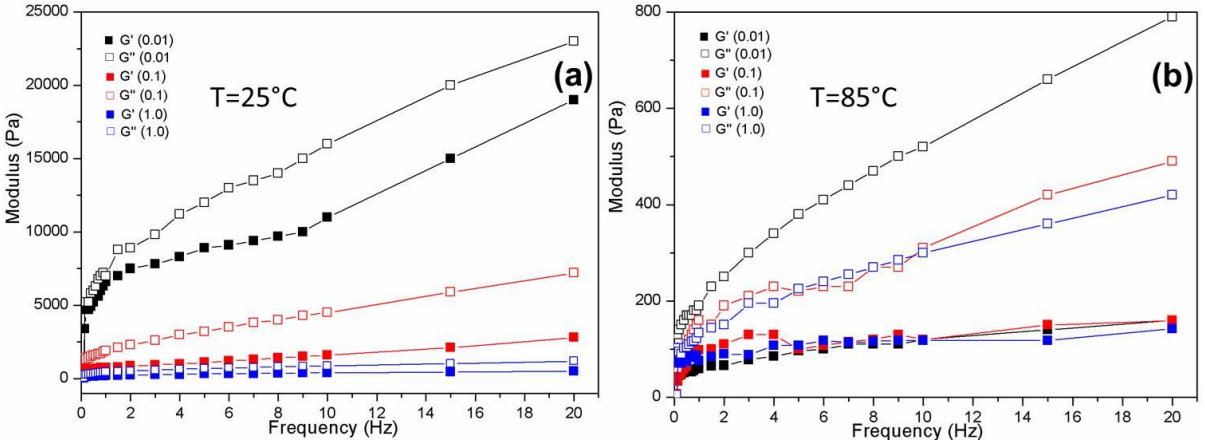

Figure S10. Rheological behaviors of solvent-free DNA-surfactant melts (here taking 14mer DNA-0.5DOAB-0.5DEAB as the example). Storage (G') and loss (G'') modulus curves of the DNA-0.5DOAB0.5DEAB liquid crystal at 25 °C (a) and liquid at 85 °C (b) as a function of frequency with varying strain (0.01, 0.1 and 1.0). In the mesophase, the frequency-dependent G'' and G' moduli values decreased with increasing strain amplitudes, implying that the existing lamellar structure was disrupted over the course of the experiment. In contrast, the isotropic liquids did not show such a strong dependence on the shear strain.

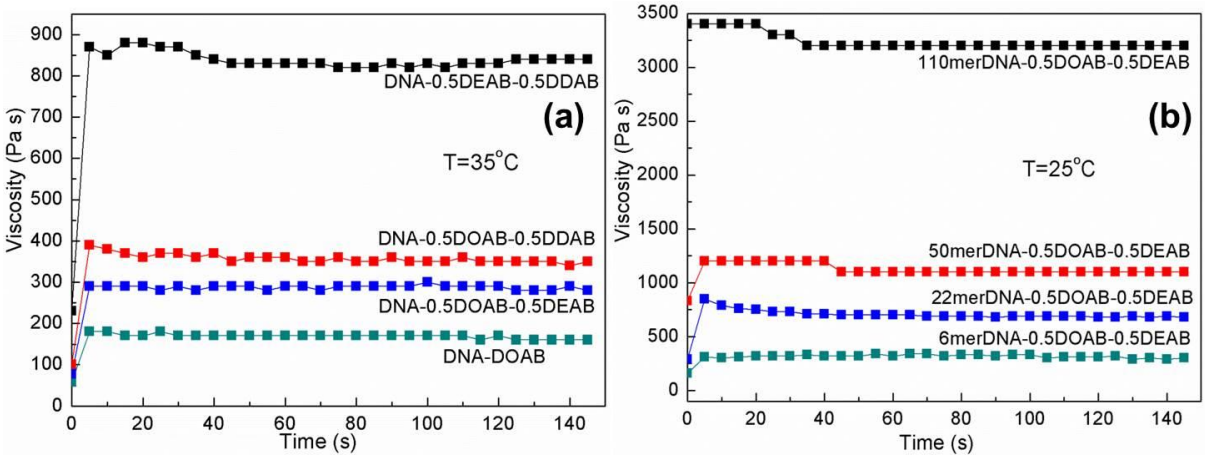

Figure S11. Rheological behaviors of solvent-free DNA-surfactant melts (here taking 14mer DNA-0.5DOAB-0.5DEAB as the example). Dependence of the viscosity of the DNA-surfactant complex with respect to the alkyl chain length of the surfactants (a) and the length of the single stranded DNA (b) (f = 1Hz, γ = 10%).

References

1. N. C. Seeman, Nature 2003, 421, 427.
2. P.W. K. Rothemund, Nature 2006, 440, 297.
3. M. Nakata, G. Zanchetta, B. D. Chapman, C. D. Jones, J. O. Cross, R. Pindak, T. Bellini, N. A. Clark, Science 2007, 318, 1276.
4. W. Guo, C. Lu, X. Qi, R. Orbach, M. Fadeev, H. Yang, I. Willner, Angew. Chem. Int. Ed. 2014, 53, 10134.
5. A.V. Pinheiro, D. Han, W.M. Shih, H. Yan, Nat. Nanotechnol. 2011, 6, 763.
6. J. W. de Vries, F. Zhang, A. Herrmann, J. Controlled Rel. 2013, 172, 467.
7. Y. He, T. Ye, M. Su, C. Zhang, A.E. Ribbe, W. Jiang, C. Mao, Nature 2008, 452, 198.
8. M. Kwak, A. Herrmann, Angew. Chem. Int. Ed. 2010, 49, 8574.
9. M. Kwak, A. Herrmann, Chem. Soc. Rev. 2011, 40, 5745.
10. J. B. Lee, S. M. Peng, D. Y. Yang, Y. H. Roh, H. Funabashi, N. Park, E. J. Rice, L. W. Chen, R. Long, M. M. Wu, D. Luo, Nat. Nanotechnol. 2012, 7, 816.
11. I. Koltover, T. Salditt, J. O. Rädler, C. R. Safinya, Science 1998, 281, 78.
12. S. Zhou, D. Liang, C. Burger, F. Yeh, B. Chu, Biomacromolecules 2004, 5, 1256.
13. A. Krivtsov, A. Bilalov, U. Olsson, B. Lindman, Langmuir 2012, 28, 13698.
14. DNA Interactions with Polymers and Surfactants, (Eds.: R. Dias, B. Lindman), Wiley-VCH, Weinheim, 2008.
15. K. Tanaka, Y. Okahata, J. Am. Chem. Soc. 1996, 118, 10679.
16. Y. Okahata, T. Kobayashi, K. Tanaka, M. Shimomura, J. Am. Chem. Soc. 1998, 120, 6165.
17. T. Neumann, S. Gajria, N. F. Bouxsein, L. Jaeger, M. Tirrell, J. Am. Chem. Soc. 2010, 132, 7025.
18. S. Gajria, T. Neumann, M. Tirrell, Wiley Interdiscip. Rev. Nanomed. Nanobiotechnol. 2011, 3, 479.
19. J. Yuan, D. Mecerreyes, M. Antonietti, Prog. Polym. Sci. 2013, 38, 1009.
20. K. Liu, L. Zheng, Q. Liu, J. W. de Vries, J. Y. Gerasimov, A. Herrmann, J. Am. Chem. Soc. 2014, 136, 14255.
21. Y. J. Min, M. Akbulut, K. Kristiansen, Y. Golan, J. Israelachvili, Nat. Mater. 2008, 7, 527.
22. J. Bonnet, M. Colotte, D. Coudy, V. Couallier, J. Portier, B. Morin, S. Tuffet, Nucleic Acids Res. 2009, 38, 1531.
23. J. M. Lehn, Chem. Soc. Rev. 2007, 36, 151.
24. M. D. Pluth, K. N. Raymond, Chem. Soc. Rev. 2007, 36, 161.
25. C. K. McLaughlin, G. D. Hamblin, H. F. Sleiman, Chem. Soc. Rev. 2011, 40, 5647.
26. K. Liu, D. Chen, A. Marcozzi, L. Zheng, J. Su, D. Pesce, W. Zajaczkowski, A. Kolbe, W. Pisula, K. Müllen, N. A. Clark, A. Herrmann, Proc. Natl. Acad. Sci. U. S. A. 2014, 111, 18596.
27. A. B. Bourlinos, S. R. Chowdhury, R. Herrera, D. D. Jiang, Q. Zhang, L. A. Archer, E. P. Giannelis, Adv. Funct. Mater. 2005, 15, 1285.
28. A. M. Leone, J. D. Tibodeau, S. H. Bull, S. W. Feldberg, H. H. Thorp, R. W. Murray, J. Am. Chem. Soc. 2003, 125, 6784.
29. A. W. Perriman, H. Colfen, R. W. Hughes, C. L. Barrie, S. Mann, Angew. Chem. Int. Ed. 2009, 48, 6242.
30. C. F. J. Faul, Acc. Chem. Res. 2014, 47, 3428.
31. Smectic Liquid Crystals, (Eds.: G. W. Gray, J. W. G. Goodby), Leonard Hill, Glasgow, 1984.
32. C. Tschierske, Angew. Chem. Int. Ed. 2013, 52, 8828.
33. S. S. Babu, J. Aimi, H. Ozawa, N. Shirahata, A. Saeki, S. Seki, A. Ajayaghosh, H. Mçhwald, T. Nakanishi, Angew. Chem. Int. Ed. 2012, 51, 3391.
34. K. Sato, Chem Eng Sci. 2001, 56, 2255.
35. J. Zhou, S. K. Gregurick, S. Krueger, F. P. Schwarz, Biophys. J. 2006, 90, 544.
36. A. S. Mocanu, M. Amela-Cortes, Y. Molard, V. Cîrcu, S. Cordiera, Chem. Commun. 2011, 47, 2056.
37. D. J. Broer, C. M. W. Bastiaansen, M. G. Debije, A. P. H. J. Schenning, Angew. Chem. Int. Ed. 2012, 51, 2.
38. D. A. Coleman, J. Fernsler, N. Chattham, M. Nakata, Y. Takanishi, E. Korblova, D. R. Link, R.F. Shao, W. G. Jang, J. E. Maclennan, O. Mondainn-Monval, C. Boyer, W. Weissflog, G. Pelzl, L. C. Chien, J. Zasadzinski, J. Watanabe, D. M. Walba, H. Takezoe, N. A. Clark, Science 2003, 301, 1204.
39. O. Lenz, F. Schmid, Phys. Rev. Lett. 2007, 98, 058104:1.
40. W. Pisula, Z. Tomović, C. Simpson, M. Kastler, T. Pakula, K. Müllen, Chem. Mater. 2005, 17, 4296.
41. N. J. Servers, Nat. Protoc. 2007, 2, 547.
42. E. Polushkin, G. Alberda van Ekenstein, O. Ikkala, G. ten Brinke, Rheol Acta 2004, 43, 364.

Chapter 4

Phase-dependent DNA electrochromics: controlling the volatility of the written optical state

Abstract

Liquid crystal electro-optic materials are familiar from their wide use in displays for portable electronic information display. This success has stimulated exploration of soft materials technologies for a broader array of applications, among the most promising of which are smart windows and panels for energy conservation and harvesting. Such applications require electro-optic effects with characteristics and behavior that are rather different from those needed for displays. Thus, some requirements, such as that for speed, are relaxed, but new ones, such as polarizer-free operation and permanent memory of a written state, become keys to success. Of interest in the energy domain are electrochromic materials, in which the absorption of infrared or visible light by dyes is put under electrical control. Here, we describe an anhydrous nanoDNA-surfactant thermotropic liquid crystal system, which exhibits distinctive electrically tunable optical absorption, and thermally tunable memory. In the liquid crystal isotropic phase, electric field-induced coloration and bleaching have a switching time of seconds. Upon transition to the smectic liquid crystal phase, a remarkable optical memory of the written state is observed without color decay for many hours in the absence of applied voltage. Interestingly, we found that reorientation of the DNA-surfactant lamellar layers plays an important role in preventing color decay. Thereby, the volatility of optoelectronic state can be controlled simply by changing the phase of the material. This research paves the way for developing a new generation of DNA-based, phase-modulated, energy-saving photoelectronic devices.

Introduction

Electrochromism, or the electrical control of a material's interaction with light[1-3], has led to the development of many technological applications that span dynamic tinting windows and mirrors, color changing displays, smart cards, and e-paper[4]. Several distinct classes of materials have been extensively investigated for their usefulness in electrochromic applications, including organic systems (e.g., bipyridilium salts)[5-9], electroactive conducting polymers (e.g., polyaniline, polythiophenes)[1,10-13], metal-organic systems (e.g., Prussian blue, Fe-terpyridines coordination polymer, Zn-pyrazolate metal-organic frameworks)[14-17] as well as inorganic systems based on transition metal oxides (e.g., WO_3)[18-21]. Despite these advances, there is a strong need for more accessible and easily processable materials with a greater degree of tunability of electrochromic behavior. Challenges to be achieved include control over the duration of an electronic state in the absence of electrical input or in response to temperature changes. Therefore, the development of new electrochromic materials is an attractive goal.

Liquid crystals (LCs) as a soft condensed state of molecules, have anisotropic structures with an enormous variety of functional properties[22,23]. The flexibility in LC physical structures, correlated with changes in electronic structures for redox-active functionality of the mesogens, seems to be regarded as a desirable property for electrochromism[24-26]. Furthermore, this flexibility in LC ordering may lead to novel electrochromic behaviors different from traditonal disordered electrochromic materials.

Thus far, little effort has been invested in studying the electrochromic properties of DNA, which is appealing as an electrochromic material due to its ubiquity and uniform distribution of redox-active sites (nucleotide bases) along its polymer backbone[27-29]. Recently, we have prepared a series of thermotropic LCs based on DNA-surfactant complexes that are produced by a simple preparation protocol[30,31]. Phase transition temperatures from the isotropic liquid phase to the LC phase to the crystalline phase can be modulated over a broad temperature range by controlling the average length of the cationic surfactant that is complexed to the negatively charged single-stranded nucleic acid molecule. Here, we report the development of DNA-LC-based electrochromic devices that are readily switchable between the colored and colorless states in the isotropic phase. The rate of coloration decay can be regulated by adjusting the phase of the DNA-surfactant complex, the length of the DNA oligomer and the identity of the complexing surfactant. A color impression can thus be preserved for several hours in the absence of applied voltage if the temperature of the system is adjusted to accommodate the LC phase or the crystalline phase. Moreover, in response to temperature changes above the clearing temperature immediate color loss is observed. This phenomenon allows for controlling the volatility of stored information in a simple and practical manner and might allow the fabrication of smart tags with clock- and thermometer functions.

Results and discussion

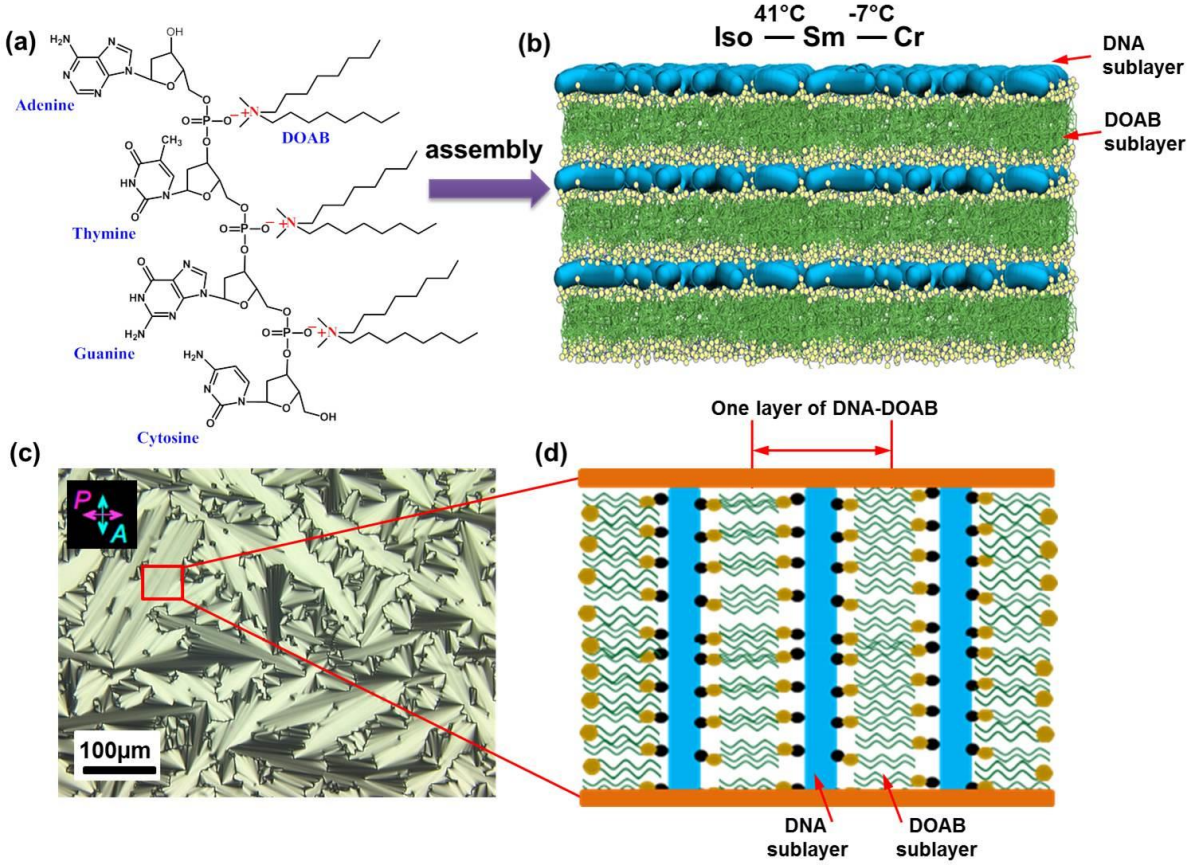

Figure 1. Schematic illustration of the DNA-surfactant complex formation, driven by ionic self-assembly. (a) Molecular structure of DNA-surfactant complex using dioctyldimethylammonium bromide (DOAB) as a representative cationic surfactant that electrostatically interacts with the oligonucleotide backbone. With increasing temperature, the DNA-surfactant complexes transition from crystalline state to the LC state and further to the isotropic liquid state. (b) The lamellar bilayer structure in the LC phase is made of one sublayer of single stranded DNA and one sublayer of interdigitated surfactants, where the phosphate groups of DNA electrostatically interact with the cationic head groups of surfactants. (c) A polarized optical microscopy (POM) image of the DNA-surfactant LC phase in a LC cell (here taking 14mer DNA-DOAB as an representative complex, 25 °C, cell gap ~6.8 μm) shows well-defined focal-conic textures of the smectic phase. (d) An illustration of the alignment of the DNA-surfactant LC in the cell shows that the DNA-surfactant smectic layers are vertical to the ITO coated glass slide surface. In d, black ball represents phosphate anions of oligonucleotide and yellow ball represents ammonium cations of surfactant.

Preparation and characterization of DNA-surfactant LCs. DNA-surfactant materials were prepared by electrostatic complexation of single-stranded oligonucleotides (6mer, 14mer, 22mer, and 50mer) with a single type of cationic surfactant (dioctyldimethylammonium bromide (DOAB), didecyldimethylammonium bromide (DEAB), and didodecyldimethylammonium bromide (DDAB)) or with a two-component mixture of surfactants (DOAB+DEAB and DEAB+DDAB). DNA-surfactant LCs were obtained according to a previously published protocol[30] that requires precipitating the DNA out of solution using the cationic surfactant, extracting the solid

product by centrifugation, and lyophilizing the complex to remove any excess water. The resulting product exhibits discrete phase transitions from the isotropic liquid, to the LC and crystalline phases at temperatures characteristic of the material. For example, the DNA-DOAB complex exhibits a smectic LC phase between -7 and 41 °C (Figure 1 and Figure S1). In this lamellar LC phase, DNA sublayers are alternatingly intercalated between aliphatic hydrocarbon sublayers (Figure 1b). Each repeating layer consists of a cationic surfactant bilayer that electrostatically interacts with an anionic oligonucleotide sublayer30. Long range periodic layer structures in the LC phase have been directly visualized by freeze-fracture transmission electron microscopy (Figure S2). The degree of crystallinity was also investigated by wide angle X-ray scattering. When the DNA-DOAB sample is heated above 41 °C, the X-ray scattering peak that was observed in the LC phase disappears, indicating a transition to the disordered liquid state (Figure S1b). If the sample is cooled below -7 °C, a series of sharp, high-intensity diffraction peaks provide evidence of crystallinity (Figure S1d). The phase transition temperatures of DNA-surfactant complexes can be controlled over a wide temperature range by varying the alkyl chain length of surfactants and employing mixtures of surfactants complexed to the DNA (Figure S3). In order to study the optoelectronic behavior of the samples, a LC cell was used that consists of two ITO-coated glass plates separated by a gap of ~6.8 μm. The LC cell was filled with the sample in the isotropic state by capillary action. When the samples were cooled to the smectic LC phase, focal-conic domains were observed by polarizing optical microscopy (POM) (Figure 1c). In these homogenous alignments, the smectic layers of the DNA-surfactant LC were oriented perpendicular to the electrode surface (Figure 1d).

Electrochemical properties of DNA-surfactant LCs. In the bulk LC state, the electrochemical spectrum of the DNA-surfactant complex was acquired in a two-ITO-electrode LC cell, where direct current (DC) electric field was applied in the direction of the DNA-surfactant smectic layers (Figure S4). Indeed, reversible anodic oxidation and cathodic reduction processes of DNA were observed at the half-wave potentials of + 2.4 and – 2.15 V, respectively. The redox behavior of the DNA-surfactant complex in a CH_2Cl_2 solution was also investigated by cyclic voltammetry (Figure S5). The DNA-surfactant complex exhibits a reversible anodic oxidation at the potential of + 1.8 V versus Ag^+/Ag. This can be attributed to the formation of radical cations at the nucleobases[29,32].

Switchable electrochromic behavior in the isotropic liquid phase. The DNA-surfactant complex exhibits reversible electrochromic switching in the isotropic liquid phase in the absence of external liquid electrolyte (Figure 2). A DC voltage step from 0 V to 4 V causes the DNA-DOAB material to change color from clear to magenta at the

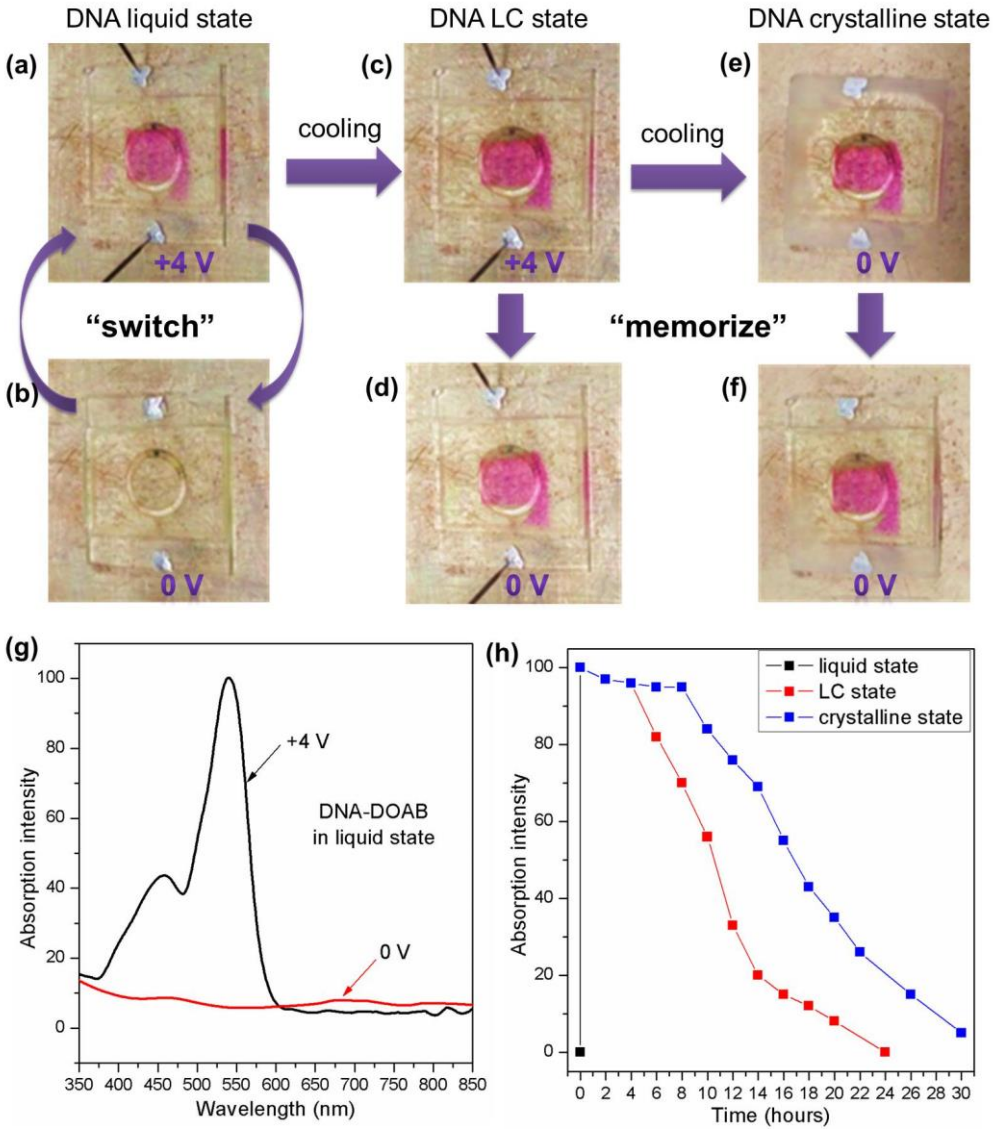

Figure 2. Phase-dependent electrochromism of DNA-surfactant complex in a LC cell in the absence of an external electrolyte layer using the 14mer DNA-DOAB complex as a representative example. The ring in the images is a part of the hot stage, which is affixed to the cell by vacuum. (a, b) Switchable electrochromism between the colored (magenta) and colorless states occurred at the anode in the isotropic liquid phase (45 °C, switch time ~30 seconds). (c) When the colored DNA-DOAB liquid was cooled to the LC phase (25 °C, cooling rate 5 °C/min) in the presence of applied voltage, the coloration state was preserved. (d) When the bias was removed, remarkable optical memory of the DNA-DOAB smectic LC can be observed as a persistent colored state. (e) Further cooling the colored DNA-DOAB LC phase to the crystalline phase (-20 °C) without the application of voltage, (f) the relaxation rate of the colored state was significantly reduced. (g) Strong absorption bands in the UV-visible absorption spectrum of the DNA-DOAB liquid (45 °C) appeared in the region of 350 to 600 nm under applied voltage (black curve) and disappear shortly after the voltage was removed. (h) Decay kinetics of the colored state in different phases. In the isotropic liquid phase, the color decayed completely within ~30 seconds after a removal of bias (black curve). In the smectic LC phase (red curve, corresponding to Figure 2d), the color intensity was maintained above 95% for 4 hours and the colorless state was recovered within 24 hours. In the crystalline phase (blue curve, corresponding to Figure 2e and 2f), the color intensity is maintained above 95% for ~8 hours and complete bleaching was only evident at 30 hours.

anode of the cell (Figure 2a and 2b). The transparent state can then be recovered within several seconds when the voltage across the electrochromic cell is again returned to 0 V. Thus, the DNA-DOAB complex exhibits reversible electrochromic properties in the isotropic liquid phase. Combined with the redox behavior analysis of the complex, it can be seen that DNA in the liquid state achieved a reversible anodic oxidation when a positive potential was applied. Radical cations of nucleobases were produced[29,32], which gave rise to absorption in the region from 350 to 600 nm (Figure 2g). This involved a color change of the DNA-surfactant complex from colorless to magenta at the anode of the cell. Control experiments showed that such color changes did not occur in the pristine surfactant material that lacks a redox-active moiety. Thus, we determine that the solvent-free DNA-surfactant complex can be considered the first example of DNA electrochromism. Previously, DNA has only acted as an electrolyte or as the host for dispersing electrochromic materials in electrochromic devices[33,34].

DNA length	Switch on	Switch off
6mer DNA	~15s	~14s
14mer DNA	~30s	~26s
22mer DNA	~80s	~70s
50mer DNA	~120s	>100s

Table 1. Switching times of the DNA electrochromics in the isotropic liquid phase using the DNA-DOAB complex as a representative example (45 °C). The electrochromic response time of these materials is correlated with the length of the DNA used.

Optical switching rates of the DNA-surfactant complexes in the isotropic phase were examined by applying a double potential step from 0 V to 4 V and back to 0 V. It was found that the electrochromic response time of these materials is correlated with the length of the DNA used (Table 1 and Figure S6), suggesting that the rate of DNA oxidation is limited by the rate of mass transport to the anode. The 6mer DNA-DOAB liquid exhibited response time of about 15 s in switching between the colored and colorless states whereas the 14mer, 22mer and 50mer had significantly longer response times of 30 s, 80 s and 120 s, respectively. These results indicate that increasing the dynamic radius of the DNA component leads to a reduction in the rate of DNA diffusion and thus affects the molecular mobility of the chromogenic component. To investigate the electrochromic stability of these DNA-surfactant ionic materials, 30 cycles of coloration and bleaching were carried out in a sequence of double-potential steps (Figure S7a, last seven cycles shown for 6mer DNA-DOAB; Figure S7c, last two cycles shown for 22mer DNA-DOAB). The color switching remained reversible and switching time of the last cycle did not significantly deviate from that of the first cycle (Figure S6).

Homogeneous focal-conic textures were recovered after cooling the electrochemically cycled samples to the LC phase (Figures S7b and S7d), indicating that the ionic DNA-surfactant complexes are stable within this timeframe.

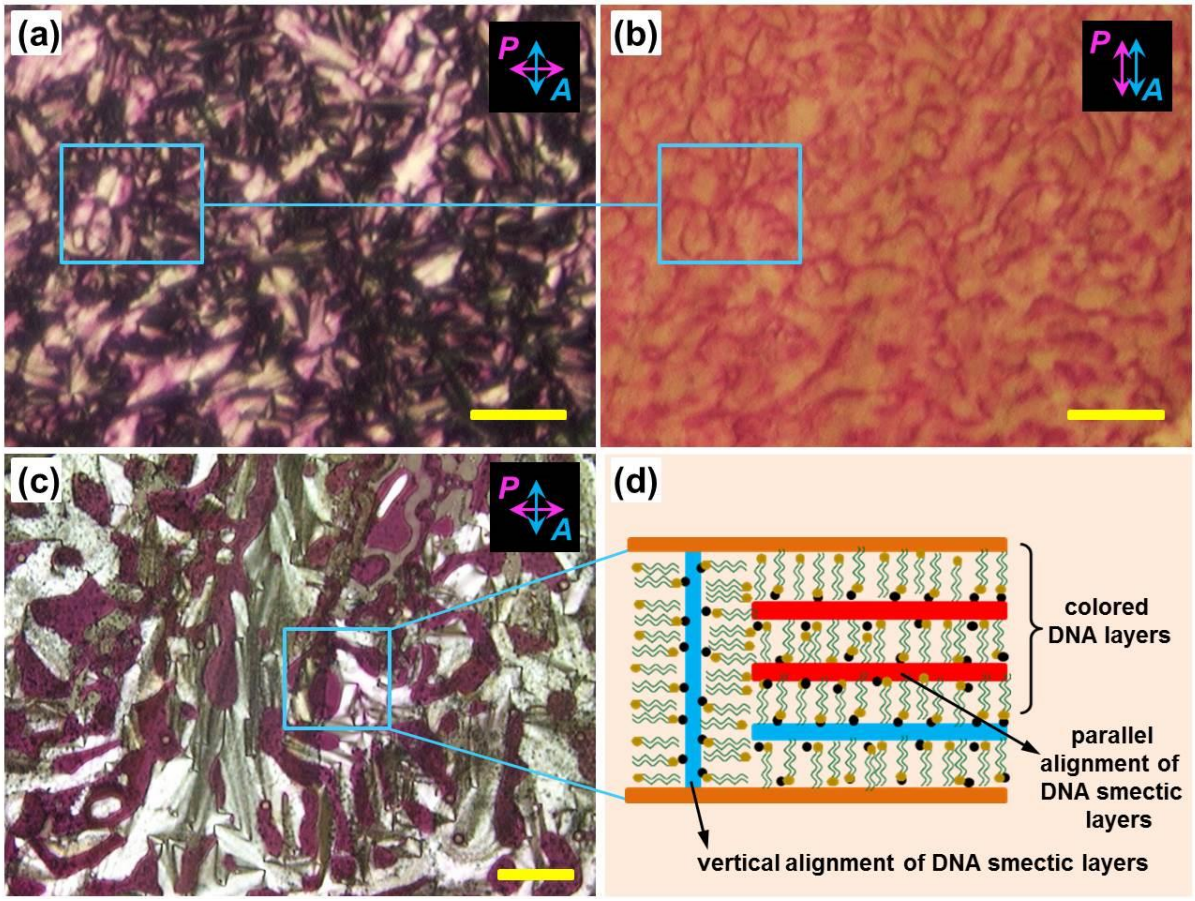

Figure 3. Investigation of birefringence textures, orientation, and color domains of the colored DNA-surfactant complex in the LC state (25 °C) in the absence of an applied voltage (corresponding to Figure 2d, 14mer DNA-DOAB with almost no color decay within 4 hours). The image of the colored DNA-DOAB textures obtained with crossed polarizer and analyzer (a) and the corresponding image (b) where the polarizer and analyzer were parallel. The focal-conic textures became much smaller or disappear in the colored DNA-DOAB domains when compared with the uncolored DNA-DOAB domains, indicating a reorientation of the colored smectic layers. The colored DNA-DOAB smectic layers oriented parallel to the electrode surface, whereas the uncolored DNA-DOAB layers remained vertical to the electrode surface. (c) This reorientation effect became more apparent after 10 cycles of applying a positive potential in the isotropic state, cooling to the LC state, removing the potential, and again heating to the isotropic state. (d) The corresponding sketch of the orthogonal alignment of the colored and the uncolored DNA-DOAB domains. (scale bar is 50 μm)

Optical memory behaviors of DNA in the LC and crystalline phases. When the DNA-surfactant liquid was cooled to the smectic LC phase while an applied voltage of 4 V was maintained, the magenta color was conserved (Figure 2c). Even after the cell voltage was returned to 0 V, the coloration state was temporally preserved in the smectic LC phase (Figure 2d) and completely bleached within 24 hours (Figures 2h, red curve and Figure S8). Further cooling the DNA-DOAB material in the magenta color state

from the LC to the crystalline phase in the absence of applied voltage (Figure 2e and 2f) extended the persistence time of the magenta state (Figures 2h, blue curve and Figure S9). The complete recovery of the colorless state in the crystalline phase was observed within about 30 hours. These results clearly indicated that the radical cations of nucleotide bases can be stabilized in the ordered DNA-surfactant structures. Thus, a method to modulate the volatility of the optical memory was developed by controlling the phase of the DNA-surfactant complex.

POM was used to investigate the birefringence textures and persistent color domains in the LC and polycrystalline phases. It was found that the focal-conic textures became much smaller or disappeared in the colored DNA-DOAB domains when compared to the uncolored DNA-DOAB birefringence domains (Figure 3a and 3b). We assume that reorientation of the oxidized DNA-DOAB smectic layers took place due to the applied voltage during the transition process from the isotropic to the LC phase (Figure 2, from a to c). In the presence of an applied voltage, the capacitive positive charge at the anode may attract the negative charged DNA, favoring a horizontal alignment of the nucleic acid layers in relation to the anode surface. This reorientation effect (compare Figures 2d and 3d) became more apparent after many cycles of applying a positive potential in the isotropic state, cooling to the LC state, removing the potential, and again heating to the isotropic state (Figure 3c). Furthermore, the alignment of the DNA-DOAB lamellar layers was maintained after the color decays completely (Figure S10a-c). The perpendicular orientation of the bleached DNA-DOAB smectic layers was recovered after an annealing treatment without application of voltage (Figure S10d), confirming the integrity of the ionic DNA-DOAB complexes. Further cooling of the colored LC sample to the crystalline phase preserved the reorientation of oxidized DNA-DOAB smectic layers (Figure S11 and S12).

When a potential of 4 V was applied directly to the DNA-DOAB material in the LC phase at 25 °C, the color impression appeared much slower and with lower intensity than in the isotropic liquid phase (Figure S13). This can be attributed to the lower mobility of DNA molecules in the smectic LC phase. In contrast to the coloration attained in the isotropic phase prior to transition to the LC phase, the coloration attained in the LC phase decayed completely within 3 hours (Figure S13), indicating that the relaxation time of DNA radical cations was significantly shorter than in the colored LC sample annealed from the isotropic phase (Figure 2d and Figure 2h, red curve). Interestingly, POM analysis did not reveal a difference in the alignments of colored and uncolored DNA-DOAB domains, as both exhibited perpendicular orientation of the smectic layers on the ITO surface (Figure 4).

The above results suggest that the reorientation of the oxidized DNA-DOAB smectic layers played an important role in trapping and protecting the colored radical cations and thus, in achieving the storage characteristics of optical information in the LC and

crystalline states. Due to the parallel alignment of the oxidized DNA-surfactant complex (Figure 3d), the surfactant sublayers may act as insulating barrier and prevent electron hopping. Therefore, the reduction process of DNA radical cations might be slowed down. It should be also noted that oxidized DNA molecules diffuse further away from anode surface in the isotropic phase than in the LC state. Therefore, in cooled samples from the isotropic melts the DNA radical cations are trapped and the colored state requires a longer time to relax back to the colorless state compared to samples that are directly oxidized in the LC state. Due to the mechanisms discussed above, the decay of a colored state of DNA-surfactant material can be controlled via a simple phase transition strategy in the absence of applied voltage.

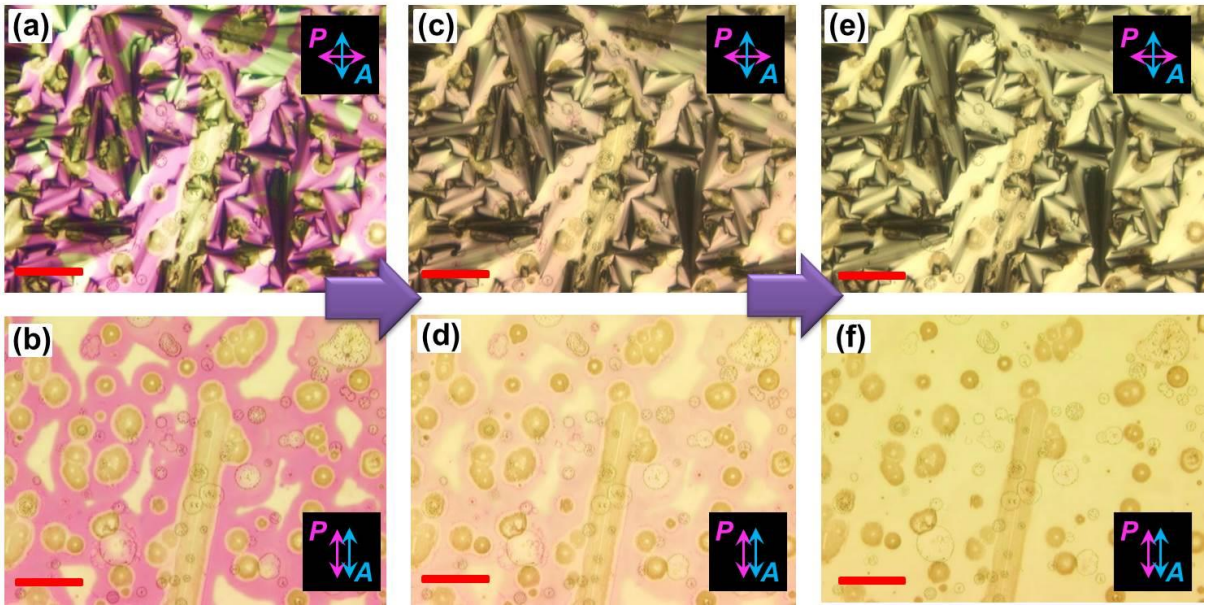

Figure 4. Investigation of birefringence textures, orientation, color domains, and color-decay after the application of 4 V directly to a DNA-DOAB complex in the LC phase (scale bar represents 100 µm). The optical images between crossed polarizer and analyzer (a, 0 hours; c, 2 hours; e, 4 hours) and the corresponding images with parallel polarizer and analyzer (b, 0 hours; d, 2 hours; f, 4 hours) showed that the alignment of colored DNA-DOAB smectic layers remained unaltered, exhibiting perpendicular orientation. The colorless state was recovered in ~3-4 hours, which was a significantly shorter recovery time than when the colored LC state was obtained from the isotropic phase.

Tunability of optical memory performance. To further illustrate the importance of material phases (isotropic liquid-LC-crystal) for tuning durability of stored optical information, a series of DNA-surfactant complexes with phase transition temperatures that range from -20 to 130 °C have been prepared (Figure S3). It can be seen that the magenta color of the DNA-DOAB liquid decays within 30 seconds after removing the potential at 45 °C (Figure 5a, black curve and Figure S6b). At the same temperature, DNA-0.5DOAB-0.5DEAB adopted the smectic LC phase and the color impression, after activation in the isotropic state, is decaying within ~10 hours (Figure 5a, red curve and Figure S14). This indicates that the lamellar layers of the DNA-surfactant complex can trap and stabilize the radical cations much more efficiently than the disordered liquid

phase. At 25 °C, the DNA-DOAB smectic LC exhibited an extended optical memory, showing full color decay within ~24 hours after removal of applied potential (Figure 5a, blue curve and Figure S8). The crystalline state of the DNA-DEAB at this temperature showed a longer memory time of ~28 hours until full bleaching occurred (Figure 5a, green curve and Figure S15). We attribute the differences in the rates of color formation and decay among the different phases and surfactant compositions to differences in the ionic mobility of the colored DNA component. We have previously reported that the viscosity of the DNA-surfactant complex, which was inversely proportional to ionic mobility, increased with the increasing surfactant alkyl chain length[31]. It is thus reasonable that the rate of decay of the magenta color impression correlated inversely with LC viscosity (Figure 5b and Figure S16, S17).

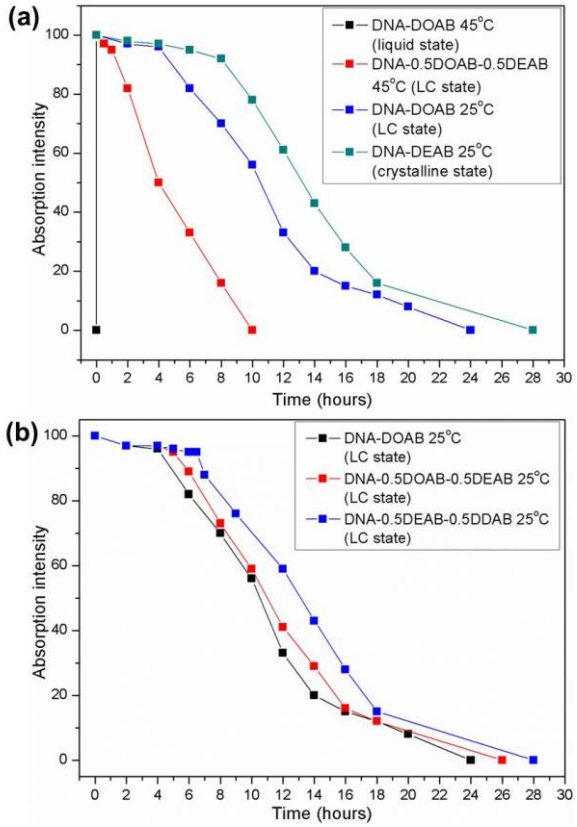

Figure 5. Color decay kinetics of the DNA-surfactant samples complexed with different surfactants, surfactant mixtures and 14mer DNA. (a) Phase-dependent memory behavior of the materials. The magenta color of DNA-DOAB isotropic liquid was bleached in 30 seconds at 45 °C after removal of bias (black curve). At the same temperature, the color impression of the DNA-0.5DOAB-0.5DEAB smectic LC phase was preserved almost completely for ~1 hours after the removal of the bias (black curve). At 25 °C, the DNA-DOAB smectic LC exhibited enhanced optical memory with negligible color decay within ~4 hours (blue curve). The crystalline state of the DNA-DEAB at this temperature showed a much longer relaxation time of ~7.5 hours (green curve). (b) Viscosity-dependent memory behaviors of the materials. The magenta color impression of the DNA-surfactant smectic LCs (25 °C) was extended from ~4 hours (DNA-DOAB, black curve) to ~5.5 hours (DNA-0.5DOAB-0.5DEAB, red curve) and further to ~7 hours (DNA-0.5DEAB-0.5DDAB, blue curve) with increasing the alkyl chain lengths of the surfactants.

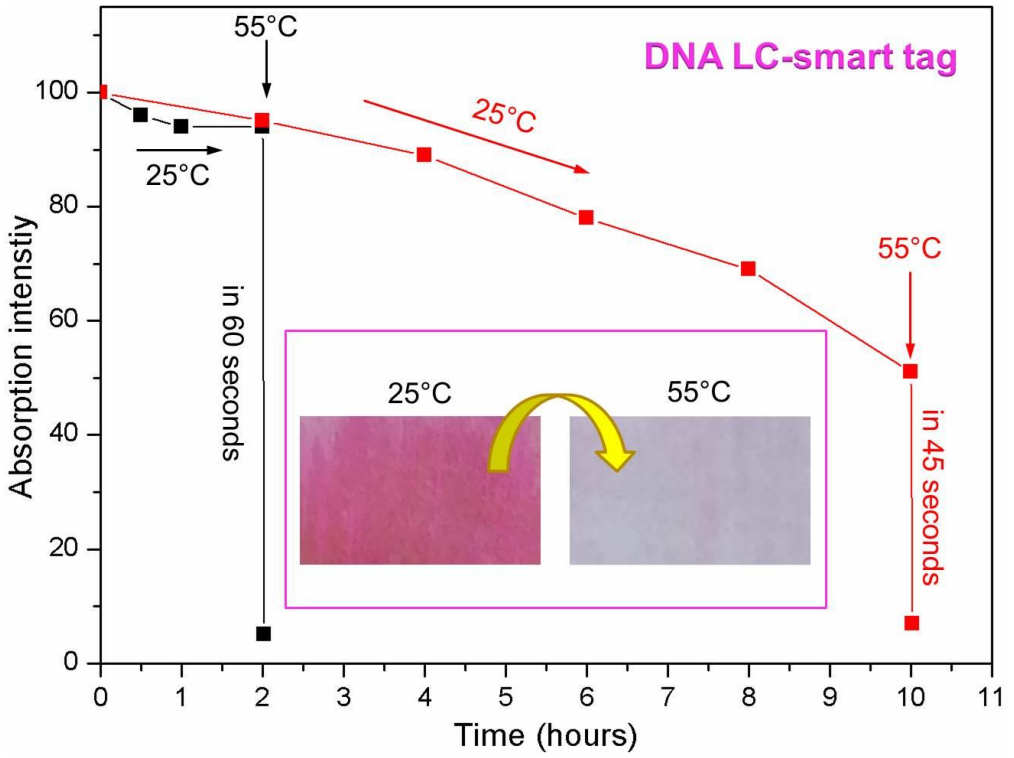

Figure 6. Decay kinetics of the colored DNA-surfactant sample with the interference of temperature (here using the 14mer DNA-DOAB LC as a representative example). At 25 °C, the color-activated sample has very slow color decay in the absence of applied voltage. Once the sample was in 55 °C (e.g., after 2 or 10 hours of the memory device), the color decayed completely within 60 seconds. The corresponding photographs of the color memorized (25 °C) and bleached (55 °C) samples are given in the insets. This time-temperature-sensitive behavior of the DNA-LC optical memory device shows great opportunies for smart tag application (e.g., time-temperature indicator).

DNA-LC optical memory device for smart tag application. Two important features of the electrochromic behavior of DNA-surfactant complexes have been demonstrated above. 1) The decay time of the colored state in the isotropic melt is in the range of seconds depending slightly on the length of the DNA molecule. 2) The decay in the LC state occurs within several hours and can be tuned by the selection of the surfactant complexed with DNA. These intriguing material characteristics can be combined and exploited for the fabrication of smart tags that exhibit a clock function and a ceiling temperature indicator. For demonstration of this dual functionality we have chosen the 14mer DNA-DOAB complex as an example. After activation of the tag in the isotropic melt, cooling and removal of voltage, the colored state decayed slowly at room temperature. However, when the temperature was raised to 55 °C, after two hours, the magenta color disappeared within 60 seconds (Figure 6, black curve; and Figure S18). Similar, a sample with ~50% color decay after 10 hours was bleached within 45 seconds when the temperature was adjusted to 55 °C (Figure 6, red curve; and Figure S19). Taking into account that the liquid-LC transition in the DNA surfactant materials can be conveniently tuned in the wide range between 130 °C and 41 °C (Figure S3), one can imagine that these behaviors of DNA-surfactant LCs offer great opportunities for

developing smart tag applications, especially with respect to packed perishable products inspection.

Conclusions

A new type of electrochromic material based on redox-active nucleic acids has been developed by mixing DNA and cationic surfactant. Phase-dependent electrochromism is an inherent characteristic of the DNA-surfactant complex, where fluidity and ordering are introduced by ionic self-assembly[35-37]. The rate of color decay was modulated very broadly, simply by controlling the phase of the material. In the isotropic liquid phase, the DNA-surfactant complex exhibits stable, reversible switching between the colorless and magenta states. In stark contrast to conventional LC electrochromic devices[7,24-26], the coloration state can be maintained over an extended period of time in the smectic LC phase or the crystalline phase without applying voltage. The time required for complete decay can range from a few seconds to over a day, which provides for a simple and effective way to modulate the volatility of stored optical information. This new type of DNA materials can be easily processed to fabricate single-layer electrochromic devices without the need for external electrolyte layers. To the best of our knowledge, the approach to controlling the volatility of stored optoelectronic information by modulating the phase of the material has never previously been proposed or attempted. Due to the broad and stable phases, these DNA-surfactant materials hold great promise for the realization of novel types of smart tags or optical devices as well as for diagnostic devices where recognition or biocatalytic events lead to phase transitions.

Experimental Section

Materials

The surfactants used for the DNA complex formation, including dioctyldimethylammonium bromide (DOAB) and didodecyldimethylammonium bromide (DDAB) were purchased from ABCR (Germany), and didecyldimethylammonium bromide (DEAB) was aquired from Sigma–Aldrich. Single-stranded DNA, including 6mer (5'-CCT CGC-3', Mw=1728g/mol), 14mer (5'-CCT CGC TCT GCT AA-3', Mw=4175g/mol) and 22mer (5'-CCT CGC TCT GCT AAT CCT GTT A-3', Mw=6612g/mol) were synthesized by conventional solid-phase synthesis method. The 50mer DNA strand (5'-CCT CGC TCT GCT AAT CCT GTT ACC TCG CTC TGC TAA TCC TGT TAC CTC GC-3', Mw=15077g/mol) was purchased from BIOMERS (Germany). Tetrabutylammonium perchlorate (Bu_4NClO_4, Mw= 341.91 g/mol), used as the supporting electrolyte for cyclic voltammetry measurements was purchased from Sigma.

DNA-surfactant complex preparation

The single-stranded DNA (6mer, 14mer, 22mer and 50mer) was pretreated by precipitating a ~300 μM DNA solution containing 5 M NaCl with cold ethanol (-20 °C). From this precipitate an aqueous DNA solution (~300 μM) was prepared in ultrapure water. In a second solution made from ultrapure water, the concentration of single surfactant (DOAB, DEAB and DDAB) or a two-surfactant mixture (DOAB:DEAB, DOAB:DDAB, and DEAB:DDAB, molar ratios 7:3, 5:5 and 3:7) were adjusted to 5-10 mM at room temperature. Both the DNA and surfactant solutions (~5 mol equivalents of surfactant relative to nucleotides of the DNA) were mixed together and as a result the insoluble complexes precipitated from the aqueous phase. After centrifugation, the water and unreacted surfactants were removed, and finally the complexes were lyophilized overnight before further characterization.

Electrochromic device fabrication

The prepared DNA-surfactant complexes were filled into a commercial liquid crystal cell consisting of two ITO-coated glass plates (LC4-6.8, ITO area 5mm×5mm, gap 6.8μm, INSTEC, USA). There are two openings on the cell. A small amount of the DNA-surfactant sample was placed over one opening, which lead to capillary forces pulling the liquid crystal material into the empty cell. This process can be accelerated by heating the materials to the isotropic states.

Electrochromic measurement

The DNA-surfactant complex was introduced into the electrochemical cell and heated to the isotropic phase. The potential was then switched between 4 V and 0 V over the course of the switching response studies. Subsequently, the complex was cooled to the smectic LC phase (cooling rate 5 °C/min) under an applied potential of 4 V. After cooling, the electric field was switched off to study the relaxation time of the colored state. In other experiments, the colored LC state was immediately cooled to the polycrystalline phase (cooling rate 5 °C/min) in the absence of an applied electric field.

Characterization

Thermal behaviors of the DNA-surfactant complexes were investigated by differential scanning calorimetry (DSC) using a TA Instruments Q1000 system in a nitrogen atmosphere with a heating/cooling rate of 5 °C/min. The structural features of the DNA-surfactant complexes were analyzed by wide-angle X-ray scattering (WAXS). WAXS with heating and cooling systems was carried out by a custom, rotating-anode-based setup, made in-house, where the sample-to-detector distance was 13 cm and a conventional X-ray source with radiation wavelength of λ = 1.54 Å was employed. Smectic layer structures of the DNA-surfactant complexes were carried out by freeze-fractured transmission electron microscopy (FF-TEM) according to a standard protocol.

FF-TEM was performed by sandwiching the samples between 2 mm by 3 mm glass planchettes and cooling from the isotropic melt to a selected temperature in the LC range. The samples were then rapidly quenched to T < -180 °C by immersion in liquid propane, fractured in vacuum at -140 °C, and then coated with 2 nm of platinum deposited at 45° and then with 25 nm of carbon deposited at 90°. After dissolving the liquid crystal, the Pt–C replicas were placed in the TEM, where the topographic structure of the fracture plane was observed. Textures and orientation analysis of the complexes were studied by polarized optical microscopy (POM). POM was conducted on a Zeiss Axiophot using the same temperature program that was employed for the DSC experiments. Electrochemical behaviors of the DNA-surfactant complexes were investigated in the solution and in the bulk material. Standard cyclic voltammetry (CV) in solution was performed in a three-electrode cell equipped with a Pt working electrode, a Pt counter electrode, and an Ag^{+}/Ag reference electrode. A solution of Bu_4NClO_4 in CH_2Cl_2 (0.10 M) was used as the supporting electrolyte. The sweep rate is 100 mVs-1. The electrical spectrum in the bulk (in the electrochromic cell described above) was measured by a semiconductor parameter analyzer (4155B, Hewlett packard). Electrochromic behaviors were examined on a hot stage (heating/cooling rate of 5 °C/min) with DC voltage control. Ultraviolet-visible absorption spectra were recorded with a JASCO V-630 spectrophotometer for the study of the reversible electrochromism and optical memory (decay kinetics) properties. Electrochromic switching time between coloration and bleaching of the DNA-surfactant complexes in the isotropic liquid phases were measured and analyzed by processing the recorded videos with the ImageJ software (National Institutes of Health).

Supplementary Figures

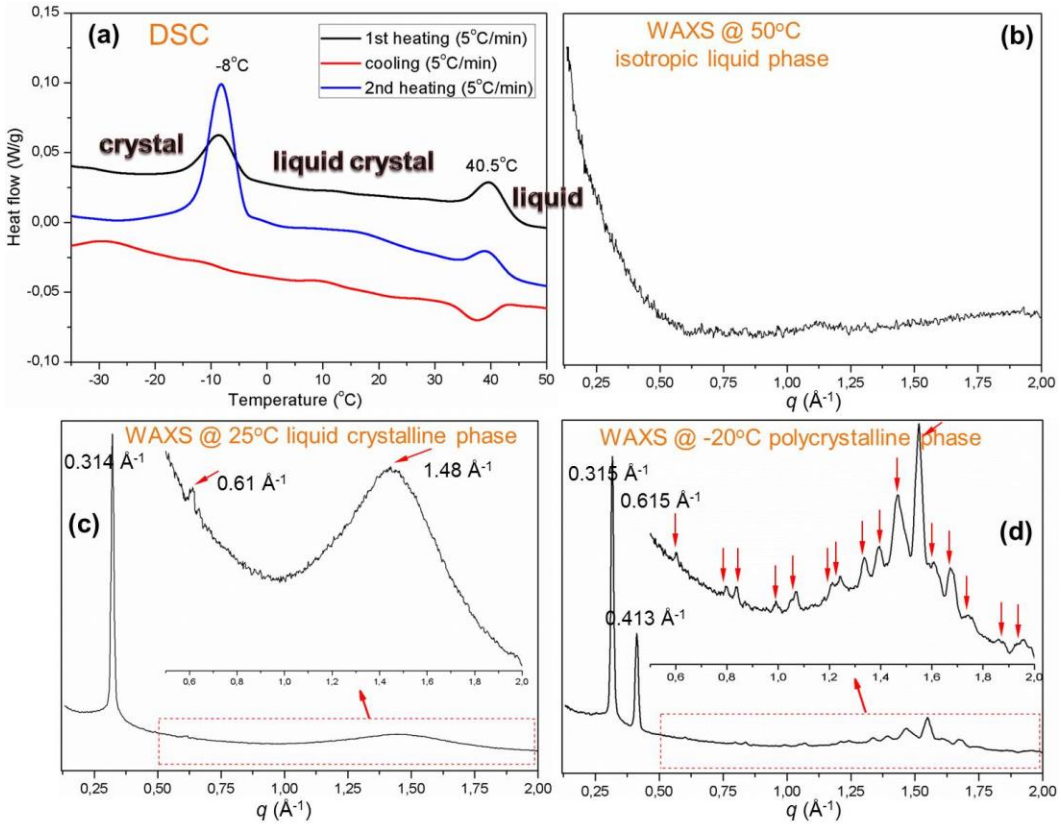

Figure S1. Characterization of the DNA-surfactant complexes (here taking 14mer DNA-DOAB as an example). (a) Thermal behavior of the DNA-DOAB by differential scanning calorimetry (DSC) analysis. The DNA-DOAB exhibits continuous phase transitions from the isotropic liquid (above 41 °C) state to the liquid crystalline (from 41 to -7 °C) state to the polycrystalline state (below-7 °C). (b-d) Structural study of the DNA-DOAB complex by wide-angle X-ray scattering (WAXS). In the isotropic liquid state (b), no any X-ray diffraction peak was observed because the DNA-DOAB molecules are disordered. In the mesophase (c), a sharp first order peak (0.314 $Å^{-1}$) and the following harmonic (second order diffraction 0.61 Å-1), and the diffraction halo (1.48 $Å^{-1}$) are characteristic of long-range ordered lamellar structure. In the crystalline phase (d), a series of diffraction peaks that are strong and narrow indicate the crystallinity of the as-prepared DNA-DOAB in -20 °C.

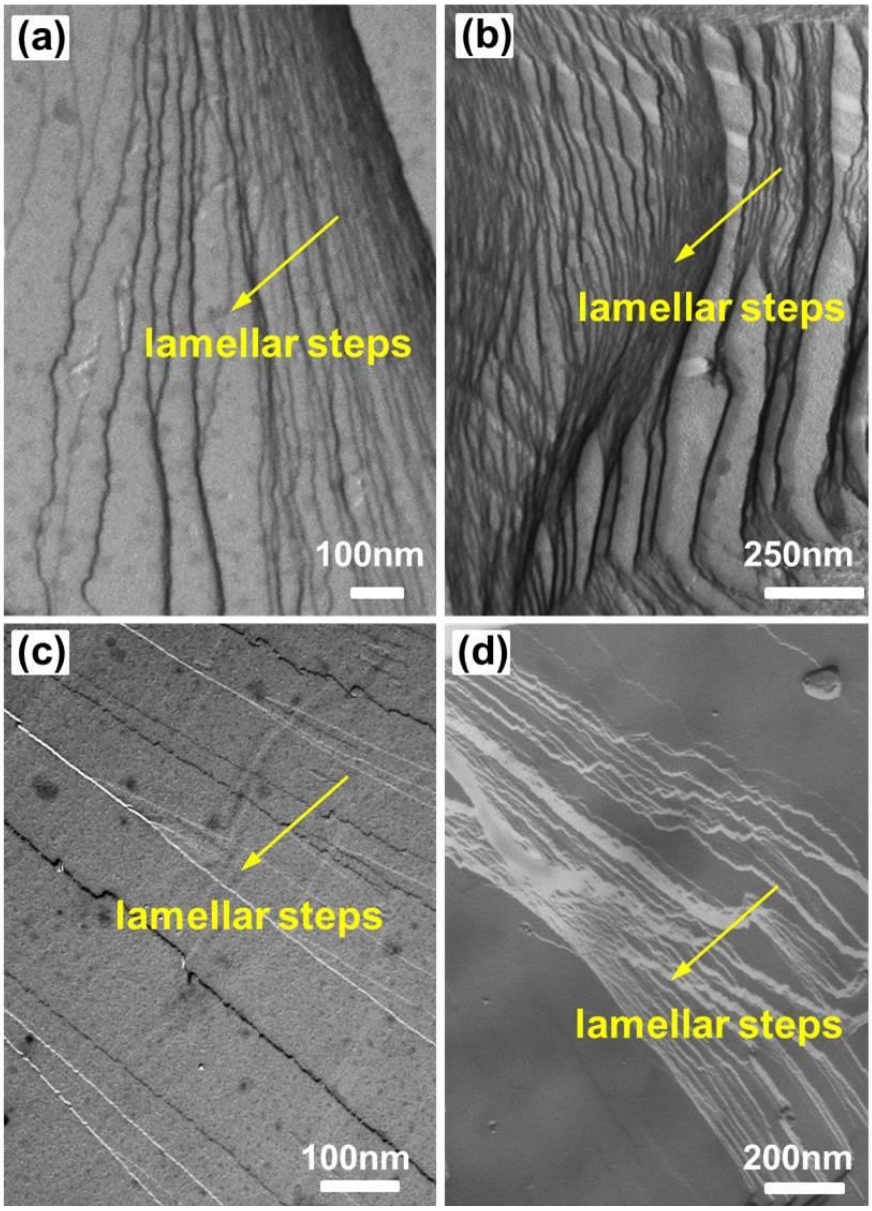

Figure S2. The lamellar structure characterization of the DNA-surfactant mesophases by freeze-fracture transmission electron microscopy (FF-TEM). (a) DNA-DOAB (25 °C). (b) DNA-DEAB (70 °C). (c) DNA-0.5DOAB-0.5DEAB (25 °C). (d) DNA-0.5DEAB-0.5DDAB (25 °C). In all the samples, smectic layer surfaces are generally smooth but have occasional layer steps that are distinct and can be identified unambiguously.

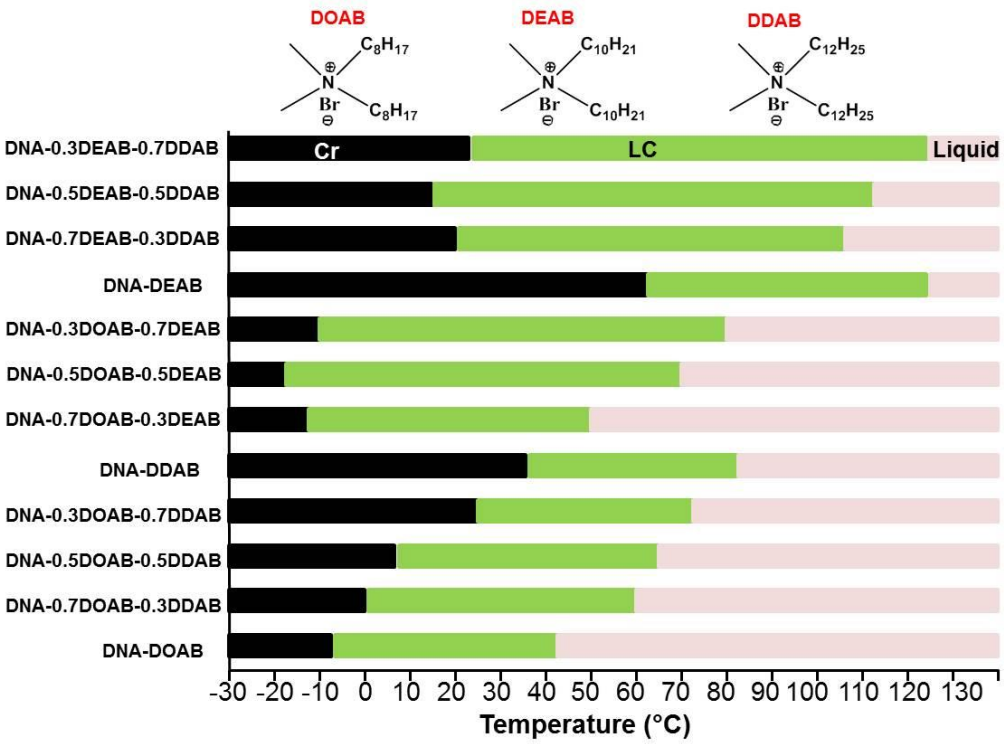

Figure S3. Overview of thermal behaviors of binary and ternary DNA-surfactant complexes. The phase transition temperatures from crystalline (Cr) to liquid crystalline (LC) and then to isotropic liquid can be controlled over a wide temperature range. Melting temperatures are tunable from around -20°C to 65 °C, and clearing temperatures are broadly dispersed between 41 °C and ~130 °C, respectively. These behaviors are strongly dependent on the specific length of the aliphatic chains of the surfactants, and marginally influenced by the lengths of the DNA.

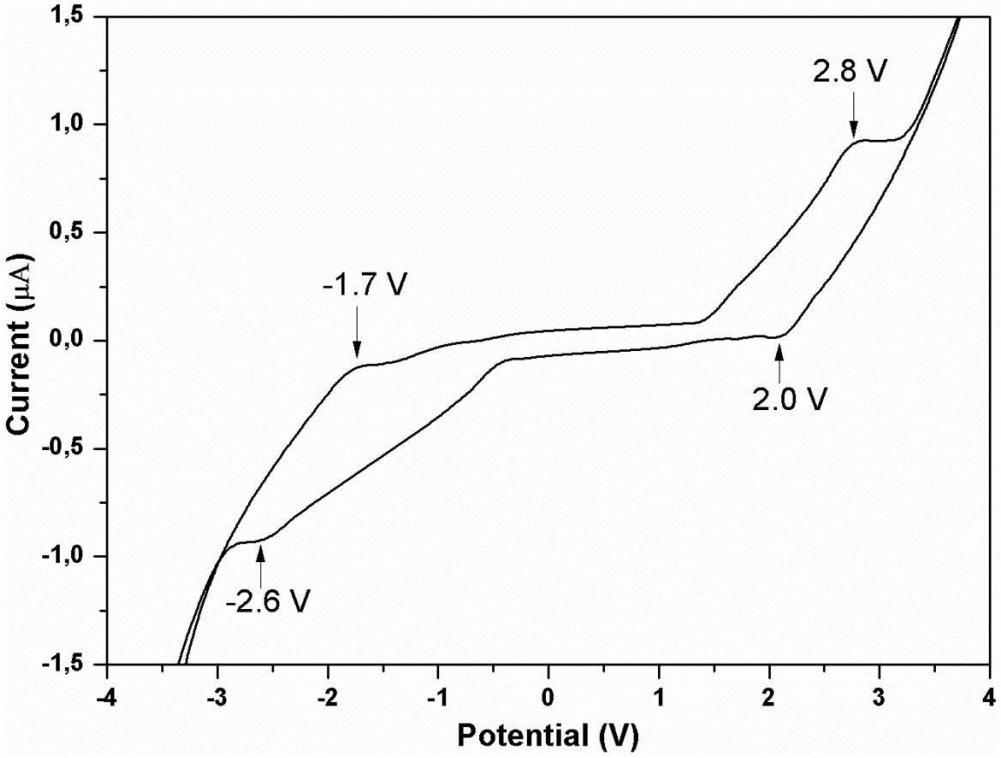

Figure S4. Electrochemical spectrum of the DNA-surfactant LC in the bulk state (here taking DNA-DOAB as an example). The DNA-DOAB liquid crystal was filled into a two-ITO-electrode LC cell by capillary force. Direct current (DC) electric field was applied in the direction of the DNA-DOAB smectic layers at 25 °C. Reversible anodic oxidation and cathodic reduction processes of DNA were observed at the half-wave potentials of + 2.4 and – 2.15 V, respectively.

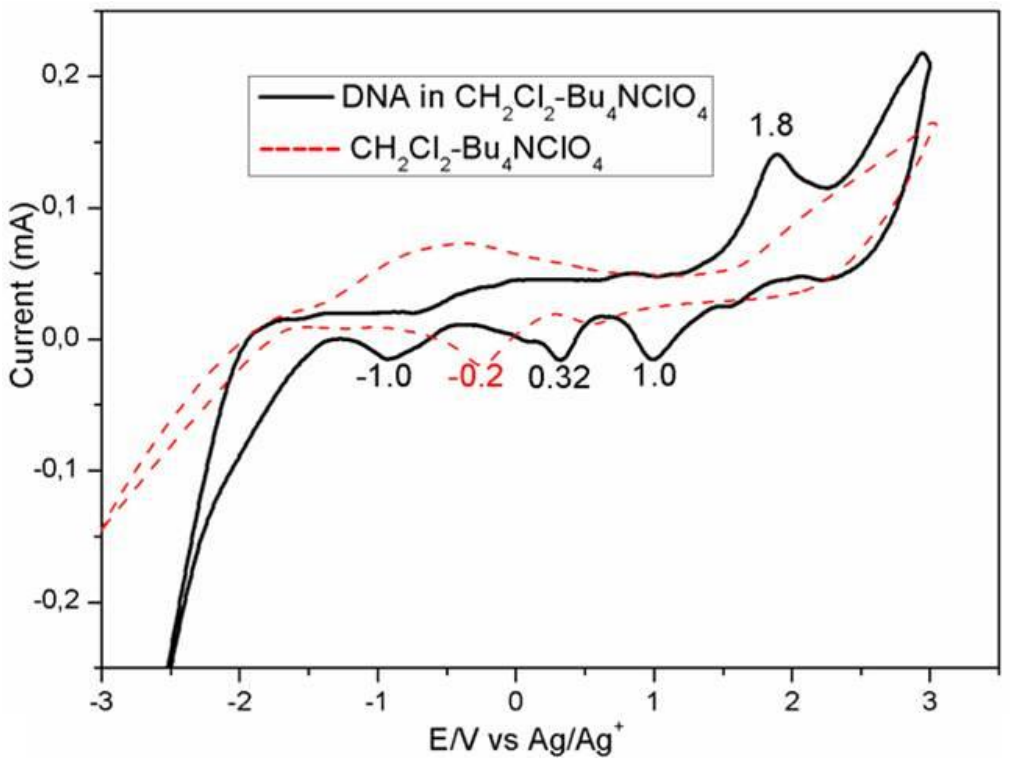

Figure S5. Electrochemical properties of the DNA-surfactant complexes in the solution (here taking DNA-DDAB as an example, ~0.5 mM in CH2Cl2) investigated by standard cyclic voltammetry measurement with a Pt working electrode. Bu4NClO4 (0.1 M) was used as the supporting electrolyte. All potentials were measured using a Ag/AgCl electrode as a reference. Reversible anodic oxidation was observed at the potential of +1.8 V versus Ag+/Ag.

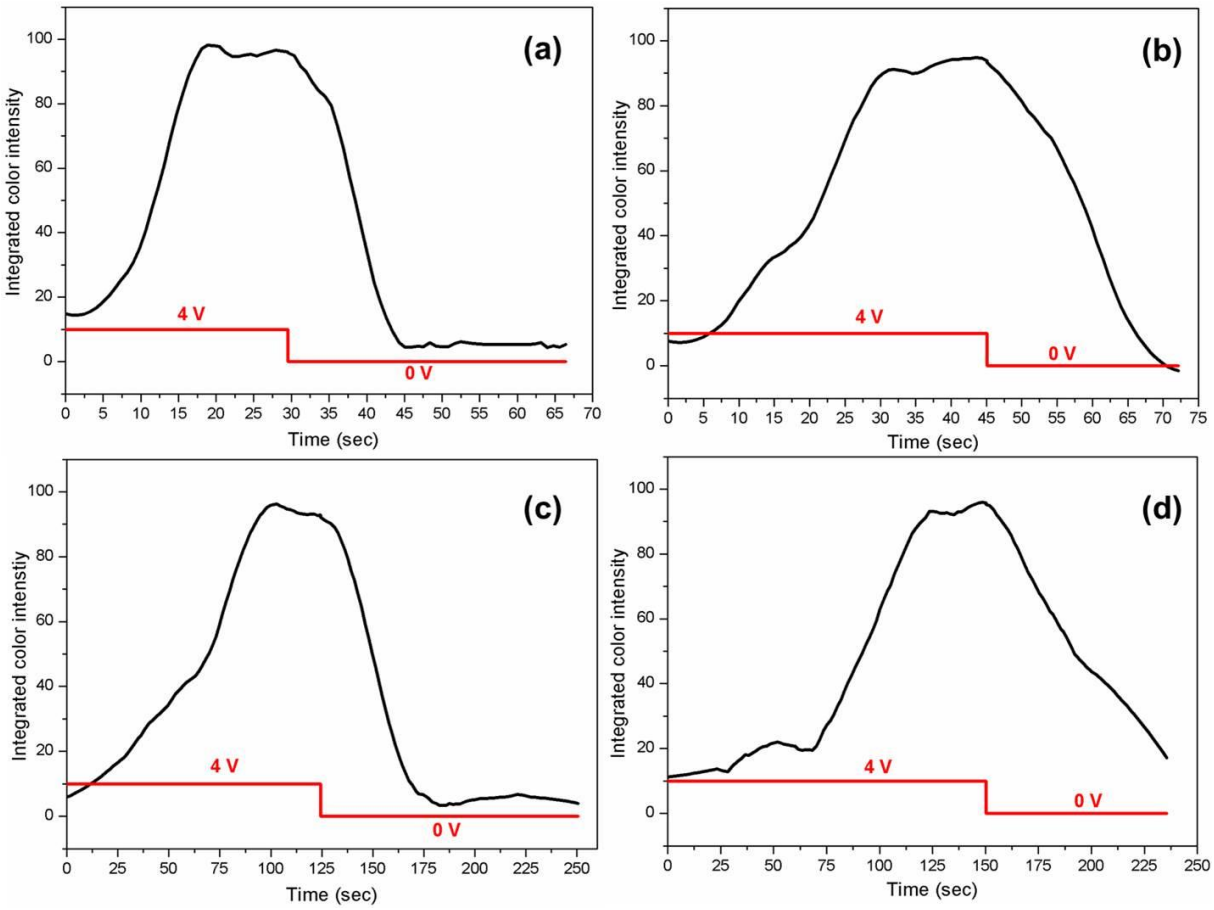

Figure S6. Electrochromic switching between colored and colorless state of the DNA-DOAB complex with different DNA lengths in the isotropic liquid phases (45 °C) upon the application of double-potential steps between +4 and 0 V. The electrochromic response time of these DNA materials is 15 s (a, 6mer), 30 s (b, 14mer), 80 s (c, 22mer) and 120 s (d, 50mer), indicating DNA length plays an important role in controlling the switching rate. The time-dependent color curves were acquired by analyzing recorded videos with ImageJ software.

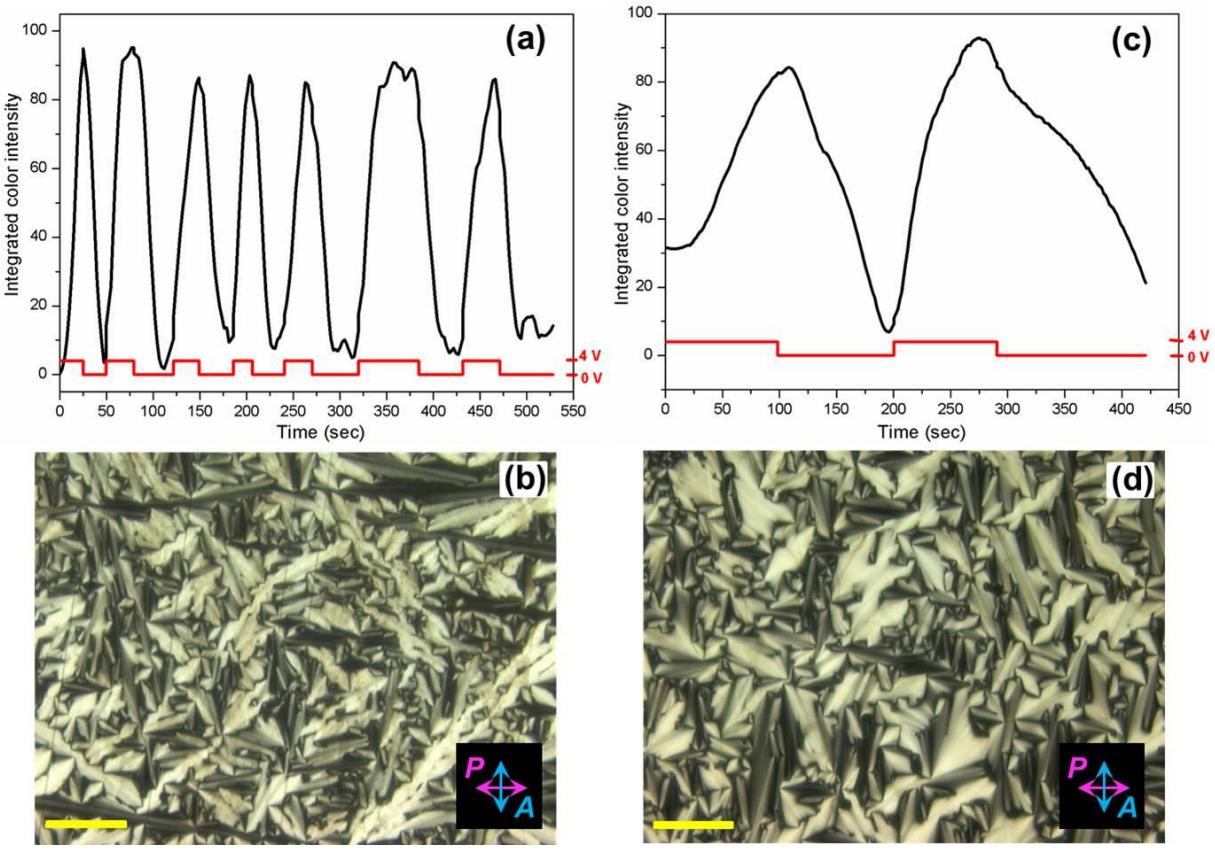

Figure S7. Switching response of the electrochromic DNA-DOAB complexes in the liquid phase (45 °C) upon the repeatedly stepping the potential between 4 and 0 V for 30 cycles (a, the last seven cycles for 6mer DNA-DOAB; b, the last two cycles for 22mer DNA-DOAB). The color switching remained reversible and switch time is comparable with the freshly prepared samples (Figure S6). After 30 cycles, the focal-conic birefringent textures were reproduced in the liquid crystal phase (25 °C) (b, 6mer DNA-DOAB; d, 22mer DNA-DOAB), indicating the redox-active DNA-surfactant materials are stable within this timeframe (scale bar represents 100 μm).

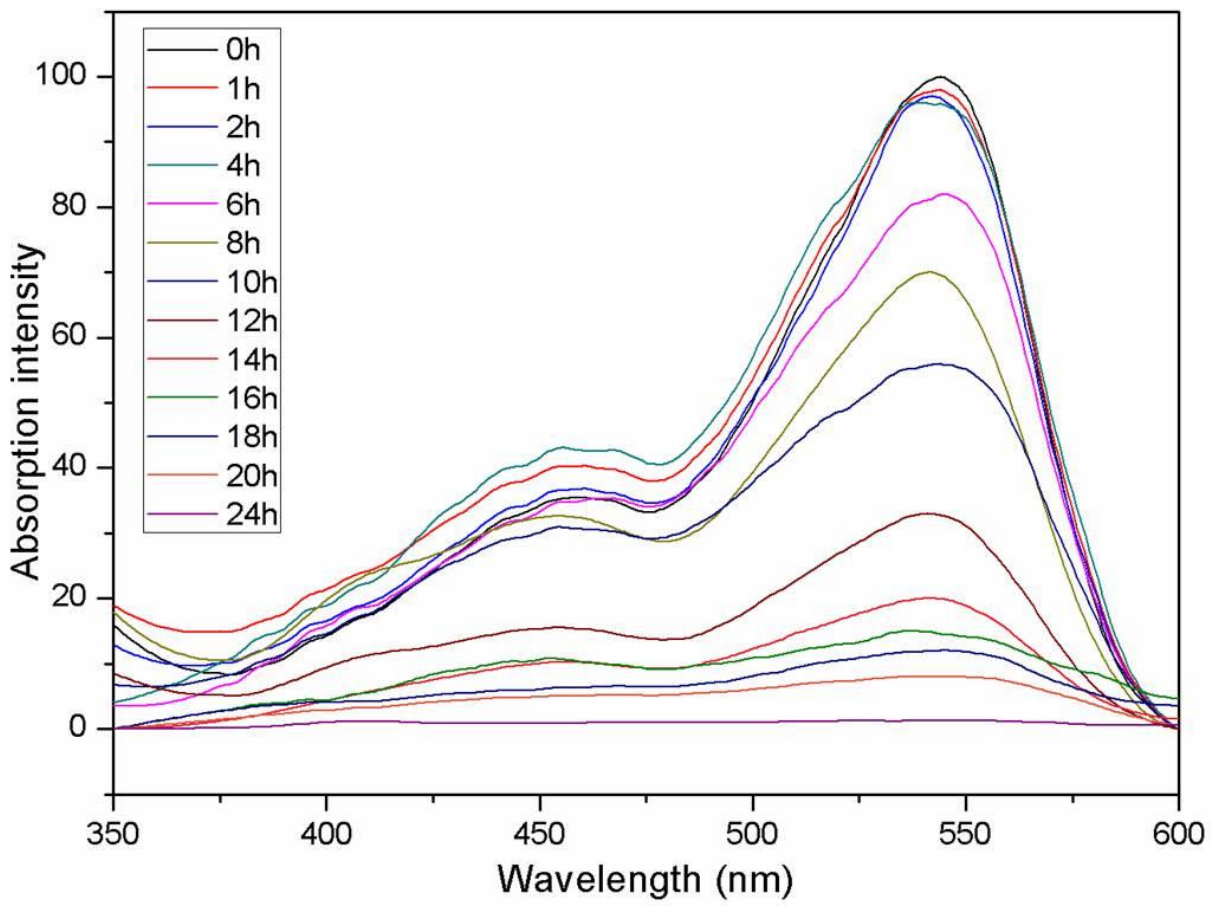

Figure S8. Time-dependent optical absorption of the colored DNA-DOAB liquid crystal after bias was removed (corresponding to the treated sample in Figure 2d). The coloration state maintains an intensity within 95% of the original intensity for ~4 hours, indicating its potential as a basis for optical memory devices.

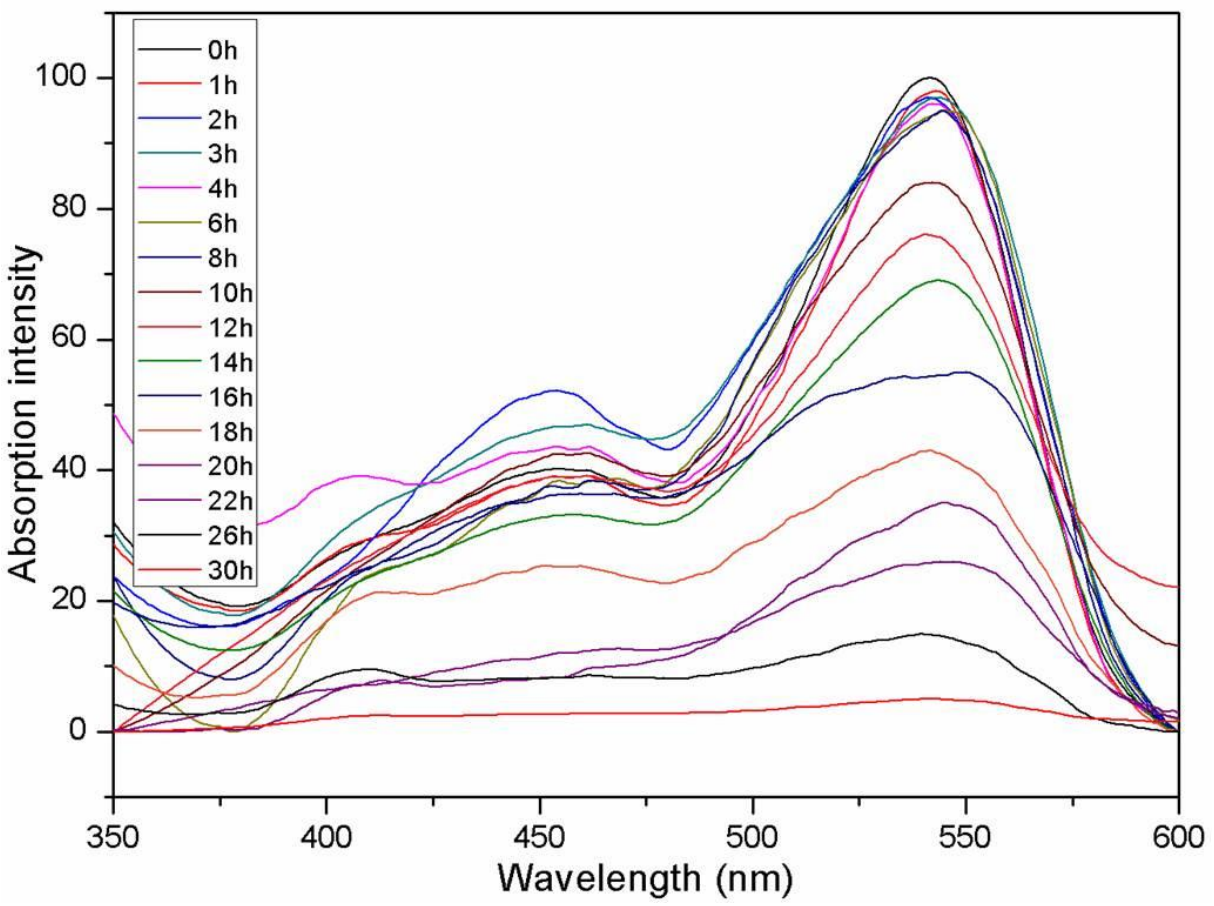

Figure S9. Time-dependent optical absorption of the colored DNA-DOAB crystalline phase after bias was removed (corresponding to the treated sample in Figure 2e,2f). The coloration state maintains an intensity within 95% of the original intensity for ~8 hours.

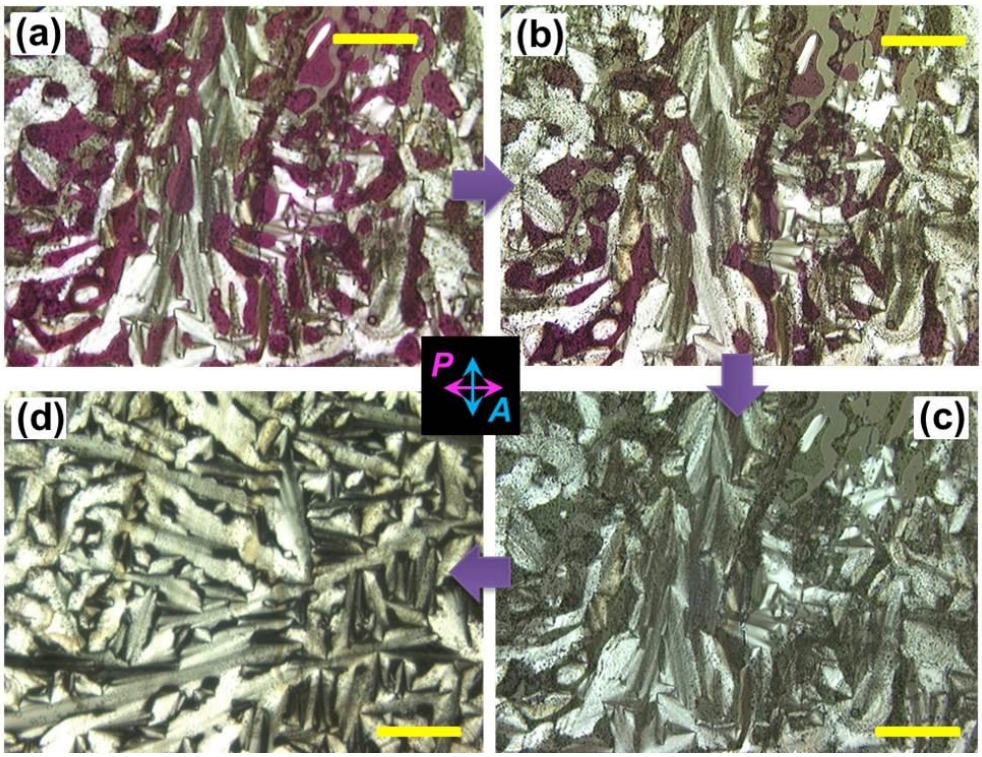

Figure S10. Investigation of birefringence textures, orientation, and color-decay of the colored DNA-DOAB complex in the liquid crystalline phase (25 °C) in the absence of applied voltage. The sample was obtained after the many repeated treatment of applying a positive potential in the isotropic state, cooling to the LC state, removing the potential, and again heating to the isotropic state. (a) The colored DNA-DOAB smectic layers are orientated parallel to the electrode surface, whereas the uncolored DNA-DOAB layers remain perpendicular to electrode surface. There is almost no color decay within 4 hours. (b) After 15 hours, the color decays a lot. The bleached DNA-DOAB smectic layers keep the parallel alignment. (c) After the color decays completely (24 hours), the alignment of the bleached DNA-DOAB lamellar layers remain parallel to electrode surface. (d) The completely reproduced birefringent textures with normal lamella orientation after annealing treatment of the bleached sample, provides evidence for the stability of the ionic DNA-surfactant complex. (Scale bar represents 100 μm).

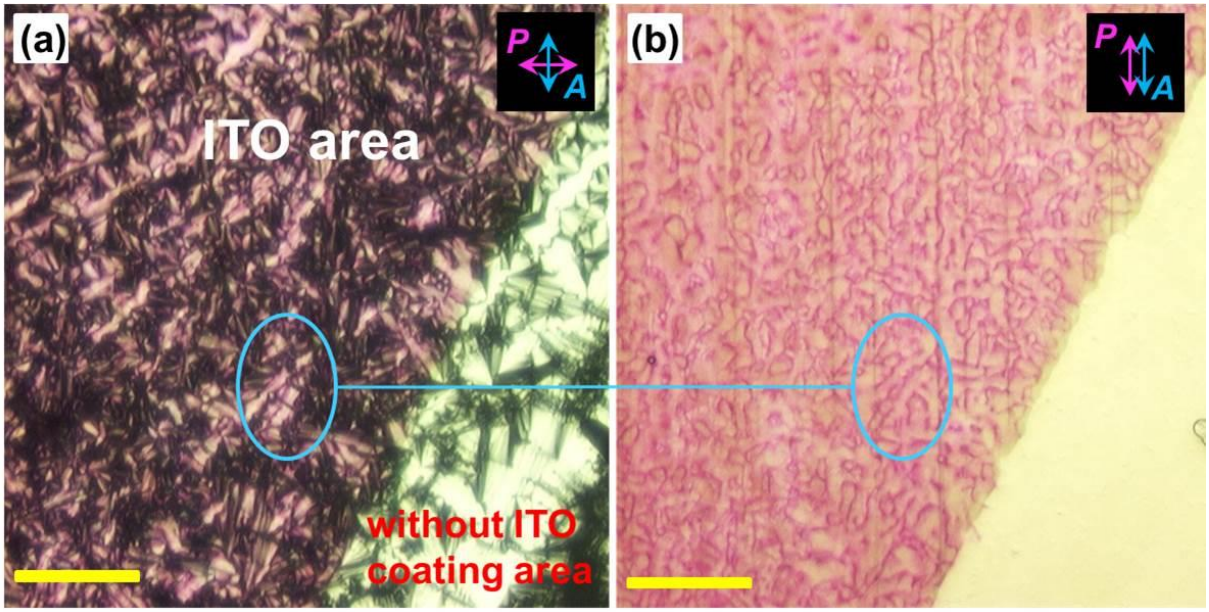

Figure S11. Investigation of birefringence textures, orientation, and color domains of the colored DNA-surfactant complex when cooling to the polycrystalline state (-20 °C) in the absence of applied voltage. The polarized (a) and depolarized (b) images of the colored DNA-DOAB textures. As in the LC phase, the colored DNA-DOAB smectic layer becomes parallel to the electrode surface, whereas the uncolored DNA-DOAB layers remain vertical to electrode surface. (Scale bar represents 100 μm).

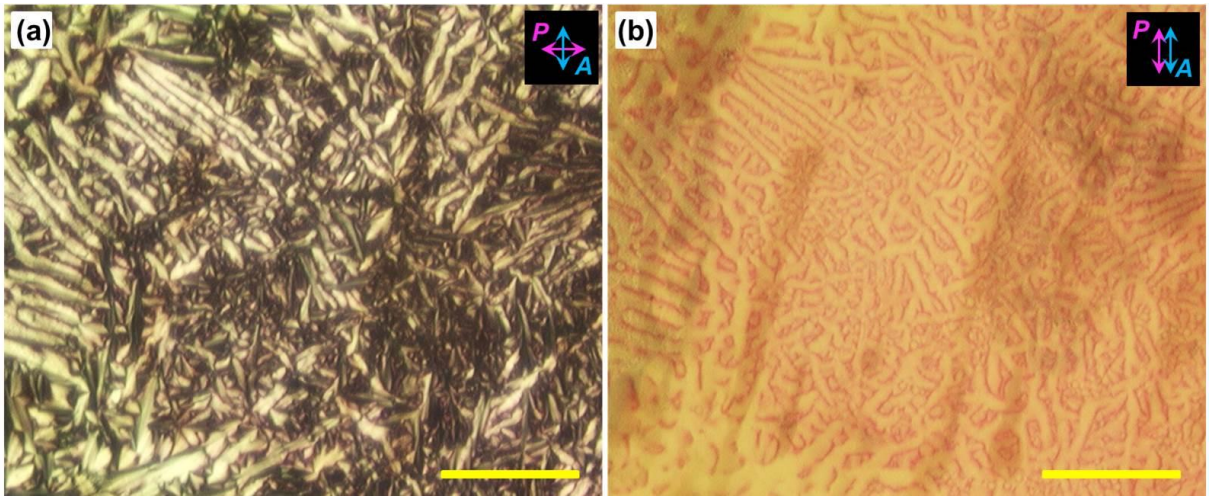

Figure S12. Investigation of birefringence textures, orientation, and color domains of the colored DNA-DOAB crystal (-20 °C) after a decay time of 24 hours. The polarized (a) and depolarized (b) images of the DNA-DOAB complex show that the orientation of color-decayed DNA-DOAB smectic layers are orthogonal to the uncolored DNA-DOAB layers (perpendicular orientation). (Scale bar represents 100 µm).

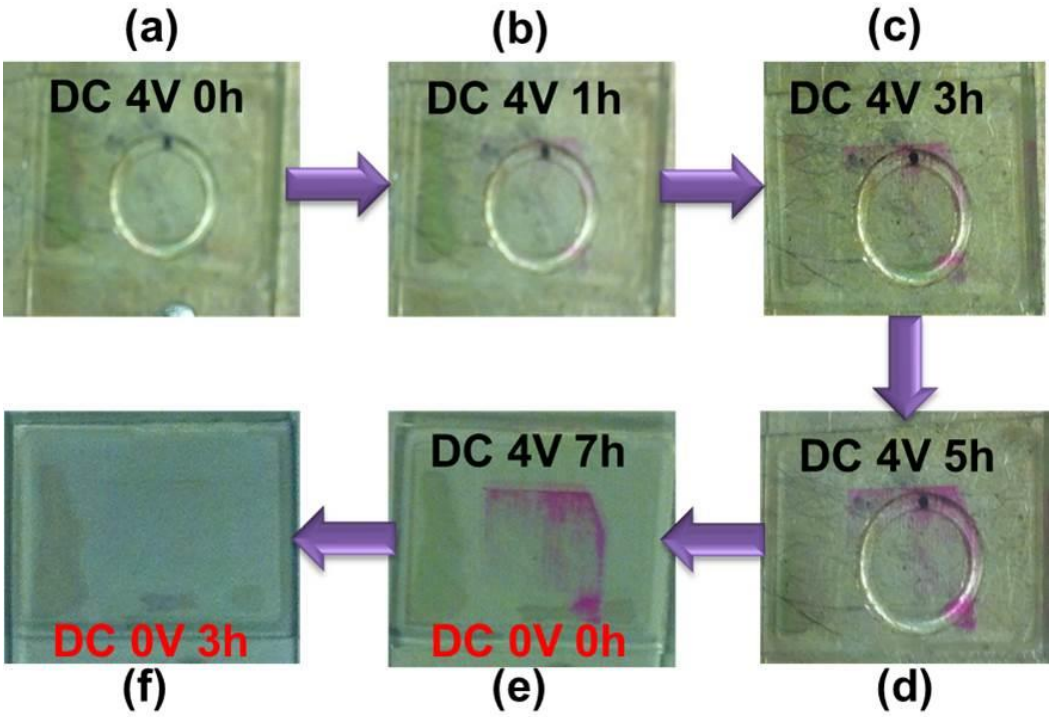

Figure S13. Electrochromism (coloration and coloration decay) of the DNA-DOAB complex with voltage (+4 V) applied directly to the LC phase (25 °C). The coloration process proceeds very slowly. The color decay is complete within 3 hours of removing the bias.

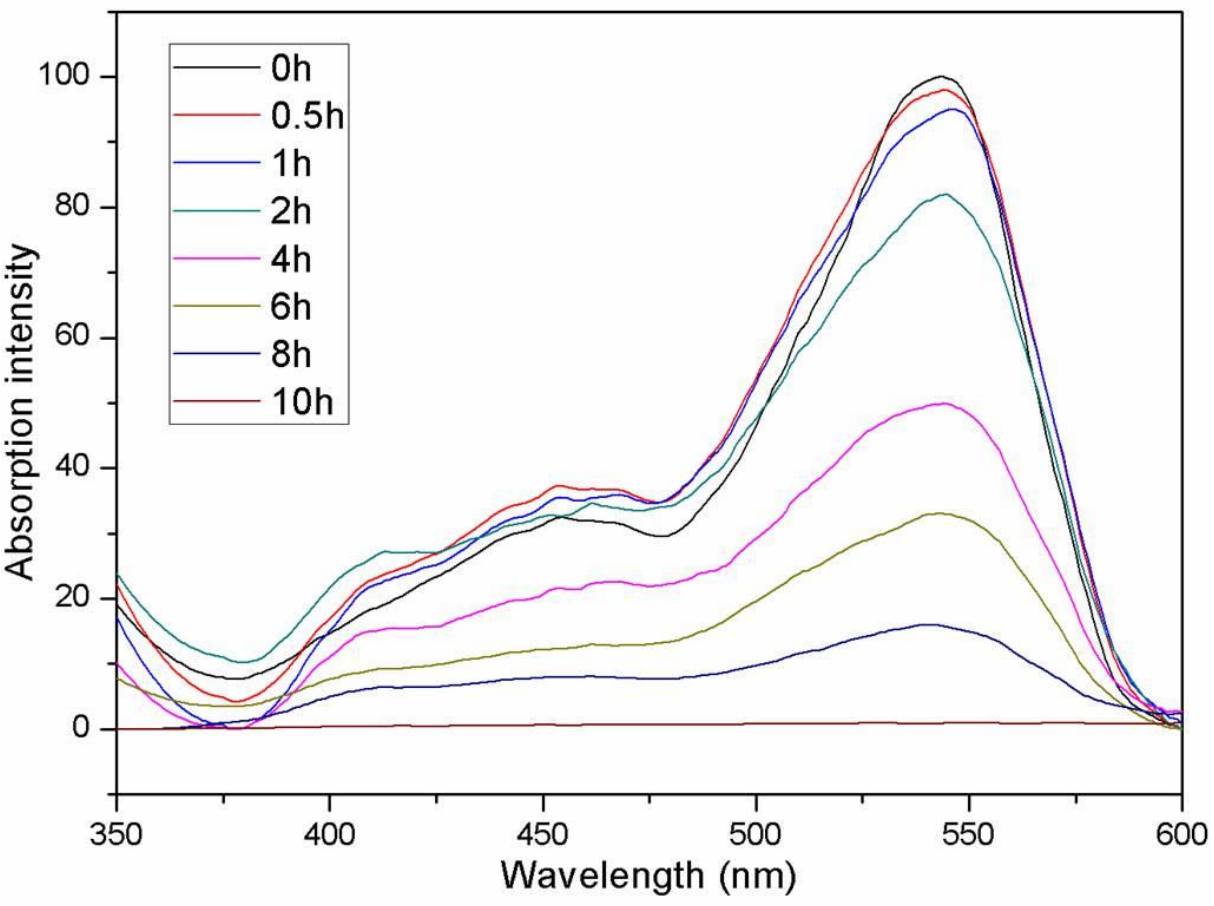

Figure S14. Time-dependent optical absorption of the colored DNA-0.5DOAB-0.5DEAB liquid crystal (45 °C) within a given time of removing the bias. The coloration state maintains an intensity within 95% of the original intensity for ~1 hours.

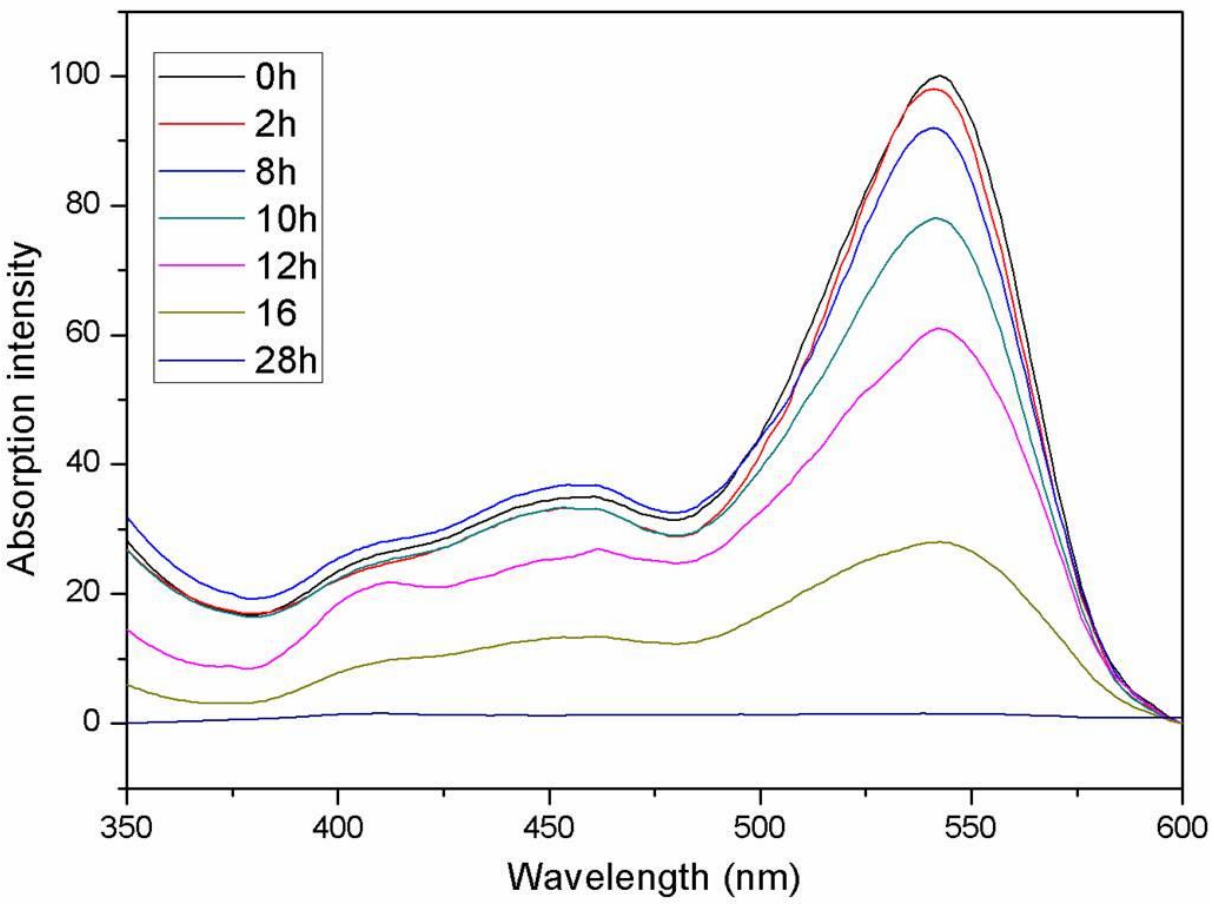

Figure S15. Time-dependent optical absorption of the colored DNA-DEAB complex when cooling to the polycrystalline phase (25 °C) in the absence of applied voltage. The coloration state maintains an intensity within 95% of the original intensity for ~ 7.5 hours.

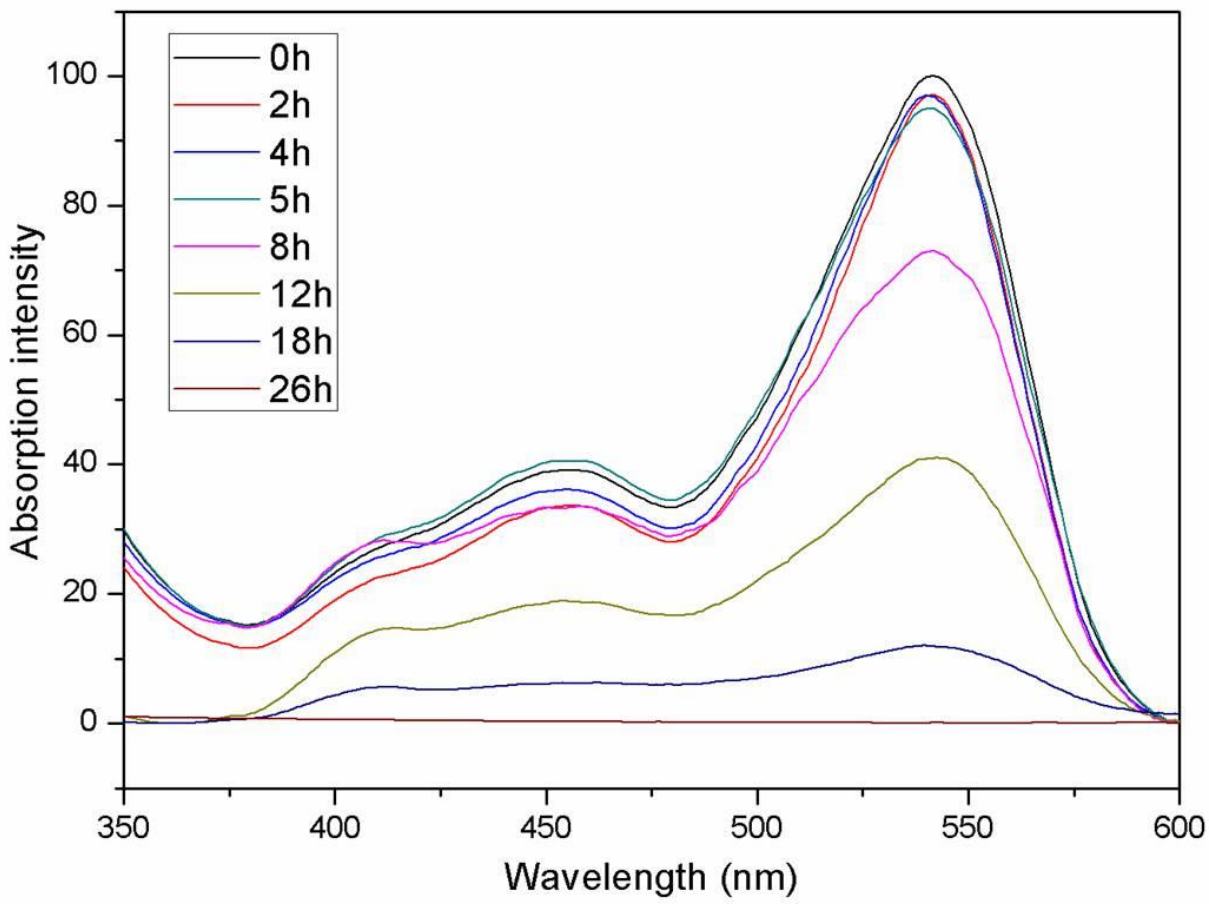

Figure S16. Time-dependent optical absorption of the colored DNA-0.5DOAB-0.5DEAB liquid crystal (25 °C) in the absence of applied voltage. The coloration state maintains an intensity within 95% of the original intensity for ~5 hours.

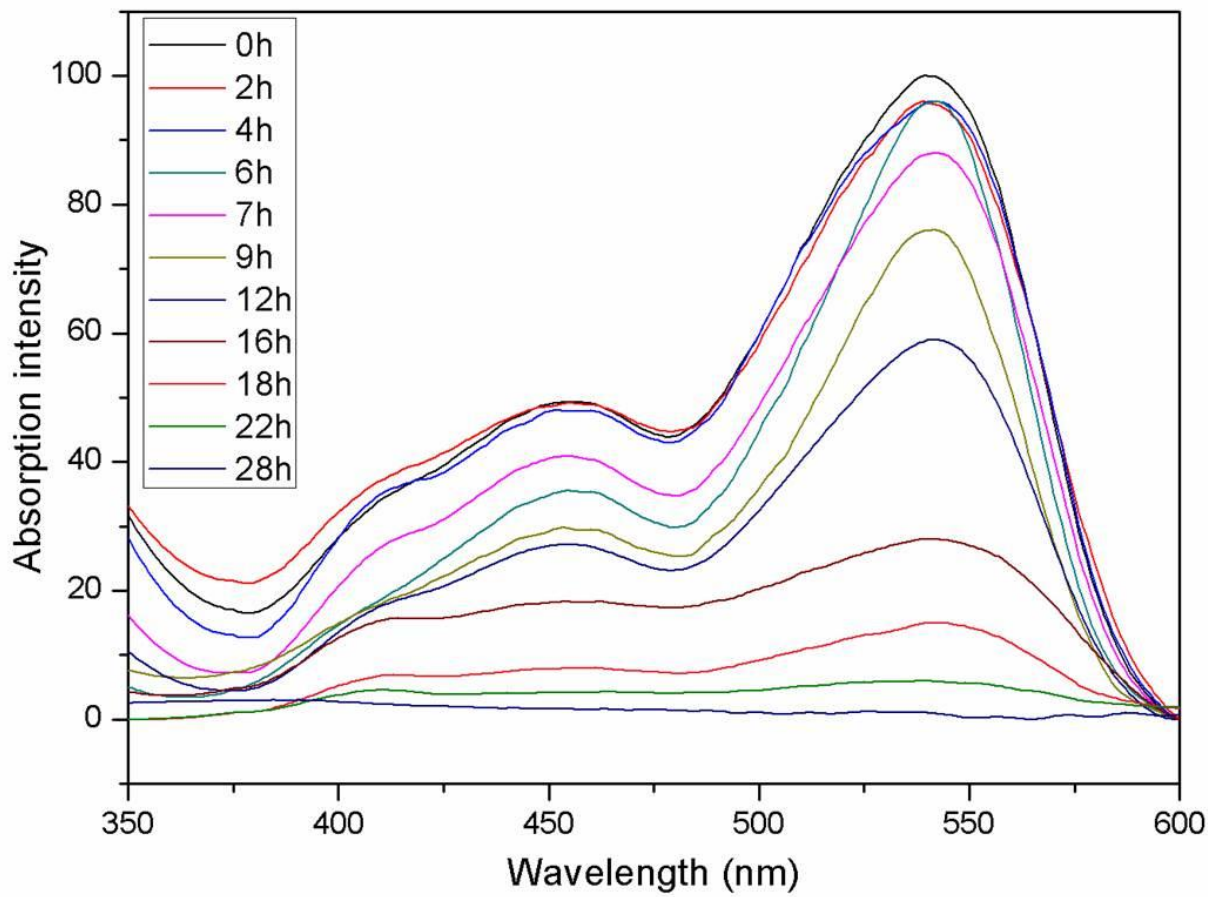

Figure S17. Time-dependent optical absorption of the colored DNA-0.5DEAB-0.5DDAB liquid crystal (25 °C) in the absence of applied voltage. The coloration state maintains an intensity within 95% of the original intensity for ~6 hours.

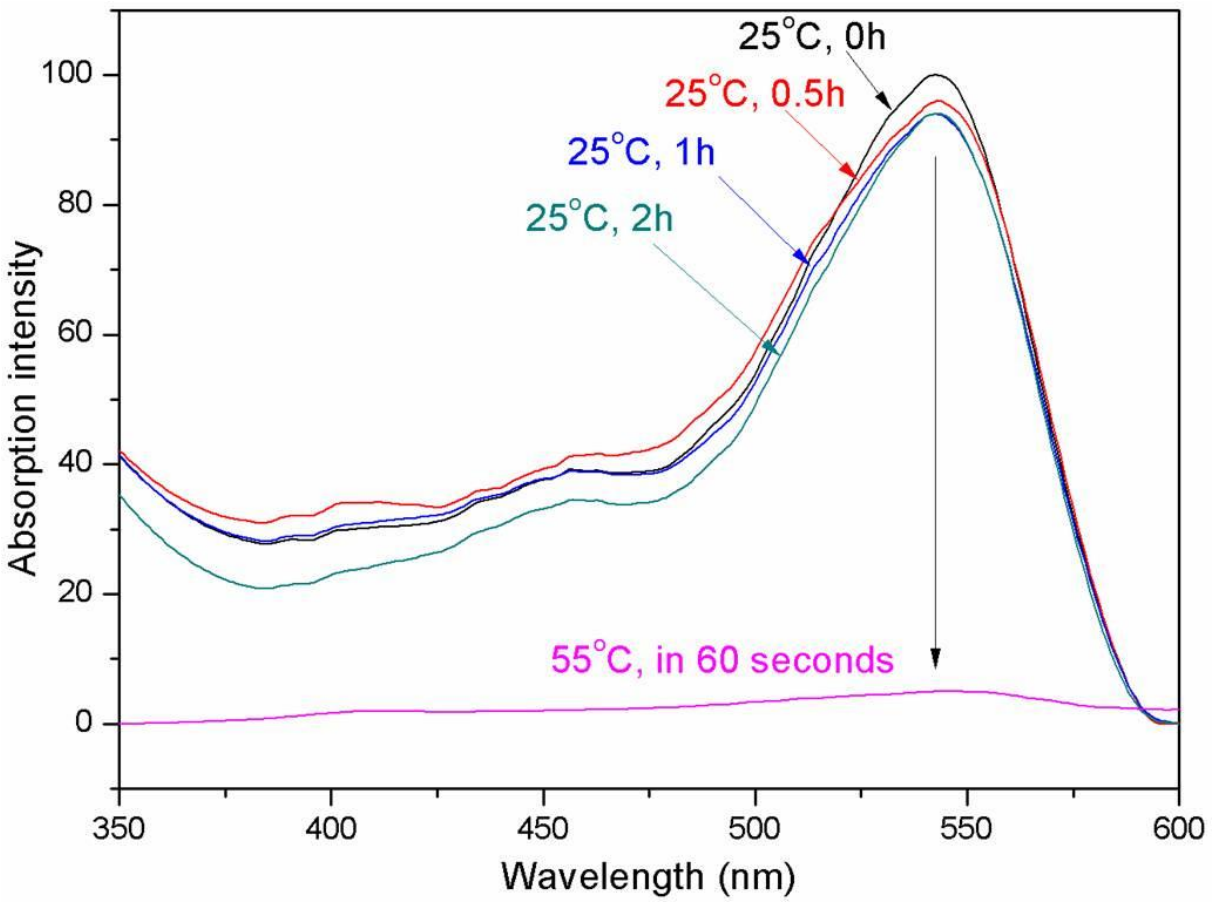

Figure S18. Temperature-sensitive optical absorption of the colored DNA-DOAB LC sample. At 25 °C, the color-activated sample has no color decay for many hours in the absence of applied voltage. Once the sample was in 55 °C (e.g., after 2 hours of the memory device), the color decayed completely in 60 seconds.

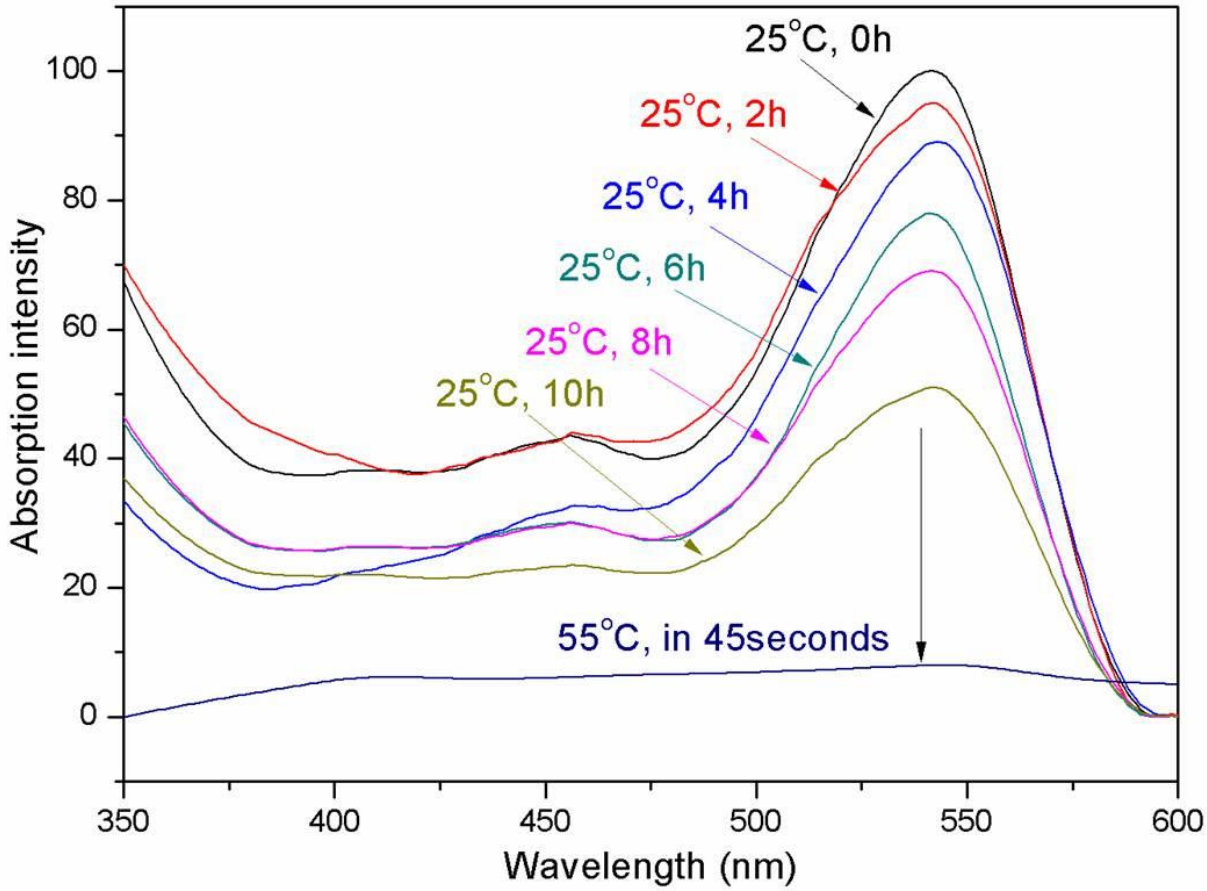

Figure S19. Temperature-sensitive optical absorption of the colored DNA-DOAB LC sample. At 25 °C, the color-activated sample has very slow color decay in the absence of applied voltage. Once the sample was in 55 °C (e.g., after 10 hours of the memory device), the color decayed completely in 45 seconds.

Reference

1. Beaujuge, P. M. & Reynolds, J. R. Color control in pi-conjugated organic polymers for use in electrochromic devices. Chem. Rev. 110, 268-320 (2010).
2. Mortimer, R. J. Electrochromic materials. Chem. Soc. Rev. 26, 147-156 (1997).
3. Rosseinsky, D. R. & Mortimer, R. J. Electrochromic systems and the prospects for devices. Adv. Mater. 13, 783-793 (2001).
4. Monk, P. M. S., Mortimer, R. J. & Rosseinsky, D. R. Electrochromism and electrochromic Devices, Cambridge University Press, Cambridge, 2007.
5. Bird, C. L. & Kühn, A. T. Electrochemistry of the viologens. Chem. Soc. Rev. 10, 49-82 (1981).
6. Schoot, C. J., Ponjee, J. J., van Dam, H. T., van Doorn, R. A. & Bolwijn, P. T. New electrochromic memory display. Appl. Phys. Lett. 23, 64-65 (1973).
7. Yamamura, K., Okada, Y., Kominami, S. O. K. & Tabushi, I. New liquid crystalline viologens exhibiting electric stimulus-response behavior. Tetrahedron Lett. 28, 6475-6478 (1987).
8. Tanabe, K., Yasuda, T., Yoshio, M. & Kato, T. Viologen-based redox-active ionic liquid crystals forming columnar phases. Org. Lett. 9, 4271 (2007).
9. Sanehira, Y., Uchida, S., Kubo, T. & Segawa, H. A distinguished retentive memory using polyethylene glycol electrolyte solvent for viologen modified titania electrochromic device. Electrochemistry 76, 150-153 (2008).
10. Lu, W. et al. Use of ionic liquids for conjugated polymer electrochemical devices. Science, 297, 983-987 (2002).
11. Jensen, J., Dyer, A. L., Shen, D. E., Krebs, F. C. & Reynold, J. R. Direct photopatterning of electrochromic polymers. Adv. Funct. Mater. 23, 3728-3737 (2013).
12. Alamer, F. A., Otley, M. T., Ding, Y. & Sotzing, G. A. Solid-state high-throughput screening for color tuning of electrochromic polymers. Adv. Mater. 25, 6256-6260 (2013).
13. Yen, H., Chen, C. & Liou. G. Flexible multi-colored electrochromic and volatile polymer Memory devices derived from starburst triarylamine-based electroactive polyimide. Adv. Funct. Mater. 23, 5307-5316 (2013).
14. de Tacconi, N. R., Rajeshwar, K. & Lezna, R. O. Metal Hexacyanoferrates: Electrosynthesis, in Situ Characterization, and Applications. Chem. Mater. 15, 3046-3062 (2003).
15. Wade, . C. R., Li, M. & Dincă, M. Facile deposition of multicolored electrochromic metal–organic framework thin films. Angew. Chem. Int. Ed., 52, 13377-13381 (2013).
16. Han, F. S., Higuchi, M. & Kurth, D. G. Metallo-supramolecular polymers based on functionalized bis-terpyridines as novel electrochromic materials. Adv. Mater. 19, 3928-3931 (2007).
17. Kurth, D. G., López, J. P. & Dong, W. F. A new Co(II)-metalloviologen-based electrochromic material integrated in thin multilayer films. Chem. Commun. 2119-2121 (2005).
18. Deb, S. K. A novel electrophotographic system. Appl. Optics., Suppl. 3, 192-195 (1969).
19. Zhang, Y., Lee, Mascarenhas, S., A. & Deb. S. K. An UV photochromic memory effect in proton-based WO3 electrochromic devices. Appl. Phys. Lett. 93, 203508 (2008).
20. Liu, S., Kurth, D. G., Möhwald, H. & Volkmer, D. A thin-film electrochromic device based on a polyoxometalate cluster. Adv. Mater. 14, 225-228 (2002).
21. Liu, J. et al. Ultrathin W18O49 nanowire assemblies for electrochromic devices. Nano Lett. 13, 3589-3593 (2013).

22. Handbook of Liquid Crystals 2nd Edition, (Eds. Goodby, J. W., Collings, P. J., Kato, T., Tschierske, C., Gleeson, H. & Raynes, P.) Wiley-VCH Verlag GmbH & Co. KGaA, (2014).
23. Clark, N. A. & Lagerwall, S. T. Submicrosecond bistable electro-optic switching in liquid crystals. Appl. Phys. Lett. 36, 899-901 (1980).
24. Yazaki, S., Funahashi, T. & Kato, M. An electrochromic nanostructured liquid crystal consisting of π-conjugated and ionic moieties. J. Am. Chem. Soc. 130, 13206-13207 (2008).
25. Yazaki, S., Funahashi, M., Kagimoto, J., Ohno, H. & Kato, T. Nanostructured liquid crystals combining ionic and electronic functions. J. Am. Chem. Soc. 132, 7702-7708 (2010).
26. Beneduci, A., Cospito, S., La Deda, M., Veltri, L. & Chidichimo, G. Electrofluorochromism in π-conjugated ionic liquid crystals. Nat. Commun. 5, 3105 (2014).
27. Dryhurst, G. & Elving, P. J. Electrochemical oxidation-reduction paths for pyrimidine, cytosine, purine and adenine: Correlation and application. Talanta 14, 855-874 (1969).
28. Caruso, T. Capobianco, A. & Peluso, A. The oxidation potential of adenosine and adenosine-thymidine base pair in chloroform solution. J. Am. Chem. Soc. 129, 15347-15353 (2007).
29. Psciuk, B. T., Lord, R. L., Munk, B. H. & Bernhard Schlegel, H. Theoretical determination of one-electron oxidation potentials for nucleic acid bases. J. Chem. Theory Comput. 8, 5107-5123 (2012).
30. Liu, K. et al. Thermotropic liquid crystals from biomacromolecules. Proc. Natl. Acad. Sci. U. S. A. 111, 18596-18600 (2014).
31. Liu, K. et al. Solvent-free Liquid Crystals and Liquids from DNA. Chem. Eur. J. 21, 4898-4903 (2015).
32. Steenken, S. Purine Bases, Nucleosides, and nucleotides: aqueous solution redox chemistry and transformation reactions of their radical cations and e- and OH adducts. Chem. Rev. 89, 503-520 (1989).
33. Pawlicka, A. et al. Ionically conducting DNA-based membranes for eletrochromic devices. Synthetic Metals 161, 2329-2334 (2011).
34. Kakibe, T. & Ohno, H. Quasi-reversible electrochromic behavior of alkyl viologens dispersed mono-molecularly in double-stranded DNA chains. J. Mater. Chem. 19, 4960-4964 (2009).
35. Faul, C. F. J. & Antonietti, M. Ionic self-assembly: facile synthesis of supramolecular materials, Adv. Mater. 15, 673-683 (2003).
36. Kato, T., Mizoshita, N. & Kishimoto, K. Functional liquid-crystalline assemblies: self-organized soft materials. Angew. Chem. Int. Ed. 45, 38 (2006).
37. Stephen, M. Self-assembly and transformation of hybrid nano-objects and nanostructures under equilibrium and non-equilibrium conditions. Nat. Mater. 8, 781-792 (2009).

Chapter 5

Nucleic acid chemistry in organic phase: terminal functionalization of oligonucleotides

Abstract

DNA-incorporating hydrophobic moieties can be synthesized by either solid-phase or solution-phase coupling. On a solid support the DNA is protected and hydrophobic units are usually attached employing phosphoramidite chemistry involving a DNA synthesizer. On the other hand, solution coupling in aqueous medium results in low yields due to the solvent incompatibility of DNA and hydrophobic compounds. Hence, the development of a general coupling method for producing amphiphilic DNA conjugates with high yield in solution remains a major challenge. Here, we report an organic-phase coupling strategy for nucleic acid modification by introducing a hydrophobic DNA-surfactant complex as a reactive scaffold. A remarkable range of amphiphile-DNA structures (DNA-pyrene, DNA-triphenylphosphine, DNA-hydrocarbon, and DNA block copolymers) are produced efficiently. We believe that this method is an important breakthrough in developing a generalized approach to synthesizing functional DNA molecules for self-assembly and related technological applications.

Introduction

The combination of the sequence addressability of DNA and the diversity of functional groups that may be introduced at various sites of the molecule (nucleobase, sugar, or phosphodiester backbone) by conventional synthesis[1-6] has led to the widespread implementation of DNA in diverse applications[7-12]. Conjugates of DNA with organic molecules[13-16], polymers[17-20], metal coordination complexes[21], and nanoparticles[22,23], have served as important tools in the development of new biohybrid materials and reagents that are designed for use in template-directed synthetic chemistry[24,25], catalysis[26,27], biomimetics[28], magnetics[29], optoelectronics[30-32], diagnostics[33-35], biomedicine[36-38], and therapeutics[39,40].

Presently, solid-phase synthesis and solution-phase coupling are the two methodologies one can employ to chemically modify the natural DNA scaffold. Solid-phase synthesis of functionalized DNA most often relies on a commercially available automated DNA synthesizer. Terminal functionalization or the introduction of non-natural nucleotides can be easily integrated into the automated synthesis protocol mostly relying on phosphoramidite chemistry. Alternatively, post-synthetic modification may be carried out on the solid support outside of the synthesizer. In this case, not only phophoramidite chemistry is useful for functionalization but also other transformations are suited for DNA modification including amide formation, Michael addition, or Huisgen cycloaddition[2,3]. However, all the approaches on solid phase have the following general limitations: (I) Yields are usually lower compared to reactions in solution due to the heterogeneous character of the reaction. (II) Special care needs to be taken in solvent selection if a polymer support is employed for DNA synthesis due to solvent-dependent swelling properties of cross-linked polymer resins. (III) Finally, the new products or introduced functional groups need to be stable against the harsh basic deprotection conditions used for removing the protective groups on the nucleic acid scaffold. Thus, modification strategies of DNA based on solid-phase synthesis remain prohibitive for some well-established coupling reactions and chemical functionalities. The absence of a general methodology to introduce various functional moieties renders DNA modification by full solid-phase synthesis a realistic approach only when significant effort can be dedicated to overcoming the many synthetic challenges involved.

Solution-phase DNA modification in the aqueous environment has proven to be highly versatile and efficient in coupling hydrophilic molecules at various DNA positions. However, the synthesis of amphiphilic DNA hybrid materials containing hydrophobic functional moieties is less efficient due to the difficulty of finding solvents that accommodate both extreme lipophiles and hydrophilic DNA strands[2-6]. To overcome this incompatibility, we employ a method of solubilizing DNA in organic solvents by exchanging the counter-ions, which are present along the charged DNA backbone, with

quaternary ammonium surfactants. In doing so, we neutralize the charge on the DNA and provide a hydrophobic coating that can shuttle DNA into the organic phase[41-44].

Inspired by previous work that utilizes DNA-surfactant complexes for DNA-templated reactions and DNA-lipid conjugation[45,46], here, we demonstrate that the DNA-surfactant complex can be much more broadly applied as a simple, generic strategy for overcoming incompatibilities in solubility in the production of functionalized DNA molecules. The prepared DNA-surfactant complex permits the terminal acylation of 3'-amine modified oligonucleotides (ODNs) by a series of hydrophobic NHS esters or acyl chlorides, including pyrene (PY), triphenylphosphine (TPP), hydrocarbon (HC), poly(propylene oxide) (PPO), polyisoprene (PI) and polystyrene (PS).

Results and discussions

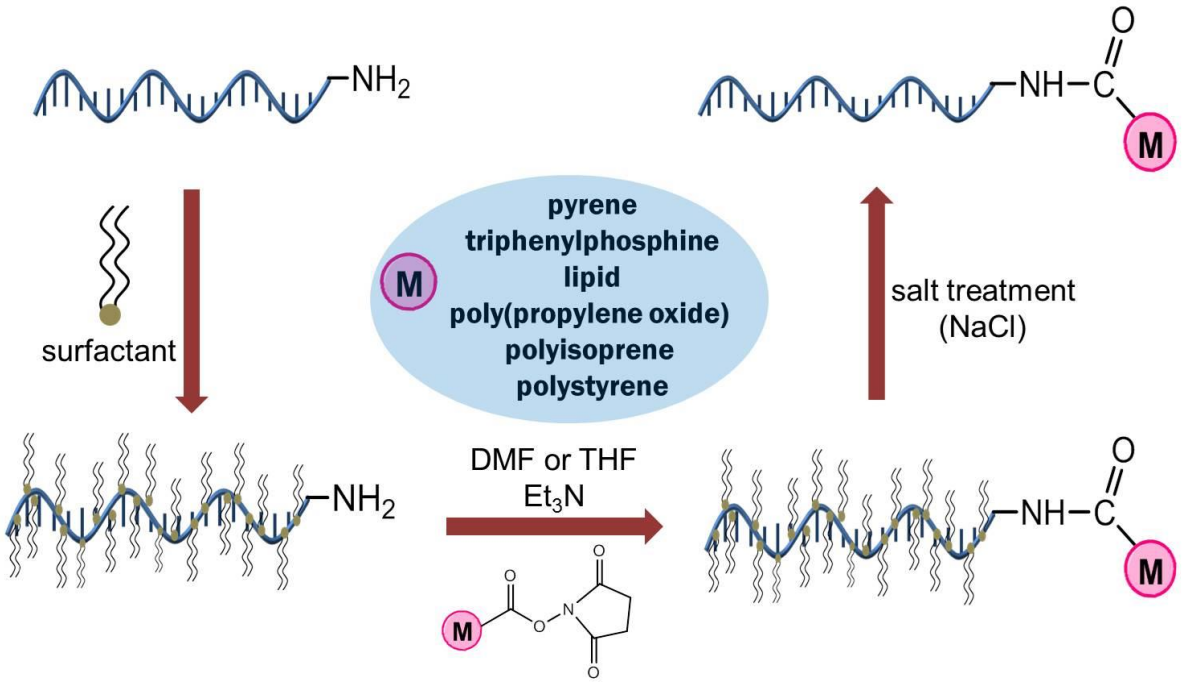

Figure 1. Scheme of the organic-phase synthesis of functional DNA, nucleic acid amphiphiles and DNA block copolymers employing activated esters. Amine modified DNA is precipitated out of the aqueous phase through the complexation with cationic surfactants. The insoluble complex is then extracted and redissolved in an organic solvent, in the present case, DMF or THF. The activated ester form of the hydrophobic unit, which is prepared separately, is then coupled to the terminal amine of the DNA in the homogenous organic phase. Finally, DNA conjugates are obtained after a mold sodium chloride treatment to remove surfactant.

A general scheme of the pathway taken to functionalize a terminal reactive amine group is presented in Figure 1. First, DNA-surfactant complexes were prepared by electrostatic complexation of 3'-amino modified oligonucleotides (6mer, 14mer and 22mer) with the cationic surfactant didodecyldimethylammonium bromide (DDAB) in the aqueous phase. Complex formation leads to the precipitation of the DNA from the aqueous solution and allows the recovery of the surfactant-coated DNA by centrifugation.

Following lyophylization, the DNA-DDAB complex is soluble in organic solvents such as DMF, DMSO, THF and $CHCl_3$. Separately, activated ester derivatives of hydrophobic small molecules and polymers were prepared by the reaction of a carboxylate group with N-hydroxysuccinimide (NHS)[47]. Here, carboxylic acid functionalized PY, TPP, HC, PPO, PI and PS are selected as representative hydrophobic moieties for the NHS ester formation in either DMF or THF. The homogeneous amine acylation reaction between DNA-DDAB and the hydrophobic moiety is carried out in an organic solvent, after which the products are recovered by means of highly concentrated salt solution treatment to release the DNA from the surfactant shell. The as-prepared samples were investigated by denaturing polyacrylamide gel electrophoresis (PAGE), reverse-phase high-performance liquid chromatography (HPLC) and matrix-assisted laser desorption/ionization time-of-flight mass spectrometry (MALDI-TOF MS) (see Table 1 and supplementary figures).

Coupling efficiencies of amphiphilic DNA conjugates

	(**PY** Mw=288)	(**TPP** Mw=306)	(**HC** Mw=340)	(**PPO** Mn=2500)	(**PI** Mn=3500)	(**PS** Mn=900)
Solvent	DMF	DMF	THF	DMF	THF	DMF
6merODN	n.c.	n.c.	n.c.	55%	42%	47%
14merODN	74%	70% (92%)	33%	36%	46%	23%
22merODN	70%	72%	27%	32%	43%	22%

Table 1. Summary of coupling efficiencies of ODN conjugates by means of NHS ester amine acylation in organic solvent (n.c. represents not conducted; coupling efficiencies of ODN-PY, ODN-TPP, and ODN-HC were determined by integrating the HPLC eluting peak intensities measured at an absorption wavelength of 260 nm; coupling efficiencies of ODN-PPO, ODN-PI, and ODN-PS were calculated according to the integration of PAGE lane intensity by ImageJ software; coupling yield presented in parentheses was obtained by the acyl chloride reaction.

Coupling efficiencies from the reaction of ODN (14mer and 22mer) with PY were determined by HPLC to be above 70% (supplementary Figure S2). The UV and visible light spectra of the purified ODN-PY solutions show two absorption bands below 400 nm, which are consistent with DNA (~260 nm) and pyrene (~350 nm) (supplementary Figure S3)[48]. MALDI-TOF MS analysis verified the formation of ODN-PY conjugates, which are characterized by an amide bond (supplementary Figure S4). A control synthesis carried out with 14mer ODN lacking the terminal amine yielded only pristine ODN (supplementary Figure S5), indicating that the amine groups of nucleobases do not react with NHS ester of PY under the same experimental conditions. Thus, it was confirmed that our designed synthetic approach is simple and effective in coupling hydrophobic molecules at terminal ODN functionalities without byproduct formation.

Another hydrophobic molecule, TPP, was coupled with 14mer and 22mer ODN by the same amine acylation in absolute DMF, which efficiently generated amide products of ODN-TPP (coupling efficiency, 70% for 14mer and 72% for 22mer), as determined by HPLC and MALDI-TOF MS (supplementary Figures S6 and S7). These results demonstrate that the length of the ODN does not significantly influence the coupling efficiency between the ODN and the hydrophobic small molecules. It should be noted that two products, including ODN-TPP and the oxidized conjugate, were obtained. The oxidation of ODN-TPP occurs during the post-synthetic handling, the HPLC purification step, and was observed previously as well[27]. Besides the aromatic molecules, which can be effectively conjugated with the ODN by our organic-phase conjugation method, long-chain aliphatic compounds were also successfully coupled to the ODN terminus. In the synthesis of ODN-HC(C22), THF was used as the organic solvent because HC(C22) is insoluble in DMF, while ODN-DDAB also dissolves in THF very well, confirming the universality of DNA-surfactant complex as the coupling scaffold in our synthetic strategy. After analysis by HPLC and MALDI-TOF MS (supplementary Figures S8 and S9), moderate coupling efficiencies for 14mer ODN-HC (33%) and 22mer ODN-HC (27%) were obtained. These values are lower than for ODN-PY and ODN-TPP conjugates, which probably can be ascribed to interference from van der Waals interactions between alkyl chains of DDAB and the HC component. High affinity of the ODN complex with HC could hinder the approach of the NHS ester to amine modified ODN terminus, thus decreasing the coupling yield of the final product.

This approach has also shown to be effective in coupling the ODN to hydrophobic polymers, including PPO, PI, and PS, highlighting the large range of polarity that reactants may exhibit. Three amine-terminated oligonucleotides of different lengths (6mer, 14mer, and 22mer) were conjugated to the activated ester form of each polymer. Our first attempt was to synthesize ODN-*b*-PPO(2.5k) block copolymer in DMF following the procedure outlined in Figure 1. PAGE analysis of the reaction mixtures of the ODN and PPO components (supplementary Figure S10) showed two distinct bands, which suggests that at least two types of ODN with different molecular weights are present. The rapidly-migrating band is assigned to the unreacted ODN due to the similarity of its mobility to pristine ODN. The second band exhibits slower mobility and is assigned to the ODN-PPO conjugate. ODN-PPO conjugation efficiencies were monitored by denaturing PAGE, which revealed 55% yield for 6merODN-*b*-PPO, 36% for 14merODN-*b*-PPO and 32% for 22merODN-*b*-PPO. Using the same procedure, we were also able to conjugate PI(3.5k) and PS(900) to 6mer, 14mer, and 22mer ODN. The ODN-PI and ODN-PS block copolymers were generated efficiently with similar yields to ODN-*b*-PPO (Table 1), as analyzed by PAGE (supplementary Figures S11 and S12).

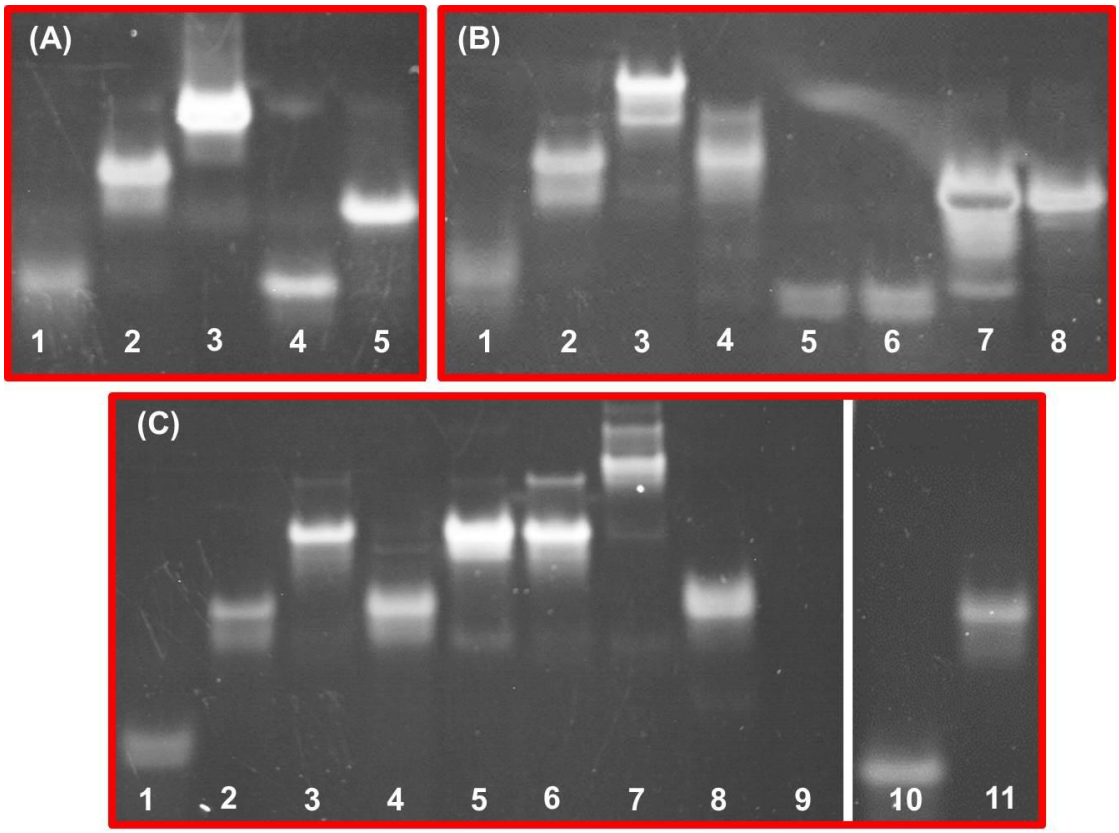

Figure 2. Denaturing polyacrylamide gel electrophoresis (20%, stained by SYBER Gold) analysis of the purified ODN conjugates and ODN block copolymers obtained by amide bond formation. (A) The purified ODN-*b*-PPO block copolymers and ODN-PY conjugates. 1, 6merODN-*b*-PPO(2.5k); 2, 14merODN-*b*-PPO(2.5k); 3, 22merODN-*b*-PPO(2.5k); 4, 14merODN-PY; 5, 22merODN-PY. (B) The purified ODN-*b*-PI block copolymers, ODN-TPP and ODN-HC conjugates. 1, 6merODN-*b*-PI(3.5k); 2, 14merODN-*b*-PI(3.5k); 3, 22merODN-*b*-PI(3.5k); 4, 14merODN-*b*-PI(5.1k); 5, 14merODN-TPP; 6, 14merODN-HC; 7, 22merODN-TPP; 8, 22merODN-HC. (C) The purified ODN-PS diblock and triblock copolymers. 1, 6merODN-*b*-PS(900); 2, 14merODN-*b*-PS(900); 3, 22merODN-*b*-PS(900); 4, 14merODN-*b*-PS(800); 5, 14merODN-*b*-PS(800)-*b*-14merODN; 6, 22merODN-*b*-PS(800); 7, 22merODN-*b*-PS(800)-*b*-22merODN; 8, 14merODN-*b*-PS(4.7k); 9, 6merODN (electrophoretic mobility was too high to be captured on the gel); 10, 14mer ODN; 11, 22merODN. The number in brackets indicates the number average molecular weight Mn of the synthetic polymer.

To further prove the generality of the approach, telechelic PS(800) terminated with carboxylic acid at both ends was coupled to 14mer and 22mer ODN. Diblock ODN-*b*-PS and triblock ODN-*b*-PS-*b*-ODN were obtained simultaneously by one-flask reaction with moderate coupling yields (supplementary Figure S13a). Furthermore, polymers with higher molecular weight PI(5.1k) and PS(4.7k) were efficiently grafted with 14mer ODN, and generated the conjugated products, 14merODN-*b*-PI, 14merODN-*b*-PS, in 40% and 35% yields, respectively (supplementary Figure S13b and 13c). As additional structural proof, the molecular weight of some ODN-polymer conjugates was obtained by MALDI-TOF MS (supplementary Figures S14-S16), further confirming the formation of ODN hybrid copolymers by amide formation in the organic phase. Moreover, the separation of purified diblock and triblock amphiphile ODN conjugates, are clearly

observed by 20% denaturing PAGE (Figure 2). It indicated the change of electrophoretic mobility of the ODN conjugates due to the appended different hydrophobic groups, further confirming the formed ODN amphiphiles. The present coupling efficiencies of ODN to large hydrophobic polymer moieties were at least comparable or even higher than those from solid-phase and other heterogeneous solution grafting approaches[17-20,49-51]. Our strategy, however, requires neither the purchase and maintenance of an in-house DNA synthesizer nor the use of sophisticated and expensive reagents, greatly reducing the investment cost of attempting problematic syntheses via the absolute organic-phase coupling method. Therefore, the DNA-surfactant complex could offer a new platform to functionalize DNA with various previously inaccessible hydrophobic adducts in a facile and efficient way.

We additionally developed an alternative method of synthesizing amphiphile-ODN conjugates by inducing amide bond formation through the reaction of acyl chloride-containing hydrophobic molecules and amine-terminated ODN. It is well known that a carboxylate group can be transferred to the very active acyl chloride by thionyl chloride treatment at room temperature[52]. Here, PY and TPP are selected as the model molecules to demonstrate that 3'-amino modified oligonucleotide can be attached to the hydrophobic molecules via their acyl chlorides (Figure 3A). First, PY acyl chlorides was coupled with ODN-DDAB complexes in anhydrous $CHCl_3$. HPLC characterization revealed that self-complementary 18mer ODN-PY was produced with high coupling efficiency (above 90%, Figures 3B), which is much higher than non-self-complementary ODN-PY (20%, supplementary Figure S17). This may indicate that DNA structure can influence the PY conjugation efficiency in acyl chloride reactions. Then, TPP acyl chloride was also used for the formation of ODN conjugates. 14mer ODN-TPP conjugates (including oxidized TPP-ODN) was produced—with observed coupling efficiencies around 92% (Figures 3C). The acyl chloride reaction produces significantly higher coupling efficiencies than what was observed with NHS coupling (Table 1), presumably due to the higher reactivity of acyl chloride. In addition, the molecular weights of the above samples measured by MALDI-TOF MS (supplementary Figures S18 and S19) are in good agreement with the calculated values, further confirming the synthesis of conjugated products. As a comparison, we conducted a coupling experiment between TPP acyl chloride and the ODN that lacks a terminal amine group. We observed no generation of ODN-TPP conjugates, suggesting that the reactivity of amine groups of the bases is not enough to couple with acyl chloride (supplementary Figure S20). This result further confirms that the primary terminal amine exclusively reacts to form the conjugates at the chosen condition. Therefore, one attractive facet of the developed method is that contamination with byproducts from nucleobase conjugates may be avoided completely. We have found that this method is less suitable for the synthesis of DNA-block copolymers due to the inactivation of the acyl chloride over the long reaction times required (24 hours). In the conjugation of small,

hydrophobic molecules to DNA, however, the acyl chloride method may produce higher conversions than the NHS method.

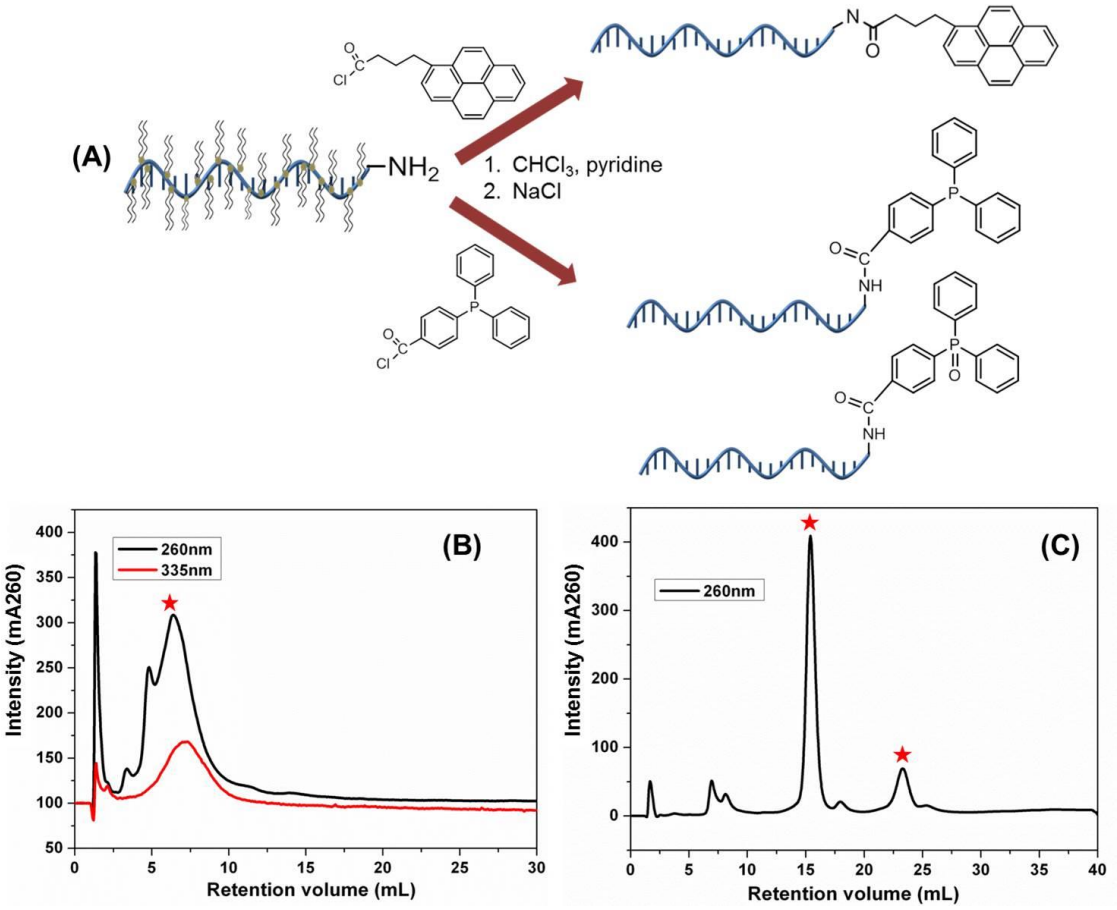

Figure 3. Preparation and purification of amphiphile ODN conjugates (ODN-PY and ODN-TPP) by means of the acyl chloride reaction in anhydrous $CHCl_3$. (A) Schematic of the synthesis route of ODN-PY and ODN-TPP. (B) Reverse phase HPLC analysis of the crude product of 18mer self-complementary ODN-PY conjugate (sequence: 5'-CGATCGATTTATCGATCG-3'). The presence of the DNA was monitored by the absorbance at 260 nm (mA260). Only one elution peak (marked with red star) corresponds to the generated ODN-PY, indicating an almost quantitative transformation. Due to the self-complementary nature of the ODN sequence, hairpin, dimer and multimer duplexes by different hybridization paths could be formed. These structures presumably lead to the broad peak observed in reverse phase HPLC. (C) Reverse phase HPLC analysis of 14merODN-TPP conjugate, suggests a coupling efficiency of 92%. ODN-TPP and oxidized TPP-ODN are the actual products (marked with red star) due to TPP oxidation during the purification process outside of an inert atmosphere.

Conclusions

In this work, a facile synthetic method for nucleic acid functionalization in organic phase has been developed. Utilizing a DNA-surfactant complex as a versatile and general scaffold for DNA functionalization in the organic phase, we have incorporated hydrophobic modifications at terminal and internal DNA positions. Various functional moieties, from hydrophobic small molecules to polymers, including pyrene, triphenylphosphine, long hydrocarbon chains, poly(propylene oxide), polyisoprene and polystyrene, have been efficiently and conveniently coupled with DNA. The established

strategy has some striking features. First, high yields for amphiphilic DNA conjugates are achieved, relative to existing methods. Second, the coupling reactions are simple, easily controllable, and applicable to a variety of hydrophobic moieties. More importantly, this approach avoids the large instrumental investment of acquiring an automated DNA synthesizer in the laboratory, thus expanding the accessibility of problematic, custom-synthesized DNA conjugates to the level of research groups. As a consequence, this technique paves the way to the synthesis of a wide variety of amphiphilic DNA hybrids for exploring DNA applications in bio- and nanotechnology more broadly.

Experimental Section

Materials

Hydrophobic molecules used for coupling with DNA including 1-pyrenebutyric acid (PY), 4-(diphenylphosphino)benzoic acid (TPP) and behenic acid were purchased from Sigma–Aldrich. Polymers including α-methoxy-ω-COOH terminated poly(propylene glycol) (PPO, M_n=2500, PDI=1.25), carboxy-terminated polyisoprene (1,4-addition) (PI, Mn=3500, PDI=1.1), carboxy-terminated polyisoprene (1,2 and 3,4-addition) (PI, Mn=5100, PDI=1.1), carboxy-terminated polystyrene (PS, M_n=900, PDI=1.5; M_n=4700, PDI=1.1) and α,ω-dicarboxy-terminated polystyrene (PS, M_n=800, PDI=1.4) were purchased from Polymer Source. Surfactant (DDAB, didodecyldimethylammonium bromide) used for the DNA complex formation was purchased from Sigma-Aldrich. 3'-NH2 modified DNA including 6mer (5'-CCTCGC-3'), 14mer (5'-CCTCGCTCTGCTAA-3'), 22mer (5'-CCTCGCTCTGCTAA-3') and 18mer self-complementary (5'-CGATCGATTTATCGATCG-3') were synthesized by standard phosphoramidite chemistry. Custom Primer Support C6 amino 200 was purchased from GE Healthcare Lifescience. Other solvents and reagents for DNA synthesis were aquired from Sigma-Aldrich. During all experiments, ultrapure water (18.2 MΩ) purified by a MilliQ-Millipore system (Millipore, Germany) was used.

Characterization

The NHS esters and acyl chlorides of hydrophobic molecules were characterized by ^{1}H NMR measurements and recorded on a Bruker AV400 FT NMR spectrometer (at 400 MHz). Functional DNA molecules and amphiphilic DNA conjugates were purified by high-performance liquid chromatography (HPLC, ÄKTA DNA explorer, GE Healthcare). Analysis of the DNA block copolymers crude products was carried out by denaturing polyacrylamide gel electrophoresis (PAGE) (20 w% TBE gel, Invitrogen life technologies) with subsequent SYBR Gold staining, and photographs of the gels were taken with a LAS-3000 Image Reader (Fuji Photo Film (Europe) GmbH, Dusseldorf, Germany). Purification of the DNA block copolymers was carried out by preparative PAGE (20 w%, Acr/Bis = 19:1, ~10 M Urea). Mass spectrometry of the synthesized DNA

and DNA conjugates was performed using a 4800 MALDI-TOF/TOF Analyzer (Applied Biosystems, Foster City, CA, USA) with 3-hydroxypicolinic acid (HPA) as matrix.

DNA-surfactant complex preparation

Aqueous solutions (0.5 mM) of 3'-amino modified ODN (6mer, 14mer, 22mer, and a pair of self-complementary 18mers) were prepared by dissolving the purified ODN in ultrapure water. In a second solution made from ultrapure water, the concentration of surfactant of didodecyldimethylammonium bromide (DDAB) was adjusted to 5-10 mM at room temperature. When the ODN and surfactants solutions (~5 mol equivalents of surfactant relative to nucleotides of the ODN) were mixed together, the insoluble complex precipitated from the aqueous phase. After centrifugation, the water and unreacted surfactants were removed, and finally, the complexes were lyophilized overnight before further dissolving in organic solvents for coupling with hydrophobic molecules.

NHS ester preparation

Small molecules and polymers (0.1 mmol) (1-pyrenebutyric acid, 4-(diphenylphosphino)benzoic acid, α-methoxy-ω-COOH terminated poly(propylene glycol), and carboxy terminated polystyrene) were first dissolved in 1.0 mL DMF, respectively. Then N-hydroxysuccinimide (NHS, 0.12 mmol) was added into the above DMF solutions with stirring. After 5min, 0.5 mL of DMF containing N,N'-dicyclohexylcarbodiimide (DCC, 0.12 mmol) was added dropwise to the reaction solution. The final mixture was stirred at room temperature under argon and white precipitate of dicyclohexylurea (DCU) appeared. After purification, the obtained products were used for the coupling experiments with DNA-surfactant complexes. NHS esters of behenic acid and carboxy-terminated polyisoprene were prepared following the same procedures except THF as the organic solvent.

Acyl chloride preparation

1.0 mL of $CHCl_3$ solution containing 1-pyrenebutyric acid and 4-(diphenylphosphino)benzoic acid (0.1 mmol) were prepared, respectively. To the solution, 1.0 mL of thionyl chloride ($SOCl_2$, 13 mmol) was added dropwise. The mixtures were stirred at room temperature under argon. After 5h, $SOCl_2$ was evaporated and the formed acyl chloride was used for the coupling experiments with DNA-surfactant complexes.

Synthesis of amphiphile DNA conjugates by amide bond formation

The prepared ODN-DDAB complexes (1.0 μmol) were dissolved in 200 μL DMF. Then, the prepared NHS esters (15.0 μmol) of small molecules (1-pyrenebutyric acid and 4-(diphenylphosphino)benzoic acid) and polymers (poly(propylene glycol) and

polystyrene) in 500 µL DMF and triethylamine (Et_3N, 1.4 mmol, 200 µL) were added to ODN-DDAB solutions. The final mixtures were stirred 24h at room temperature under argon. After that, saturated NaCl aqueous solution (150 µL) was added into the above organic solutions and stirred for another 3h. After evaporation of DMF, 500 µL MilliQ water was added and the mixtures were filtered to separate the unreacted esters of hydrophobic molecules and polymers. Then desalting process was carried out using a centrifugal concentrator (Vivaspin). Finally, the crude products were purified before further characterization. The coupling between ODN-DDAB and NHS ester of behenic acid or polyisoprene was carried out using the same procedures, except using THF as the organic solvent. For the synthesis of ODN triblock polystyrene, 4 µmol of ODN-DDAB complexes in 300 µL DMF were used to react with NHS ester of α,ω-dicarboxy terminated polystyrene (2 µmol in 100 µL DMF). Furthermore, the acyl chloride of 1-pyrenebutyric acid and 4-(diphenylphosphino)benzoic acid were reacted with ODN-DDAB complexes in $CHCl_3$ with argon protection for 3~5h following the above protocol.

Purification and coupling efficiency calculation of amphiphile DNA conjugates

Reverse phase HPLC was used to purify the DNA conjugated small molecules (1-pyrenebutyric acid, 4-(diphenylphosphino)benzoic acid, and behenic acid). HPLC information: RESOURCE™ RPC column (1 mL), 0-100 %B gradient, flow rate 2 mL/min, 0.1 M triethylammonium acetate buffer containing 2.5% acetonitrile as buffer A, 0.1 M triethylammonium acetate buffer containing 65% acetonitrile as buffer B. Coupling efficiencies of the above conjugates were determined by integrating the eluting peak intensities of 260 nm. Denaturing PAGE (20%) was used to analyze crude products of the 14mer and 22mer ODN block copolymer with SYBER Gold staining. Coupling efficiencies were calculated according to the integration of PAGE lane intensity by ImageJ software. Preparative PAGE (8%) was used to purify 6mer, 14mer, and 22mer ODN block copolymers. Coupling efficiencies of 6mer ODN block copolymers were determined by analysis of the preparative PAGE (8%).

Supplementary Figures

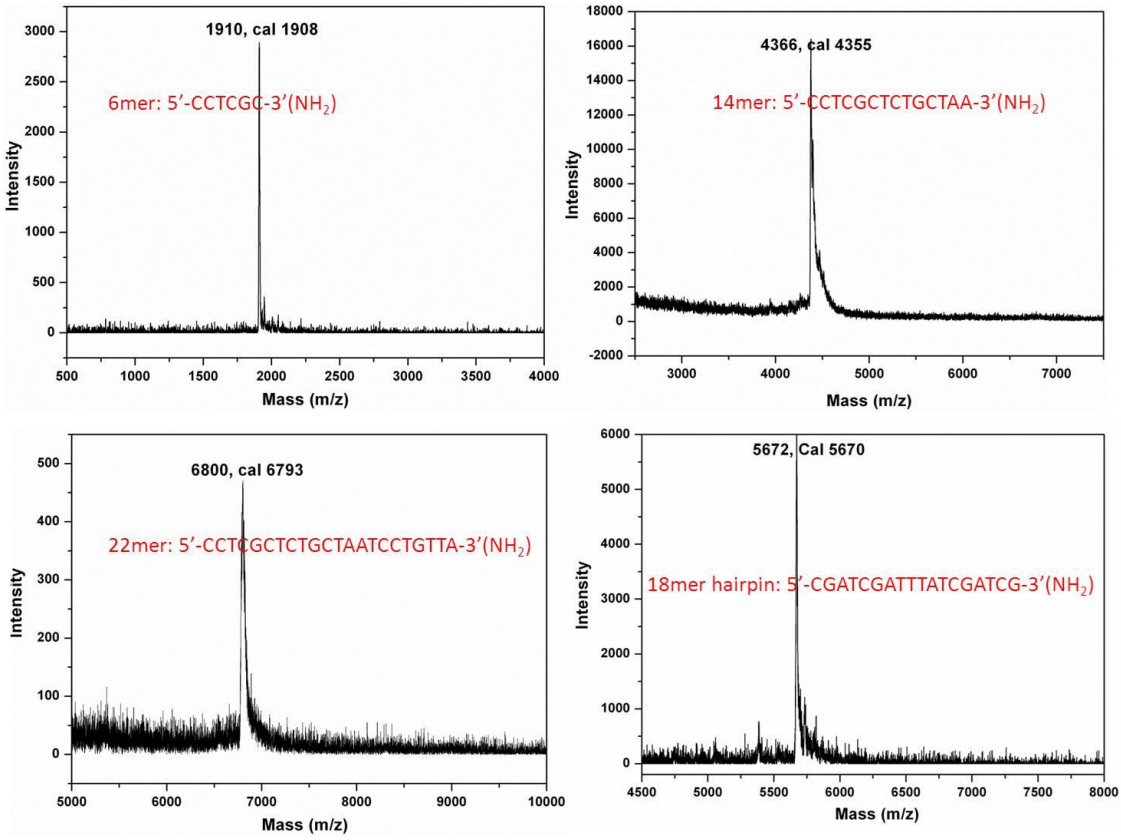

Figure S1. MALDI-TOF mass spectra of the 3'-amino-modified DNA. The oligonucleotides were synthesized by standard phosphoramidite chemistry using C6-amino-modified solid-support. After anion exchange HPLC purification, MALDI-TOF MS measurements were carried out with 3-hydroxypicolinic acid (HPA) as matrix. All spectra confirm the identity of the corresponding DNA molecules.

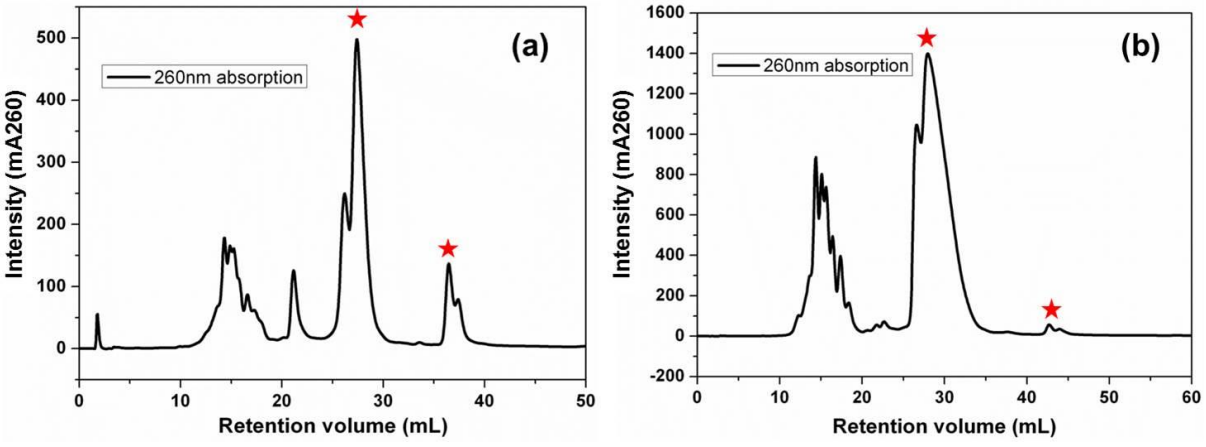

Figure S2. Reverse phase HPLC elugrams of the reaction mixtures of the 14merDNA-PY (a) and 22merDNA-PY (b). Combined with the following MALDI-TOF MS results, the elution peaks marked with red star represent the generated conjugates with coupling efficiencies of 74% (14merDNA-PY) and 70% (22merDNA-PY), respectively. The peaks at higher elution volumes (>35 mL) marked with a star represent micelle aggregates of DNA-PY.

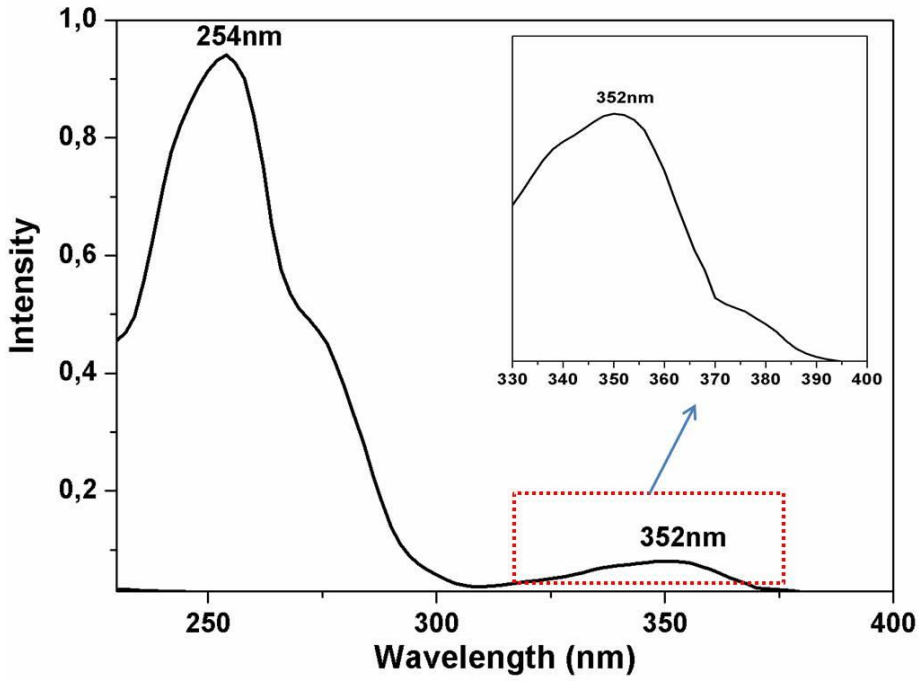

Figure S3. UV absorption of the purified 22mer DNA-PY conjugate. Two UV bands appear, corresponding to the absorptions of DNA at ~260 nm and pyrene at ~350 nm, suggesting the successful formation of the DNA-PY conjugate.

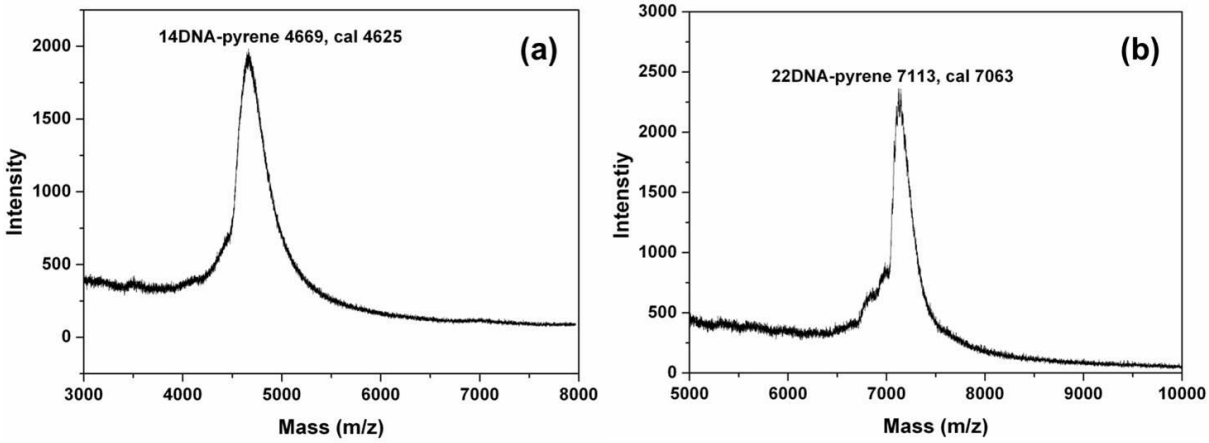

Figure S4. MALDI-TOF mass spectra of the purified 14merDNA-PY (a) and 22merDNA-PY (b) measured with HPA as matrix. The mass peaks are in good agreement with the calculated values.

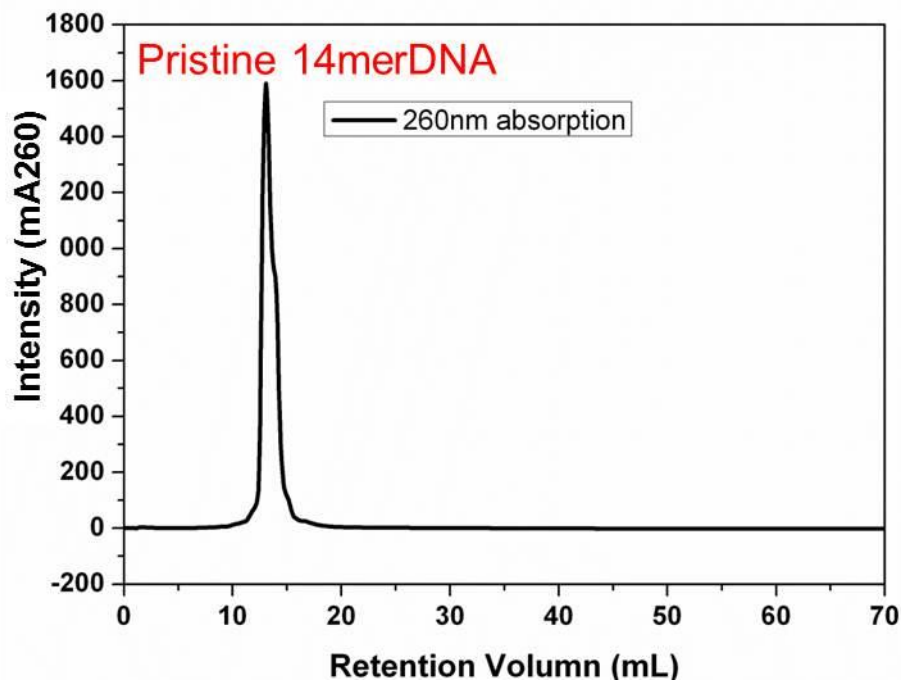

Figure S5. HPLC analysis of the reaction mixture of 14mer DNA without 3'-NH_2 group reacted with pyrene NHS ester. In the control experiment, only uncoupled DNA appeared, indicating that the amine groups of nucleobases do not react with NHS ester under the experimental conditions.

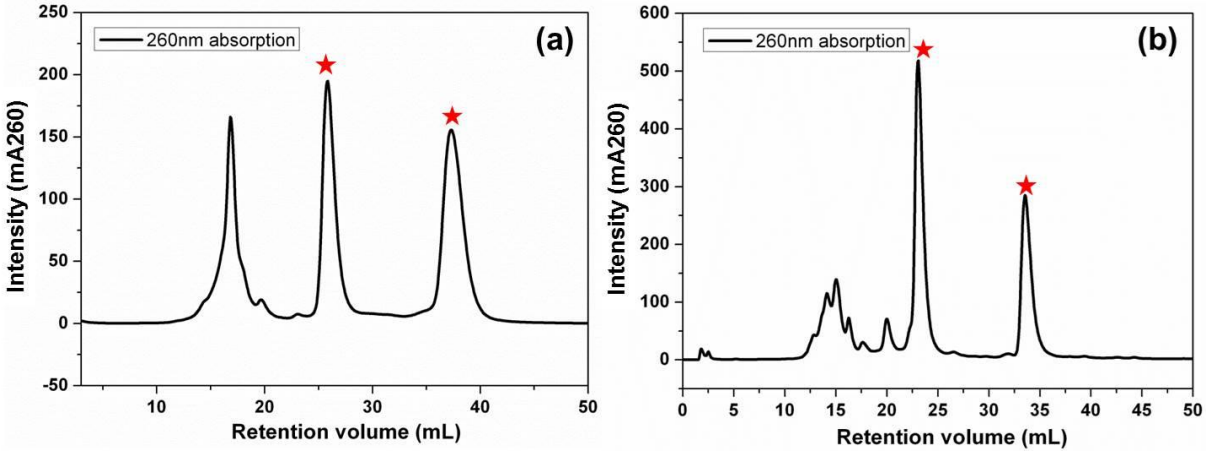

Figure S6. Reverse phase HPLC elugram of the reaction mixture of 14merDNA-TPP (a) and 22merDNA-TPP (b). According to the following MALDI-TOF MS results, the two elution peaks marked with red star are the products that were obtained with coupling efficiencies of 70% and 72%, respectively. The oxidized TPP-DNA conjugate (first peak marked with a star) was produced simultaneously, which indicated that the oxidation of DNA-TPP happened during the post-treatment, especially in the HPLC purification process without any inert gas protection. The used buffer solutions were not deoxygenated.

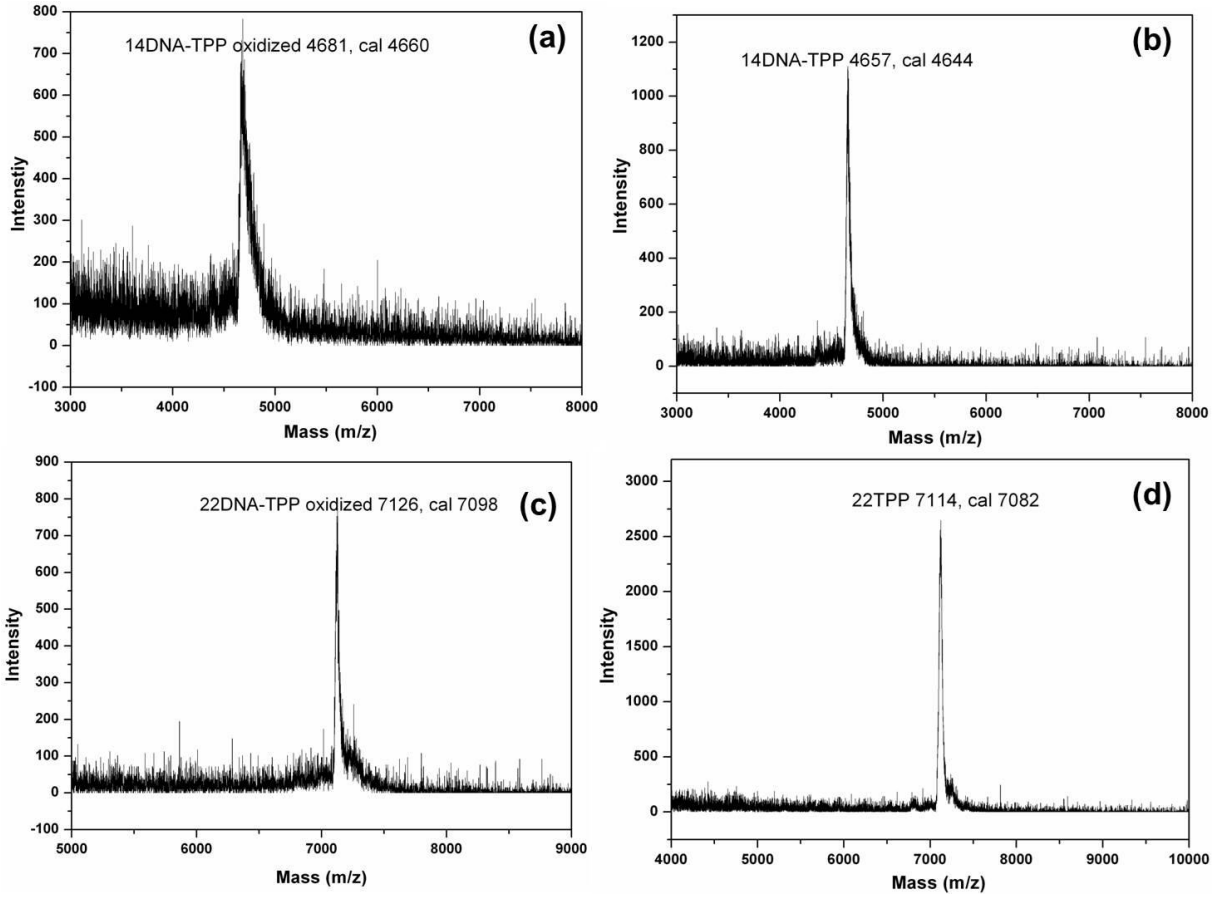

Figure S7. MALDI-TOF mass spectra of the 14mer (a and b) and 22mer (c and d) DNA-TPP and oxidized TPP-DNA conjugates measured with HPA as matrix. The mass peaks are in good agreement with the calculated values.

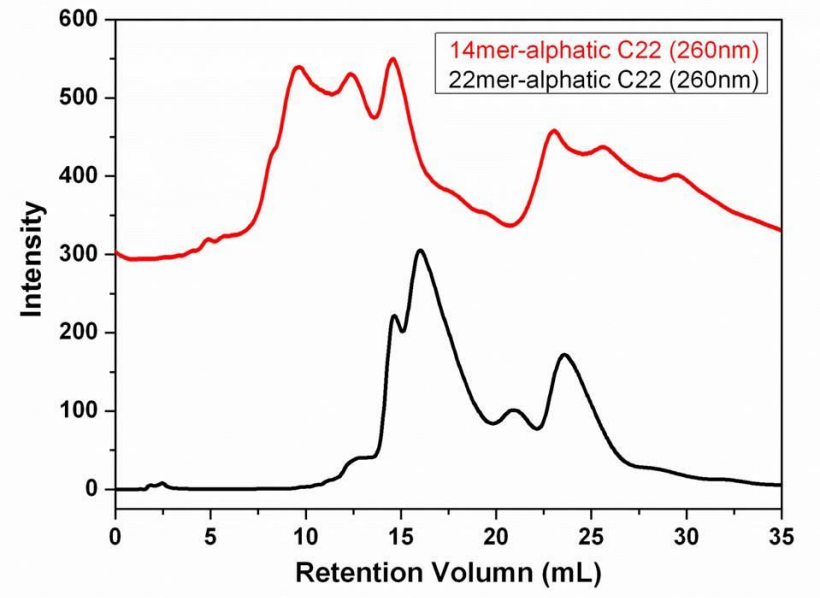

Figure S8. Reverse phase HPLC analysis of DNA lipid conjugates (14mer, red; 22mer, black). According to the following MALDI-TOF MS results, the elution peaks marked with red star represent the products that were obtained with coupling efficiencies of 33% and 27%, respectively.

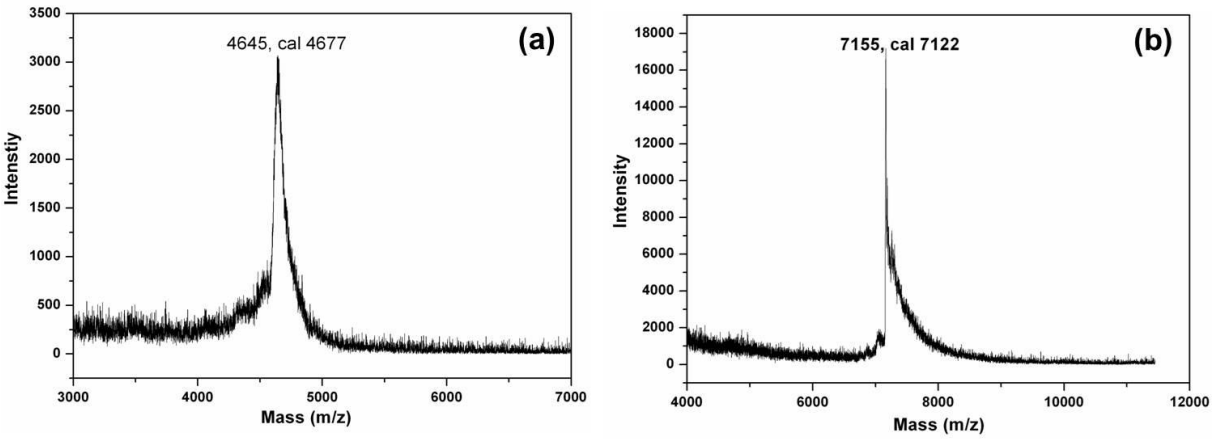

Figure S9. MALDI-TOF mass spectra of the purified 14merDNA-lipid (a) and 22merDNA-lipid (b) obtained with HPA as matrix. The measured mass peaks are in good agreement with the calculated values.

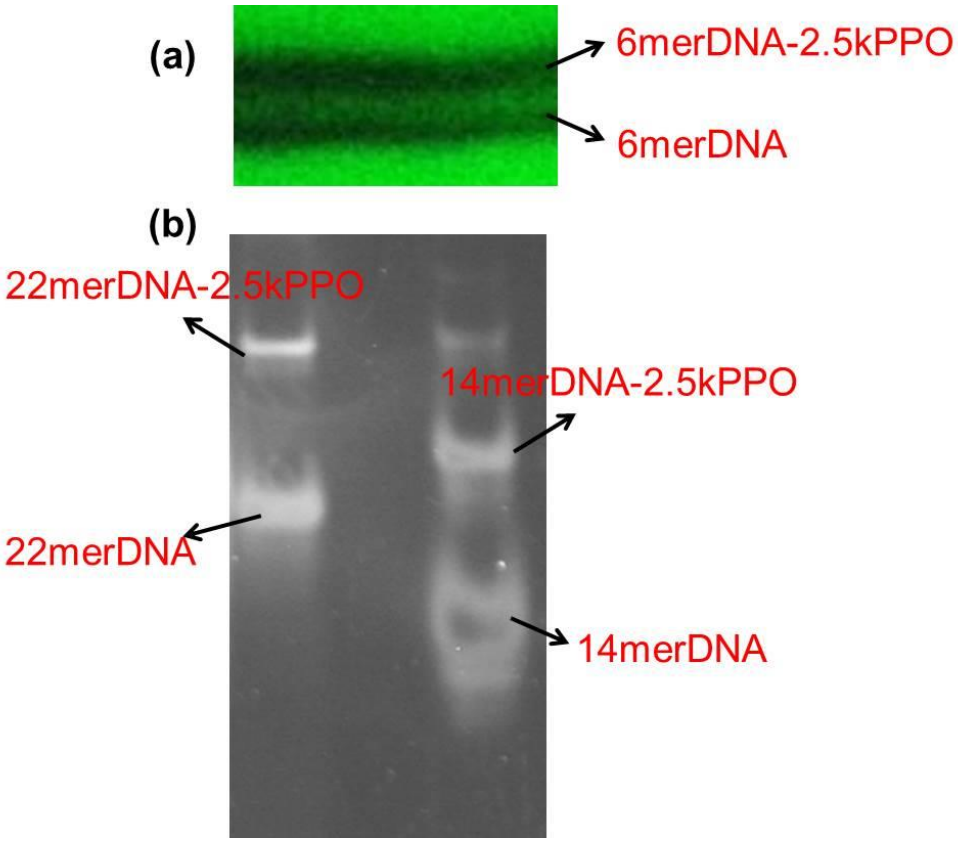

Figure S10. PAGE analysis of DNA-*b*-PPO crude products: (a) 6merDNA coupled with PPO (preparative PAGE), (b) 14mer and 22merDNA coupled with PPO. Combined with the following MALDI-TOF MS analysis, the upper bands marked with arrows are DNA-*b*-PPO conjugates with coupling efficiencies of 55% for 6merDNA-*b*-PPO(2.5k), 36% for 14merDNA-*b*-PPO(2.5k), and 32% for 22merDNA-*b*-PPO(2.5k), respectively. The number in brackets indicates the number average molecular weight M_n of the polymer.

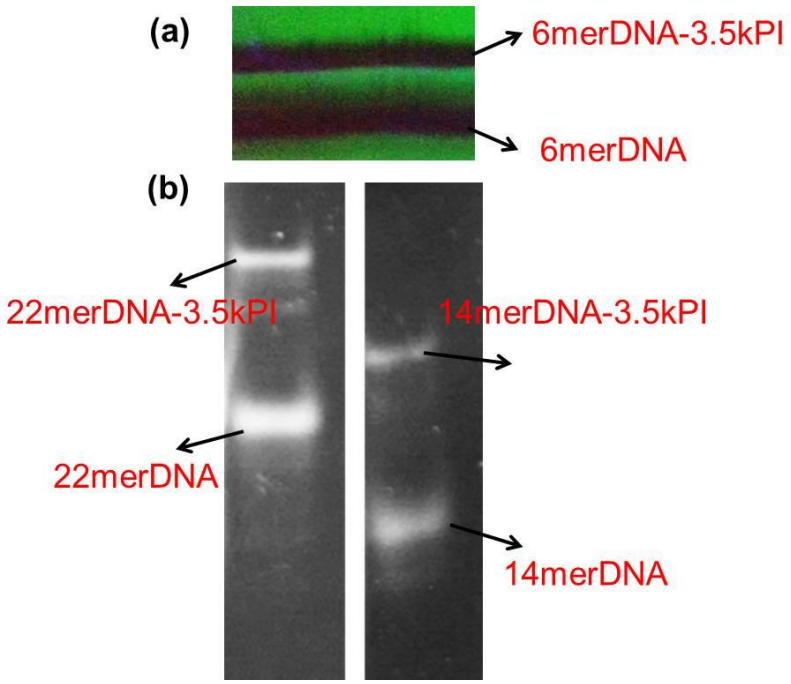

Figure S11. PAGE analysis of DNA-*b*-PI crude products: (a) 6merDNA coupled with PI (preparative PAGE), (b) 14mer and 22merDNA coupled with PI. Combined with the following MALDI-TOF MS analysis, the upper bands marked with arrows are DNA-*b*-PI conjugates with coupling efficiencies of 42% for 6merDNA-*b*-PI(3.5k), 46% for 14merDNA-*b*-PI(3.5k), and 43% for 22merDNA-*b*-PI(3.5k), respectively. The number in brackets indicates the number average molecular weight M_n of the polymer.

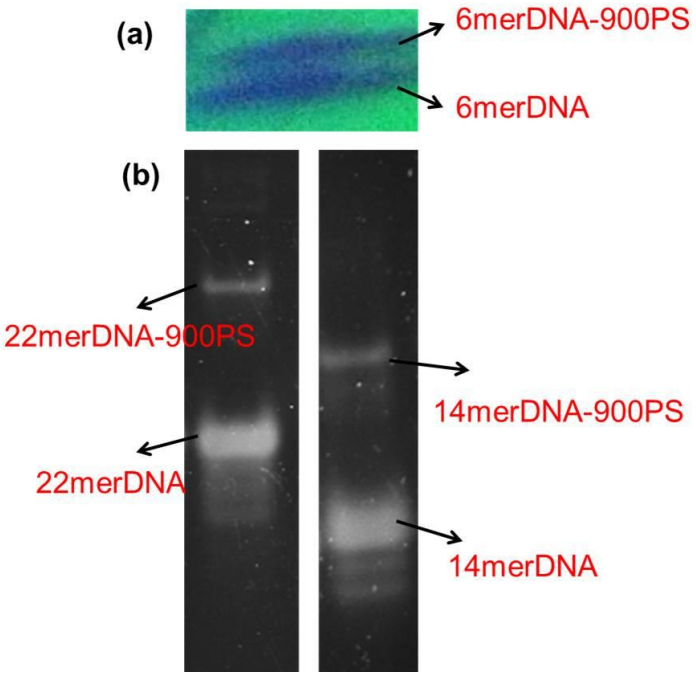

Figure S12. PAGE analysis of DNA-*b*-PS crude products: (a) 6merDNA coupled with PS (preparative PAGE), (b) 14mer and 22merDNA coupled with PS. Combined with the following MALDI-TOF MS analysis, the upper bands marked with arrows are DNA-*b*-PS conjugates obtained with coupling efficiencies of 47% for 6merDNA-*b*-PS(900), 23% for 14merDNA-*b*-PS(900), and 22% for 22merDNA-*b*-PS(900), respectively. The number in brackets indicates the number average molecular weight M_n of the polymer.

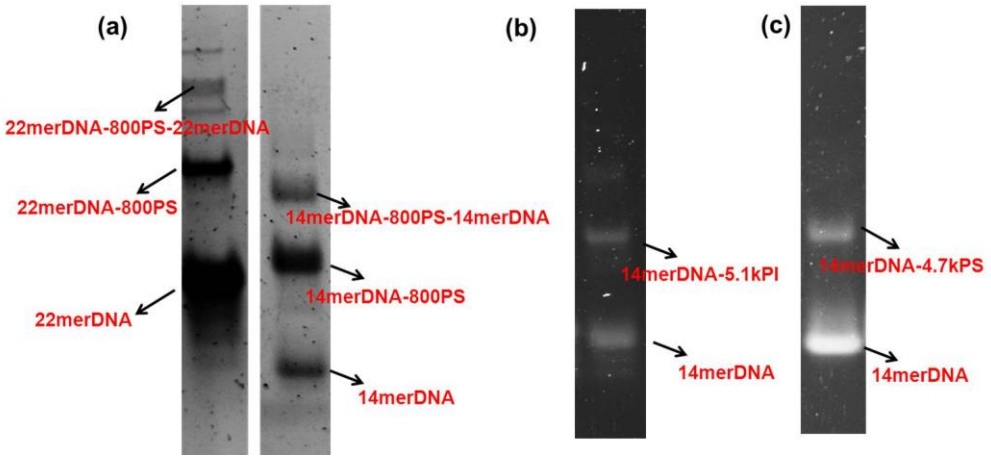

Figure S13. PAGE analysis of DNA block copolymer crude products: (a) dicarboxy-terminated polystyrene was conjugated with 14mer and 22merDNA, forming DNA-*b*-PS(800) diblock and DNA-*b*-PS(800)-*b*-DNA triblock copolymers; (b) 5.1kPI and 4.7kPS were employed for coupling with 14merDNA, resulting in 14merDNA-*b*-PI(5.1k) (40% coupling efficiency) and 14merDNA-*b*-PS(4.7k) (35% coupling efficiency). The number in brackets indicates the number average molecular weight M_n of the polymer.

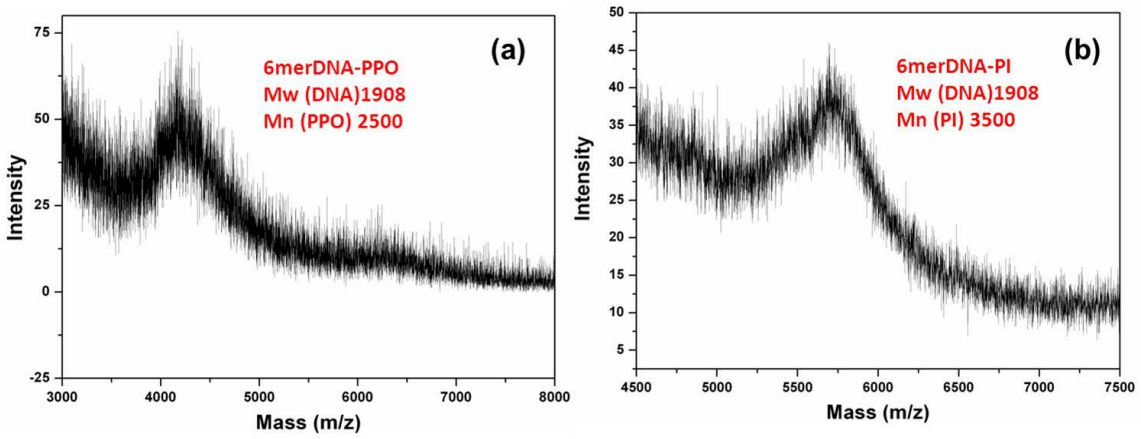

Figure S14. MALDI TOF mass spectra of the 6merDNA-*b*-PPO(2.5k) and 6merDNA-*b*-PI(3.5k) block copolymers. The number in brackets indicates the number average molecular weight M_n of the polymer.

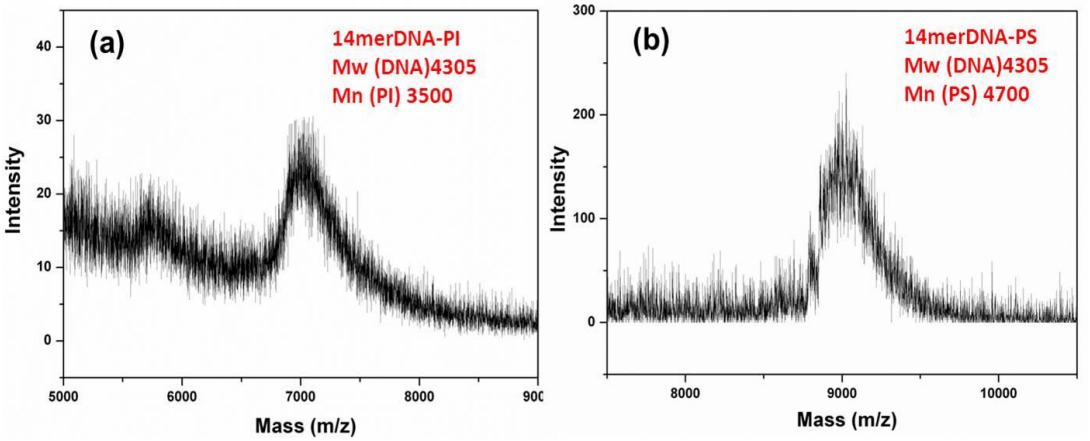

Figure S15. MALDI TOF mass spectra of 14merDNA-*b*-PI(3.5k) and 6merDNA-*b*-PS(4.7k) block copolymers. The number in brackets indicates the number average molecular weight M_n of the polymer.

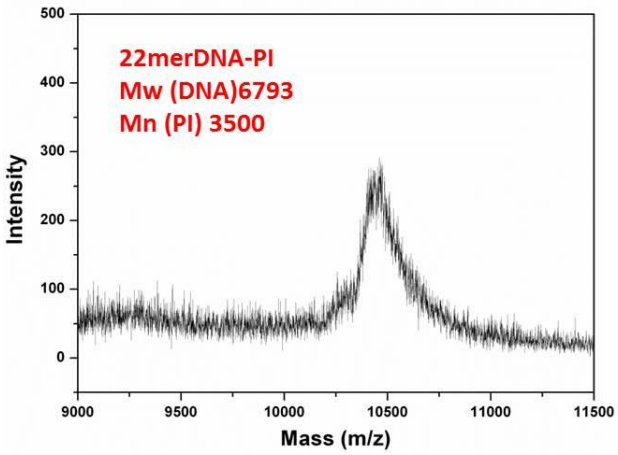

Figure S16. MALDI TOF mass spectrum of 22merDNA-*b*-PI(3.5k) block copolymer. The number in brackets indicates the number average molecular weight M_n of the polymer.

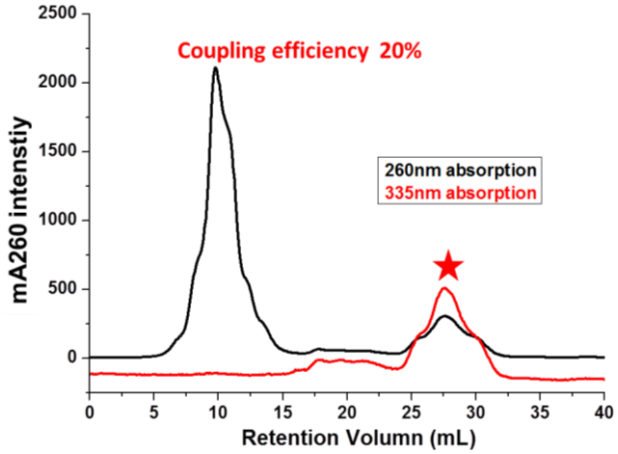

Figure S17. Reverse phase HPLC elugrams of the reaction mixtures of the non-self-complementary ODN-PY by acyl chloride coupling (sequence: 5'-CCTCGCTCTGCTAATCCT-3'). The elution peak marked with red star represent the generated conjugate, where the PY absorption at 335 nm is overlapped with the DNA absorption at 260 nm.

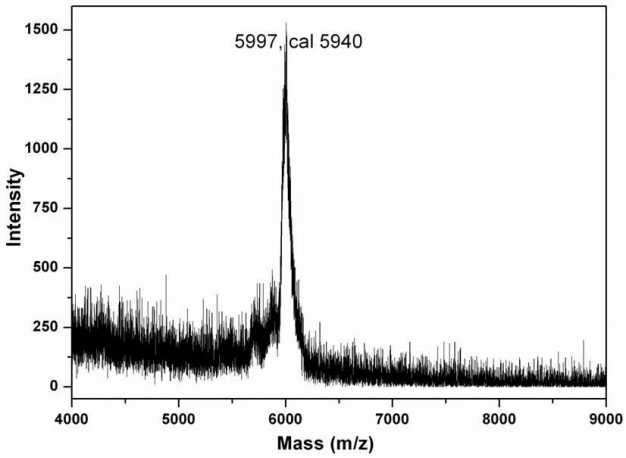

Figure S18. MALDI-TOF mass spectrum of 18mer self-complementary DNA-PY conjugate formed with pyrene functionalized acyl chloride as starting material.

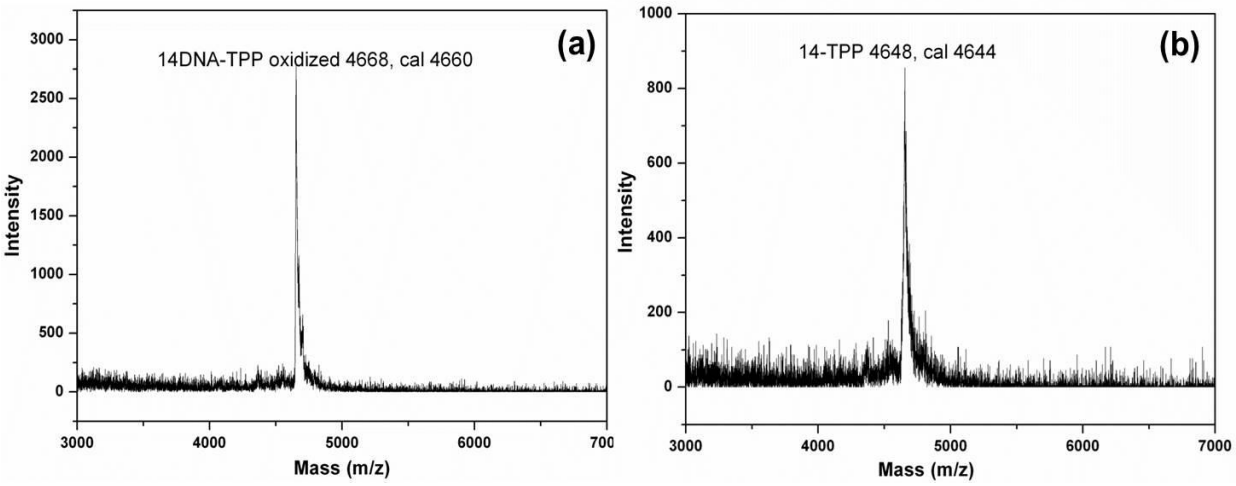

Figure S19. MALDI-TOF mass spectra of 14mer DNA-TPP conjugates formed by acyl chloride route. Two products of TPP-DNA and oxidized TPP-DNA are obtained due to TPP oxidation during the purification process.

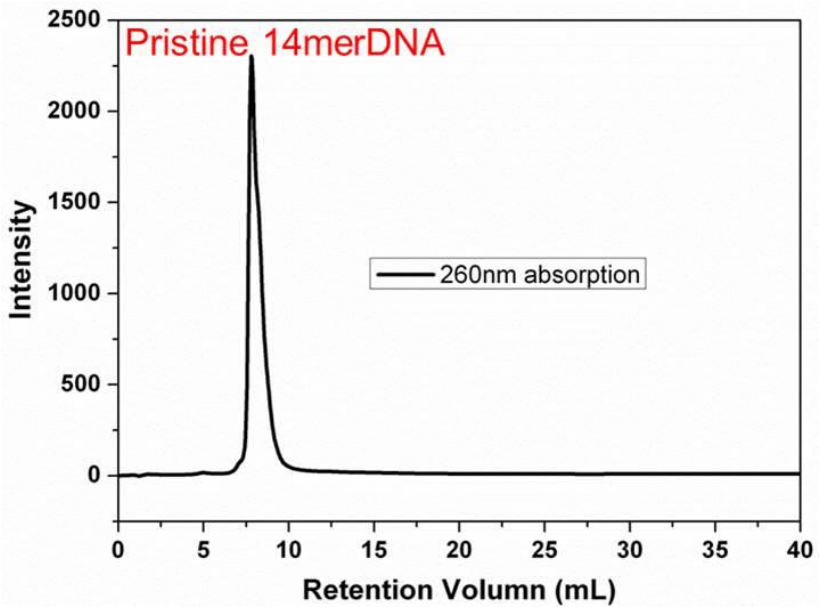

Figure S20. HPLC elugram of the reaction mixture of 14mer DNA without 3'-NH2 group reacted with TPP acyl chloride. In this control experiment, only uncoupled DNA appeared, indicating that the amine groups of nucleobases do not react with TPP acyl chloride under the experimental conditions.

References

1. M. D. Matteucci, M. H. Caruthers, J. Am. Chem. Soc. 1981, 103, 3185.
2. M. Kwak, A. Herrmann, Angew. Chem. Int. Ed. 2010, 46, 8574.
3. T. Schnitzler, A. Herrmann, Acc. Chem. Res. 2012, 45, 1419.
4. T. J. Bandy, A. Brewer, J. R. Burns, G. Marth, T. Nguyen, E. Stulz, Chem. Soc. Rev. 2011, 40, 138.
5. F. Amblard, J. H. Cho, R. F. Schinazi, Chem. Rev. 2009, 109, 4207.
6. S. H. Weisbrod, A. Marx, Chem. Commun. 2008, 5675.
7. N. C. Seeman, Annu. Rev. Biochem. 2010, 79, 65.
8. A.V. Pinheiro, D. Han, W.M. Shih, H. Yan, Nat. Nanotechnol. 2011, 6, 763.
9. L. H. Eckardt, K. Naumann, W. M. Pankau, M. Rein, M. Schweitzer, N. Windhab, G. von Kiedrowski, Nature 2002, 420, 286.
10. O. I. Wilner, I. Willner, Chem. Rev. 2012, 112, 2528.
11. H. Rosemeyer, Chem. Biodiversity 2005, 2, 977.
12. T. Wang, A. Pfisterer, S. L. Kuan, Y. Wu, O. Dumele, M. Lamla, K. Müllen, T. Weil, Chem. Sci. 2013, 4, 1889.
13. (13) J. Shi, D. E. Bergstrom, Angew. Chem., Int. Ed. 1997, 36, 111.
14. B. Datta, G. B. Schuster, J. Am. Chem. Soc. 2008, 130, 2965.
15. T. Zhou, P. Chen, L. Niu, J. Jin, D. Liang, Z. Li, Z. Yang, D. Liu, Angew. Chem., Int. Ed. 2012, 51, 11271.
16. M. Schade, A. Knoll, A. Vogel, O. Seitz, J. Liebscher, D. Huster, A. Herrmann, A. Arbuzova, J. Am. Chem. Soc. 2012, 134, 20490.
17. M. Lemaitre, B. Bayard, B. Lebleu, Proc. Natl. Acad. Sci. U. S. A. 1987, 84, 648.
18. Z. Li, Y. Zhang, P. Fullhart, C. A. Mirkin, Nano Lett. 2004, 4, 1055.
19. F. E. Alemdaroglu, K. Ding, R. Berger, A. Herrmann, Angew. Chem. Int. Ed. 2006, 45, 4206.
20. M. P. Chien, A. M. Rush, M. P. Thompson, N. C. Gianneschi, Angew. Chem. Int. Ed. 2010, 49, 5076.
21. C. K. McLaughlin, G. D. Hamblin, H. F. Sleiman, Chem. Soc. Rev. 2011, 40, 5647.
22. M. Endo, H. Sugiyama, ChemBioChem 2009, 10, 2420.
23. W. Cheng, M. J. Campolongo, J. J. Cha, S. J. Tan, C. C. Umbach, D. A. Muller, D. Luo, Nat. Mater. 2009, 8, 519.
24. R. E. Kleiner, C. E. Dumelin, D. R. Liu, Chem. Soc. Rev. 2011, 40, 5707.
25. M. L. McKee, P. J. Milnes, J. Bath, E. Stulz, A. J. Turberfield, R. K. O'Reilly, Angew. Chem. Int. Ed. 2010, 49, 7948.
26. H. Abe, N. Abe, A. Shibata, K. Ito, Y. Tanaka, M. Ito, H. Saneyoshi, S. Shuto, Y. Ito, Angew. Chem. Int. Ed. 2012, 51, 6475.
27. D. K. Prusty, M. Kwak, J. Wildeman, A. Herrmann, Angew. Chem. Int. Ed. 2012, 51, 11894.
28. K. Börjesson, J. Tumpane, T. Ljungdahl, L. M. Wilhelmsson, B. Nordén, T. Brown, J. Mårtensson, B. Albinsson, J. Am. Chem. Soc. 2009, 131, 2831.
29. G. H. Clever, S. J. Reitmeier, T. Carell, O. Schiemann, Angew. Chem. Int. Ed. 2010, 49, 4927.
30. H. Nishioka, X. Liang, T. Kato, H. Asanuma, Angew. Chem. Int. Ed. 2012, 51, 1165.
31. N. Lu, H. Pei, Z. Ge, C. R. Simmons, H. Yan, C. Fan, J. Am. Chem. Soc. 2012, 134, 13148.
32. M. Kwak, J. Gao, D. K. Prusty, A. J. Musser, V. A. Markov, N. Tombros, M. C. A. Stuart, W. R. Browne, E. J. Boekema, G. ten Brinke, H. T. Jonkman, B. J. van Wees, M. A. Loi, A. Herrmann, Angew. Chem. Int. Ed. 2011, 50, 3206.
33. J. M. Gibbs, S. Park, D. R. Anderson, K. J. Watson, C. A. Mirkin, S. T. Nguyen, J. Am. Chem. Soc. 2005, 127, 1170.
34. M. Kwiat, R. Elnathan, M. Kwak, J. W. de Vries, A. Pevzner, Y. Engel, L. Burstein, A. Khatchtourints, A. Lichtenstein, E. Flaxer, A. Herrmann, F. Patolsky, J. Am. Chem. Soc. 2012, 134, 280.
35. D. K. Prusty, A. Herrmann, J. Am. Chem. Soc. 2010, 132, 12197.
36. Y. Wu, K. Sefah, H. Liu, R. Wang, W. Tan, Proc. Natl. Acad. Sci. U. S. A. 2010, 107, 5.
37. J. W. de Vries, F. Zhang, A. Herrmann, J. Controlled Rel. 2013, 172, 467.
38. F. E. Alemdaroglu, C. N. Alemdaroglu, P. Langguth, A. Herrmann, Adv. Mat. 2008, 20, 899.
39. T. Chen, C. S. Wu, E. Jimenez, Z. Zhu, J. G. Dajac, M. You, D. Han, X. Zhang, W. Tan, Angew. Chem. Int. Ed. 2013, 52, 2012.
40. J. I. Cutler, E. Auyeung, C. A. Mirkin, J. Am. Chem. Soc. 2012, 134, 1376.
41. L. E. Bromberg, A. M. Klibanov, Proc. Natl. Acad. Sci. USA 1994, 91, 143.
42. K. Tanaka, Y. Okahata, J. Am. Chem. Soc. 1996, 118, 10679.

43. V. G. Sergeyev, S. V. Mikhailenko, O. A. Pyshkina, I. V. Yaminsky, K. Yoshikawa, J. Am. Chem. Soc. 1999, 121, 1780.
44. S. Gajria, T. Neumann, M. Tirrell, Wiley Interdiscip Rev Nanomed Nanobiotechnol. 2011, 3, 479.
45. M. M. Rozenman, D. R. Liu, ChemBioChem 2006, 7, 253.
46. T. R. Pearce, B. Waybrant, E. Kokkoli, Chem. Commun. 2014, 50, 210.
47. A. J. Lomant, G. J. Fairbanks, Mol. Biol. 1976, 104, 243.
48. M. E. Østergaard, P. J. Hrdlicka, Chem. Soc. Rev. 2011, 40, 5771.
49. F. Teixeira, Jr. P. Rigler, C. Vebert-Nardin, Chem. Commun. 2007,1130.
50. C. J. Yang, M. Pinto, K. Schanze, W. Tan, Angew. Chem. Int. Ed. 2005, 44, 2572.
51. J. Jeong, T. Park, Bioconjugate Chem. 2001, 12, 917.
52. J. Azéma, B. Guidetti, J. Dewelle, B. L. Calve, T. Mijatovic, A. Korolyov, J. Vaysse, M. Malet-Martino, R. Martino, R. Kiss, Bioorg. Med. Chem. 2009, 17, 5396.

Summary

Complex formation between cationic surfactants and oppositely charged nucleic acids has been studied extensively in recent years. Three types of DNA-surfactant assemblies, including bulk films, lyotropic liquid crystals and hydrogels have been reported. The driving force for the formation of these systems is the long-range electrostatic interaction between molecules of opposite charge i.e. the polyelectrolyte DNA and positively charged surfactants. To understand these interactions is very important to realize different packing modes of the complexes and to achieve different structures. Thus, the influence of DNA chains, headgroup charge and chain length of chosen surfactants, counterions, and other polyelectrolytes on the complex structures have been investigated intensitvely and are reviewed in **chapter 1**. In part, these structural investigations were motivated by the application of DNA-surfactant complexes in the fields of optoelectronic devices and gene delivery. Due to their physicochemical properties such as good temperature stability, wide HOMO/LUMO band-gap, low optical absorption and propagation, low optical scattering loss and mechanical robustness, DNA-surfactant complexes have been used in lasing, nonlinear optics, light-emitting diodes, and solar cells. Equally important is potential application as efficient non-viral vectors for gene transfection and gene silencing. The study of lyotropic liquid crystals of DNA-surfactant complexes has revealed that the assembled mesophase structures (e. g., lamellar, hexagonal, and cubic phases) are very important in determining delivery efficiencies. Furthermore, the advantages and disadvantages of DNA-surfactant complexes for gene therapy and drug delivery have been discussed in this chapter.

Aside from these achievements on DNA-surfactant assemblies (bulk films, lyotropic liquid crystals, and hydrogels), here, a new class of DNA-surfactant materials has been developed, that represent solvent-free thermotropic liquid crystals. This new soft DNA structures was prepared by electrostatic complexation of a single-stranded oligonucleotide with a cationic surfactant containing two aliphatic chains (DOAB: dimethyldioctylammonium bromide) (**chapter 2**). After one-step precipitation and final lyophylization, solvent-free thermotropic mesophases were obtained at room temperature. Lamellar structures of the DNA-DOAB complexes are formed, in which the bilayer is composed of a ssDNA sublayer of ~10 Å thickness that electrostatically interacts with a interdigitaed DOAB sublayer of ~10 Å. Thermal measurements of the smectic DNA-DOAB mesophase indicated its stability from -7 to 41 °C, which enables the study and application of DNA thermotropic liquid crystalline phase behavior without thermal degradation of the biomolecular components. Moreover, this method is also applicable to RNA-surfactant complexes, which exhibit very similar liquid crystalline properties as DNA.

It is known that solid-state DNA undergoes thermal degradation at elevated temperatures, so the realization of solvent-free DNA fluids remains a challenge. Here we found that the combination of DNA with suitable cationic surfactants, followed by

dehydration, can be extended as a simple generic scheme for producing solvent-free DNA fluid systems (**chapter 3**). Three surfactants with two aliphatic chains of variable lengths, i.e. dioctyldimethylammonium bromide (DOAB), didecyldimethylammonium bromide (DEAB), and didodecyldimethylammonium bromide (DDAB), were used to prepare the DNA-surfactant fluids including the stable liquid crystals and isotropic liquids. It was found that the phase transition temperatures of DNA-surfactant complexes can be controlled over a wide temperature range. Smectic DNA mesophases have been achieved at temperatures as low as -20 °C and also can be adjusted up to 65 °C. In particular, we found a new class of modulated smectic liquid crystalline phase in DNA-DDAB complex, which exhibits an additional periodicity perpendicular to the layer normal, i.e. an in-plane layer undulation. The disordered DNA liquids were achieved between 41 °C and 130 °C by selection of the appropriate surfactants. Viscoelastic properties of the developed DNA fluids have been investigated, which are strongly dependent on the surfactant alkyl chain length and molecular weight of the DNA part.

Our solvent-free DNA-surfactant complexes are fluid, and exhibit high DNA content, which make it suitable to be used as easily-processable biomaterials for optoelectronic device fabrication. In **chapter 4** we report a novel electrochromic device by directly injecting DNA-DOAB in a liquid crystal cell. Extraordinary electrochromics without supported electrolyte solution are achieved by the soft condensed material. When the voltage was switched from 0 to 4 V, the appearance of DNA-DOAB in the isotropic liquid phase changed from transparent to magenta. The bleaching state was recovered in several seconds when the voltage was switched back to 0 V. In this process, reversible anodic oxidation of DNA took place, and the produced radical cations of nucleotide bases are responsible for the color appearance. Thus, the isotropic liquid state of DNA-DOAB complex exhibits switchable electrochromic properties. Switching rates of the DNA-DOAB fluids in the isotropic phase have been investigated. We found that the response time is correlated with the length of the used oligonucleotides. For instance, switch time can be controlled from 15, 30, 80 to 120 seconds by increasing the DNA length gradually (6mer, 14mer, 22mer, and 50mer). When cooling the colored DNA-DOAB to the LC phase while keeping the applied voltage at 4 V, the magenta color was conserved. More importantly, the complete coloration state can be continuously maintained without decay over an extended period of time (few hours) even after removal of the applied voltage. The optical relaxation can be further elongated in the crystalline phase (up to 30 hours). Further experiments indicated that the reorientation of the DNA-DOAB lamellar layers plays an important role in controlling the long-term color relaxation. Thus, a novel optical memory system based on nucleic acid fluids has been realized in a simple way. The volatility of stored optical information can be modulated conveniently by exploiting the phase behavior of the materials. Due to the optoelectronic characteristics of the DNA-surfactant complex LCs, these materials are suited for utilization as smart tags with built-in time-temperature functions.

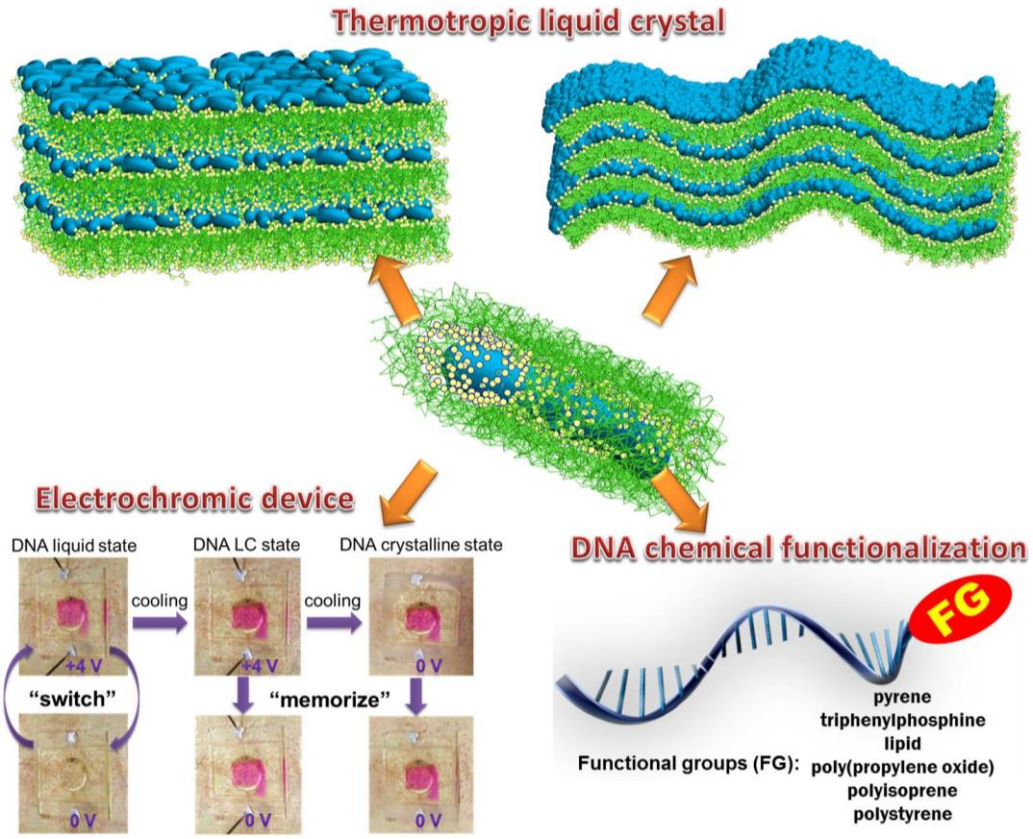

Figure 1. Summary of the new developments based on DNA-surfactant complex.

Apart from the development of solvent-free nucleic acid fluids and their optoelectronic applications, the complexation of DNA with surfactants can also be used as a chemically reactive scaffold for the fabrication of amphiphilic oligonucleotides in organic phase (**chapter 5**). We first produced the amino terminated DNA-DDAB complex that can be dissolved in a wide range of organic solvents (e.g., DMF, DMSO, THF, and $CHCl_3$). Then, a series of activated ester derivatives of hydrophobic molecules (e.g., pyrene, triphenylphosphine, and long hydrocarbon chains) were reacted with DNA-DDAB complex by amine acylation in a homogeneous organic environment. After treatment with highly concentrated salt in solutions, amphiphilic DNA conjugates were released from the surfactant shell and the resulting DNA hybrid structure were obtained with high coupling efficiencies. We have developed an alternative method of synthesizing amphiphile-DNA conjugates by inducing amide bond formation through the reaction of acyl chloride-containing hydrophobic molecules (pyrene and triphenylphosphine) and amine-terminated DNA-DDAB complexes. Even higher coupling efficiencies (>90%) of the target conjugates were achieved without formation of any byproducts conjugated at the nucleobase. Moreover, hydrophobic polymers (poly(propylene oxide), polyisoprene, and polystyrene) were efficiently coupled with DNA by our novel strategy. DNA diblock and triblcok copolymers (DNA-*b*-PPO, DNA-*b*-PI, DNA-*b*-PS, and DNA-*b*-PS-*b*-DNA) were produced. The present coupling efficiencies of DNA to large hydrophobic polymer moieties were at least comparable or even higher than those from solid-phase and other

heterogeneous solution grafting approaches. Therefore, the introduction of DNA-surfactant complexes as a reactive scaffold for nucleic acid functionalization overcomes solubility incompatibilities of in-solution coupling and avoids the harsh reactions of deprotection in solid phase synthesis.

In conclusion, as summarized in Figure 1, we have developed a new soft condensed state of DNA-surfactant complexes i.e. DNA thermotropic liquid crystals. Their thermal behaviors, mesophase structures, and electrochromic applications have been investigated successfully. We also found that DNA-surfactant complexes offers extraordinary opportunities for the synthesis of functional DNA molecules in organic solvents without the need of any expensive DNA synthesizer. It is believed that the results presented in this thesis are crucial for the further development of several fields where nucleic acids play an important role like DNA nanotechnology, chemical biology and bioelectronics.

Samenvatting

Complexvorming tussen kationische oppervlakteactieve stoffen en tegengesteld geladen nucleïnezuren zijn uitgebreid bestudeerd in de afgelopen jaren. Drie typen DNA-surfactant samenstellingen, waaronder solid-state films, lyotrope vloeibare kristallen en hydrogels zijn gerapporteerd. De drijvende kracht in de formatie van deze systemen is de lange-afstands elektrostatische interactie tussen moleculen van tegengestelde lading, d.w.z. tussen het polyelectrolitische DNA en de positief geladen surfactants. Het is zeer belangrijk om een uitgebreide kennis te vergaren van deze interacties om verschillende structuren en verpakkings wijzes van deze samenstellingen te realizeren. Om deze reden zijn de invloed van DNA-ketens, kopgroep lading en ketenlengte van de gekozen surfactanten, tegenionen en andere polyelektrolyten op de complexe structuren systematisch onderzocht en beschreven in **hoofdstuk 1**. Het belang van deze studies is ingegeven door de groeiende interesse in de toepassing van DNA-surfactant samenstellingen in optisch-elektronische apparatuur en genetische afgiftesystemen. Vanwege hun uitstekende fysico-chemische eigenschappen zoals een goede temperatuurs stabiliteit, een brede HOMO/LUMO bandkloof, lage optische absorptie en verspreiding, een laag optisch verstrooiings verlies en mechanische robuustheid, zijn DNA-surfactant samenstellingen gebruikt in laseren, niet-lineaire optica, licht-uitstralenden dioden en zonnecellen. Even belangrijk is de potentiele toepassing als efficiënte niet-virale vectoren voor gen transfectie en gen stillegging. De studie van lyotrope vloeibare kristallen van DNA-surfactant samenstellingen heeft aangetoond dat geassembleerde mesofase structuren (bijvoorbeeld lamellaire, hexagonale en kubische fasen) zeer belangrijk zijn in het bepalen van leverings efficiënties. Bovendien zijn de voor- en nadelen van DNA-surfactant samenstellingen voor gentherapie en geneesmiddelen afgifte in dit hoofdstuk besproken.

Naast deze successen op DNA-surfactant samenstellingen (solid-state films, lyotrope vloeibare kristallen en hydrogels), is hier een nieuwe klasse van DNA-surfactant samenstellingen ontwikkeld, welke oplosmiddelvrije thermotrope vloeibare kristallen vertegenwoordigt. Deze nieuwe type zachte DNA materiaal werd bereid door elektrostatische complexvorming van enkelstrengs oligonucleotiden met kationische surfactanten met dubbele alifatische ketens (DOAB: dioctadecyl dimethyl ammonium bromide) (**hoofdstuk 2**). Na één-staps precipitatie en uiteindelijke lyofilisatie, werden oplosmiddelvrije thermotrope mesofasen bij kamertemperatuur verkregen. Lamellaire structuren van het DNA-DOAB complex werden gevormd, waarbij de dubbellaag is samengesteld uit een ssDNA sublaag van ~10 Å dik welke elektrostatisch samenwerkt met een inter-grijpende DOAB sublaag van ~10 Å. Thermische metingen van de smectische DNA-DOAB mesofase gaven een stabiliteit van -7 tot 41 ° C aan, welke de studie en toepassing van het DNA thermotrope vloeibare kristallijne fase gedrag zonder thermische afbraak van de biomoleculaire componenten mogelijk maakt. Bovendien is deze werkwijze ook toepasbaar op RNA-surfactant samenstellingen, welke soortgelijke kristallijne eigenschappen vertoond als DNA.

Het is bekend dat DNA in vaste toestand thermische degradatie bij verhoogde temperaturen ondergaat, waardoor de realisatie van oplosmiddelvrije DNA vloeistoffen problematisch blijft. Nu hebben we bevonden dat de combinatie van DNA met geschikte kationische surfactanten, gevolgd door dehydratatie, kan worden uitgebreid als een eenvoudige algemene concept voor het produceren van oplosmiddelvrije DNA vloeistofsystemen (**hoofdstuk 3**). Drie surfactanten met twee alifatische ketens van verschillende lengtes, d.w.z. dioctadecyl dimethyl ammonium bromide (DOAB), didecyl dimethyl ammonium bromide (DEAB), en didodecyl dimethyl ammonium bromide (DDAB), werden gebruikt om DNA-surfactant vloeistoffen te bereiden waaronder stabiele vloeibare kristallen en isotrope vloeistoffen. Het was bevonden dat de faseovergangs temperatuur van DNA-surfactant samenstellingen geregeld kan worden over een breed temperatuurbereik. Smectische DNA mesofasen zijn bij temperaturen zo laag als -20 ° C bereikt en kunnen ook worden aangepast tot 65 ° C. In het bijzonder tonen we een nieuwe klasse van gemoduleerde smectische vloeibare kristallijne fase in DNA-DDAB complexen, welke een aanvullende periodiciteit vertoont loodrecht op de horizontale laag, d.w.z. een in-vlak laag golving. De wanordelijke DNA vloeistoffen zijn reeds afgesteld tussen 41 ° C en 130 ° C door de keuze van een geschikte surfactant. Visco-elastische eigenschappen van de ontwikkelde DNA vloeistoffen zijn onderzocht, welke sterk afhankelijk zijn van de surfactant alkyl ketenlengte en het molecuulgewicht van het gebruikte DNA.

Onze oplosmiddelvrije DNA-surfactant samenstellingen zijn vloeibaar en vertonen een hoog DNA gehalte, welke het geschikt maakt voor gebruik als gemakkelijk-verwerkbare biomaterialen voor opto-elektronische apparatuur fabricage. In **hoofdstuk 4** beschrijven we een nieuw elektrochromisch apparaat door het direct injecteren van DNA-DOAB in een vloeibare kristallen cel. Bijzondere elektrochromen zonder ondersteunde elektrolyt oplossing wordt bereikt door het zachte gecondenseerde materiaal. Wanneer de spanning werd overgeschakeld van 0 tot 4 V, veranderde het uiterlijk van DNA-DOAB in de isotrope vloeibare fase van transparant naar magenta. De blekende staat werd in enkele seconden hersteld wanneer de spanning werd teruggeschakeld naar 0 V. In dit proces vindt omkeerbare anodische oxidatie van DNA plaats, en de geproduceerde radicale kationen van de nucleotide basen zijn verantwoordelijk voor de kleurweergave. Hierdoor vertoont de isotrope vloeibare staat van het DNA-DOAB complex omschakelbare electrochromische eigenschappen. De schakelings snelheid van de DNA-DOAB vloeistoffen in de isotropische fase zijn onderzocht. We vonden dat de responstijd correleerd met de lengte van de gebruikte oligonucleotiden. Zo kan schakelingstijd worden bediend van 15 seconden, 30 seconden, 80 seconden tot 2 minuten door het geleidelijk verhogen van de DNA lengte (6-mer, 14-mer, 22-mer en 50-mer). Bij koeling van het gekleurde DNA-DOAB naar de vloeibare kristal fase terwijl de aangelegde spanning bij 4 V wordt gehouden, werd de magenta kleur behouden. Belangrijker, de volledige gekleurde staat kan continu gehandhaafd houden zonder afbraak gedurende een lange periode (vele uren) zelfs na verwijdering

van de aangelegde spanning. De optische ontspanning kan verder worden verlengt in de kristallijne fase (tot 30 uur). Verdere experimenten gaven aan dat de heroriëntatie van de DNA-DOAB lamellaire lagen een belangrijke rol speelt bij het regelen van de kleur relaxatie op langetermijn. Aldus is een nieuw optisch geheugen systeem gebaseerd op nucleïnezuren vloeistoffen gerealiseerd op een eenvoudige manier. De volatiliteit van de opgeslagen optische informatie kan gemakkelijk worden gemoduleerd door het fase gedrag van de materialen te exploiteren. Door de opto-elektronische eigenschappen van de DNA-surfactant vloeibare kirstallen, zijn deze materialen veelbelovend voor de toepassing in elektrochrome aparaten met een laag energieverbruik en ingebouwde tijd-temperatuurs functies.

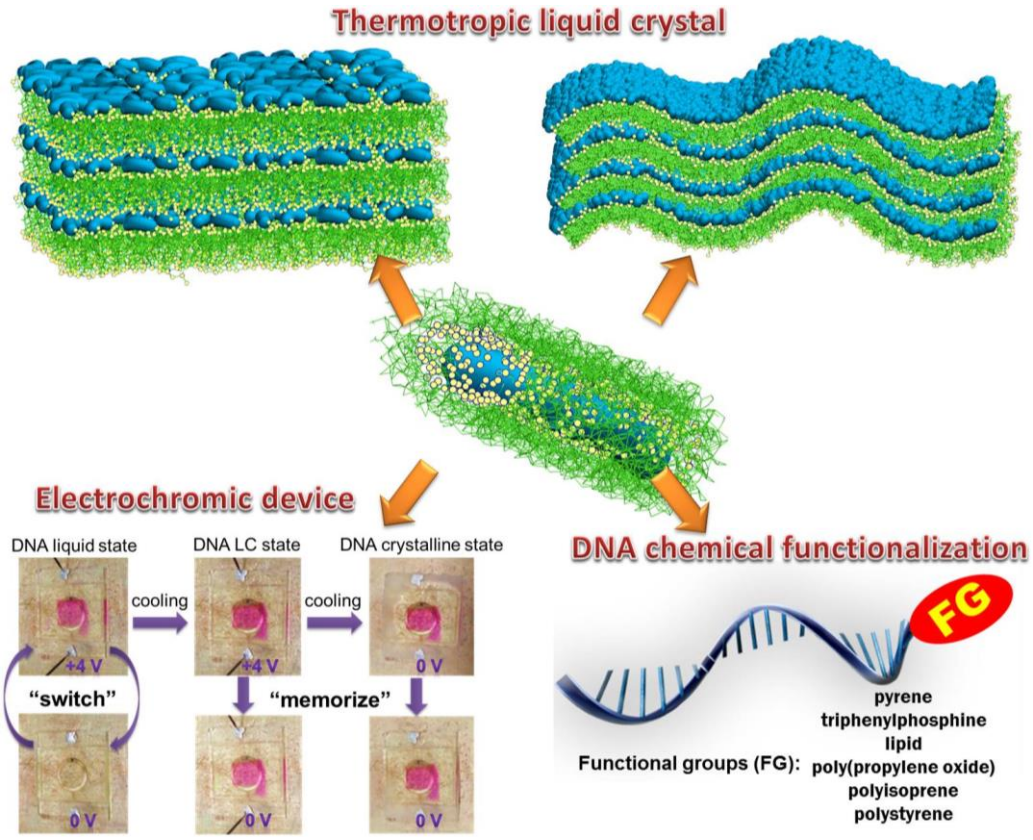

Figuur 1. Samenvatting van de nieuwe ontwikkelingen op basis van DNA-surfactant samenstellingen.

Naast de ontwikkeling van oplosmiddelvrije nucleïnezuur vloeistoffen en de opto-elektronische toepassingen, kan de complexering van DNA met surfactanten ook gebruikt als een chemisch reactieve matrix voor amfifiele oligonucleotiden synthese in organische fase (**hoofdstuk 5**). We hebben eerst amino-beëindigde DNA-DDAB complexen geproduceerde welke opgelost kunnen worden in een groot aantal organische oplosmiddelen (bijvoorbeeld DMF, DMSO, THF en $CHCl_3$). Vervolgens werden een reeks geactiveerde ester derivaten van hydrofobe moleculen (bijvoorbeeld, pyreen, trifenylfosfine en lange koolwaterstofketens) gereageerd met het DNA-DDAB complex door amine acyletylatie in een homogene organische omgeving. Na behandeling met een geconcentreerd zout in oplossing, werden de amfifiele DNA

conjugaten vrijgemaakt uit het surfactant omhulsel en de resulterende DNA hybride structuren werden verkregen met een hoge koppeling efficiëntie. Wij hebben een alternatieve methode ontwikkeld voor het synthetiseren van amfifiel-DNA conjugaten door het induceren van de vorming van amidebindingen door reactie van acyl chloride-bevattende hydrofobe moleculen (pyreen en trifenylfosfine) en amine-beëindidgde DNA-DDAB complexen. Nog hogere koppelings efficiënties (> 90%) van de bedoelde conjugaten werden behaald zonder verontreiniging van bijproducten van nucleobase conjugaten. Belangrijker nog is dat hydrofobe polymeren (poly(propyleenoxide), polyisopreen en polystyreen) efficiënt en eenvoudig werden gekoppeld met DNA door onze gevestigde strategie. DNA di-blok en tri-blok copolymeren (DNA-*b*-PPO, DNA-*b*-PI, DNA-*b*-PS en DNA-*b*-PS-*b*-DNA) zijn geproduceerd. De huidige koppelings efficiënties van DNA aan grote hydrofobe polymeer groepen waren ten minste vergelijkbaar of zelfs hoger dan die van vaste-fase en andere heterogene oplossings beëntings benaderingen. Daarom overkomt de introductie van DNA-surfactant samenstellingen als een reactieve matrix voor nucleïnezuur functionalisering de onverenigbaarheden van in-oplossing koppeling en vermijdt het de ruwe reacties van deprotectie in vaste fase synthese.

Concluderend, zoals samengevat in Figuur 1, hebben we een nieuwe zachte gecondenseerde toestand van DNA-surfactant samenstellingen ontwikkeld, d.w.z. DNA thermotrope vloeibare kristallen. Hun thermische gedrag, mesofase structuren, en elektrochromische toepassingen zijn succesvol onderzocht. We bevonden ook dat de DNA-surfactant samenstellingen buitengewone mogelijkheden bieden voor de fabricatie van functionele DNA moleculen in organische oplosmiddelen zonder de noodzaak om een kostbare DNA synthesizer te gebruiken. Er wordt aangenomen dat de in dit proefschrift beschreven resultaten cruciaal zijn voor de verdere ontwikkeling van verschillende onderzoeksvelden waar nucleïnezuren een belangrijke rol spelen, zoals DNA nanotechnologie, chemische biologie en bio-elektronica.

Publications

1. **K. Liu**, D. Pesce, C. Ma, M. Tuchband, M. Shuai, D. Chen, J. Su, Q. Liu, J. Y. Gerasimov, A. Kolbe, W. Zajaczkowski, W. Pisula, K. Müllen, N. A. Clark, A. Herrmann, *Solvent-free liquid crystals and liquids based on genetically engineered supercharged polypeptides with high elasticity*, ***Adv. Mater.*** 2015, *27*, 2459-2465. (highlighted as front cover)

2. **K. Liu**, M. Shuai, D. Chen, M. Tuchband, J. Y. Gerasimov, J. Su, Q. Liu, W. Zajaczkowski, W. Pisula, K. Müllen, N. A. Clark, A. Herrmann, *Solvent-free liquid crystals and liquids from DNA*, ***Chem. Eur. J.*** 2015, *21*, 4898-4903. (highlighted as frontispiece)

3. **K. Liu**, D. Chen, A. Marcozzi, L. Zheng, J. Su, D. Pesce, W. Zajaczkowski, A. Kolbe, W. Pisula, K. Müllen, N. A. Clark, A. Herrmann, *Thermotropic liquid crystals from biomacromolecules*, ***Proc. Nat. Acad. Sci. USA*** 2014, *111*, 18596-18600. (Highlighted in *Liquid Crystals Today* 2015, 24(4), 132)

4. **K. Liu**†, L. Zheng†, Q. Liu, J. Willem de Vries, J. Y. Gerasimov, A. Herrmann, *Nucleic acid chemistry in organic phase: from functionalized oligonucleotides to DNA side chain polymers*, ***J. Am. Chem. Soc.*** 2014, *136*, 14255-14262. (†equal contribution)

5. W. Chen, J. Y. Gerasimov, P. Zhao, **K. Liu**, A. Herrmann, *High density functionalization of DNA by electrostatic interactions*, ***J. Am. Chem. Soc.*** 2015, *137*, 12884-12889.

6. H. Yang, C. Ma, K. Li, **K. Liu**, M. Loznik, R. Teeuwen, J. C. M. van Hest, X. Zhou, A. Herrmann, J. Wang, *Tuning ice nucleation with supercharged polypeptides*, 2015, **under revision**.

7. **K. Liu**, J. Varghese, J. Y. Gerasimov, A. O. Polyakov, M. Shuai, J. Su, D. Chen, W. Zajaczkowski, A. Marcozzi, W. Pisula, B. Noheda, T. T. M. Palstra, N. A. Clark, A. Herrmann, *Phase-dependent DNA electrochromics: controlling the volatility of the written optical state*, 2015, **submitted**.

8. **K. Liu**, L. Zheng, J. Y. Gerasimov, A. Herrmann, *DNA-surfactant complexes: self-assembly properties and applications*, **to be submitted**. (a review)

9. **K. Liu**, C. Ma, J. Sun, L. Zheng, A. Herrmann, *Supercharged polypeptide doing it all in mechanics: from ultra-strong adhesion for glue application to biomimetic fibers with greater strength and stiffness than natural spider silk*, **in preparation**.

10. **K. Liu**, C. Ma, W. Zajaczkowski, W. Pisula, A. Herrmann, *Polypeptide-based liquid crystalline fibers with outstanding mechanical performance mediated by genetic engineering*, **in preparation**.

11. **K. Liu**, A. Herrmann, *Thermotropic liquid crystals from biomacromolecules*, **in preparation**. (a review)

Acknowledgments

The last section of my thesis comes to my fingers. It is the right moment to look back the past few years in Groningen. It would not be possible to finish all the work without the help of a large number of people. Now it is the great time to acknowledge all of you who contributed on this work.

First and foremost, I would like to give my sincere and deepest gratitude to my supervisor Prof. Andreas Herrmann. Andreas, thank you very much for offering me the opportunity to pursue my Ph. D study in PCBE group at University of Groningen. Many special thanks for introducing me to the exciting nucleic acid and biomaterial research filed. I really appreciate for your guidance on this topic throughout the four years especially the discussions we had before. You gave me a lot of freedom to work and at the meantime helped me to establish the framework of my Ph. D research. I learned a lot from your inspiring ideas, broad knowledge, and attitude in scientific researches. In particular, I greatly enjoy the interdisciplinary research environment in our lab. I also appreciate very much your scientific suggestions and most of all, that my opinions were also heard and taken into account. You provided me so many opportunities to collaborate with other groups and present our work in many conferences. I really appreciate your continuous support for my research work and the amount of time you spent on the results analysis, paper and thesis writing. Your sharp mind and enormous energy on science are so inspiring , which I have learnt a lot and will be a great treasure in my life.

Next, I am deeply grateful to Prof. Noel Clark in University of Colorado. It was an amazing experience to participate in the ILCC2012 held in Mainz and then to start the fruitful collaboration with your group. Thank you very much for your patience and dedicated time on experimental design, data analysis, and paper writings. I enjoyed the meetings with you and Andreas, which were always full of scientific discussion. I am really impressed on your broad knowledge and can consult almost everything from you. At the meantime, I would like to take this opportunity to thank your group members: Dr. Dong Chen-my dear friend, Dr. Min Shuai, and Mr. Michael Tuchband. Dear guys, I really appreciate all of your continuous support on my work including FF-TEM measurements, results discussions, and manuscript polish.

Then, many sincere thanks to Prof. Klaus Müllen and Dr. Wojciech Pisula in Max Planck Institute for Polymer Research. I am really grateful to you for the valuable discussions on my projects. Thanks a lot for offering me many opportunities to access your WAXS machine. I also appreciate your willingness of reading and evaluating my manuscript. Your comments and suggestions helped a lot to improve my scientific work. I want to thank your Ph. D student Wojciech Zajaczkowski for dedicated time to do WAXS measurements together with me. Hi! man, I really enjoyed the time spent together with you, Mengmeng Li, and Shuhao Wang for the impressive chatting and dinners in Mainz.

Additionally, I would like to thank other collaborators involved in my project. Dear Prof. Thomas Palstra, Prof. Beatriz Noheda, Dr. Justin Varghese, and Mr. Alexey O. Polyakov, I really appreciate your contributions on liquid crystal device measurements, results analysis, and paper writing. My work would never be done without your continuous support. I am also pleased to give my gratitude to Prof. Justin Jianting Ye and Mr. Lei Liang, I really enjoyed the discussions with you. As physicists, your suggestions for my research are very valuable.

I would like to express my sincere gratitude to the reading committee members: Prof. Tanja Weil, Prof. Sébastien Lecommandoux, and Prof. Gerard Roelfes. Thanks a lot for your patience and dedicated time to read and evaluate my thesis. Your comments and advices helped a lot to polish my thesis.

Very special thanks to Dr. Evgeny Polushkin for your invaluable technical support on my project. You helped me a lot with the characterization of liquid crystals by SAXS and Rheometer. Thank you very much for the constant help in the lab work. I am grateful to you for sharing your knowledge and experience with me. The results presented in my thesis would not have been possible without your help.

Moreover, I want to express my great gratitude to Prof. Kajta Loos and Mr. Gert Alberda van Ekenstein. Thanks a lot for your agreement and offering me many opportunities to operate the machines in polymer lab. Dear Katja, it is grateful that you arrange me to work as teaching assistant for undergraduate practical course. I learnt a lot! Dear Gert, you are so busy in taking care of all the instruments in Lab-0303. I cannot remember how many times I came to you with some questions concerning the POM and DSC. But you are always patient for teaching and helping me with all the problems. Thank you so much for your help and your brilliant ideas for the POM measurements. I wish you all the best in the future!

Now, it is time to gratefully acknowledge the members of PCBE group and polymer chemistry department. Dear colleagues, I am really lucky to meet all of you who make my stay in Groningen really a wonderful memory. Karin, Martine, Yvonne, and Andrea, thank you so much for all your kind help in the administrative work. Jan Willem, Dr. de Vries, thank you so much for your supports and translations in any aspect. I really appreciate that you are always willing to contribute your time for the computers, equipment, and chemicals. My great thanks go to Lifei for very useful daily discussions and suggestions in my entire studies. You supported me in any manner and enabled so much joyful time inside and outside of the lab. You are a smart scientist and a qualified father, I wish you all the best for your family and a bright future for your career! Wei, thank you for many suggestions and enlightening discussions. You are my first contacted colleague in Groningen. Dr. Xingfei Zhou, I am so lucky to have you as my colleague during my Ph. D study in the first year. Thank you so much for all advices in questions and your encouragement when I struggled. Jun, it is very lucky that we

become colleagues again in PCBE group. I am grateful to you and your wife Pei for all kinds of helps. In particularly, I really enjoyed the Chinese food you cooked. Diego, Alessio, my dear Italian friends, I really appreciate our collaborations, your advice, and fruitful discussions. Pavlo, you are always willing to help me in experiments. Thanks a lot! Jennifer, I am sincerely thankful to you for polishing my papers and the thesis as well. Qing, Chao and Jing, I really appreciate your efforts on our collaborated experiments. Good luck for your Ph. D study! Dear Mark, thanks a lot for your efforts on my thesis! Dear Dr. Bart Crielaard, it is great that we have many valuable discussions on research. Lei, Jingyi, Zhuojun, Agnieszka, Tiancai, Hongyan, Gurudas, Karolin, Kseyniya, Konstantin, Jur, Eliza, Alina, Daniel, Avishek, Gert-Jan, Konstantin, Stefano, Alberto, Manfred, Anke, Deepak, and Minseok, thank you for being my colleagues in PCBE group. It is indeed a very wonderful experience to work together. I really enjoyed our trips to conferences and the annual Christmas dinners with all of you. I want to express my gratitude to Prof. Gerrit ten Brinke, Prof. Arend Jan Schouten, Prof. Ton Loontjens. Thanks for helping me in one way or another. Thanks to Jin, I really enjoyed the enlightening discussions with you. Best wishes to you and your boyfriend in your pursuing Ph. D study! Anton, thanks for your patience to help me some Dutch translations. I want to express my thanks to all the former and present members of polymer chemistry department for the supports and accompany during coffee breaks, VvP activities, and trips although it would be impossible to mention all the names: Zhen, Qiuyan, Yi, Yexing, Albert, Steven, Samomeh, Milica, Dejan, Jelena, Jakob, Erythrina, Vincent, Azis, Ivana, Martijn, Martin, Nanda, Ralph, Thomas, and Giuseppe.

I would like to thank all the other friends I met during my stay in Groningen, who helped me a lot and shared a lot of wonderful moments with me and my family. Dear Mr. Tao Zhang and Mrs. Wenjun Wang, thank you very much for mixing wines and alcohols, cooking tasty foods. Especially, your Northwestern broad-noodles is so an amazing food that I decided to learn it and now cook it very frequently at home. I really appreciate your whole-night accompanies during my wife delivery in Martini Hospital. I wish that both of your careers proceeds very well and may you soon have a dear baby! Dear Floris, it was an enjoyable memory that you drove a Minibus and took us to catch oyster in North Sea. Thanks a lot for your cooked Dutch food and your constant helps to my family. Dear Tao Yuan couple, Shuo Yang, Zhongtao Wu, Yun Liu, Jiquan Wu couple, Bo Zhang and your xiaoqi, Chenyu Shi couple, Huanlin Lang and your private doctor Shaochong Bu, Linlin Li couple, Jinfeng Shao, Zilin Yu, Jie Yin and your daughter, Zheng Zhang and your Jan, Bin Mao, Wenqiang Zou, Jiawen Chen and your beibei, Depeng Zhao, Zhiyuan Zhao, Yuehu Wang, Guowei Li, Feng Zhang, Jianwei Li, Yajun Gao, other Groningen funny football teammates, and ..... the list is endless, I really enjoyed the delighted time spent together with you for dinners and parties. I am so lucky to have you as my dear friends, the Groningen study life became more colorful because of you.

Many sincere thanks to my master supervisor Prof. Hongpeng You. Thank you so much for encouraging me to pursue Ph. D study abroad. I deeply appreciate your endless support and help. What I learnt from you will be a treasure in my life.

Finally and most importantly, I would like to give my deepest gratitude to my family. Dear Dad and Mom, thank you very much for your continuous support in my life. Love from you is beyond word! I am gratefully acknowledge to my deeply-loved wife, Juanjuan Su, thank you for being next to my side, your constant understanding, support, encouragement, and also some collaborations on modeling liquid crystal structures. Thank you for giving me the most important and invaluable gift in Nov. 8th 2013, our lovely angel–Esther Yige Liu. She is so cute and brings us endless joys and happiness. I express my sincere gratitude to my parents-in-law, thanks for your love! I wish you all the best! Many special thanks to my sisters, Yan Liu and Fang Liu, your encouragement and support are always there. My dearest, thanks for everything you have done for me. You provide all my needs and give me the capability to pursue a Ph. D in my life, so the thesis is dedicated to you.